

The development of microfluidic platforms for environmental analysis

Ivan Maguire, B.Sc. (Hons)

Doctor of Philosophy

to



Dublin City University

July 2018

Supervisor: Prof. Fiona Regan

School of Chemical Sciences

Supervisor: Prof. Jens Ducreé

School of Physical Sciences

Declaration

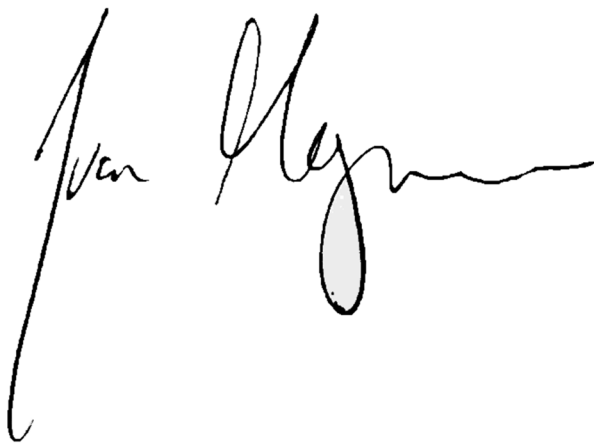
Name: Ivan Maguire

(Candidate) ID No.: 14211797

Date: 09/ 07/2018

I hereby certify that this material, which I now submit for assessment on the programme of study leading to the award of Doctor of Philosophy (PhD) is entirely my own work, that I have exercised reasonable care to ensure that the work is original, and does not to the best of my knowledge breach any law of copyright, and has not been taken from the work of others save and to the extent that such work has been cited and acknowledged within the text of my work. In the specific cases where collaboration between scientific papers has occurred within a specific chapter, due diligence of the paper's co-authors has been provided in the form of a breakdown of work within the chapters forward.

Signed:

A handwritten signature in black ink, appearing to read 'Ivan Maguire', written in a cursive style.

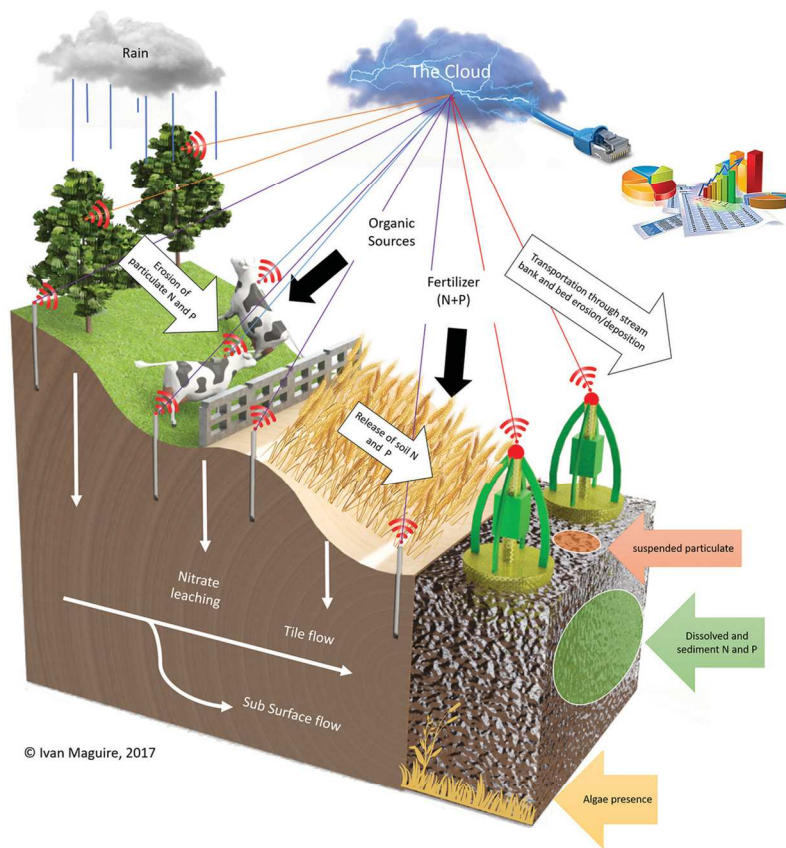
Ivan Maguire, BSc. (Hons)

Thesis Abstract

There is currently a gap in the use of centrifugal microfluidics in the field environmental sensing. The purpose of this thesis was to develop new and innovative centrifugal microfluidic platforms, which could enhance current environmental monitoring strategy limitations; portability and *in-situ* capability, cost-effectiveness, generical design for multi-analyte detectability, and the minimal required end-user interaction. Included in the main body of the thesis will be a review article, providing the theoretical perspectives which have been demonstrated for microfluidic applications in other domains and recommendations for adaptation towards environmental sensing using centrifugal microfluidics, and three novel papers on the staged development of a multi-toxin detection platform aimed to be incorporated within the fully deployable MariaBox (*Marine environmental in-situ assessment and monitoring toolBox*, co-funded by the European Commission: contract no.614088) system. The aspects covered across these three original articles includes the development of a centrifugal microfluidic platform with complementary fluorescence detection system as an initial test bed for toxin bio-assay integration on-disc, progression of current centrifugally-automatable pneumatic microvalve mechanisms for increased actuation predictability, and the further combination of both of these detection and microvalve mechanisms for a complete on-disc, multi-toxin detection platform which has been designed specifically to be compatible with the deployable MariaBox platform.

Analyst

rsc.li/analyst



ISSN 0003-2654



Table of Contents

Declaration	ii
Thesis Abstract.....	iii
Dissemination history (2014-2018).....	xi
Conference oral presentations	xi
Conference poster presentations	xiii
Workshop demonstrations	xv
Papers accepted and published	xvi
Paper submitted	xviii
Acknowledgments	xx
Publications and Author Contribution	xxiii
Thesis Foreword.....	xxv
Chapter 1: Introduction to The Theory of Pressure-Driven Laminar Flow	1
Chapter Foreword.....	1
1.1 Surface tension and cohesion	1
1.2 Capillary action and adhesion	3
1.3 Laminar flow.....	4
1.4 Navier–Stokes equation	5
1.5 Poiseuille flow	6
1.6 Hagen–Poiseuille’s law	7
1.7 Reynolds number	9
1.8 Hydraulic resistance	10
1.9 Extra fluid movement considerations within a rotating system	12
1.10 Particle sedimentation through a fluid within a rotating system.....	13
1.11 References.....	15
Chapter 2: Literature review: A review of centrifugal microfluidics in environmental monitoring 17	
Chapter Foreword.....	17
2.1 Abstract	19
2.2 Introduction to microfluidics platforms	20
2.3 Development of centrifugal microfluidics for environmental monitoring.....	26

2.4	Environmental assay integration on a centrifugal microfluidic platform.....	27
2.5	Detection strategies on centrifugal microfluidic platforms for environmental assay integration	32
2.5.1	Acoustic transducers	33
2.5.2	Electrochemical transducers	39
2.5.3	Optical transducers	43
2.6	Opportunity for LOAD modifications in environmental monitoring	48
2.7	Conclusions	50
2.8	References.....	52

Chapter 3: A novel microfluidic analytical sensing platform for the simultaneous detection of three algal toxins in water 71

Chapter Foreword.....	71
3.1 Abstract	74
3.2 Introduction	75
3.3 Results and discussion.....	79
3.3.1 Microfluidic disc characterisation	79
3.3.2 Biosensor characterisation	81
3.4 Conclusion	90
3.5 Materials and methods	91
3.5.1 Chemical and biological reagents used	91
3.5.2 Preparation of conjugates and fluorescent antibodies	91
3.5.3 Microfluidic disc manufacturing.....	92
3.5.4 Preparation of reservoir surface for bio-activation.....	92
3.5.5 Amine surface functionalisation of biosensor reservoir floor by liquid phase.....	93
3.5.6 Microfluidic disc characterisation	94
3.5.7 Optimisation of antibody concentration.....	96
3.5.8 Toxin Conjugate and control antibody binding to biosensor surfaces	96
3.5.9 Manufacture of the detection platform.....	97
3.5.10 Measurement of toxin binding.....	98
3.6 Acknowledgment	99
3.7 Author Information	99
3.8 Supplementary Information	99
3.9 References.....	100

Chapter 4: Enabling fluidic predictability using a pneumatic valve enhancement strategy for highly integrated Lab-on-a-disc platforms 107

Chapter Foreword:.....	107
4.1 Abstract	109
4.2 Introduction	110
4.3 Results and discussion.....	116

4.3.1	Disc characterisation	117
4.3.2	Outlier removal	120
4.3.3	Initial Model generation.....	121
4.3.4	Spin protocol generation.....	124
4.3.5	Summary	126
4.4	Conclusion	130
4.5	Acknowledgment	131
4.6	Materials and Methods.....	131
4.6.1	Microfluidic disc manufacturing.....	131
4.6.2	Microfluidic disc characterisation	131
4.7	Reference	132

Chapter 5: A Centrifugal Microfluidic-Based Approach for Multi-Toxin Detection for Real-Time Marine Water-Quality Monitoring 138

Chapter Foreword:.....	138	
5.1	Abstract	140
5.2	Introduction	140
5.2.1	Overview of the problem	140
5.2.2	Current approaches for toxin analysis.....	142
5.2.3	A Lab-On-A-Chip (LOAC) solution to toxin monitoring.....	143
5.2.4	Proposed Lab-On-A-Disc (LOAD) alternative solution	144
5.3	Results and discussion.....	145
5.3.1	Characterisation of sample handling.....	146
5.3.2	Fluorescent assessment of microfluidic	146
5.3.3	Next steps to be taken	147
5.4	Conclusion	147
5.5	Methods and Materials	148
5.5.1	Chemical and biological reagents used:	148
5.5.2	Preparation of MC-LR and DA conjugates and fluorescent antibodies:.....	149
5.5.3	Microfluidic disc manufacturing:.....	149
5.5.4	Dissolvable film valves:.....	149
5.5.5	Preparation of reservoir surface for bio-activation:.....	152
5.5.6	Amine surface functionalisation of biosensor reservoir floor by liquid phase:.....	152
5.5.7	Toxin conjugate binding/Control antibody binding to biosensor surface:.....	153
5.5.8	Microfluidic disc characterisation:	153
5.5.9	Fluorescent microscope analysis:.....	154
5.6	Acknowledgment	154
5.7	References.....	155

Chapter 6: Development of a novel multi-analyte marine bio-sensor lab-on-a-disc platform: A design pipeline from concept to actuality	160
Chapter Foreword:.....	160
6.1 Abstract	162
6.2 Introduction	163
6.3 Methodology.....	164
6.3.1 Chemical and biological reagents used	164
6.3.2 Microfluidic disc manufacturing.....	165
6.3.3 Microfluidic disc fluidic characterisation.....	165
6.3.4 Pre-storage of analyte conjugate and control on disc	165
6.3.5 Biosensor integration	166
6.3.6 Heavy metals assay integration.....	166
6.3.7 Manufacturing of a detection platform	167
6.4 Discussion.....	168
6.4.1 Analytes.....	168
6.4.2 Disc development process.....	171
6.4.3 Summary and lessons learned.....	188
6.5 Conclusion	193
6.6 Acknowledgment	193
6.7 Supplementary Information	194
6.8 References.....	195
Chapter 7: Final Conclusion	199
7.1 References.....	204

Table of Figures

Figure 1.1: Graphical illustration of surface tension.	2
Figure 1.2: Graphical illustration of capillary action.	4
Figure 1.3: Graphical illustration of laminar flow.....	5
Figure 1.4: Graphical demonstration of Poiseuille flow.	7
Figure 1.5: Graphical demonstration of Hagen-Poiseuille flow.	9
Figure 1.6: The forces operating on a rotating LOAD system.	12
Figure 1.7: The forces acting on a centrifugally driven particle in a fluid.	14
Figure 2.1: Manufacturing a NP-based centrifugal microfluidic platform.	21
Figure 2.2: The Photolithography process used in constructing P-based platforms.....	22
Figure 2.3: Lab-On-A-Chip (LOC)(left) and Lab-On-A-Disc(LOAD)(right) platforms.....	24
Figure 2.4: Keyword publications trends per annum with respect to microfluidic research.....	24
Figure 2.5: A graphical breakdown of assay protocol conversion to microfluidic features.	28
Figure 2.6: Designing reservoirs to avoid sample loss.	30

Figure 2.7: Percentage of reservoir filled before sample leakage occurs vs liquid viscosity.....	31
Figure 2.8: Graphical illustrations of Surface acoustic wave (SAW) biosensors.....	38
Figure 2.9: Amperometric-based electrochemical detection on a LOAD platform (49).	40
Figure 2.10: Potentiometric-based electrochemical detection on a LOC platform (77).	42
Figure 2.11: Absorbance-based optical detection on LOAD based platforms.	44
Figure 2.12: Analyte capture and optical detection.....	46
Figure 2.13: SPR optical detection on LOAD based platforms, as described by Hemmi et al (115).....	47
Figure 2.14: Future developments for Lab-On-A-Disc platforms studies.....	49
Figure 3.1: The chemical structures of microcystin-LR (MC-LR), domoic Acid (DA) and saxitoxin (STX) in their predominant congener form.	76
Figure 3.2: Fluid dynamic characterisation of microfluidic disc using a coloured-aqueous solution.....	80
Figure 3.3: The comparison of the performance of the microcystin scFv vs scAb antibody form.	81
Figure 3.4: In-house highly specific recombinant antibody technology vs. commercial counterparts (supplied by Abcam Ltd.).....	82
Figure 3.5: Direct binding assay measured by the system.	83
Figure 3.6: Intra-assay analysis (n=3) for microcystin (MC-LR), domoic acid (DA) and saxitoxin (STX) measured on the microfluidic sensor.....	87
Figure 3.7: Inter-assay analysis for microcystin (MC-LR), domoic Acid (DA) and saxitoxin (STX) measured on the microfluidic sensor.....	88
Figure 3.8: The competitive toxin detection assay protocol represented by functional microfluidic reservoirs.....	94
Figure 3.9: The 'Spin stand' used for microfluidic characterisation.	95
Figure 3.10: The Detection system.....	98
Figure 4.1: The Lab-On-A-Disc (LOAD) platform concept.....	111
Figure 4.2: Active valving systems integrated into microfluidic platforms.	112
Figure 4.3: Passive valving solutions for microfluidic platforms.	114
Figure 4.4: The development stages of a highly integrated LOAD microfluidic platform summarised as three microfluidic platforms.	115
Figure 4.5: The Microfluidic disc with spiral arraying of reservoir-reservoir-Pneumatic-chamber (RRPC) microfluidic features.	118
Figure 4.6: The averaged (n=3) rotational frequency vs positional radius from centre of rotation, whereby liquid phase change occurred.	119
Figure 4.7: Averaged rotational frequency vs positional radius of feature from centre of rotation, whereby liquid phase change occurred, with outliers excluded as per settings described in Table 7. ...	121
Figure 4.8: The averaged rotational frequency (with outliers excluded) at the inverse square root positional radius of feature from centre of rotation, whereby liquid phase change occurred.	123
Figure 4.9: Averaged (n=3) rotational frequency vs positional radius from centre of rotation whereby liquid phase change occurred (including outliers) compared to model.....	125
Figure 4.10: Raw rotational frequencies of the three discs vs positional radius from centre of rotation whereby liquid phase change occurred (including outliers) compared to model.	126
Figure 4.11: Ideal dissolvable valve locations.	128
Figure 4.12: The rotational frequency protocol used for the MariaBox microfluidic platform(40), either by varying radius (top) or time (below), based on the normalisation, passthrough and compression models.....	129

Figure 5.1: The chemical structures of microcystin-LR (left) and domoic acid (right) in their predominant congener forms	142
Figure 5.2: The MARIABOX platform and detection.	145
Figure 5.3: – Microfluidic disc characterisation.	147
Figure 5.4: – Fluorescent microscopy images taken from the test reservoir floors.....	148
Figure 5.5: – An illustration to demonstrate how sample progression can be halted for a set period of time using a pneumatic stop approach, which was determined by a specific disc spin cycle.	150
Figure 5.6: – An illustration of a triple-test assay on the disc, with the 5-step assay protocol in triplicate;	151
Figure 6.1: The inverse assay protocols used for fluorescence detection of both non-heavy metal analytes (A) and heavy metals (B), illustrated as a centrifugal microfluidic processing unit.	169
Figure 6.2: Layer-by-layer disc design approach using CAD software for ease of compatibility and rapid modification.	172
Figure 6.3: The design tree for the MariaBox centrifugal processing unit (mCPU).....	173
Figure 6.4: Initial conceptualisation of the MariaBox centrifugal processing unit (mCPU).	174
Figure 6.5: The single assay concept (v1.0).....	175
Figure 6.6: The design refinement process of the initial assay development with manual microvalve mechanism (V1.1-1.5).	176
Figure 6.7: Flowchart of the APTES-EDC/NHS surface functionalisation chemical method.....	177
Figure 6.8: The detection optimised mCPU with manual microvalve mechanism (V1.6), and reservoir replica chip and holder for rapid biosensor integration.	178
Figure 6.9: The Evolution of the detection platform for the MariaBox centrifugal processing unit.	180
Figure 6.10: The microvalve mechanisms investigated for autonomous assay execution.	183
Figure 6.11: Modifications and calibration discs required for integration of microfluidic platform with autonomous MariaBox platform.....	185
Figure 6.12: The deployable 3-day, 3 analyte (3D3A) MariaBox centrifugal processing unit.	186
Figure 6.13: Issues associated with the optical transparency of the discs during transportation.	187
Figure 6.14: The deployable 3-day, 8 analyte (3D8A) MariaBox centrifugal processing unit.	188

Dissemination history (2014-2018)

Conference oral presentations

1. Title: Novel One-Step Centrifugal Sensor System for the Detection of Cyanobacterial Toxin Microcystin-LR

Authors: J. Fitzgerald, I. Maguire, B. Heery, C. Murphy, C. Nwankire, R. O’Kennedy, J. Ducreé and F. Regan

Conference: 2015 ASLO Aquatic Sciences Meeting, Granada, Spain, 22-27 February 2015

2. Title: Atalanta: The autonomous analytical algal toxin platform

Authors: I. Maguire, J. Fitzgerald, B. Heery, C. Murphy, C. Nwankire, R. O’Kennedy, J. Ducreé and F. Regan

Conference: Euroanalysis 2015, Bordeaux, France, 6-10 September 2015

Award (Yes, No) – Yes, best presenter award

3. Title: A centrifugal lab-on-a-disc device for the in-situ determination of dissolved reactive phosphate in water

Authors: G. Duffy, B. Heery, I. Maguire, C. Nwankire, J. Ducreé, F. Regan

Conference: Euroanalysis 2015, Bordeaux, France, 6-10 September 2015

4. Paper: A centrifugal lab-on-a-disc device for determination of phosphate in water

Authors: G. Duffy, B. Heery, I. Maguire, C. Nwankire, J. Ducreé, F. Regan

Conference: YoungChem 2015, Krakow, Poland 7-11 October 2015

5. Title: Atalanta: The autonomous analytical algal toxin platform

Authors: I. Maguire, J. Fitzgerald, B. Heery, C. Murphy, C. Nwankire, R. O’Kennedy, J. Ducreé and F. Regan

Conference: SWIG meeting 2016, Dublin, Ireland, 25-28 January 2016

6. Title: In-Situ detection of microcystin in a pre-lysed freshwater sample using an integrated centrifugal microfluidics platform

Authors: I. Maguire, J. Fitzgerald, B. Heery, C. Murphy, C. Nwankire, R. O’Kennedy, J. Ducreé and F. Regan

Conference: Biosensors 2016, Gothenburg, Sweden, 25–27 May 2016

7. Title: HONEY, I SHRUNK THE LABORATORY (WITH SCIENTISTS ALSO INCLUDED)

Authors: I. Maguire

Conference: Thesis-in-3, Dublin, Ireland, 9 September 2016

8. Title: A Physicist's Paradigm to crafting chemistry contraptions for the scientist *et al.*

Authors: I. Maguire

Conference: Chemistry Day, DCU, Dublin, Ireland, 11 May 2017

9. Title: A Centrifugal Microfluidic-Based Approach for Multi-Toxin Detection for Real-Time Marine Water-Quality Monitoring

Authors: I. Maguire, J. Fitzgerald, D. McPartlin, B. Heery, C. Murphy, C. Nwankire, R. O’Kennedy, J. Ducreé, F. Regan

Conference: Oceans ’17, Aberdeen, Scotland, 19 June 2017

10. Title: From Um to Ah! A journey of discovery

Authors: I. Maguire

Conference: A taste of DCU, an age-friendly event, Dublin, Ireland, 29 September 2017

11. Title: ToxiSense: A centrifugal microfluidic sensor for the simultaneous detection of the algal toxins; Microcystin-LR, Domoic Acid and Saxitoxin.

Authors: I. Maguire, J. Fitzgerald, B. Heery, C. Murphy, C. Nwankire, R. O’Kennedy, J. Ducreé and F. Regan

Conference: BRS research Day, DCU, Dublin, Ireland, 25 January 2018

12. Title: ToxiSense: A centrifugal microfluidic sensor for the simultaneous detection of the algal toxins; Microcystin-LR, Domoic Acid and Saxitoxin.

Authors: I. Maguire

Conference: Amgen Biotech Experience Talk, Dublin, Ireland, 31 January 2018

Conference poster presentations

1. Title: Novel method for the detection of cyanobacterial toxin microcystin-LR using a centrifugal microfluidic (Lab-On-A-Disc) sensing system

Authors: I. Maguire, J. Fitzgerald, B. Heery, C. Murphy, C. Nwankire, R. O’Kennedy, J. Ducreé and F. Regan

Conference: Environ 2015, Sligo IT, Sligo, Ireland, April 8th-10th 2015

2. Title: The ToxiSense detection system: a novel centrifugal-based microfluidic (lab-on-a-disc) system for detecting cyanobacterial toxin microcystin-LR

Authors: I. Maguire, J. Fitzgerald, B. Heery, C. Murphy, C. Nwankire, R. O’Kennedy, J. Ducreé and F. Regan

Conference: MicroTas 2015, Gyeongju, South Korea, 25-29 October 2015

Award (Yes, No): Unsuccessful finalist for best poster

3. Title: ToxiSense v2.0: The next generation autonomous analytical algal toxin platform

Authors: I. Maguire, J. Fitzgerald, B. Heery, C. Murphy, C. Nwankire, R. O’Kennedy, J. Ducreé and F. Regan

Conference: Europt[r]ode XIII, Graz, Austria, 20-23 March 2016

4. Title: A fully integrated centrifugal lab-on-a-disc platform for onsite measurement of phosphate in water

Authors: G. Duffy, I. Maguire, B. Heery, C. Nwankire, J. Ducreé, F. Regan

Conference: Europt[r]ode XIII, Graz, Austria, 20-23 March 2016

Award (Yes, No) Yes – 2nd place in Best poster competition

5. Title: Novel One-Step Centrifugal Sensor System for the Detection of Cyanobacterial Toxin Microcystin-LR

Authors: J. Fitzgerald, I. Maguire, B. Heery, C. Murphy, C. Nwankire, R. O’Kennedy, J. Ducreé and F. Regan

Conference: SETAC 2015, Barcelona, Spain, 3-7 May 2015

6. Title: An in-situ Marine Pollution Monitoring Device, based on new Biosensors, designed for long-term Unsupervised Autonomy: System Requirements and Design Approach

Authors: A. Giusti, S. Hadjiyiannis, P. Philimis, P. Barattini, M. Bonasso, E. Garces, K. Thomas, S. Mier, A. Varriale, S. D’Auria, R. McNulty, F. Regan, J. Fitzgerald, I. Maguire, S. Mier, R. Isticato, G. Donadio, E. Ricca

Conference: CEST 2015, Rhodes, Greece, 3-5 September 2015

7. Title: A microfluidic lab-on-a-disc device for in situ measurement of phosphate in water

Authors: G. Duffy, I. Maguire, B. Heery, C. Nwankire, J. Ducreé, F. Regan

Conference: CASi, Dublin City University, Dublin, Ireland, 14-15 April 2016

8. Title: Development of novel centrifugal separation device - addressing the challenges of size and shape of microplastics with results from Irish rivers

Authors: I. Maguire, L. Mata, C. Gourvennec, K. Alazet, S. Mc Gowan, F. Regan

Conference: IWA Conference, DCU Dublin, Ireland 15 November 2016

13. Title: Development of an autonomous algal-toxin analytical platform for aquatic monitoring

Authors: J. Fitzgerald, I. Maguire, B. Heery, C. Murphy, C. Nwankire, R. O’Kennedy, J. Ducreé and F. Regan

Conference: Digital Oceans Conference, SeaFest ’16, Galway, Ireland, 29 June 2016

14. Title: Battery-powered microcontroller with wireless communication for random, ohmic actuation of novel wax valves on a lab-on-a-disc platform

Authors: I. Maguire, B. Heery, B. Andlauer, S. Gribbin, C. Nwankire, J. Ducreé, A. Morrin and F. Regan

Conference: MicroTAS 2016, Dublin, Ireland 9-13 October 2016

15. Title: A centrifugal microfluidic platform for Chromium speciation on a lab-on-a-disc

Authors: I. Maguire, G. Duffy, B. Heery, P. Gers, J. Ducreé, F. Regan

Conference: Europt(r)ode XIV, Naples, Italy 25-28 March 2018

16. Title: Design features for enhancing optical detection on Lab-on-a-disc platforms

Authors: I. Maguire, J. Fitzgerald, G. Duffy, B. Heery, J. Ducreé, F. Regan

Conference: Europt(r)ode XIV, Naples, Italy 25-28 March 2018

Workshop demonstrations

1. Workshop title: Centrifugal microfluidic systems

Authors: I. Maguire and F. Regan

Conference: Water conference, DCU Water institute, Dublin, Ireland, 9 September 2015

2. Workshop title: Designing, manufacturing and testing of centrifugal microfluidic systems for rapid prototyping of environmental detection systems

Authors: I. Maguire, J. Ducreé and F. Regan

Conference: IAH meeting 2016, Tullamore, Ireland, 12-13 April 2016

3. Workshop title: Microplastics: What are they, where do they come from, and where do they go?

Authors: I. Maguire, G. Duffy and F. Regan

Conference: 35th ChemEd-Ireland Conference, Dublin, Ireland, 22nd October 2016

4. Workshop title: Microplastics: What are they, where do they come from, and where do they go?

Authors: I. Maguire, G. Duffy and F. Regan

Conference: Sensors workshop, DCU Water institute, Dublin, Ireland, 29 November 2018

Papers accepted and published

1. Paper title: SIZE- and deformability-based particle sorting by strategic design of obstacle arrays in continuous centrifugal sedimentation mode

Authors: C. E. Nwankire, I. Maguire, D. Kernan, M. Glynn, D. Kirby and J. Ducreé

Journal name: IEEE

Volume: 2015 Transducers - 2015 18th International Conference on Solid-State Sensors, Actuators and Microsystems (TRANSDUCERS)

Page range: 1854 - 1856

Date of Conference: 21-25 June 2015

DOI: 10.1109/TRANSDUCERS.2015.7181310

2. Paper title: PhosphaSense: A fully integrated, portable lab-on-a-disc device for phosphate determination in water

Authors: G. Duffy, I. Maguire, B. Heery, C. Nwankire, J Ducreé, F Regan

Journal name: Sensors & Actuators: B. Chemical

Year: 2017

Volume: 246

ISSN: 0925-4005

DOI: 10.1016/j.snb.2016.12.040

3. Paper title: A centrifugal microfluidic-based approach for multi-toxin detection for real-time marine water-quality monitoring

Authors: I. Maguire, J. Fitzgerald, D. McPartlin B. Heery, C. Murphy, C. Nwankire, R. O’Kennedy, J. Ducreé and F. Regan

Journal name: IEEE OCEANS 2017 - Aberdeen

Year: 2017

Pages: 1-8

DOI: 10.1109/OCEANSE.2017.8084975

4. Paper title: MariaBox: First prototype of a novel instrument to observe natural and chemical pollutants in seawater

Authors: M. Bonasso, P. Barattini, R. Isticato, G. Donadio, A. Giusti, P. Philimis, S. D’Auria, A. Varriale, M. Staiano, A. Pennacchio, I. Maguire, J. Fitzgerald, F. Regan and J. Ducreé

Journal name: IEEE OCEANS 2017 - Aberdeen

Year: 2017

Pages: 1-5

DOI: 10.1109/OCEANSE.2017.8084860

5. Paper title: ChromiSense: A colourimetric lab-on-a-disc sensor for chromium speciation in water

Authors: G. Duffy, I. Maguire, B. Heery, C. Nwankire, J Ducreé, F Regan

Journal name: Talanta

Year: 2018

Volume: 178

Issue: Supplement C

Pages: 392-399

ISSN: 0039-9140

DOI: 10.1016/j.talanta.2017.09.066

6. Paper title: Centrifugal microfluidics and its potential in environmental monitoring (REVIEW)

Authors: I. Maguire, R. O’Kennedy, J. Ducreé and F. Regan

Journal name: Analytical methods

Year: 2018

Volume: 10

Issue: 13

Pages: 1497-1515

DOI: 10.1039/C8AY00361K

7. Paper title: A novel microfluidic analytical sensing platform for the simultaneous detection of three algal toxins in water

Authors: I. Maguire, J. Fitzgerald, B. Heery, C. Nwankire, R. O’Kennedy, J. Ducreé and F. Regan

Journal name: Analytical Chemistry Society Omega

Year: 2018

Volume: 3

Issue: 6

Pages: 6624-6634

DOI: 10.1021/acsomega.8b00240

Paper submitted

1. Paper title: A characterisation technique for predicting centrifugal microvalve operational conditions

Authors: Ivan Maguire, Kevin Alazet, Niamh Aine Kilcawley, Turlough Downes, Jens Ducreé, Fiona Regan

Journal name: Sensors & Actuators: B. Chemical

2. Paper title: Development of a novel multi-analyte marine bio-sensor lab-on-a-disc platform: A design pipeline from concept to actuality

Authors: I. Maguire, J. Fitzgerald, C. Murphy, R. O’Kennedy, J. Ducreé, F. Regan, A. Giusti, P. Philimis, R. Isticato, G. Donadio, S. D’Auria, A. Varriale, M. Staiano, A. Pennacchio, K. Thomas, S. J. Sayfritz

Journal name: Emerald Sensors Review

Acknowledgments

I would like to thank first my supervisor Prof. Fiona Regan for her constant support throughout my PhD, often trusting wildly imaginative ideas even when I had no idea how they would be implemented, and for convincing me that a simple physicist could feel at home in the field of chemistry and biology. Thank you for all of the travel and opportunities which you so eagerly encouraged me to do during my PhD, and for your endless positivity, even when things went wrong. But I think it's safe to say, we got a lot more things right!

Secondly, I would like to thank Dr. Jenny Fitzgerald for being my mentor, and above all else, a true friend! This PhD would not have been completed without her guidance, nor would I have survived the rabbit-hole that is biotechnology! Thank you for always taking the time to help, for enduring long meetings and dodgy skype calls, for laughing at all the failures with me, and for the perpetual mothering of me over the years. It was greatly appreciated!

Thank you to my co-supervisor Prof. Jens Ducreé for his help and access to equipment. Thanks to Danielle, Éanna, Éadaoin and Daniel K. for some great fun over the years.

A special thank you must go to the wonderful analytical chemist, Dr. Gillian Duffy, who took the time to teach me chemistry, and so enthusiastically endured when I taught her physics in return... We'll always have PhosphaSense and ChromiSense, remember that!

Alan, Ciprian, Maria, and Lisa, Brendan thanks for the friendship and support over the years. Also, a massive thank you to all of my first-rate final year, INTRA and international students; Alex, Alexandra, Aurelie, Bastien, Célia, Kévin A., Kevin M., Lise, Manon, Sean, and Steven.

Thank you to Prof. Richard O'Kennedy for access to his facilities and to his wonderful team. Daniel McP., Jonathan, Aoife and Arabelle, this last year has been filled with so much science, laughter and abuse. It has been a wonderful distraction from this thesis. I probably should have been finished an awful lot sooner... but where's the fun in that?

Many thanks to the DCU Water Institute, SmartBay Ireland, Dublin City University and the European Commission for funding all of my PhD escapades and giving me the opportunity to pursue my ambitions.

Thanks to all Biotechnology and Chemistry postgrads, and technical staff, past and present, for the friendship and fun every day. Thanks to the NRF staff and Pat Wogan for all the help.

Thank you to my brothers, John and Adrian, both of whom helped me in one way or another during the years... and in particular Adrian, as if you hadn't completed your PhD, I probably wouldn't have had the same drive to complete mine either... After all, I couldn't let you be the only doctor in the family.

Finally, a massive thank you to my incredible parents, Michael and Ann, for their unwavering support, encouragement and unwavering belief in me, particularly when I made it more difficult than necessary. This thesis is dedicated to you.

“Nobody ever figures out what life is all about, and it doesn't matter. Explore the world. Nearly everything is really interesting if you go into it deeply enough.”

— Richard Feynman

Publications and Author Contribution

This thesis includes three original manuscripts published in peer-reviewed journals and two chapters that are submitted to peer-reviewed journals. At the core of the thesis is the development process and implementation of low cost centrifugal microfluidic based analysers for monitoring of the aqueous environment. The ideas, development and writing up of all manuscripts in the thesis were the principal responsibility of me, the candidate, working within the School of Chemical Sciences under the supervision of Prof. Fiona Regan, and with significant assistance with regards to the biological integration and data analysis viewed in chapter 3 and 5 also provided by Dr. Jenny Fitzgerald. The inclusion of co-authors in Chapter 2 to 6 reflects the fact that part of the work came from active collaborations between researchers. In the case of these chapters, my contribution to the work involved the following:

Chapter	Sensor	Nature and extent of candidate's work
3	Single Toxin detector	Joint first author, initiation, key ideas, design and engineering of platform, integration of electronic components (<i>collaboration with Dr. Brendan Heery</i>), disc fabrication, biosensor integration (<i>collaboration with Dr. Jenny Fitzgerald</i>), data collection and analysis (<i>collaboration with Dr. Jenny Fitzgerald</i>), manuscript development and writing up (<i>collaboration with Dr. Jenny Fitzgerald</i>).
4	Autonomous Microvalve	First author, initiation, key ideas, disc fabrication (<i>collaboration with Kevin Alazet and Niamh Aine Kilcawley</i>), data collection, data analysis (<i>collaboration with Prof. Turlough Downes</i>), manuscript development and writing up.
5	Multi-toxin detector	First author, initiation, key ideas, design and engineering of platform, disc fabrication,

biosensor integration (*collaboration with Dr. Jenny Fitzgerald*), data collection and analysis (*collaboration with Dr. Jenny Fitzgerald*), manuscript development and writing up.

6	System integration of multi-toxin detector	First author, initiation, key ideas, input and management of biosensor, microvalves and total system integration design strategies, large scale fabrication, assisted in integration troubleshooting, collection of all relevant 'MARIABOX' project information and analysis from partners, manuscript development and writing up.
----------	--	--

Signed: _____ Date: _____

Ivan Maguire

Signed: _____ Date: _____

Prof. Fiona Regan

Thesis Foreword

With the ever-increasing demand on our natural environment, environmental sensors for monitoring should be considered a high priority. The focus of this thesis is to contribute to the field of environmental sensors.

The purpose of this thesis was to develop new and innovative centrifugal microfluidic platforms, which could enhance current environmental monitoring strategy limitations; portability and in-situ capability, cost-effectiveness, generical design for multi-analyte detectability, and the minimal required end-user interaction. Included in the main body of the thesis will be a review article, providing the theoretical perspectives which have been demonstrated for microfluidic applications in other domains and recommendations for adaptation towards environmental sensing using centrifugal microfluidics, and four novel papers on the staged development of a multi-toxin detection platform aimed to be incorporated within the fully deployable MariaBox (*Marine environmental in-situ assessment and monitoring toolBox*, co-funded by the European Commission: contract no.614088) system. The aspects covered across these four original articles includes the development of a centrifugal microfluidic platform with complementary fluorescence detection system as an initial test bed for toxin bio-assay integration on-disc, progression of current centrifugally-automatable pneumatic microvalve mechanisms for increased actuation predictability, and the further combination of both of these detection and microvalve mechanisms for a complete on-disc, multi-toxin detection platform which has been designed specifically to be compatible with the deployable MariaBox platform and the design strategy implemented during this development process. During the course of the PhD, a reoccurring theme of research was the investigation of the use of centrifugal microfluidics for environmental analysis and monitoring. This included the study of centrifugal microfluidics for:

- Biological studies, such as toxin detection using recombinant antibody technologies with future interests in DNA sensors.
- Chemical studies, using absorbance-based on-disc detection of chromium and phosphate.
- Centrifugal microfluidic disc enhancements for easier assay integration including: advanced microvalve development for more reliable assay performance (graphite-Wax, pneumatic, hydrophobic), electrification and digital-integration of electrical components for on-disc heating, optical and electrochemistry detection, wireless disc-to-PC communications for absolute assay automation, and investigation into reusable and cost effective centrifugal microfluidic solutions.

The PhD programme was funded by the FP7 EU-Funded MARIABOX project, as part of the European Union Seventh Framework Program (grant agreement No: 614088), whereby the candidate was required to develop a centrifugal microfluidic platform with eight separate on-board biosensors (four biological, four chemical). This platform was also required to be compatible with a deployable analytical system developed by partners, in which contained modules of sample preparation and delivery, disc and reagent storage, fluorescent detection capabilities, as well as network communications. The project involved the procurement of device components, off-the-shelf chip integration, module integration, laboratory testing, field testing and marinization. As part of this project, a proof-of-concept, fluorescence-based centrifugal microfluidic toxin detection system was also developed and tested. While this platform was successful in the use of anti-body technology for 3 separate toxins, current investigations are underway for use as a highly portable fluorescence-based DNA detector. While MARIABOX was the core project of the PhD, several side-project were also investigated. This included the investigation of integrating enhancements into the centrifugal microfluidic platform for increased performance and capabilities. One such example was the integration of electronic components, in combination with graphite-paraffin wax, for automated, wirelessly-operated microvalves actuated through melting. Another example was the development of highly reliable pneumatic valves which opened through increased disc rotational speed, and which was incorporated within the MARIABOX 8-analyte discs for synchronised multi-assay execution. A third project

included the conversion of a spectrophotometer into a highly portable centrifugal microfluidic platform whereby the detection of both chromium and phosphate was demonstrated. A final project was the anti-fouling assessment of bio-inspired microstructures using a centrifugal microfluidic platform. This included a comprehensive surface characterisation of the marine-based species as well as the development of a centrifugal microfluidic platform for assessing relative adhesion rates of variant diatom species through centrifugation.

It is hoped that these investigations will not just lead to more complete, cost-effective sensors targeting long-term autonomous deployment of marine-based environments, as well as being adaptable to other fields due to the generic design and flexibility of the centrifugal microfluidic platform.

Chapter 1: Introduction to The Theory of Pressure-Driven Laminar Flow

Chapter Foreword

A complete understanding of hydrodynamics is essential in developing successful, pressure-driven microfluidic systems.⁽¹⁾ Therefore, the theory behind how hydrodynamics systems operate must be considered comprehensively, and in particular how they function in microfluidic network-based devices. In this section, theoretical fluid flow will be discussed with particular attention to laminar flow in both rectangular and circular channels. These theories apply to both Lab-on-a-Chip (LOAC) and Lab-on-a-Disc (LOAD) systems, but the additional forces which only occur in LOAD platforms will also be discussed. This section will comprehensively cover all the important hydrodynamic derivations that must be considered when designing and developing of microfluidic technologies.

1.1 Surface tension and cohesion

Surface tension, often overlooked for being negligible in the world of macrofluidics, plays an important role in microfluidics. Surface tension is as a consequence of the force of cohesion of the fluids molecules at the free surface. This force is due to the molecules being pulled in less directions by molecular forces, such as hydrogen bonding, thus resulting in a stronger cohesion at the surface, with respect to the bulk of the liquid (Figure 1.1, top). The surface tension of a liquid can be measured by stretching a liquid membrane, using a wire edge as shown in liquid (Figure 1.1, bottom), and by where the surface tension can be determined using Equation 1.1.

Equation 1.1: Determining the Surface tension of a liquid

$$\sigma = \frac{F_{\sigma}}{l}$$

Where 'σ' is surface tension (N/m), 'F_σ' is the counteracting force (N) due to surface tension which opposes the pulling force F and 'l' is the length of the wire (m). (See Figure 1.1, bottom).

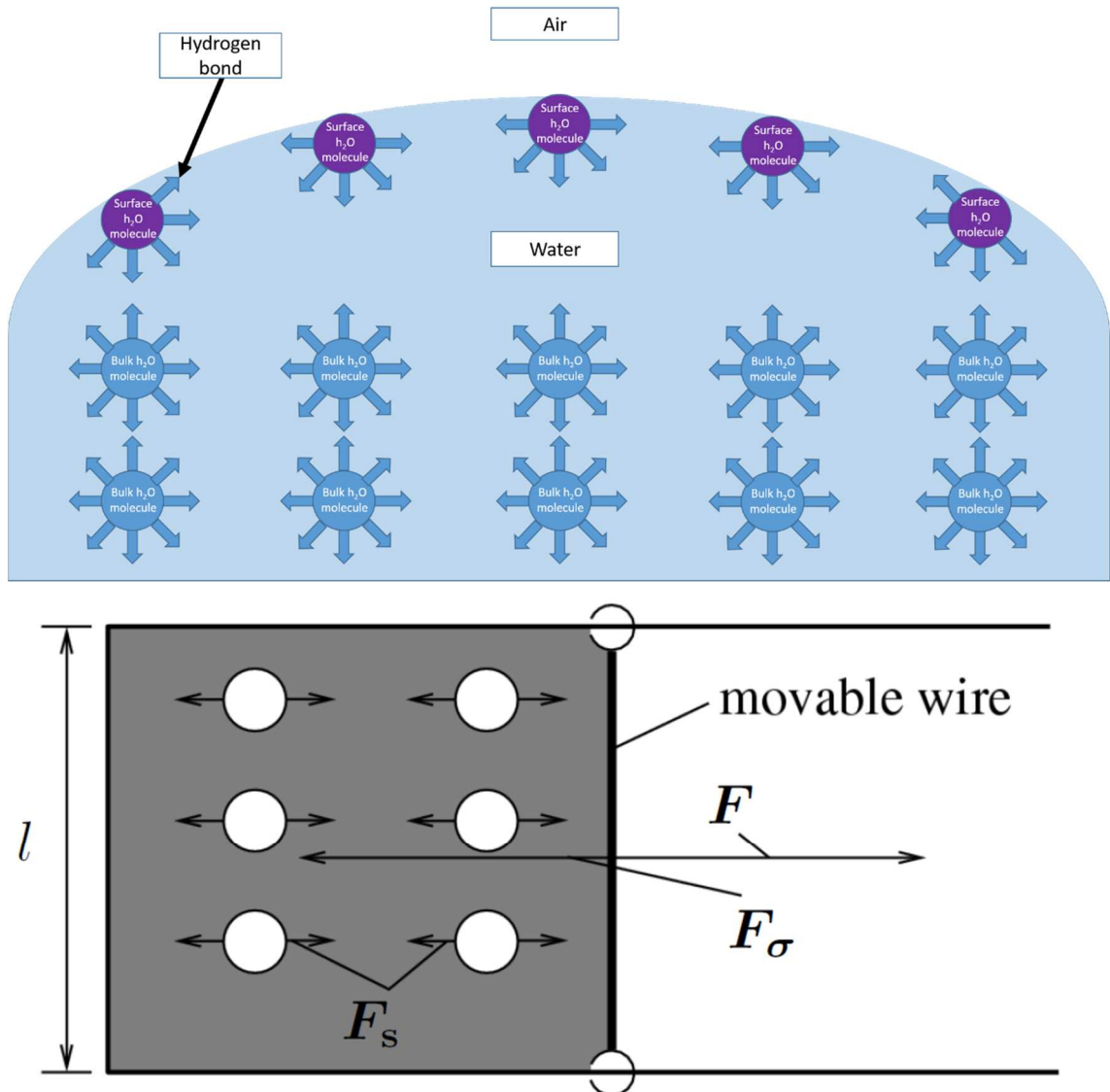


Figure 1.1: Graphical illustration of surface tension.

This phenomenon occurs due to molecular cohesion at the free surface (Top) and how it is measured (Bottom). Top: At the surface, there is less hydrogen bond pairs, which would otherwise normalise within the bulk of the water, thus resulting in a tighter compacting of the molecules at the free surface. Bottom: Surface tension σ can be measured by pulling a liquid membrane by a wire of edge length l with the force F which counteracts the overall forces due to surface tension ($F_{\sigma} = \sum F_s$). (2)

1.2 Capillary action and adhesion

Capillary action is a feature that a liquid possesses by where it can flow through narrow passages without the assistance of, and often counteracting, external forces like gravity. Capillary action occurs due the intermolecular adhesion forces between the liquid and its surrounding solid surface. Its magnitude is inversely proportionally to the cross-sectional area of the passage, and in combination with surface tension, can actively lift the liquid (capillary attraction, see Figure 1.2, Left). Alternatively, if the forces within the bulk of the liquid are larger than the combination of the surface tension and adhesion forces, capillary action will work in reverse (capillary repulsion, see Figure 1.2, Right). Mathematically, this phenomenon can be described as shown in Equation 1.2.

Equation 1.2: Capillary pressure in a circular tube

$$p_{\theta} = \frac{2\sigma}{r} \cos \theta$$

Where p_{θ} is the Capillary pressure, σ is the surface tension of the liquid, r is the radius of the tube, and θ is the contact angle between the liquid and the solid surface (perfect wetting occurs at $\theta = 0$, and the surface is considered hydrophobic where $\theta > 90^{\circ}$).

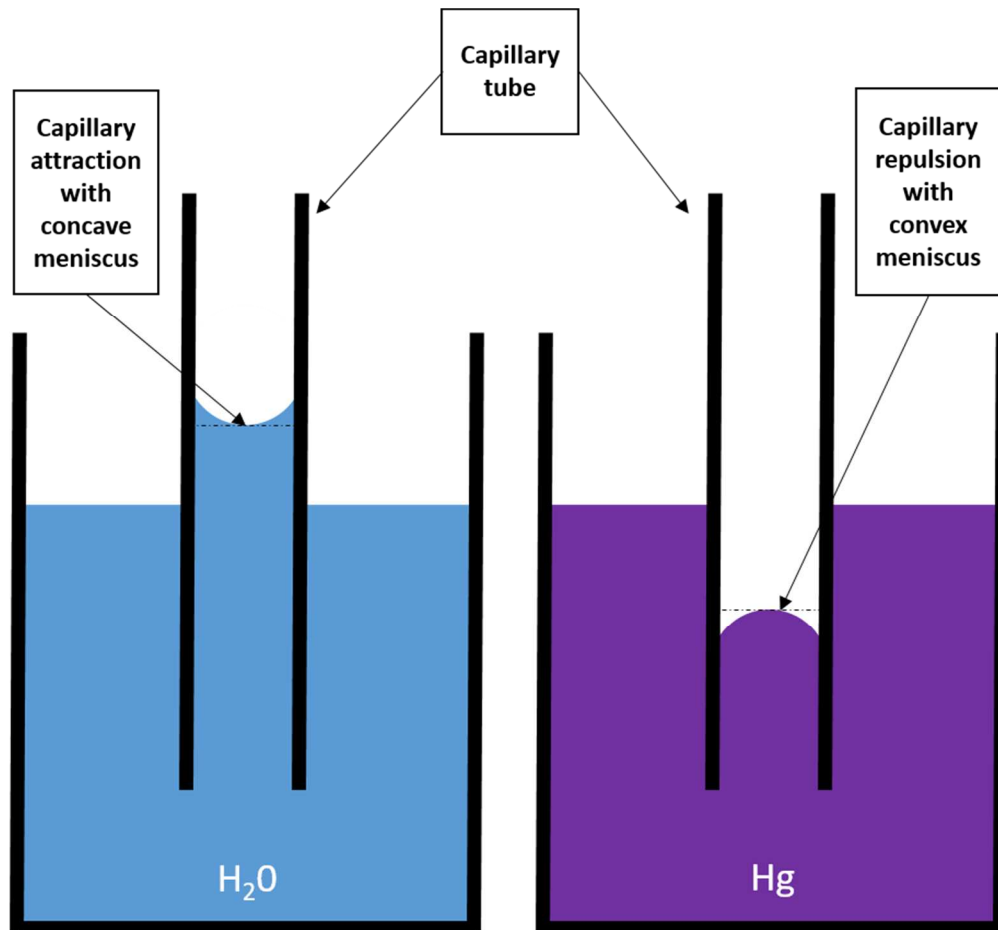


Figure 1.2: Graphical illustration of capillary action.

Left: Capillary attraction occurs between water and a glass capillary tube as the capillary forces are larger than the internal forces of the liquid. Right: Capillary repulsion occurs between the mercury and a glass capillary tube as the capillary forces are smaller than the internal forces of the liquid.

1.3 Laminar flow

Laminar flow is a non-turbulent fluid flow that will occur naturally in microfluidic systems. The fluid movement can be considered similar to multiple sheet-like segments of fluid, which travel in the same direction, without mixing occurring with adjacent layers. Laminar flow is related to fluid viscosity, where the viscosity of a fluid is the fluid's resistance to flow. Laminar flow is often described as non-turbulent streamline flow also. In laminar flow, parallel layers are referred to as the lamina. A case of laminar flow is demonstrated in Figure 1.3.

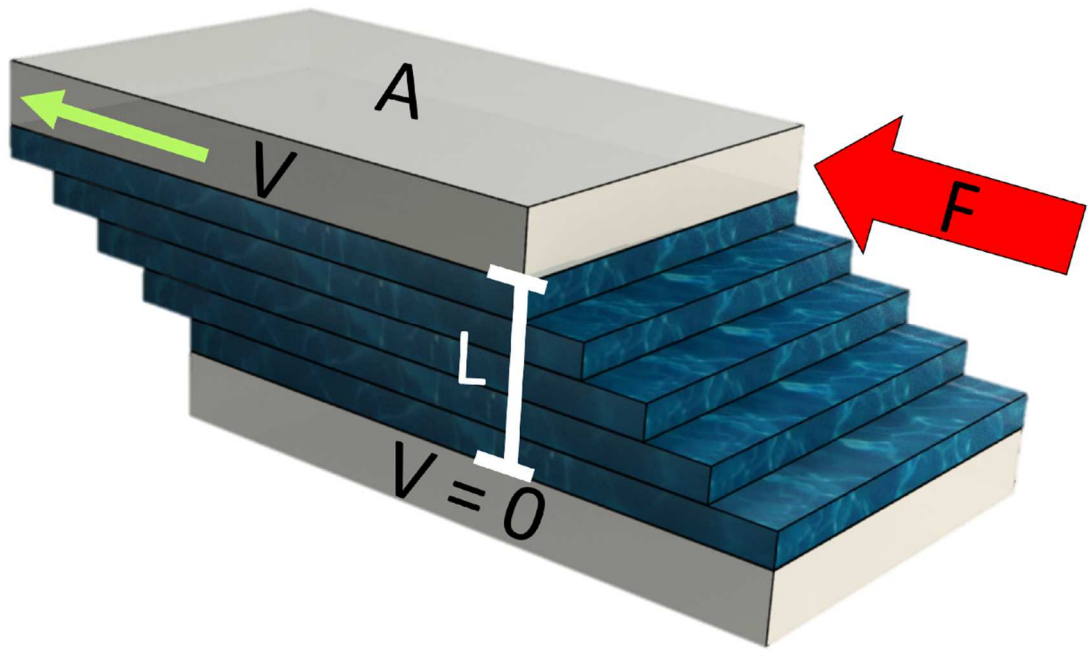


Figure 1.3: Graphical illustration of laminar flow.

The graphic demonstrates fluidic movement between a moving plate at velocity 'V' and stationary plate. With the top plate, of surface area 'A', undergoing a force (f), the fluid would resultantly divide into lamina. This is due to the fluid resisting against the flow of the above lamina.(3)

1.4 Navier–Stokes equation

Micro-fluids are considered to be incompressible due to the high surface to volume ratio.(4) The Navier–Stokes equation (Equation 1.3) is therefore applicable. The most basic scenario of the Navier-Stokes equation for uniform-viscous Newtonian fluids (when the viscous stresses of a fluid are proportional to the rate of change of the fluids deformation with respect to time), with no additional bodies in sedimentation, is given by:

Equation 1.3: The Navier–Stokes equation:

$$\rho \frac{d\vec{u}}{dt} = (-\rho)(\vec{u} \cdot \nabla \vec{u}) + (-\nabla p) + (\eta \nabla^2 \vec{u})$$

(Rate of change of momentum)

= (convective force) + (Pressure force) + (viscous force)

'u', 'ρ', 'η' and 'p' are the system flow velocity, fluid density, the fluid viscosity, and fluid pressure respectively.

This equation demonstrates that 'u', representing the flow velocity (m.s⁻¹) within the system, and 'ρ', 'η' and 'p', being the fluid density (kg.m⁻³), the fluid viscosity (Pa.s) and the fluid pressure (Pa) respectively, are all relatable. Viscosity of a fluid is also proportional to the fluids temperature. This is a factor that may also need to be considered during testing as results may be affected.

1.5 Poiseuille flow

Poiseuille flow is the case where a flowing, but non-accelerating, laminar and unidirectional fluidic motion occurs through a long cylindrical channel. It is described mathematically as Equation 1.4:

Equation 1.4: Basic Poiseuille flow

$$\nabla p = \eta \nabla^2 u$$

Where 'p' is pressure, 'η' = viscosity and 'u' = flow speed.

Equation 1.4 demonstrates the proportionality between the net pressure of the fluid and the net viscosity of the fluid. By applying a boundary condition and using geometric simplification (*by specifying that $u = 0$ at $r = R$, where $r =$ radius of the cylindrical channel, see Figure 1.4*), then the complete derivation of Poiseuille flow in the case of a pressure driven motion within a circular channel of radius 'R' (m) is given by:

Equation 1.5: Complex Poiseuille flow

$$u = \frac{R^2 - r^2}{4\eta} \cdot \left(-\frac{dp}{dx}\right) = u_{max} \left(1 - \frac{r^2}{R^2}\right)$$

where u_{max} is the maximum velocity: $\frac{R^2}{4\eta} \cdot \left(-\frac{dp}{dx}\right)$ at $r = 0$ (see Figure 1.4)

From Equation 1.5, it is evident that at the centre of the circular channel ($r=0$), the speed of the flow (u) will be at a maximum compared to the null value achieved at the channel walls ($r=R$), thus creating parabolic flow conditions (Figure 1.4).

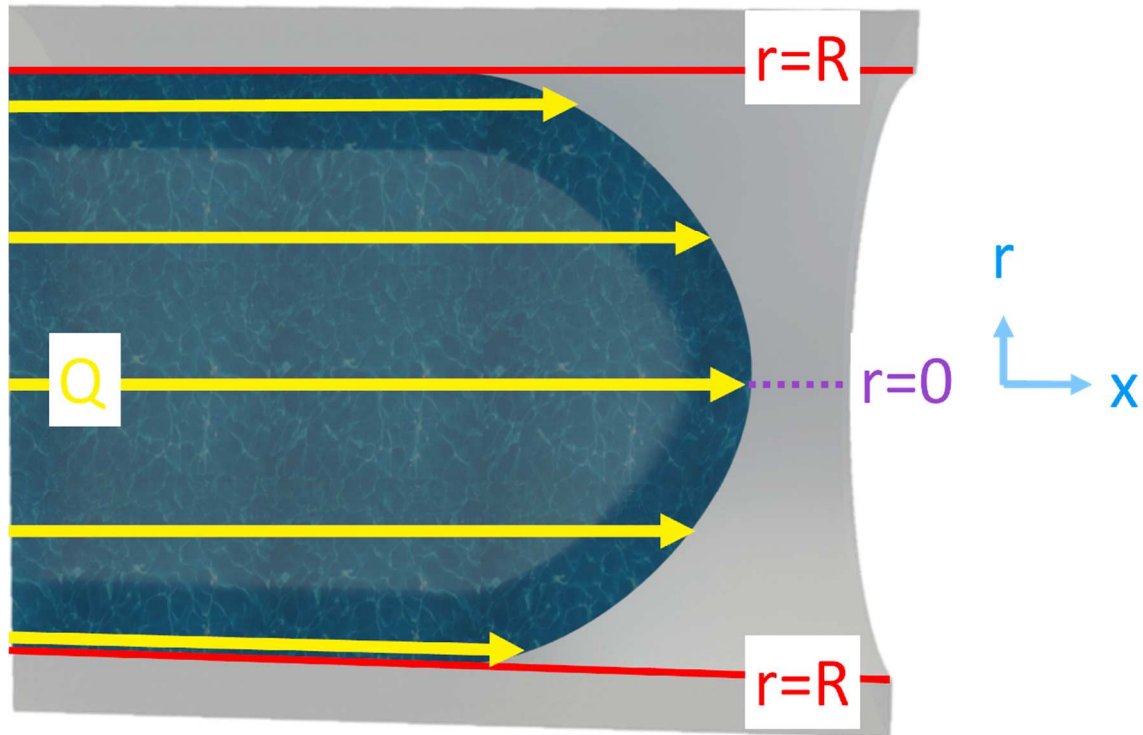


Figure 1.4: Graphical demonstration of Poiseuille flow.

A fluid flowing at a systematic rate of Q , in the direction of x , is the summation of the individual flow rates of the lamina flow rates. These individual lamina flow rates, which are proportional to the radial distance from the centre to the max distance R (at the boundaries), can be determined from complex Poiseuille flow (Equation 1.5).

1.6 Hagen–Poiseuille’s law

Hagen-Poiseuille law can be derived directly from Poiseuille flow (Equation 1.5) to determine the volumetric flow rate ($\text{m}^3 \cdot \text{s}^{-1}$). This scenario only applies where the channel used is both perfectly straight and infinitely long channel. To reach this derivation, integration of the Poiseuille flow (Equation 1.5), with respect to the flow speed of each the lamina with the fluid motion, is required. The degree of volumetric flow, in the case of the previously discussed of non-accelerating, pressure-driven fluid flow (Equation 1.6), through a circular chamber is given by:

Equation 1.6: Hagen-Poiseuille law

$$Q = \frac{\pi R^4}{8\eta} \cdot \left(-\frac{dp}{dx}\right)$$

Normalisation of (Equation 1.6) using the cross-sectional area will return the area-normalised flow velocity rate ($\text{m}\cdot\text{s}^{-1}$) (see Equation 1.7):

Equation 1.7: Normalized Hagen-Poiseuille law

$$U = \frac{Q}{\pi R^2} = \frac{R^2}{8\eta} \cdot \left(-\frac{dp}{dx}\right)$$

By using (Equation 1.7) for channel length 'L', certain conditions must be assumed. The first assumption that must be made is that the fluid is moving in a fully developed flow with the length of the channel 'L' being significantly greater than the circular channel radius 'R'. For this to hold true, then $(L/R) \gg 1$ and $(L/R) \gg \text{Re}$, where Re represents Reynolds number (see section 1.7), must be true. The assumption that must be made is that the pressure acclivity across the channel wall, in the case of pressure-driven microfluidic systems, is constant. This then allows suggestion that ' dp/dx ' is approximately equal to ' dp/dL '. Taking these assumptions into consideration, (Equation 1.8) resolves to the following:

Equation 1.8: Resolved Hagen-Poiseuille law

$$uQ = \frac{\pi R^4 \Delta p}{L}$$

With the overall system flow rate 'Q' determining direction of system flow (in such that a positive value is the equivalent of travel from the inlet to outlet). The hydraulic resistance (see section 1.8) can then be further derived from Equation 1.8.

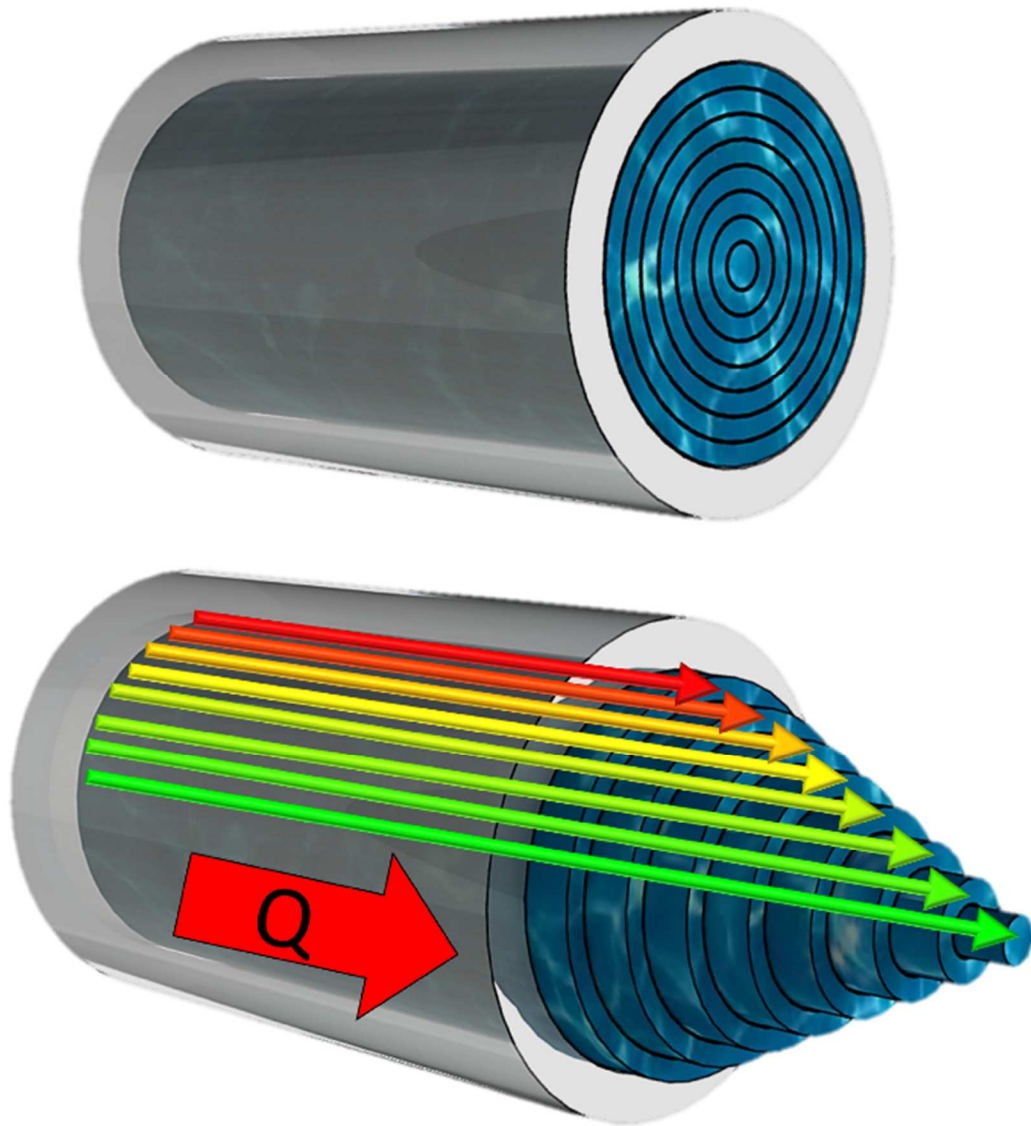


Figure 1.5: Graphical demonstration of Hagen-Poiseuille flow with the overall system flow rate 'Q'.

The top image illustrates the fluid moving in circular lamina, with the bottom image demonstrating the difference in flow speeds from the outer radius to the centre of the channel. This difference in speed is as a result of inter-lamina frictional forces, which are highest at the channel boundaries and lowest at channel centre.

1.7 Reynolds number

The Reynolds number (Re), mentioned in the previous section, is the standard measurement that determines the turbulence level of a fluid flow. It is defined as the quotient of the inertial and viscous forces (Equation 1.9). It has been determined that for flow in straight, smooth channels, that laminar flow exists at $Re < 2300$ with turbulent

flow occurring at $Re \geq 2300$.(5) The Re can be described in terms of characteristic length 'D' (m) and the velocity 'V' ($m.s^{-1}$) of flow. This may also be described in terms of the area-normalised velocity 'U' (Equation 1.7) and the hydraulic diameter (D_H). Resultantly, the Reynolds number is defined as:

Equation 1.9: The Reynolds Number

$$R_e = \frac{\text{(inertia force)}}{\text{(viscous force)}} = \frac{\rho V D}{\eta} \approx \frac{\rho U D_H}{\eta}$$

1.8 Hydraulic resistance

By modifying Equation 1.8 further, the simplified Hagen-Poiseuille law can be achieved:

Equation 1.10: Simplified Hagen-Poiseuille law

$$Q = \frac{\Delta p}{R_H}; \Delta p = Q R_H$$

Where the hydraulic resistance ' R_H ' ($Pa.s^3.m^{-1}$) being defined as:

Equation 1.11: Hydraulic resistance

$$R_H = \frac{8\eta L}{\pi R^4} \approx \frac{8\eta L}{\pi r_H^4}$$

As microfluidic channels are regularly designed to be of rectangular dimensions, particularly due to the difficulty with manufacturing circular channels, Equation 1.11 should be modified to be valid for non-circular channels also. This is achieved by exchanging the radius R with the hydraulic radius (r_H), or hydraulic diameter D_H , being twice the hydraulic radius ($2r_H$). The hydraulic radius (r_H) can then be defined in this scenario as $r_H = (2A/P)$, where 'A' represents the channel's cross-sectional area (m^2) and P is the wetted perimeter (m). This can also be formulated as:

Equation 1.12: Simplified Hydraulic resistance of a rectangular channel

$$r_H = \frac{w \cdot h}{w + h}$$

This resolves the formula in terms of channel dimensions (channel width 'w' and channel height 'h'). This computes a solution to within a 20% error approximation for a square

cross section.(6) Solving Poiseuille flow (Equation 1.4) in a rectangular channel is a computationally intense task as it normally determined through a Fourier series summation (7), and therefore the non-simplified hydraulic resistance can be given by:

Equation 1.13: Hydraulic resistance of a rectangular channel

$$R_H = \frac{12\eta L}{wh^3 \left(1 - \frac{h}{w} \left(\frac{192}{\pi^5} \sum_{n=1}^{\infty} \frac{1}{(2n-1)^5} \tanh h \left(\frac{(2n-1)\pi w}{2h} \right) \right) \right)}$$

Through combining (Equation 1.11, Equation 1.12 & Equation 1.13) and making the assumption that the aspect ratio is high in a microfluidic channel (where $R_H|_{n=1}$ is true at $\frac{h}{w} < 1$), Hagen–Poiseuille’s equation for a rectangle can be further generalized as:

Equation 1.14: Generalised Hagen–Poiseuille’s equation for a rectangle

$$\Delta p = QR_H ;$$

$$\Delta p = \frac{12\eta QL}{wh^3} \left[1 - \frac{192h}{w\pi^5} \tanh h \left(\frac{\pi w}{2h} \right) \right]^{-1}$$

From Equation 1.14, the following conclusions can be drawn:

- a) A Pressure change occurring within a channel will proportionally affect both the hydraulic resistance and the volumetric flow rate, especially since the volumetric flow is dependent on the variance of the pressure at both the channel inlet and outlet.(8)
- b) The Hydraulic resistance of the system is normally of constant value, as it is the by-product of the unvarying conditions of the fluid viscosity and cross-sectional area of the channel.
- c) The hydraulic resistance will be reciprocal to the channel length. Again, this is due to unchanging system conditions.

These conclusions forge the foundation of microfluidic manipulation and demonstrate that fluids can be controlled provided that the system has no unconsidered changes to either the pressure or fluid flow of the system.

1.9 Extra fluid movement considerations within a rotating system

When working with the Lab-on-a-disc (LOAD) platform, all the forces of the system must be considered carefully. A liquid travelling through a system with angular velocity will be exposed to the centrifugal force, the Euler force and the Coriolis force of the system (Figure 1.6).

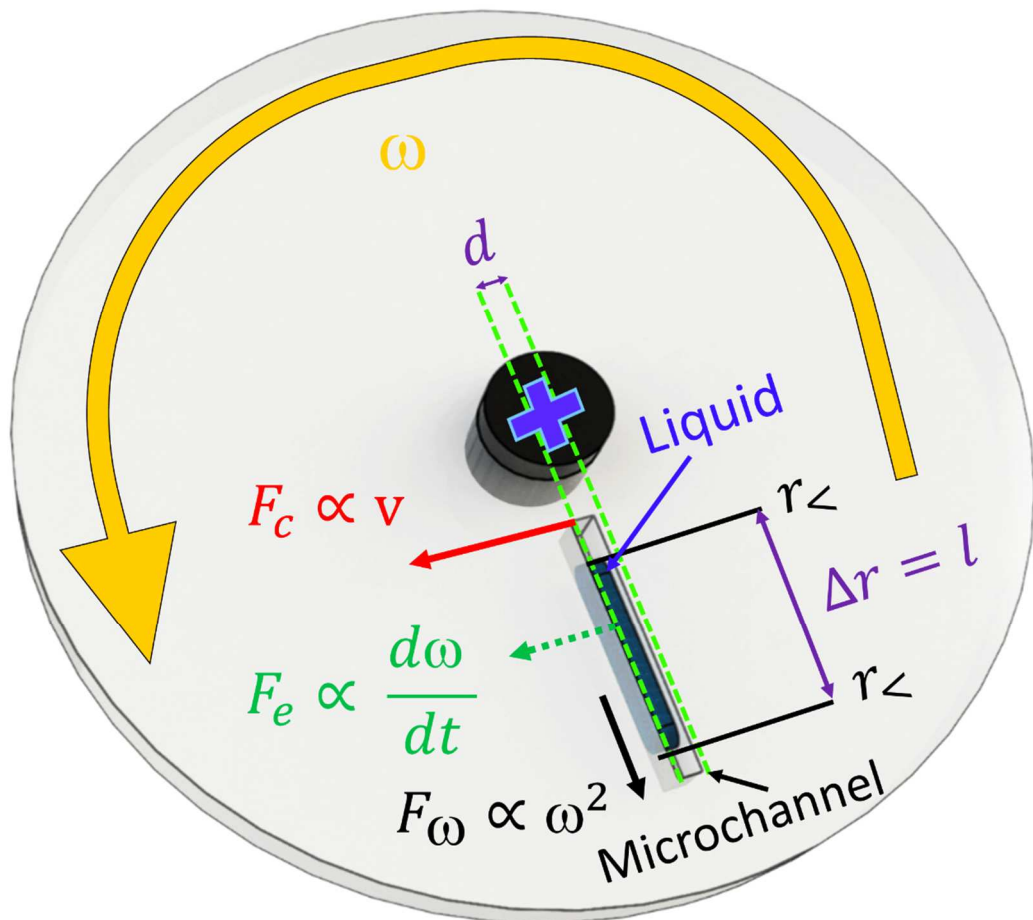


Figure 1.6: The forces operating on a rotating LOAD system.

A disk, with geometry extruding towards reader, rotating at an angular velocity ' ω '. Using the radial coordinates ' r ', the channel diameter ' d ', the absolute length ' l ' can be discussed in terms of radial positions ' $r_<$ and $r_>$ '. Liquid travelling from $r_<$ to $r_>$ will be affected by the centrifugal force (F_ω) (Equation 1.15), Euler force (F_e) (Equation 1.16) and the Coriolis force (F_c) (Equation 1.17) of the system. (9)

The centrifugal force is defined as a force which occurs due to the inertia of a body, which acts on a body that is travelling in a circular path, causing the body to move away from the radial centre of the circular path (Equation 1.15). (9)

Equation 1.15: The Centrifugal Force

$$f_{\omega} = \rho r \omega^2$$

Where ' f_{ω} ' represents the centrifugal force (N), ' ρ ' represents the density of the body (kg.m^{-3}), ' r ' represents the distance (m) from the centre of rotation and ' ω ' represents the angular velocity (rad.s^{-1}) of the system.

The Euler force is a pseudo-force which a body experiences due to Euler acceleration, which acts in a perpendicular direction with respect to centrifugal force and is within the plane of rotation.

Equation 1.16: The Euler force

$$f_e = \rho r \frac{d\omega}{dt}$$

Where ' f_e ' represents the Euler force (N), ' ρ ' represents the density of the body (kg.m^{-3}), ' r ' represents the distance (m) from the centre of rotation and $\frac{d\omega}{dt}$ represents the angular acceleration (rad.s^{-2}) of the system.

The Coriolis force is a force which an angularly moving body experiences, which acts perpendicular to the direction of motion and the axis of rotation.

Equation 1.17: The Coriolis force

$$f_c = 2\rho\omega v$$

Where ' f_c ' represents the Coriolis force (N), ' ρ ' represents the density of the body (kg.m^{-3}), ' v ' represents the velocity (m.s^{-1}) of the body in the plane and ' ω ' represents the angular velocity (rad.s^{-1}) of the system.

1.10 Particle sedimentation through a fluid within a rotating system

A particle present with the liquid will also experience these forces but will also be affected by the buoyancy and the Stokes drag forces, which counteract the sedimentation of the particle through the liquid. (10) This is most evident when the liquid is stationary in the system with particles moving through the system. The buoyancy force is an upward force that a fluid can exert on a body which opposes the weight of the immersed body. (10)

Equation 1.18: The buoyancy force

$$f_m = \Delta m r \omega^2$$

Where ' Δm ' represents the difference in mass between the bodies, ' r ' represents the distance from the centre of rotation and ' ω ' represents the angular velocity of the system.

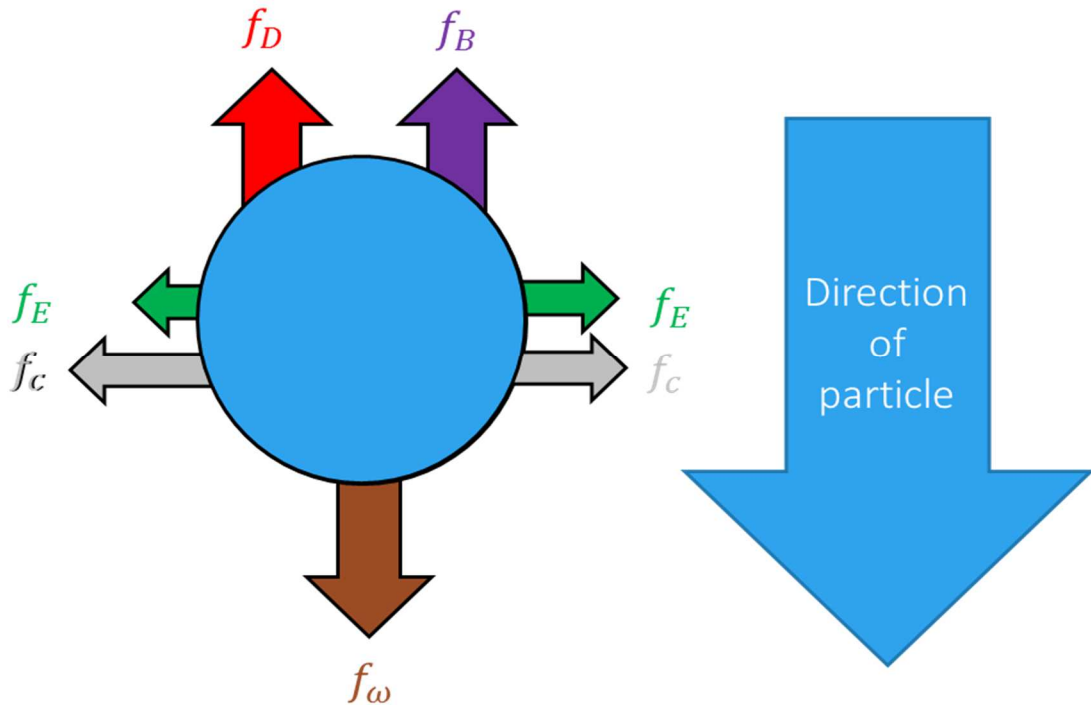


Figure 1.7: The forces acting on a centrifugally driven particle in a fluid.

The particle experiences a centrifugal force (f_ω) which is counteracted by the drag (f_d) and buoyancy (f_b) forces dependant on holding sample. It also experiences lateral forces in the form of Euler (f_E) and Coriolis forces (f_c), where by the direction of force vector is dependent on the direction of rotation.

The Stokes drag force is a force, by which a fluid can act on a body to the opposite direction of fluid flow (10).

Equation 1.19: The Stokes drag force

$$f_d = 6\pi\eta Rv$$

Where ' η ' represents the viscosity of the fluid, ' R ' represents the Radius of a spherical particle and ' v ' represents the velocity of the body in the plane.

These formulae are essential to understanding particle-fluid interaction within a rotating system.

1.11 References

1. Oh KW, Lee K, Ahn B, Furlani EP. Design of pressure-driven microfluidic networks using electric circuit analogy. *Lab a Chip - Miniaturisation Chem Biol* [Internet]. 2012 Feb 7 [cited 2013 Nov 7];12(3):515–45. Available from: <http://www.ncbi.nlm.nih.gov/pubmed/22179505>
2. Jens Ducreé, Peter Koltay RZ, Ducreé J, Koltay P, Zengerle R. *Microfluidics*. Springer; 2006.
3. OpenStax College. *Viscosity and Laminar Flow; Poiseuille's Law* [Internet]. Vol. 2013, College Physics. 2012. Available from: <http://cnx.org/content/m42209/latest/?collection=col11406/latest>
4. kirby BJ. *Micro-and nanoscale fluid mechanics*. Vol. 32. New York: Cambridge University Press; 2010.
5. Koo J, Kleinstreuer C. Liquid flow in microchannels: Experimental observations and computational analyses of microfluidics effects. *J Micromechanics Microengineering* [Internet]. 2003;13(5):568–79. Available from: <http://www.scopus.com/inward/record.url?eid=2-s2.0-0141830183&partnerID=40&md5=f62544e85caff1bd360bbb3aed0904a6>
6. Angelescu DE. Flow in a rectangular channel . In: *Highly integrated microfluidics design*. Artech House; 2011. p. 159.
7. Cornish RJ. Flow in a pipe of rectangular cross-section. *Proc R Soc London Ser A*. 1928;120(786):691–700.
8. Bao J-B, Jed Harrison D. Measurement of flow in microfluidic networks with micrometer-sized flow restrictors. *AIChE J* [Internet]. 2006;52(1):75–85. Available from: <http://dx.doi.org/10.1002/aic.10612>
9. Ducreé J, Haeberle S, Lutz S, Pausch S, Zengerle R, Stetten F Von, et al. The centrifugal microfluidic Bio-Disk platform. *J Micromechanics Microengineering* [Internet]. 2007 Jul 1 [cited 2013 Nov 7];17(7):S103–15. Available from: <http://dx.doi.org/10.1088/0960-1317/17/7/s07>

10. Burger R, Ducreé J. Handling and analysis of cells and bioparticles on centrifugal microfluidic platforms. *Expert Rev Mol Diagn* [Internet]. 2012 May;12(4):407–21. Available from: <http://www.ncbi.nlm.nih.gov/pubmed/22616705>

Chapter 2: Literature review: A review of centrifugal microfluidics in environmental monitoring

Chapter Foreword

The purpose of this chapter is to identify the current analytes of interest within the marine environment and how microfluidic platforms have been utilised to monitor these analytes within the required ranges of sensitivity, whilst also illustrating how these platforms can be adapted to detect additional analytes through minimal modification. Firstly, the reader will be presented with background information about microfluidics systems. This will include the origin of microfluidic technologies, currently used manufacturing methodologies and the Lab-on-a-Chip and Lab-on-a-Disc dissemination history. Secondly, a demonstration of how to design a centrifugal microfluidic platform for mimicking a specific bio-chemical based assay protocol is illustrated to the reader. This includes an assay-to-microfeature conversion process as well as illustrating the microfeature modifications necessary for tailoring to specific sample/reagent fluidic properties, such as viscosity. Thirdly, the reader is presented with an in-depth presentation on the current detection methodologies for monitoring key marine-based analytes of interest on both chip- and disc-based microfluidic platforms. This also covers a discussion on how different transducing elements can be transferred and implemented within centrifugal microfluidic platforms based on the sensitivity and selectivity required to detect a specific analyte. Finally, a brief insight into the author's predictions into the future trends of centrifugal microfluidics and how these enhancements will lead to more easily applicable and integrated microfluidic platforms, particularly for targeting autonomous, *in-situ* environmental monitoring.

Summary of the nature and extent of candidate's work present in this chapter:

First author, initiation, key ideas, manuscript development and writing up.

A review of centrifugal microfluidics in environmental monitoring

I. Maguire, R. O’Kennedy, J. Ducreé and F. Regan

The article was received on 15 Feb 2018, accepted on 12 Mar 2018, and first published on 13 Mar 2018.

Anal. Methods, 2018,10, 1497-1515 (DOI:10.1039/C8AY00361K)

2.1 Abstract

There is currently a gap in the use of centrifugal microfluidics in the field of environmental sensing. This review provides theoretical perspectives that have been demonstrated for applications in other domains and recommends adaptations for environmental sensing. Current approaches of centrifugal systems reported are primarily in the area of biosensing and electrochemical detection. In the case of current environmental monitoring devices discussed, a conversion process for developing centrifugal microfluidic platforms around currently reported transduction methods will be presented, covering design and manufacturing elements required for successful platforms. While the success of these reported systems is not in question, there is more to be done in advancing both automation, sample-to-detector interaction, simplification for the end user and portability, to facilitate long term deployable or in situ based environmental monitoring. Also included for discussion, are devices that have demonstrated the capability of sample processing and reagent mixing, as well as high-sensitivity sample characterisation with a number of varying detection techniques through transducer substitution. While in some cases, necessary sample preparation currently involves off-chip steps (such as cell lysis), others have incorporated these steps within the microfluidic platform, therefore through combinations of reported sample handling and detection strategies, more refined and flexible environmental monitoring tools can be achieved on a single platform using centrifugal microfluidics. Also considered will be the cost-effectiveness of the microfluidic platforms with current multi-use limitations. In the absence of suitable centrifugal microfluidic sensors,

alternative chip-based systems, with significant relevance to environmental applications and which could be easily adapted to a centrifugal platform, are suggested. The primary technical challenge of this report is to demonstrate how these current centrifugal sensing systems could offer huge potential in the environmental sensing field, with minimal systematic modification, but a myriad of applications.

2.2 Introduction to microfluidics platforms

Microfluidic systems operate using micro-scale concepts and technologies to develop micro-platforms which are aimed at controlling and manipulating fluidic samples. Within this, fluidic sample handling holds the key to miniaturising full laboratories onto a single microfluidic platform, or Lab-On-A-Chip (LOC).(1) The volumes of fluidic samples often range from as large as nano-litres (10^{-9}) to as small as atto-litres (10^{-18}). A fluidic input in this range is highly favourable. With a reduced input sample size, there is a corresponding reduction in reagent consumption and required detection time. This range also increases the systematic detection resolution and sensitivity, whilst also lowering the material quantity required to conduct an experiment. All of these virtues collectively decrease the overall cost of microfluidic system advancement, and their associated development carbon footprint.(2)

The origin of microfluidics was due to the requirement for a versatile and highly sought-after technology which became resultant bi-product of a number of fields; molecular biology and analysis, bio-defence and microelectronics.(3) In the 1980s, the evolution of genomics accelerated significantly. New analytical methods were therefore required to allow better sample processing abilities, such as wider range of detectability with greater sensitivity. Other micro-analytical methods at the time, which were based around laser optical detection, were also under development, high-performance liquid chromatography (HPLC)(4), capillary electrophoresis (CE)(5) and gas chromatography (GC)(6). These methods were hugely important for genomics because the methods can deliver the required resolution and sensitivity for low sample injection volumes. Investigation was then focused into developing new technologies capable of enhancing

the performance of these micro-analytical methods for the field of genomics. This was the initial step in the development of microfluidics technologies.

After the cold war, bio-chemical terrorism became a clear threat in the future. Therefore, in the 1990s, technology to detect a bio-chemical threat in in-field scenarios was investigated. Thus, there was significant developments in microfluidic systems. This research was carried out by the 'Defense Advanced Research Projects Agency' (DARPA) through the support of the US Department of Defence. (7–9)

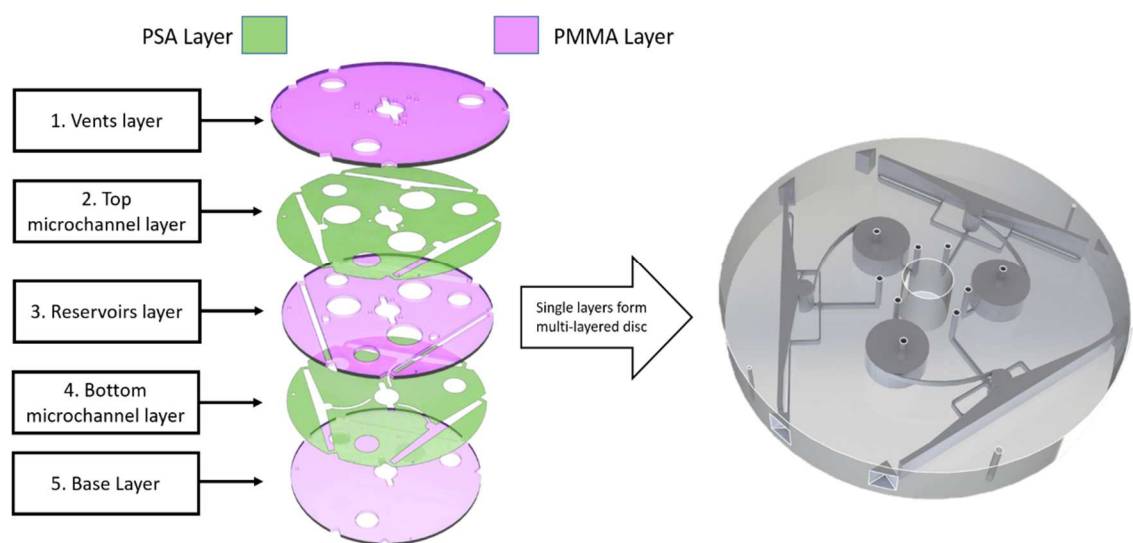


Figure 2.1: Manufacturing a NP-based centrifugal microfluidic platform.

Illustrated here is PhosphaSense platform, which comprises of multiple PMMA and PSA alternating layers (10) (Image is authors own)

Microelectromechanical systems (MEMS), which are primarily silicon-based microelectronics, became highly successful (11). This was due to the development of microfabrication technologies, such as photolithography (12–14), as well as the development of other manufacturing technologies including xurographic and laser cutting systems (15–17). These technologies were found to be also applicable in the advancing field of microfluidics. While there are a variety of approaches for producing centrifugal microfluidic platforms, only two production methods here will be presented:

- A non-photolithography(15–17) (NP) method, achieved through assembling consecutive layers of poly(methyl methacrylate) (PMMA) and adhesive polyethylene terephthalate (PET)(Figure 2.1), also previously reported for centrifugal microfluidics environmental applications (10,18).
- A photolithography(12–14) (P) method, by where exposed photoresist can be used to create microstructures on a silicon wafer (Figure 2.2), upon which polymer-based materials, such as polydimethylsiloxane (PDMS), is poured to form a mould.

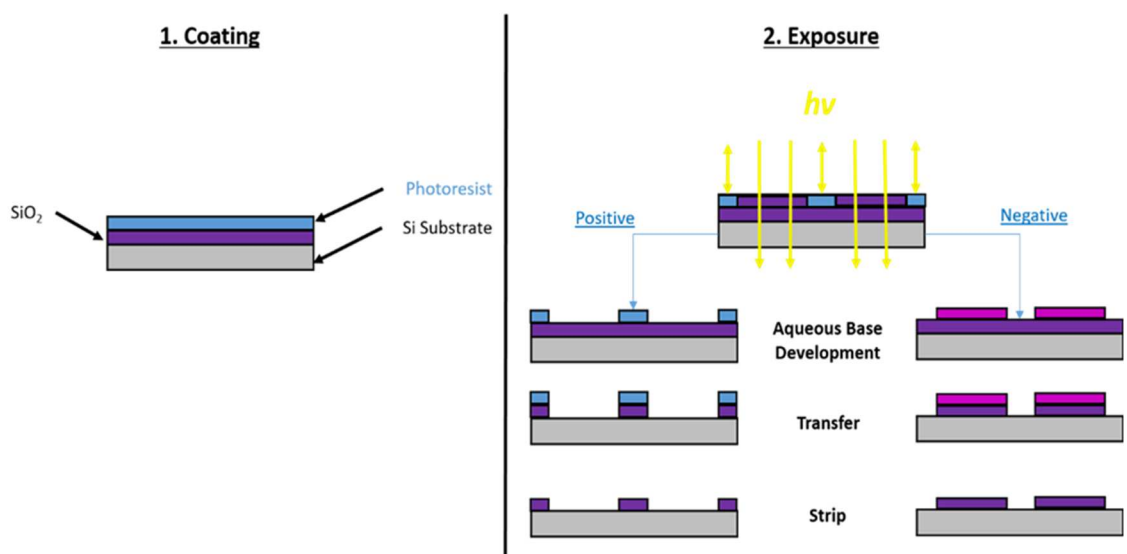


Figure 2.2: The Photolithography process used in constructing P-based platforms.

This process is used to construct a master construct of the design, on which, PDMS solution is poured to form a mould. (Image is authors own)

Both platforms have different strengths and weaknesses without comparing the actual materials themselves; a comparative list can be seen in Table 1. While P-based platforms can achieve significantly higher resolution in comparison to NP-based platforms, it comes at the cost of poor manufacturing time. However, required system resolution is usually the deciding factor on which platform was selected. Another important consideration was NP-based platforms could be easily constructed into multilayer-

varying discs, whereas P-based platforms rarely contain above 2 layers due to the associated photomask alignment difficulties.

Benefits of platform	NP Method	P Method
Min resolution	500 μm	1 μm
Cost per disc	+++	++
Manufacturing time	+++	+
Equipment for manufacturing cost	++	+++

Table 1: Comparative table of the benefits between PMMA- and PDMS- based platforms.

Microfluidic devices operate primarily through two platforms; the Lab-On-A-Chip (LOC) platform (Figure 2.3.Left), which uses pumping forces to drive the sample progression, and the Lab-On-A-Disc (LOAD) platform (Figure 2.3.Right), which uses centrifugal forces as the primary driving force in the system. As LOC platforms have a number of comprehensive review articles to date, as evident by Figure 2.4, also some of specifically relevant review also provided (19–21), thus LOC platforms will mostly fall outside the scope of this review. Both platforms are constructed from most materials, with Poly (methyl methacrylate) (PMMA) with adhesive PET and/or Polydimethylsiloxane (PDMS) often used. The LOC (Figure 2.3.Left) utilises an external pumping mechanism as a driving force for each chip. The LOAD (Figure 2.3.Right) platform does not have this requirement. This is therefore can be an advantage due to ease of use from an end used experience. However it is important to note that as LOAD platforms can often designed to be for single use scenarios (22), in contrast to LOC platforms which can be used for long-term deployment of without replacement (23).

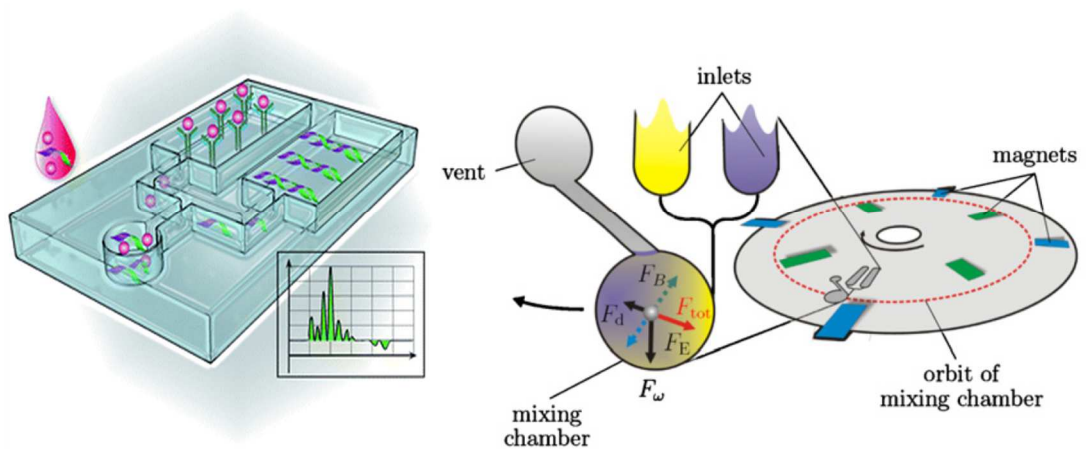


Figure 2.3: Lab-On-A-Chip (LOC)(left) and Lab-On-A-Disc(LOAD)(right) platforms.

Left) This Concept (24) demonstrates how LOC platforms are capable of multiplex analysis of complex biological samples. Right) This illustration (25) demonstrates a mixing chamber on the LOAD platform. The samples are loaded into the inlets and the LOAD is the spun. The centrifugal force $f(\omega)$ is applied to the system, where ω is the angular rotation of the system. Also, resultantly applied are the Coriolis force $f(c)$ and drag force of sample $f(d)$ which all aid in the mixing of samples as required.

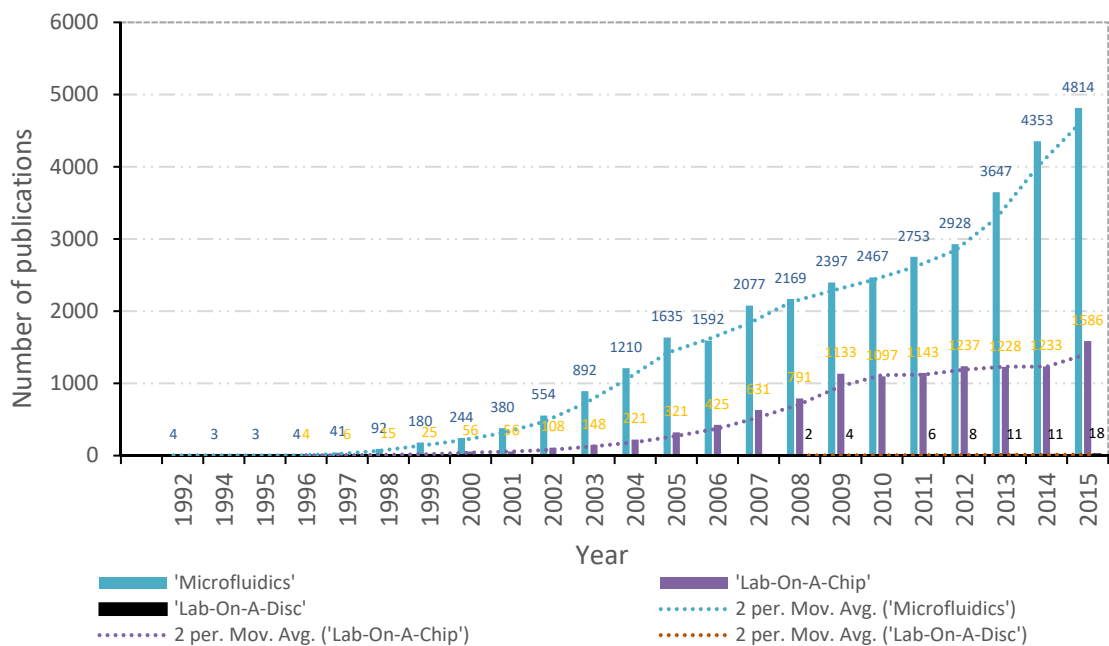


Figure 2.4: Keyword publications trends per annum with respect to microfluidic research.

This included Lab-On-A-Chip and Lab-On-A-Disc platforms, according to Clarivate Analytics' 'Web of Science' (26).

The inlet of the LOAD can have a sample injected directly into the system. The LOAD is then rotated, allowing the sample to be driven through the system by the generated centrifugal force. Another advantage of working with LOAD systems is that multiple testing mechanisms can be incorporated onto one single disc. This can mean samples can either be tested multiple times on a single disc, with the exact testing condition in each chamber, or multiple analytes can be detected simultaneously (27–30). This provides more statistically accurate and repeatable data.

When designing LOAD systems, there are three primary design criteria to be considered:

- Laminar flow;
- Micro-architectural design for sample manipulation and;
- Micro-architectural design for air manipulation.

➤ **Laminar flow will occur naturally**

Due to the flow of such small samples, laminar flow will occur. Laminar flow is a non-turbulent fluid flow, where the fluid(s) appears to travel in sectional parallel layers, known as lamina, with no apparent mixing occurring between layers. (21) However, laminar flow may be an undesirable feature as it can prevent sample-reagent mixing. Thus, turbulent flow can be introduced through the integration of micro-architectural features, such as micro-pillars, to allow sample mixing to occur as required.(31)

➤ **Micro-architectural design for sample manipulation**

In order to conduct laboratory experiments accurately on chip, the sample must be manipulated and controlled to follow a strict and exact experimental protocol or ‘assay’. To follow an assay protocol, either physically, biologically or chemically-based, will require the addition of micro-architectural structures for example; microchannels for sample progression, reservoirs for sample modifications (such as reagent introduction),

among others. Stone et al.(21) demonstrate a number of micro-architectural features to convert a microfluidic chip to the more desired LOC platform.

➤ **Micro-architectural design for air manipulation**

The interactions between sample and pre-occupied air become significantly more complex due to both fluids being on the micro-scale.(25,32) This means that the previous forces acting on both fluids, including buoyancy force and surface tension, change significantly with comparison to the macro-scale.(33) Quite often, the surface tension can be significantly stronger than the buoyancy force, due to the high surface to volume ratio of the fluid, which prevents the pre-occupied air from escaping directly through the sample. This means that an air ventilation system must be considered to prevent air-locking within microfluidic systems as this can disrupt or even halt assay progression. Alternatively, the air ventilation system can also be designed intentionally to halt sample progression (34). Whereby, if the assay requires a wait period, indirect control of the sample can be achieved by direct control of locked air discharge. These three elements, when optimised, allow accurate and controlled fluidic sample handling, inclusive of complex samples containing particle-like components.

2.3 Development of centrifugal microfluidics for environmental monitoring

The ideal environmental monitoring tools are expected to be: capable of autonomous deployment; robust and capable of providing quantitative and qualitative measurements. The requirement for autonomous and/or handheld sensors is essential in gaining temporal/timely and qualitative understanding of key environmental locations. This can include four core environments; Air (indoor and outdoor air quality, etc.), land (agriculture, residential/corporate impact, etc), life (ecology, anthropogeny, etc) and water (drinking/leisure water sources, wastewater treatment, etc). Within these core environments, where crossover between the core environments is also possible, there is also a variety of potential analytes which can be environmentally

relevant. In order to develop a centrifugal microfluidic platform for environmental monitoring, a number of considerations must be determined; sample/reagent type/size, analyte characteristics, sample matrix, assay protocols, transduction method, targeted for autonomous/handheld platform, single or multiuse. In this section, a presentation of how some of these considerations are used in manufacturing new or modifying previous adaptations of centrifugal microfluidic platforms for environmental monitoring. This specifically includes the design strategies considered in developing a LOAD platform which emphasis on selecting a transducing element.

2.4 Environmental assay integration on a centrifugal microfluidic platform

To determine the optimal approach, a complete breakdown of what laboratory steps required to perform the environmental assay are included in the design. This includes the specific duties which would be performed on the microfluidic platform. An example of a biological assay is demonstrated in Figure 2.5 for toxin detection on a LOAD platform. This Figure 2.5 demonstrates the required assay protocol associated for a fluorescence-based, inverse-assay toxin detection platform. This case illustrates the range of both external inputs and expected outcomes, performed for specific periods of time by the microfluidic platform. From this, along with further information about the sample (volume, contents, viscosity and surface tension), the required microfluidic platform was selected, with fluorescence detection selected for measurement within the range of the WHO regulation limit.

In the example of Figure 2.5, consider a sample input of 50 μL of sea water containing targeted, pre-lysed Microcystin-LR toxin. In this case, the platform does not require high resolution microstructures ($< 500 \mu\text{m}$), therefore NP method would be the preferred method for producing this platform. Further considering of the adaptation of the assay protocol found in Figure 2.5 into a microfluidic platform, adequate sample/reagent/complex-sized reservoirs with liquid-transfer and air-ventilation microchannel should be designed as required to complete the assay. As the sample liquid would then be expected to be passed to each succeeding functionalised reservoir

for assay completion (i.e. fluorescent-antibody coating, priming of capture antigen on test and control reservoirs, etc.), consideration of the sample-transfer microchannels would then be considered.

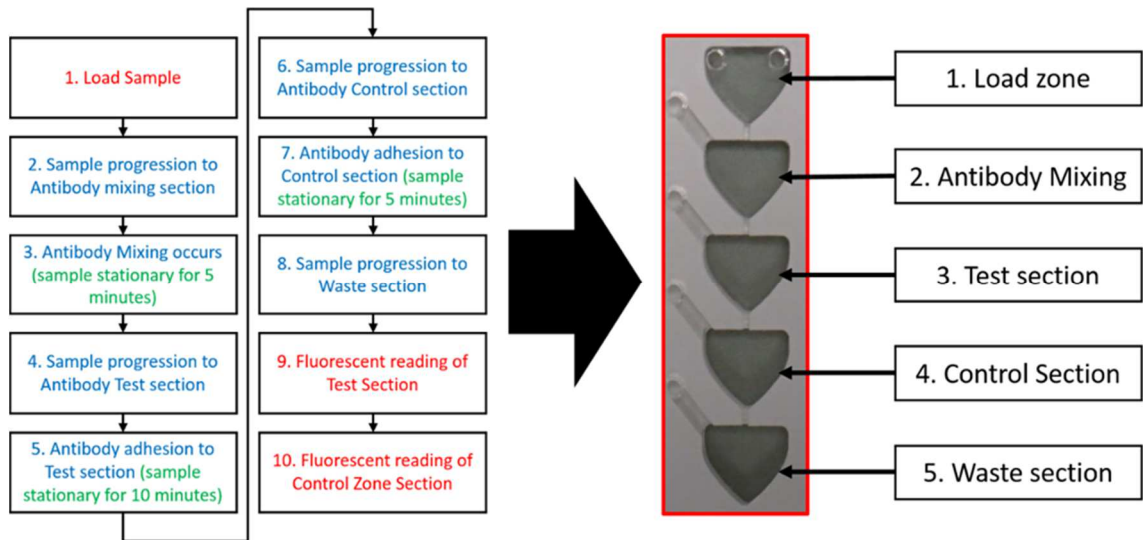


Figure 2.5: A graphical breakdown of assay protocol conversion to microfluidic features.

This illustrates the example of a toxin detection assay protocol, with the required external interactions, duties expected to be performed by the microfluidic platform (for chosen length of period), and how it can be converted to microfluidic features such as reservoirs and microchannels. (Image is authors own)

While the dimensions of the microchannels often are not critically important once a standard microfluidic channel dimension is observed, they potentially can be, as then sample attributes may need to be taken into consideration. While centrifugal forces are viewed as the primary driving forces of the reagents on disc, significantly large rotational speeds would be required for sample progression if they were the only acting forces available for liquid manipulation. Instead, the system usually minimises the microchannel cross-sectional area in order to offer ‘assisting and desisting’ capillary action forces, which complements the centrifugal forces generated, thus allow reagent actuation with greater ease. Liquids, upon meeting microchannels which have low cross-sectional areas with respect to length ($\mu\text{m}:\text{mm}$), experience capillary action. The capillary action magnitude and direction of flow is dependent on the ratio of molecular cohesion force within the reagent, and the adhesion energy between the reagent and

containing surface. Thus, if the flow speed of the sample within microchannel was important, then refining the optimum channel width and thickness would be required. However, this is often not the case and aqueous solutions were able to easily travel through microchannels, with a standard thickness of $< 200 \mu\text{m}$ and $500\text{-}700 \mu\text{m}$ channel widths, at relatively low rotational speeds (8-15 Hz). In comparison, it can be expected that for channel widths $>1 \text{ mm}$, aqueous solutions may require rotational speeds of $\geq 20 \text{ Hz}$ in order to compensate for a reduced capillary action within microchannels of a LOAD platform.

After determining the optimum microchannel dimensions and reservoir locations, the next consideration was to set the opening of the microchannel at the lowest tangential point of each reservoir, with regards to the radial centrifugal force. This was often achieved by filleting the reservoir shape to remove corners. This approach is taken to minimise any potential sample loss throughout the microfluidic platform, as shown in Figure 2.6. Another important aspect that should be considered was reservoir shape for reagent loading and storage.

Depending on the characteristics of the liquid, for example liquid viscosity, coarser reservoir shapes may also be required in order to reduce the liquid-surface attractions, as demonstrated by Duffy et al. (18). In this example (18), reservoir shape characterisation is demonstrated in Figure 2.6, where the loading of water (72.75 mN/m surface tension @ 20°C)(35) with a viscosity of $0.89 \text{ mPa}\cdot\text{s}$ into a circular reservoir (Figure 2.6.Circle) was successful, whereas loading methanol (22.95 mN/m surface tension @ 20°C)(35) with a viscosity of $0.543 \text{ mPa}\cdot\text{s}$ into the same reservoir shape resulted in an approximate 50% sample injection reduction. To counteract this, a coarser reservoir shape, shown in Figure 2.6.Shield, was also tested. It was expected that the perimeter wall wettability would be reduced as the wall shape became coarser (36), which proved to be the case (Figure 2.6.Graph).

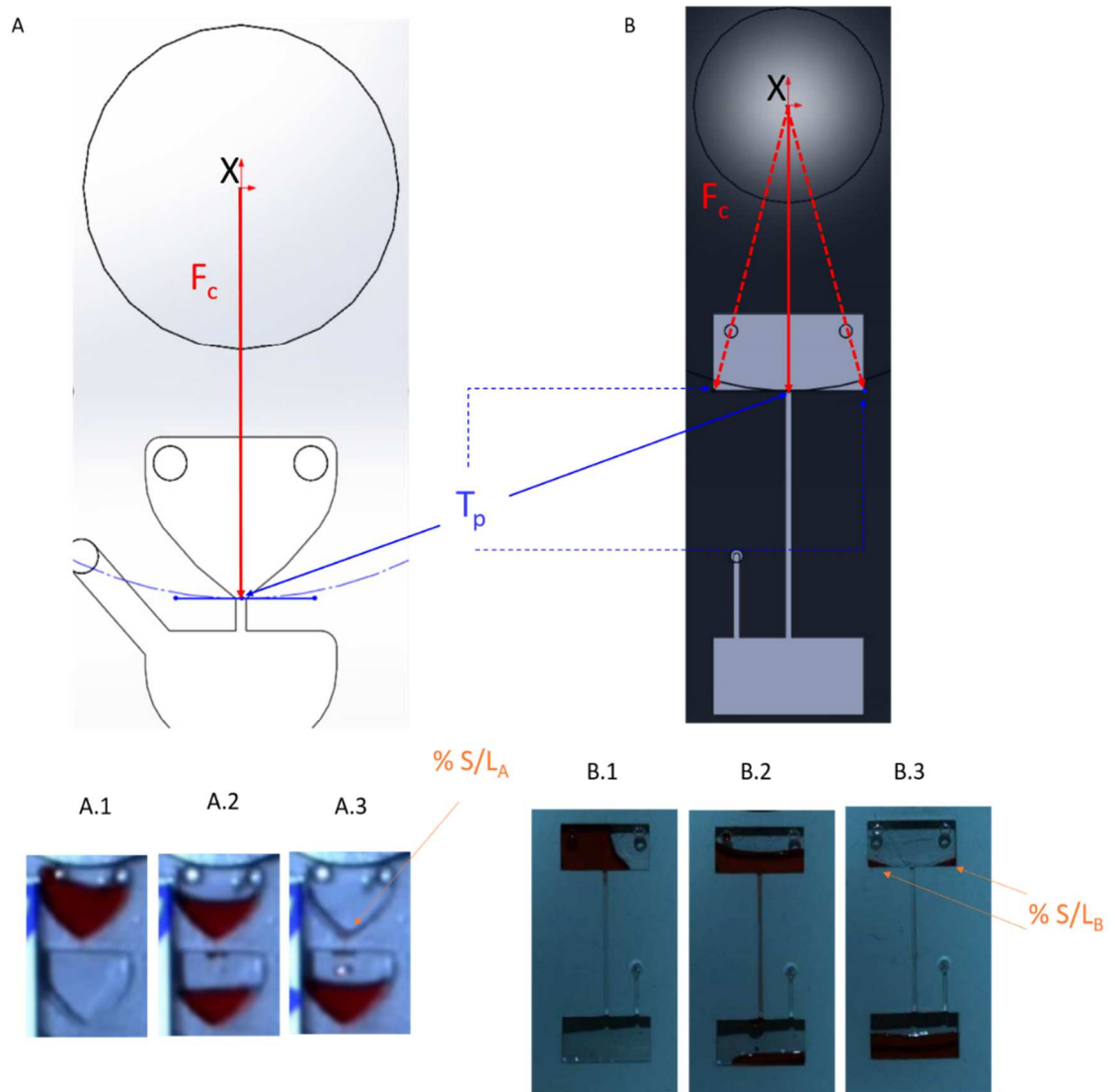


Figure 2.6: Designing reservoirs to avoid sample loss.

A) This illustration demonstrates the correct reservoir solution, by where the end of the reservoir is the lowest tangential point (T_p) with respect to the centrifugal force (F_c). A.1-3) confirms that sample loss (S/L_A) is minimal during sample progression. B) In contrast to A, this reservoir has tangential points which have a larger radial distance than the microfluidic channel's tangential point. B.1-3) confirms that sample loss (S/L_B) is occurring during sample progression. (Image is authors own)

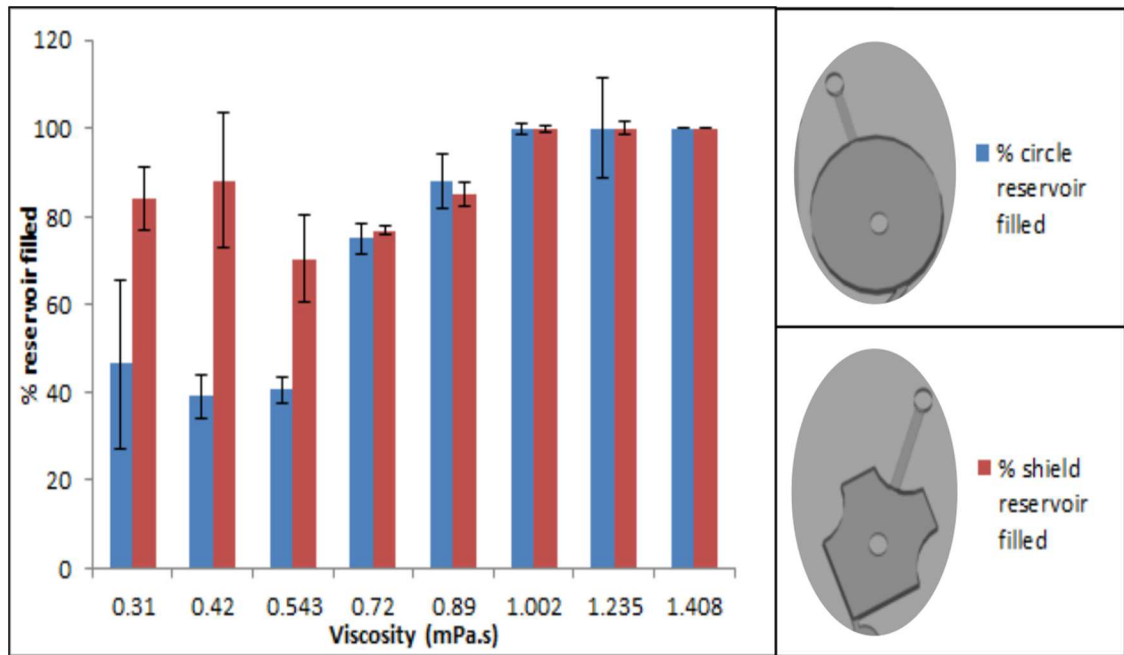


Figure 2.7: Percentage of reservoir filled before sample leakage occurs vs liquid viscosity.

This figure illustrates the how reservoir shape can impact the load-ability of a sample. The circular design has a uniform perimeter wall in comparison the more random and non-spherical ‘shield’ design. It is speculated that the circular reservoir fills too quickly, due to the wettability attraction between the sample and perimeter wall at low liquid viscosities, which can lead to air trapping and reduction in maximum liquid input. In the case of the shield, the wettability of the coarse perimeter wall is less, (36) therefore reducing the shear force acting on the liquid caused by wettability attraction, leading to a reduction in air trapping, and thus increasing sample load volume. The liquid viscosities were formed using combinations of acetone, glycerol, methanol and water at 25 °C. (Image based on Duffy et al. (36))

2.5 Detection strategies on centrifugal microfluidic platforms for environmental assay integration

There are a number of microfluidic detection strategies currently employed in the fields of biosensing (25) and electrochemical sensing (37), but there is a significant gap with regard to LOAD applications for environmental monitoring using these transducing strategies. In an effort to determine the significance of this gap, a table produced by Rodriguez-Mozaz. et al (38) for identifying environmental applications for LOC platforms, was modified to include LOAD microfluidics platforms as shown in Table 2.

Table 2 is a summary of the reported developments including the transduction element, for detection of the relevant environmental compounds and parameters, against known integrations of detection on LOAD platforms, or lab-on-a-chip (LOC) platforms if none. It is quite clear from Table 2 that if centrifugal microfluidic platforms are to be used in environmental monitoring, significantly more study is required. The key in developing such a multi-analyte environmental monitor lies within the integration and adaptation of new and current transduction elements on LOAD platforms.

As analytes levels in the environment are often in trace quantities, a low limit of detection (LOD) is required by the transducing element. Typically, a pre-concentration step would be required in order to move the analyte detection within a suitably sensitive linear range of the transducing element. If a pre-concentration step is required, it has been previously demonstrated that the pre-concentration step can be integrated within the LOAD by using silica-based gel column on a LOAD platform (39), with similar gel products found to be successful for LOC platforms also (40). Alternatively, a pre-concentration step could also be carried out prior to sample injection at a cost of reduced simplicity.

The value of the platform is assessed based on its analytical performance e.g. linear dynamic detection range and sensitivity. Therefore, the LOAD system is designed to meet current legislation (WHO, WFD etc.). Table 2 can be used to compare current detection capabilities of specific detection approaches on a microfluidic system for environmental application.

2.5.1 Acoustic transducers

2.5.1.1 *Surface acoustic wave (SAW)*

Acoustic waves have been demonstrated as suitable transducing elements for a myriad of applications, with one of the more prominent configurations being the surface acoustic wave (SAW) format (41–44). SAW-based sensors operate on the premise that a pair of piezoelectric (Pe) constructs, where the primary Pe generates acoustic waves while the secondary Pe records acoustic wave outputs through a connecting biosensor-enabled waveguide. Analyte interactions between the waveguide and sample can then distort the translating acoustic wave, where a change in total mass on the biosensor results in a shift of the wave's phase. Information about the 'capture' and 'release' rates, as well as the stoichiometry of the interaction, can be extrapolated from this phase shift. In some cases (42,45,46), antibody biosensor technology was combined with SAW-based sensors for the determination of the analytes-of-interest presence, analysis of the acoustic wave response due to competitive binding. Conformation of the molecules can also be derived from variation in the amplitude of the acoustic wave, whereby a dampening of the acoustic wave occurs with increased flexibility of the target molecule through interaction with the sample. Two examples of SAW-based sensors used on microfluidic devices are illustrated in Figure 2.8. A chip-based (Left) design and centrifugal cartridge-based (Right) platform are demonstrated. The chip-based platform(42) utilises a Al-SiO₂ interdigitated transducer (IDT) SAW platform for the detection of *Escherichia coli* with a reported limit of detection of 1.8×10^{-15} M. The centrifugal cartridge-based platform(45) demonstrates a dual IDTs Al-SiO₂ SAW platform with separate working and reference sensor pairing, achieving a 6.7 pg.mL^{-1} limit of detection.

Table 2: Current environmentally-aimed transducing elements with corresponding environmental analytes of interest.

Transducing element	Compounds or parameters	Bio-recognition element	Features	Reference (s)	Relevant LOAD reference	Relevant LOC reference
Acoustic (surface acoustic wave) (SAW)		Antibodies	LOD = 6.7 pg/mL	-	[2]	
	Salmonella Typhimurium	Antibodies	100 cells/mL	[3]	-	[4], [5]
	Escherichia Coli	Antibodies	LOD = 1.8×10^{-15} M	[6]	-	[4], [5]
Electrochemical (amperometric)	C-reactive protein (CRP)	Antibodies	LOD = 4.9 pg/mL	-	[7]–[9]	
	Inorganic phosphate	Enzymatic (trienzymatic configuration)	LOD: 0.57 mg/L	[10]	-	[11]
	EDCs	Enzymatic (Tyrosinase)	-	[12]	-	[13]–[15]
	Alkylphenols and their ethoxylates	Antibodies	LOD: $\mu\text{g/L}$ range	[16]	-	-
	Nonylphenol	Antibodies	LOD: 10 $\mu\text{g/L}$ range	[17]	-	[13]
	Pesticides (Carbofuran and/or Paraoxon)	Enzyme (AChE)	Discrimination between different AChE inhibitors by neuronal networks LOD: 0.2 $\mu\text{g/L}$	[18]	-	-
	BOD	Multispecies culture	Minimum measurable BOD=0.088 mg/L O ₂ ; (biosensor BOD/BOD ₅) ratio=0.80	[19]	-	[20]
	Organophosphorus compounds	Enzyme (organophosphorus hydrolase)	Modified carbon nanotube	[21]	-	[22]
	Phenols	Enzymatic (cellobiose dehydrogenase and quinoprotein dependent glucose dehydrogenase)	In-field measurements LOD: 0.8 $\mu\text{g/L}$	[23]	-	[24]
	Surfactants	Pseudomonas and Achromobacter (plasmid for anionic surfactant degradation)	LOD: 0.25 mg/L (SDS)	[25], [26]	-	[27]
	Oxygen reduction reaction (ORR)	-	micro-electrochemical Chip	-	-	[28]

Table 2: (Cont.) Current environmentally-aimed transducing elements with corresponding environmental analytes of interest.

Transducing element	Compounds or parameters	Bio-recognition element	Features	Reference (s)	Relevant LOAD reference	Relevant LOC reference
	LAS	Trichosporon cutaneum (LAS-degrading bacteria)	In-situ measurement LOD: 0.2 mg/L	[29]	-	-
Electrochemical (chrono-potentiometric)	Electrolytes	-	Gold sensing micro-electrodes; Cation exchange membrane (CEM)	-	-	[30]
	Chlamydia trachomatis (DNA)	DNA (hybridisation)	Previous PCR amplification LOD: 0.2 mg/L	[31]	-	[32]
	Daunomycin PCBs, Aflatoxin	DNA	LOD: 0.3 mg/L, LOD: 0.2 mg/L, LOD: 10 mg/L	[31], [33]	-	[32]
Electrochemical (potentiometric)	Nitrate ion	NO ₃ - ion-selective membrane	NO ₃ - ion recovery: 97-105%	-	-	[34]
	Escherichia Coli	Antibodies	10 cells/mL	[35]	-	[36]
Electrochemical, optical and mass signal (combination)	-	-	-	-	-	-
	Cadmium, copper and mercury	Enzyme (AChE and urease)	Array biosensor for the measurement of pH, urea, heavy metals and AChE	[37]	-	-
Electrochemical and sonochemical (combination)	-	-	-	-	-	-
	Dichlorvos, parathion, azinphos (organophosphorus pesticides)	Enzyme (AChE)	Array of microelectrodes	[38]	-	[38]
Optical (fluorescence)	Multiple compounds	Antibodies	multiplexed bead-based fluorescence immunoassays	-	[39]–[42]	-
	EDCs	Recombinant yeast	-	[43]	-	[44]
	Isoproturon, diuron simazine	Chlorella vulgaris (Algae cells)	0.025 µg/L, 0.5 µg/L	[45]	-	-
	PCBs	Antibodies	LOD: 0.1 ng/L	[46]	-	[47]
	Bisphenol A	Antibodies	Monitoring in a waterworks	[48]	[49]	-
	Naphthalene and phenanthrene	DNA	Sol-gel array	[50]	-	-

Table 2: (Cont.) Current environmentally-aimed transducing elements with corresponding environmental analytes of interest.

Transducing element	Compound s or parameters	Bio- recognition element	Features	Reference (s)	Relevant LOAD reference	Relevant LOC reference
	Nitrate	Recombinant Escherichia coli	Without interference of phosphate, chloride or nitrite	[51]	[52]	-
	Antibiotics	Antibodies	-	[53]	-	-
	Propanil	Antibodies	0.6 ng/L	[54]	-	-
	Pesticides and estrone	Antibodies	Natural water samples	[55]–[57]	[58]	-
	Hormones (estrone, progesterone, testosterone)	Antibodies	LOD: sub-ng/L	[59]–[61]	-	-
	Hormones (estrone, progesterone, testosterone)	Antibodies	LOD: sub-ng/L	[59]–[61]	-	-
Optical (luminescence)	-	-	-	-	[62], [63]	-
	Dioxin and dioxin-like chemicals	Recombinant hepatoma cells	LOD: 10 pM	[64]	-	-
	Benzene and its derivatives	Recombinant Escherichia coli	Air determination LOD: 0.5 mg/L, LOD: 0.5 mg/L	[65]	-	-
	Genotoxicity	Recombinant Escherichia coli	-	[66]	-	[67]
	Toxicity	Recombinant bioluminescent bacteria	Cell array to classify toxicity	[68]	-	[69]
	Mercury arsenite	Pseudomonas fluorescence (with sensors plasmids)	0.003 µg/kg, 0.7 µg/kg	[70]	-	-
	Heavy metals	Recombinant Escherichia coli	Bioavailable fraction in soils	[71]	-	[69]
	Chlorophenols	Enzymatic (horseradish peroxidase)	LOD: 1.4–1975 µg/L	[72]	-	-
	Toxicity	Genetically engineered bioluminescent bacteria	Portable	[73]	-	[69]

Table 2: (Cont.) Current environmentally-aimed transducing elements with corresponding environmental analytes of interest.

Transducing element	Compounds or parameters	Bio-recognition element	Features	Reference (s)	Relevant LOAD reference	Relevant LOC reference
Optical (Optic fibre)	-	-	-	-	[74]	-
Optical (Colourimetric absorbance)	Low BOD	<i>Pseudomonas putida</i>	Minimum measurable BOD=0.5 mg/L O ₂ ; comparison with BOD ₅ : R ² =0.971	[75]	-	-
	Phosphorus	blue phosphomolybdenum complex	LOD: 5 µg/L PO ₄ -P, Linear range: 14–800 µg/L Sensitivity of 0.003 AU.L/µg	[76]	-	[76]
Optical (SPR)	Chromium (III)	2,6-pyridine dicarboxylic acid	LOD: 21 mg/L Linear range: 69–1000 mg/L	[77]	-	[77]
	Chromium (VI)	1,5-diphenyl carbazide (DPC)	LOD: 4 µg/L Linear range: 14–1000 µg/L	[77]	-	[77]
	immunoglobulin A (IgA)	Antibodies	Gold surface SPR detection chamber		[78]	-
Optical (SPR)	EDCs	Estrogen receptor	LOD: 0.1 µg/L (estradiol)	[79]	-	-
	Salmonella enteritidis	Antibodies	106 cell/mL	[80]	-	-
	Carbaryl	Antibodies	Self-assembled monolayers LOD: 1.38 µg/L	[81]	-	-
	Bisphenol A	Antibodies	SPE prior to analysis to improve sensitivity	[82]	-	-

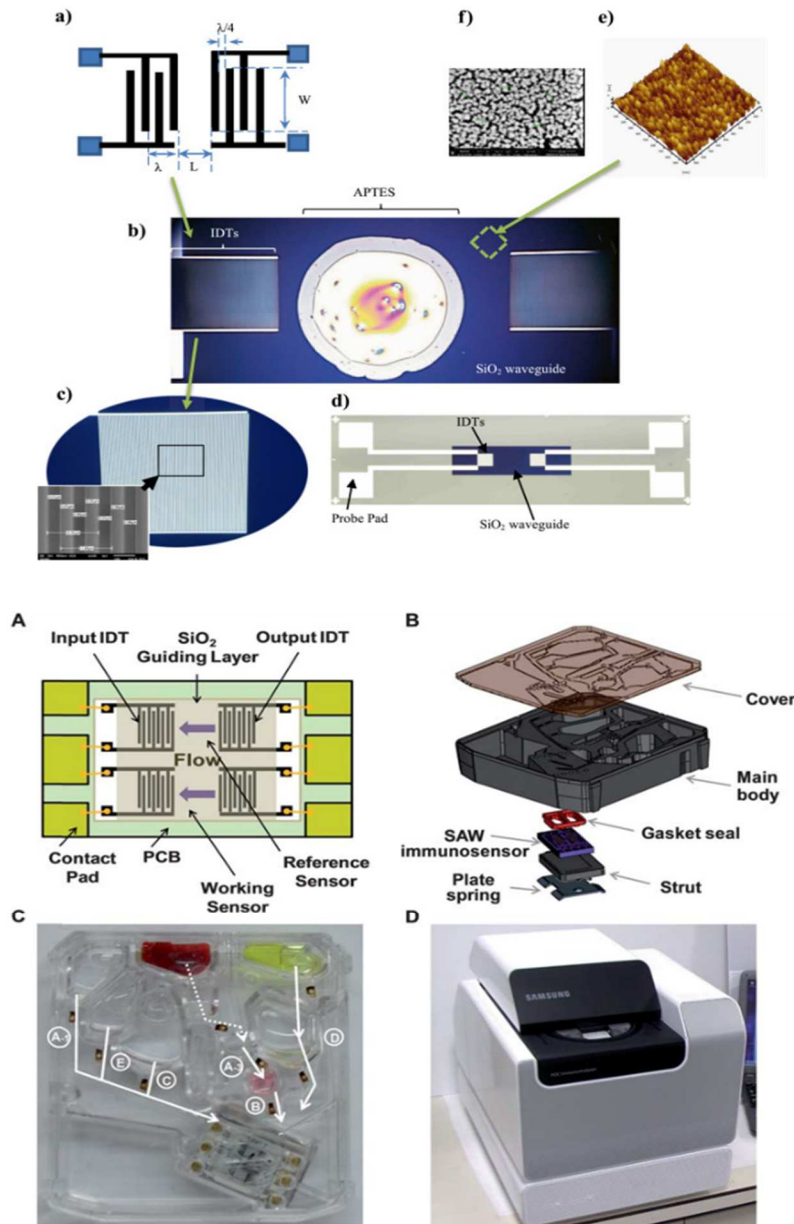


Figure 2.8: Graphical illustrations of Surface acoustic wave (SAW) biosensors.

Top) A 'shear horizontal surface acoustic wave' (SHSAW) biosensor with SiO₂ nanoparticles waveguide (42); The IDT design parameters (a), Microscope image of the SHSAW fabricated biosensor for *E. coli* O157:H7 detection with APTES (b), HPM and SEM images of the IDTs (c), Microscope image of the whole SHSAW biosensor and probe pads (d), AFM image of deposited SiO₂ layer (e) and FESEM image of the SiO₂ nanoparticles at 5 kV with 800,000 magnification (f).

Bottom) A Schematic layout of the dual-type SAW sensor packaged on a printed circuit board (top view) (A)(45); A Schematic diagram of the cartridge assembly for the integration of the SAW immunosensor (B) and image of the assembled cartridge filled with reagents and sample for troponin I (cTnI) cardiac marker analysis (C); white lines indicate the direction of flow for the implementation of the applied assay, and the dotted line indicates the flow direction for plasma purification and metering. Each reagent is transported according to the alphanumeric sequence. Picture of the centrifugal cartridge operating system (D).

2.5.2 Electrochemical transducers

Electrochemical transducers are the branch of sensors which utilises electricity as a quantitative phenomenon to investigate chemical or biological reactions(120). This is achieved through the measurement of electrical charge interactions between the electrodes and electrolytes (or ionic species in a solution). Electrochemical transducers usually consist of two or more electrodes for detection, with preference on latter for specific electrochemical studies as the collected data is more explicit and definable due to the presence of a reference electrode(120,121). Electrochemical sensors can be widely classified as two predominant categories; biosensors and chemical sensors.

Biosensor-based electrodes relate to platforms which specialise in the sensing of present biological compounds such as Proteins, nucleotides and tissues(122–124). Examples of biosensor-based electrodes in microfluidic platforms, including Lab-on-a-disc(125), Lab-on-a-Chip(126) and paper-fluidics(127), has become prevalent.

Chemical-based electrodes can be used as a catalyst for biochemical/chemical compound reactions, either through oxidisation or reduction(128,129). Examples of chemical-based electrodes in microfluidic platforms, including Lab-on-a-disc(10,18), Lab-on-a-Chip(130) and paper-fluidics(131), has become prevalent.

Through the combined efforts of these classifications, often referred to as an 'electrochemical biosensor', individual and highly selective electrochemical analysis can be achieved, including the 'capture' and 'release' rates of target analytes(132–134). Two forms of electrochemical studies will be presented here; amperometry and potentiometry.

2.5.2.1 *Amperometry*

Amperometry involves a step electrical potential applied to a 'working electrode', which causes the electroactive species to generate a current. This current is then measured across the working electrode and the counter electrode. The generated current is proportional to the concentration of the electroactive species in solution and exponentially decays with respect to time. The function of this phenomenon is described by the Cottrell equation.

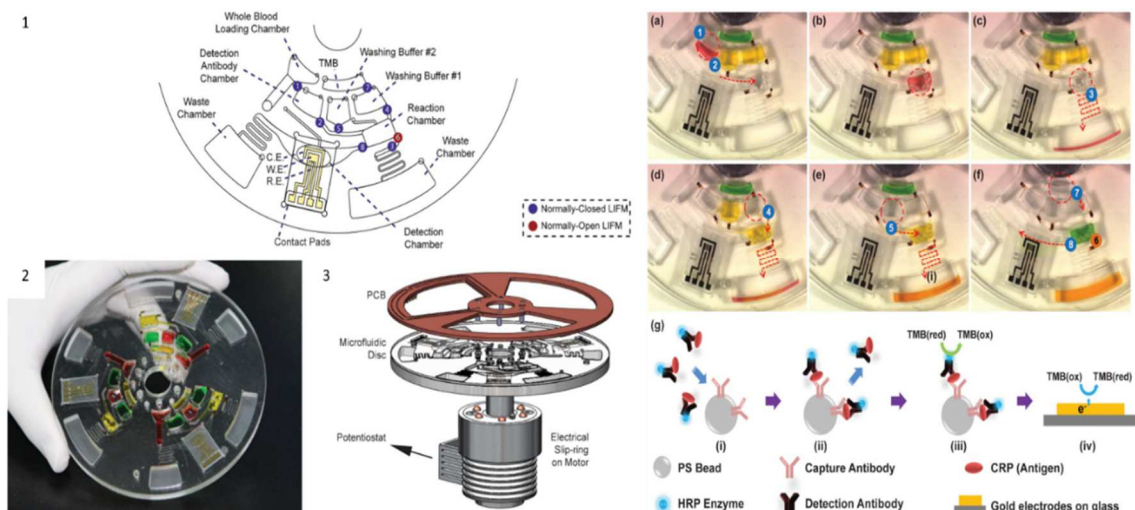


Figure 2.9: Amperometric-based electrochemical detection on a LOAD platform (49).

Left) 1) schematic of the microfluidic disc design with integrated miniaturized gold electrodes, labelled as the working (W.E.), reference (R.E.) and counter (C.E.) electrodes. (2) Image of the fabricated disc loaded with coloured water to aid visualization. (3) Setup for the on-disc electrochemical measurements. This setup includes an electrical slip-ring mounted onto a motor, a stationary potentiostat, and a PCB component that makes electrical contact with the electrodes embedded within the microfluidic disc.

Right) Stroboscopic images of the critical operational steps. For visual aid, coloured water was utilized. (a) Purified sample from the Sample Collection Chamber mixes for 10 s with a solution containing detection antibodies. (b) The mixed solution is transferred to the Reaction Chamber containing polystyrene beads coated with capture antibodies. Here, the solution is incubated for 10 min. (c) Extra solution is transferred to the Waste Chamber. (d & e) Two washing steps are applied to the beads. (f) Finally, the substrate solution (TMB) is introduced into the Reaction Chamber and is incubated for 5 min. Finally, the incubated solution flows over the electrodes in the Detection Chamber for electrochemical detection. (g: i–iv) Schematic representing the steps automated on the microfluidic disc: ELISA followed by electrochemical detection. (i) Introduction of the sample, containing the CRP antigen, to the capture antibody-coated PS beads. The CRP antigen is pre-incubated with the detection antibody. (ii) Washing of PS beads. (iii) Introduction of TMB to quantify captured CRP. (iv) Electrochemical measurement of TMB.(49)

An example of amperometry used in environmental monitoring is demonstrated by Shi et al.(135), whereby organophosphates, specifically dichlorvos, was reported with a detection limit of 10 nM in the simulated seawater during a 15 min inhibiting time. While this example only demonstrates the electrode used, development of a centrifugal microfluidic platform around this electrode could assist in automation. Another example of amperometric-based electrochemical detection on a LOAD platform using antibody

technology(49) is illustrated in Figure 2.9. In this example(49), a three-electrode system (working, counter and reference), combined with antibody-coated polystyrene (PS) beads, was employed for detecting a biomarker for cardiovascular disease (C-reactive protein) with a LOD of 4.9 pg.mL^{-1} . While this example is not a demonstration of LOAD platforms used in environmental monitoring, it demonstrates the potential for a high-sensitivity biosensor to be integrated into a LOAD platform, and with the substitution of environmental-targeted antibody technologies (as illustrated by Figure 2.9-biorecognition element), could be used to detect many different environmental analytes.

2.5.2.2 Potentiometry

Potentiometry is an electrochemical study in which a constant electrical potential is applied to one of the electrodes, referred to as the 'reference', causing a change in sample composition which can then be assessed by the second 'indicator' electrode (120). This quantification of change is based on the potential difference between the two electrodes. As potentiometry is a passive measurement of the solution, it is also considered a non-destructive measurement, under the assumption that both the material of the electrode and the solution can equilibrate. It is common practise that indicator electrodes, which have been designed to be specifically ion-selective electrodes (ISE), are used in potentiometric studies. This is because the potential is solely dependent on the activity of the target ion-of-interest; an example is described by, where a nitrite ion-selective membrane was used (75). The sensitivity and accuracy of the platform is determined by the time to reach equilibrium between the solution and the electrode. This is therefore an ideal type of detection that could be performed on LOAD based platform. In aquatic environments, platinum is regularly utilised as an electrode due to its high electron transfer kinetics (136), but a combination of metals can also be used for further enhancing electron transfer kinetics (137). Chronopotentiometry is a variant of potentiometry, first initiated by the work of *Weber*(138), in which measurement of electric potential as a function of time are performed whilst a constant current is being maintained. An example by *Gabig-Ciminska et al.* (77), also shown in Figure 2.10, demonstrates how potentiometric measurement

of a targeted enzyme product can be achieved. In this example, a silicon chip-based electric detector was coupled with bead-based sandwich hybridization (BBSH) to perform rapid analysis of specific nucleic acids, which also included characterisation of the platform using in vitro synthesized RNA oligonucleotides, followed by analysis of 16S rRNA in *Escherichia coli* extract. In the analysis of the synthesized mRNA, 200 fmol (corresponding to 10^{11} target molecules) was detected, with suggestions made on further optimisations which could further improve the detection limit to 10^9 – 10^6 target molecules.

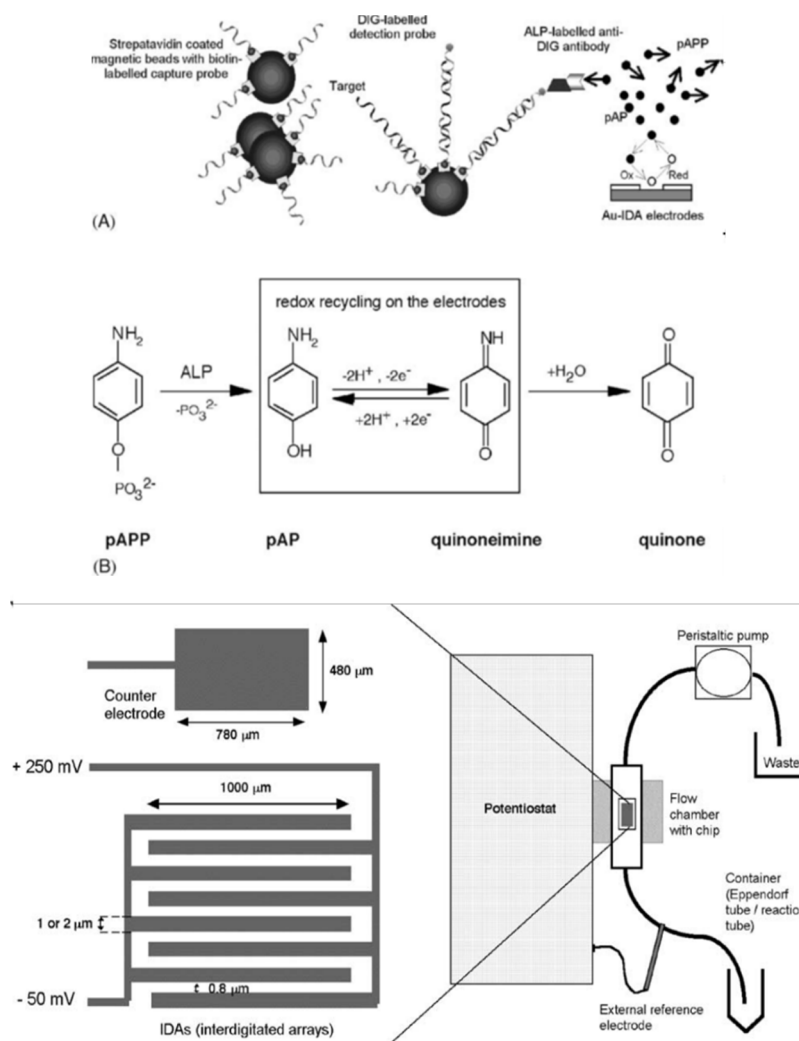


Figure 2.10: Potentiometric-based electrochemical detection on a LOC platform (77).

Top) Principle of the electric chip-based nucleic acids assay (panel A) and the redox recycling scheme (panel B).

Bottom) Top view of detailed interdigitated electrodes on the chip (left). The schematic diagram of the integrated fluidic system (right) (77).

2.5.3 Optical transducers

Optical detection is one of the most successful and common forms of detection on microfluidic platforms, primarily due to the wide availability of cheap, low-energy consumption and simplistic integration requirements, which is evident by the significant number of review articles over the past decade (139). One of the most common forms of optical transducers used are electro-optic transducers. Electro-optic transducers, usually consisting of a light source, photodiode and integrated circuit, operate through the conversion of electrical potential into light radiation. The generated light interacts with a sample, and the reemitted light is recorded and converted back to electrical signals. These electrical signals are used to quantify the sample-light interaction, dependent on the selected choice of optical arrangement. For optical transducer platforms, due to the abundance of widely available light-emitting-diodes (LEDs) and photodiodes types, detection of on-chip assay can be easily tailored to achieve optimum detectability. Three reoccurring optical arrangements which will be discussed include absorbance, fluorescently and surface plasma resonance (SPR).

2.5.3.1 Absorbance spectroscopy

Absorbance-based optical detection is a common technique used in laboratory environments in the form of a photo-spectrometer. This approach employs the use of a set wavelength, or spectrum, to characterise and analyse a sample. In this approach, both the light source and photodiode detect are set to detect only the loss in the emitted light source wavelength through sample absorption. Several sample characteristics can be determined from this approach, depending on the quanta of light used, including sample identification and quantification of component concentrations. Absorbance spectroscopic studies are relative measurements, whereby an assessed sample is contrasted against a known standard of similar composition, or blank sample. Absorbance spectroscopy on LOAD platforms has been reported for the detection of phosphate(10) and chromium (III & VI)(18), with a generalised example illustrated in Figure 2.11. In the case of the phosphate detection system(10), the ascorbic acid colourimetric absorbance assay, adapted from *Clesceri et al.*(140), was incorporated on a LOAD platform for determining phosphate with a reported sensitivity and limit of

detection of $0.003 \text{ AU L } \mu\text{g}^{-1}$ and $5 \mu\text{g L}^{-1} \text{ PO}_4\text{-P}$ respectively. In a LOAD system chromium (III) and (VI) were measured using 2,6-pyridine dicarboxylic acid and 1,5-diphenyl carbazide (DPC) respectively, forming complexes that were measured at 535 nm. The LOD for trivalent and hexavalent chromium using this device were 21 mg L^{-1} and $4 \mu\text{g L}^{-1}$, respectively. The sensitivity was found to be $0.0012 \text{ AU L } \mu\text{g}^{-1}$ for Cr(III) and $0.0017 \text{ AU L } \mu\text{g}^{-1}$ for Cr (VI).(18).

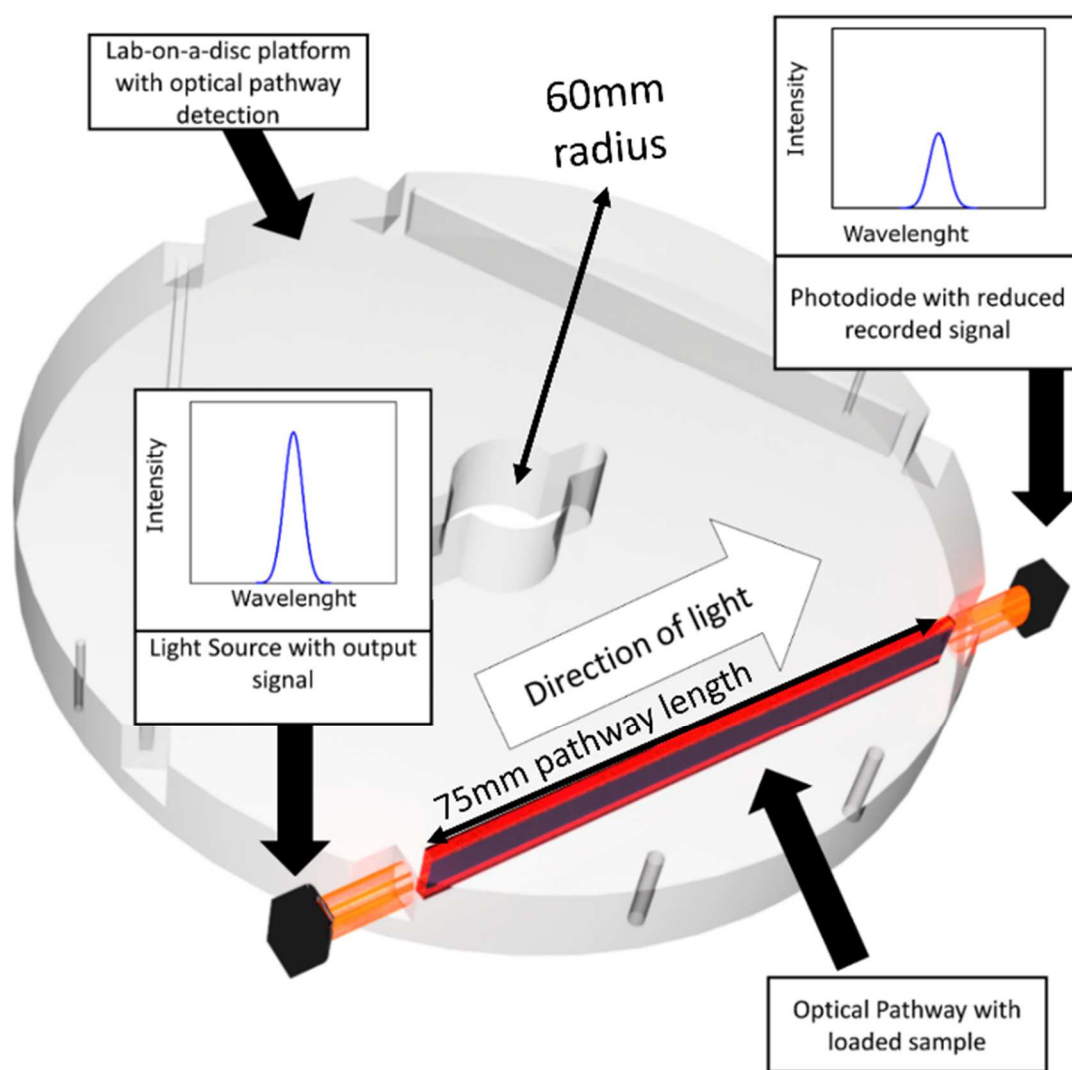


Figure 2.11: Absorbance-based optical detection on LOAD based platforms.

This LOAD platform has been designed to measure sample light absorbance through an optical pathway(10,18).

2.5.3.2 *Fluorescence spectroscopy*

Fluorescence-based optical makes use of either a particular light excitation wavelength, to interact with targeted molecules (fluorophores), which convert and reemit an emission wavelength, therefore determining the quantity of fluorophores present. Fluorophores can be easily integrated to more specific and sensitive molecules such as antibodies(141–143), proteins(144,145) and ligands(146,147) for high affinity capture targeted biological or chemical complexes in samples such as toxins, antibiotics(92), propanil(93), pesticides and estrone(94–96), naphthalene(89) and phenanthrene(89) and heavy metals(148,149). In these cases, fluorescence detection in the ng L^{-1} range is common, where in the case of PCB detection, a limit of detection as low as 0.1 ng L^{-1} was reported (86). Fluorescence is a form of luminescence, whereby luminescence occurs due to a reaction with excitation photons (photoluminescence), but luminescence can occur through other means; such as electrical(150), chemical(151), electrochemical(152) and bioluminescence(106,109,153). Figure 2.12.A illustrate how an immune complex can be formed and assessed, using a targeted antigen and fluorescently enabled antibody, with Figure 2.12.B demonstrating how heavy metals can be captured for assessment using a DNA-ligand binding. An example of how possible fluorescent detection can be integrated on a LOAD platform is illustrated in Figure 2.12.C.

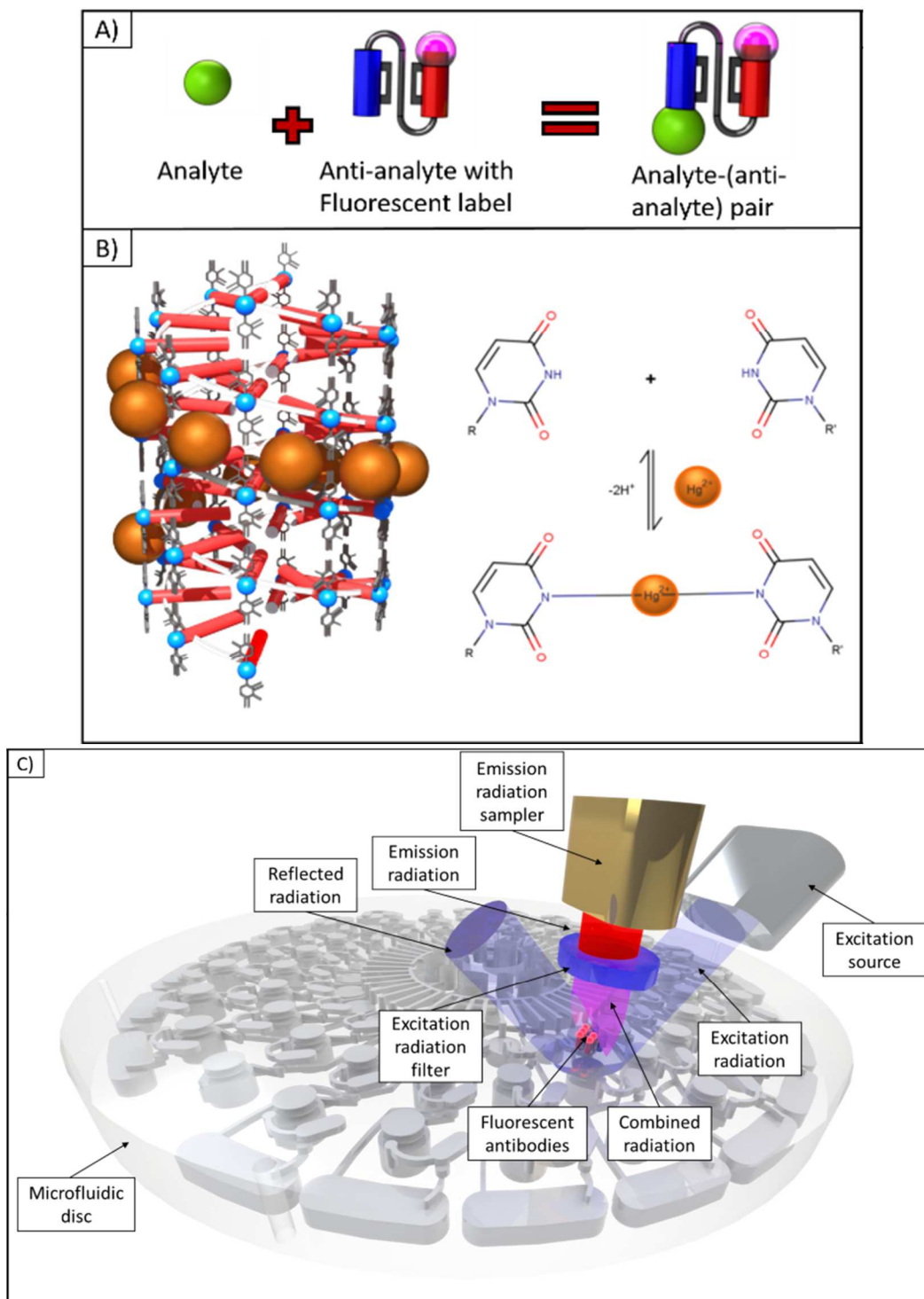


Figure 2.12: Analyte capture and optical detection.

A) Antibody technology can be used if an anti-analyte can be constructed, such as a toxin. The anti-analyte can also be fluorescently enabled to allow optical detection. B) Deoxyribonucleic acid (DNA) can be modified to collect analytes, in this case, to collect mercury(154). C) A graphical illustration of how fluorescent spectroscopy can be carried out on a LOAD platform. With the capture analyte bound to optically responsive fluorescent label, upon excitation, the emission can be recorded. This set-up can be modified for a luminescent set-up also by replacing the label and removing the laser/light source.

2.5.3.3 Surface plasmon resonance (SPR)

Surface plasmon resonance (SPR) is a label-free optical detection technique in which a reflective substrate, such as gold or silver, is coated with ligand or antibody technology and used to assess analyte-to-substrate binding rates, specificity, affinity, kinetics and analyte concentration. This is assessed by changes in the angle of reflected light, as the refractive index of the substrate is proportional to the change in surface mass, thus allowing highly sensitive quantification of analytes of interest. An example of SPR through antibody-based detection on a LOAD platform is demonstrated by *Hemmi et al* (115)(Figure 2.13). Using this device as an example, it is reasonable to expect that similar results could be obtained through substitution of the IgG antibodies with alternative ligand/antibody technology. As previously reported, SPR has been used in the detection of *Salmonella enteritidis* (117), carbaryl (118) and bisphenol A (119). While the limits of detection reported by these examples are as low as $< 2 \mu\text{g}\cdot\text{L}^{-1}$, which is significantly higher than the reported fluorescence-based limit of detection of $0.1 \text{ ng}\cdot\text{L}^{-1}$, its key advantages are the multiple characteristics which can also be quantified. SPR has been demonstrated in the detection of domoic acid in marine sensing applications (155).

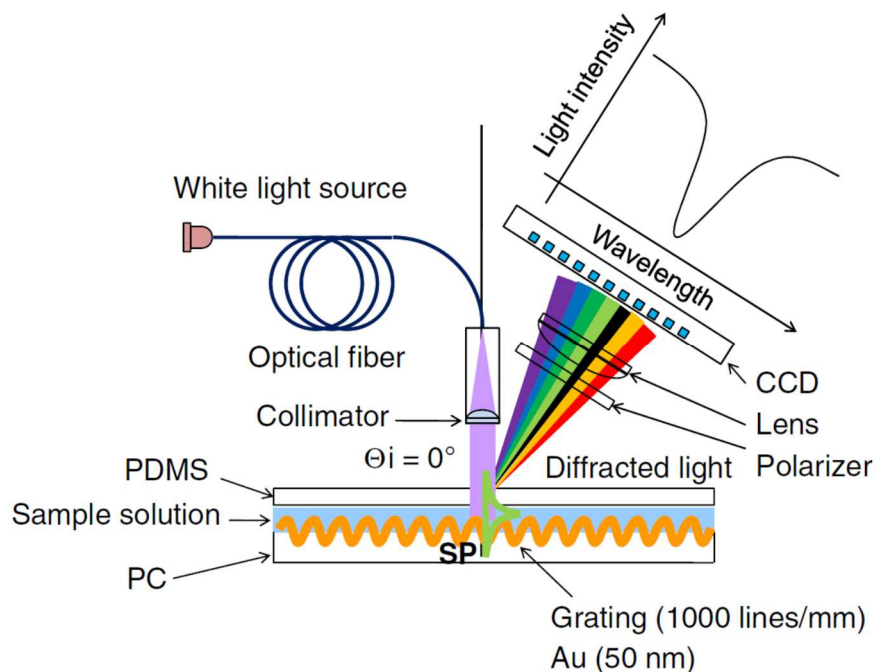


Figure 2.13: SPR optical detection on LOAD based platforms, as described by *Hemmi et al* (115).

This illustration demonstrates a particular reservoir of the microfluidic disc which has a gold grating lined in the reservoir, on which analyte-surface interactions can be analysed. This occurs due to a change on the surface's mass modifying the trajectory of the optical rays due to a change in refractive index.

2.6 Opportunity for LOAD modifications in environmental monitoring

The success of a LOAD system is dependent on its ability to mimic the specific laboratory protocols with which are required to conduct sample-to-answer analysis, and to achieve this, electrical integration is key. This would offer capability for sample treatments including sample handling and manipulation (such as mixing and separation), sample modification (including heating and redox reactions), as well as reaction detection (such as optical, electrochemical, or as required by user) on the device. Therefore, it is important to maximise the LOAD capabilities and make it would be a more attractive platform.

Currently, by comparison of the varying transducers, it is evident that electrochemical and optical integration on LOAD platforms offer a myriad of detection possibilities with minor modifications of previously successful platforms. However, electrochemical LOAD systems have been slower to be adopted due to difficulties in integration of the electrodes with external electrochemical connections. This initially requires the disc to be stationary for electrochemical detection to occur, as demonstrated by *Nwankire et al*(156). While this stopped-measurement is a less complex solution, it may not always be feasible. The inputted sample may need to be measured during electrode-passthrough, perhaps to conduct kinetic studies or identify other sample traits obtainable through SPR, or as per assay requirements. Many methods have been proposed to date to overcome the issues and allow sample-in-motion electrochemical studies, and as well as more integrated optical studies, to occur. Wireless induction-powered programmable integrated circuits with expandable capabilities through module stacking(157) (Figure 2.14.A), slip-ring based connection to external potentiostat(49,50) have been described (Figure 2.14.B), or alternatively using an on-disc, battery-powered plug-and-play electrochemical system (Figure 2.14.C). Each system has its advantage and disadvantage. While the wireless power transfer system offers a constant power solution, similar to the slip ring solution and unlike the battery powered solution, it comes with the added weight provided by induction coil. As the slip-ring solution does

not require the induction coil, it can however add significant electrical noise to the system, a feature that is undesirable for electrochemical studies. The battery-based option is expected to be the most electrically stable solution, but battery longevity for long-term deployment is a major issue. A solution may be a combination of all the systems, perhaps with a battery-based system with slip-ring or wireless charging solution.

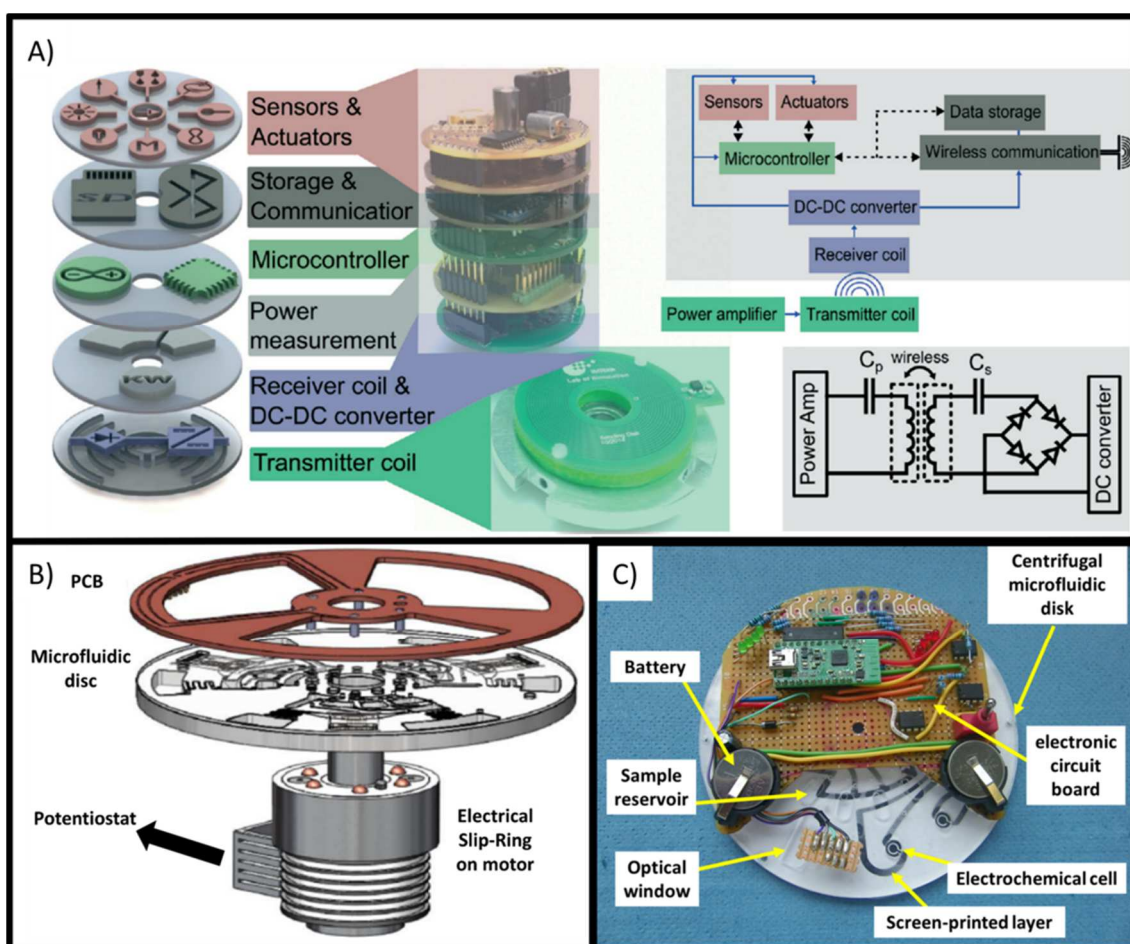


Figure 2.14: Future developments for Lab-On-A-Disc platforms studies.

A) An example of an induction-based, electrically configurable system, developed by J. Höfflin et al.(157), for performing in-motion detection which could be modified to conduct electrochemical studies on LOAD platforms. B) An example of a slip-ring based electrical system, designed by Kim et al.(49), for conducting electrochemical analysis while disc is spinning. C) An example of a battery powered system, which can perform both optical and electrochemical studies simultaneously. This system is can communicate wirelessly to transmit recordings as well as receiving commands.

It is hoped that these additions will pave the way for the next-generation LOAD platforms which be more capable of performing environmental analysis activities on a disc. Refining and optimisation of these platforms could also aid in the development of more generic LOAD platforms which can be used for observing and quantifying current environmental problems. These would then offer better environmental data, from which more informed decisions can be made.

2.7 Conclusions

While centrifugal microfluidics is an ever-evolving field, it is important to illustrate how Lab-On-A-Disc (LOAD) advances can be very useful in the field of environmental monitoring with minimal systematic modification. As with LOC systems the disadvantage of LOAD for environmental monitoring include: sample preparation (filtering, lysing, pre-concentration) currently needs to be done off chip for water samples containing cells or particulates. This is due to the potential for clogging of the channels.

Some key advantages of LOAD sensors identified:

- Cost-effective support equipment: LOADs use low cost motors as opposed to the use of LOC microfluidic pumps.
- Replacement of damaged equipment would also be minimal for LOAD vs. LOC.
- Due to the use of a compact disc based design, it has a familiarity of "spin-to-use" for the end-user/automation process, due to the resemblance of many common technology is. Cd drives, DVD players, computer consoles.
- LOCs utilise a common sample input which is directed through often an assay protocol for detection. Due to the nature of the LOAD, incorporation of multiple assay iterations can be carried out simultaneously, with separate loaded samples if desired, using a motor. This can be compared to a LOC system which would require further pumping mechanisms to achieve this.
- Pumping can cause leakages due to high pressures involved in driving liquids through small channels, especially in sandwich-constructed LOC platforms. Centrifugal forces which are utilised in LOAD systems are limited both by the radius of the disc and the mass of the loaded liquid, therefore the pressures required for driving samples is significantly less.

This review presents the relevant information for developing new and novel environmental sensing systems based on centrifugal microfluidic platforms. The key is in identifying the most suitable transducer, for application to the most common analytes-of-interest. An environmental sensing LOAD platform is designed around this transduction method and the chemical or bio-assay to measure the analyte. The review identifies the quite significant gap in the ability to detect certain environmentally relevant compounds or parameters for which monitoring is important. LOAD systems provide a robust, versatile option to developing such novel sensing systems.

2.8 References

1. Figeys D, Pinto D. Lab-on-a-chip: a revolution in biological and medical sciences. *Anal Chem*. 2000;72(9):330–A.
2. Manz A, Harrison DJ, Verpoorte EMJ, Fettinger JC, Paulus A, Lüdi H, et al. Planar chips technology for miniaturization and integration of separation techniques into monitoring systems: Capillary electrophoresis on a chip . 593(1–2):253–8. Available from:
<http://www.sciencedirect.com/science/article/pii/S0021967392802934>
3. Whitesides GM. The origins and the future of microfluidics. *Nature* [Internet]. 2006;442(7101):368–73. Available from:
<http://www.scopus.com/inward/record.url?eid=2-s2.0-33747117373&partnerID=40&md5=0074130e4ce504444efcdd2a9e1f92d4>
4. Greenblatt DJ. High-Performance Liquid Chromatography: Advances and Perspectives. *J Clin Psychopharmacol*. 1982;2(3):230.
5. Li SFY. *Capillary electrophoresis: principles, practice and applications*. Vol. 52. Elsevier; 1992.
6. Uden PC, Henderson DE. Determination of metals by gas chromatography of metal complexes. A review. *Analyst*. 1977;102(1221):889–916.
7. Ligler FS, Anderson GP, Davidson PT, Foch RJ, Ives JT, King KD, et al. Remote Sensing Using an Airborne Biosensor. *Environ Sci Technol* [Internet]. 1998 Aug 1;32(16):2461–6. Available from: <http://dx.doi.org/10.1021/es970991p>
8. Walt DR, Franz DR. Peer Reviewed: Biological Warfare Detection. *Anal Chem* [Internet]. 2000;72(23):738 A-746 A. Available from:
<http://dx.doi.org/10.1021/ac003002a>
9. Charles PT, Bart JC, Judd LL, Gauger PR, Ligler FS, Kusterbeck AW. Continuous flow fluorescence based immunosensor for the detection of explosives and environmental pollutants. In 1997. p. 80–7. Available from:
<http://dx.doi.org/10.1117/12.276137>

10. Duffy G, Maguire I, Heery B, Nwankire C, Ducreé J, Regan F. PhosphaSense: A fully integrated, portable lab-on-a-disc device for phosphate determination in water. *Sensors Actuators B Chem.* 2017;246:1085–91.
11. Noyce RN. Microelectronics. *Sci Am.* 1977;237:62–9.
12. Xia Y, Whitesides GM. Soft lithography. *Annu Rev Mater Sci.* 1998;28(1):153–84.
13. Steigert J, Brenner T, Grumann M, Riegger L, Lutz S, Zengerle R, et al. Integrated siphon-based metering and sedimentation of whole blood on a hydrophilic lab-on-a-disk. *Biomed Microdevices.* 2007;9(5):675–9.
14. Ducreé JS and SH and TB and CM and CPS and PK and NG and HR and JR and RZ and J, Steigert J, Haeberle S, Brenner T, Müller C, Steinert CP, et al. Rapid prototyping of microfluidic chips in COC. *J Micromechanics Microengineering* [Internet]. 2007;17(2):333. Available from: <http://stacks.iop.org/0960-1317/17/i=2/a=020>
15. Becker H, Locascio LE. Polymer microfluidic devices. *Talanta.* 2002;56(2):267–87.
16. Bartholomeusz DA, Boutté RW, Andrade JD. Xurography: rapid prototyping of microstructures using a cutting plotter. *J Microelectromechanical Syst.* 2005;14(6):1364–74.
17. Nayak NC, Lam YC, Yue CY, Sinha AT. CO₂-laser micromachining of PMMA: the effect of polymer molecular weight. *J Micromechanics Microengineering.* 2008;18(9):95020.
18. Duffy G, Maguire I, Heery B, Gers P, Ducreé J, Regan F. ChromiSense: A colourimetric lab-on-a-disc sensor for chromium speciation in water. *Talanta* [Internet]. 2018 Sep [cited 2017 Sep 26];178(Supplement C):392–9. Available from: <http://www.sciencedirect.com/science/article/pii/S0039914017310081>
19. Mark D, Haeberle S, Roth G, von Stetten F, Zengerle R. Microfluidic lab-on-a-chip platforms: requirements, characteristics and applications. *Chem Soc Rev* [Internet]. 2010;39(3):1153–82. Available from: <http://pubs.rsc.org/en/content/articlehtml/2010/cs/b820557b>

20. Gardeniers JGE, Van Den Berg A. Lab-on-a-chip systems for biomedical and environmental monitoring. *Anal Bioanal Chem.* 2004;378(7):1700–3.
21. Stone HA, Stroock AD, Ajdari A. ENGINEERING FLOWS IN SMALL DEVICES Microfluidics Toward a Lab-on-a-Chip. *Annu Rev Fluid Mech* [Internet]. 2004;36(1):381–411. Available from: <http://arjournals.annualreviews.org/doi/abs/10.1146/annurev.fluid.36.050802.122124>
22. Maguire I, Fitzgerald J, McPartlin D, Heery B, Murphy C, Nwankire C, et al. A centrifugal microfluidic-based approach for multi-toxin detection for real-time marine water-quality monitoring. In: *OCEANS 2017 - Aberdeen*. 2017. p. 1–8.
23. Cleary J, Slater C, McGraw C, Diamond D. An autonomous microfluidic sensor for phosphate: On-site analysis of treated wastewater. *IEEE Sens J.* 2008;8(5):508–15.
24. Liu Y, Sun Y, Sun K, Song L, Jiang X. Recent developments employing new materials for readout in lab-on-a-chip. *J Mater Chem* [Internet]. 2010;20(35):7305–11. Available from: <http://dx.doi.org/10.1039/C0JM00576B>
25. Ducrée J, Haeberle S, Lutz S, Pausch S, Zengerle R, Stetten F Von, et al. The centrifugal microfluidic Bio-Disk platform. *J Micromechanics Microengineering* [Internet]. 2007 Jul 1 [cited 2013 Nov 7];17(7):S103–15. Available from: <http://dx.doi.org/10.1088/0960-1317/17/7/s07>
26. Clarivate Analytics. Web of Science [Internet]. 2017. Available from: <http://apps.webofknowledge.com>
27. Park J, Sunkara V, Kim TH, Hwang H, Cho YK. Lab-on-a-disc for fully integrated multiplex immunoassays. *Anal Chem.* 2012;84(5):2133–40.
28. Lee BS, Lee YU, Kim H-SH, Kim T-H, Park J, Lee J-G, et al. Fully integrated lab-on-a-disc for simultaneous analysis of biochemistry and immunoassay from whole blood. *Lab Chip.* 2011;11(1):70–8.

29. Klostranec JM, Xiang Q, Farcas GA, Lee JA, Rhee A, Lafferty EI, et al. Convergence of quantum dot barcodes with microfluidics and signal processing for multiplexed high-throughput infectious disease diagnostics. *Nano Lett.* 2007;7(9):2812–8.
30. Riegger L, Grumann M, Nann T, Riegler J, Ehlert O, Bessler W, et al. Read-out concepts for multiplexed bead-based fluorescence immunoassays on centrifugal microfluidic platforms. *Sensors Actuators, A Phys.* 2006;126(2):455–62.
31. Stott SL, Hsu C-H, Tsukrov DI, Yu M, Miyamoto DT, Waltman BA, et al. Isolation of circulating tumor cells using a microvortex-generating herringbone-chip. *Proc Natl Acad Sci U S A* [Internet]. 2010;107(43):18392–7. Available from: <http://www.scopus.com/inward/record.url?eid=2-s2.0-78649872067&partnerID=40&md5=62f009f147b6d07e35a468fff7db5191>
32. Oh KW, Lee K, Ahn B, Furlani EP. Design of pressure-driven microfluidic networks using electric circuit analogy. *Lab a Chip - Miniaturisation Chem Biol* [Internet]. 2012 Feb 7 [cited 2013 Nov 7];12(3):515–45. Available from: <http://www.ncbi.nlm.nih.gov/pubmed/22179505>
33. Lam P, Wynne KJ, Wnek GE. Surface-tension-confined microfluidics. *Langmuir.* 2002;18(3):948–51.
34. R. G, C.E. N, J. G, X. Z, G.G. D, M. R, et al. Centrifugo-pneumatic valving utilizing dissolvable films. *Lab a Chip - Miniaturisation Chem Biol* [Internet]. 2012;12(16):2894–902. Available from: <http://ovidsp.ovid.com/ovidweb.cgi?T=JS&PAGE=reference&D=emed10&NEWS=N&AN=2012436014>
35. Vazquez G, Alvarez E, Navaza JM. Surface tension of alcohol water+ water from 20 to 50. degree. *C. J Chem Eng Data.* 1995;40(3):611–4.
36. Nakae H, Inui R, Hirata Y, Saito H. Effects of surface roughness on wettability. *Acta Mater.* 1998;46(7):2313–8.
37. Wang J. Electrochemical detection for microscale analytical systems: a review. *Talanta.* 2002;56(2):223–31.

38. Rodriguez-Mozaz S, Lopez De Alda MJ, Barceló D. Biosensors as useful tools for environmental analysis and monitoring. *Anal Bioanal Chem.* 2006;386(4):1025–41.
39. Lafleur JP, Salin ED. Pre-concentration of trace metals on centrifugal microfluidic discs with direct determination by laser ablation inductively coupled plasma mass spectrometry. *J Anal At Spectrom.* 2009;24(11):1511–6.
40. Hatch A V, Herr AE, Throckmorton DJ, Brennan JS, Singh AK. Integrated preconcentration SDS– PAGE of proteins in microchips using photopatterned cross-linked polyacrylamide gels. *Anal Chem.* 2006;78(14):4976–84.
41. Puiu M, Gurban A-M, Rotariu L, Brajnicov S, Viespe C, Bala C. Enhanced Sensitive Love Wave Surface Acoustic Wave Sensor Designed for Immunoassay Formats. Vol. 15, *Sensors* . 2015.
42. Ten ST, Hashim U, Gopinath SCBB, Liu WW, Foo KL, Sam ST, et al. Highly sensitive Escherichia coli shear horizontal surface acoustic wave biosensor with silicon dioxide nanostructures. *Biosens Bioelectron* [Internet]. 2017 Jul 15;93(August 2016):146–54. Available from: <http://dx.doi.org/10.1016/j.bios.2016.09.035>
43. Ritter F, Hedrich J, Deck M, Ludwig F, Shakirov D, Rapp BE, et al. Polymer Structures on Surface Acoustic Wave Biosensors. *Procedia Technol.* 2017;27:35–6.
44. Jung JH, Destgeer G, Park J, Ahmed H, Park K, Sung HJ. On-demand droplet capture and release using microwell-assisted surface acoustic waves. *Anal Chem.* 2017;89(4):2211–5.
45. Lee W, Jung J, Hahn YK, Kim SK, Lee Y, Lee J, et al. A centrifugally actuated point-of-care testing system for the surface acoustic wave immunosensing of cardiac troponin I. *Analyst* [Internet]. 2013;138(9):2558–66. Available from: <http://www.ncbi.nlm.nih.gov/pubmed/23478433>
46. Pathirana S., Barbaree JM, Chin BA, Hartell M., Neely W., Vodyanoy V. Rapid and sensitive biosensor for Salmonella. *Biosens Bioelectron* [Internet]. 2000;15(3–

- 4):135–41. Available from:
<http://linkinghub.elsevier.com/retrieve/pii/S0956566300000671>
47. Barker J, Holthouse S, Solomon M. Biological Saw Sensor [Internet]. Google Patents; 2008. Available from:
<https://www.google.com/patents/US20080241933>
48. Yeo LY, Friend JR. Surface acoustic wave microfluidics. *Annu Rev Fluid Mech.* 2014;46:379–406.
49. Kim T-H, Abi-Samra K, Sunkara V, Park D-K, Amasia M, Kim N, et al. Flow-enhanced electrochemical immunosensors on centrifugal microfluidic platforms. *Lab Chip* [Internet]. 2013;13(18):3747–54. Available from:
<http://pubs.rsc.org/en/Content/ArticleHTML/2013/LC/C3LC50374G%5Cnhttp://dx.doi.org/10.1039/C3LC50374G%5Cnhttp://www.ncbi.nlm.nih.gov/pubmed/23900555>
50. Andreasen SZ, Kwasny D, Amato L, Brøgger AL, Bosco FG, Andersen KB, et al. Integrating electrochemical detection with centrifugal microfluidics for real-time and fully automated sample testing. *RSC Adv* [Internet]. 2015;5(22):17187–93. Available from: <http://xlink.rsc.org/?DOI=C4RA16858E>
51. Burger R, Amato L, Boisen A. Detection Methods for Centrifugal Microfluidic Platforms. *Biosens Bioelectron* [Internet]. 2015;(January 2016):1–14. Available from: <http://linkinghub.elsevier.com/retrieve/pii/S0956566315302463>
52. Parellada J, Narváez A, López M a., Domínguez E, Fernández JJ, Pavlov V, et al. Amperometric immunosensors and enzyme electrodes for environmental applications. *Anal Chim Acta.* 1998;362:47–57.
53. Dempsey E, Diamond D, Collier A. Development of a biosensor for endocrine disrupting compounds based on tyrosinase entrapped within a poly(thionine) film. *Biosens Bioelectron* [Internet]. 2004;20(2):367–77. Available from:
<http://www.ncbi.nlm.nih.gov/pubmed/15308243>
54. Ha K, Joo G, Jha SK, Kim Y-S. Monitoring of endocrine disruptors by capillary electrophoresis amperometric detector. *Microelectron Eng* [Internet].

- 2009;86(4–6):1407–10. Available from:
<http://linkinghub.elsevier.com/retrieve/pii/S0167931709001439>
55. Noh H-B, Lee K-S, Lim BS, Kim S-J, Shim Y-B. Total analysis of endocrine disruptors in a microchip with gold nanoparticles. *Electrophoresis* [Internet]. 2010;31(18):3053–60. Available from:
<http://doi.wiley.com/10.1002/elps.201000112>
56. Ino K, Kitagawa Y, Watanabe T, Shiku H, Koide M, Itayama T, et al. Detection of hormone active chemicals using genetically engineered yeast cells and microfluidic devices with interdigitated array electrodes. *Electrophoresis*. 2009;30(19):3406–12.
57. Rose A, Nistor C, Emnéus J, Pfeiffer D, Wollenberger U. GDH biosensor based off-line capillary immunoassay for alkylphenols and their ethoxylates. *Biosens Bioelectron* [Internet]. 2002;17(11–12):1033–43. Available from:
<http://linkinghub.elsevier.com/retrieve/pii/S0956566302000969>
58. Evtugyn G a, Eremin S a, Shaljamova RP, Ismagilova a R, Budnikov HC. Amperometric immunosensor for nonylphenol determination based on peroxidase indicating reaction. *Biosens Bioelectron* [Internet]. 2006;22(1):56–62. Available from: <http://www.ncbi.nlm.nih.gov/pubmed/16406500>
59. Bachmann TT, Schmid RD. A disposable multielectrode biosensor for rapid simultaneous detection of the insecticides paraoxon and carbofuran at high resolution. *Anal Chim Acta* [Internet]. 1999;401(1–2):95–103. Available from:
<http://linkinghub.elsevier.com/retrieve/pii/S0003267099005139>
60. Tan TC, Wu CH. BOD sensors using multi-species living or thermally killed cells of a BODSEED microbial culture. *Sensors and Actuators B-Chemical*. 1999;54:252–60.
61. Torrents A, Mas J, Muñoz FX, Del Campo FJ. Design of a microfluidic respirometer for semi-continuous amperometric short time biochemical oxygen demand (BOD_{st}) analysis. *Biochem Eng J*. 2012;66:27–37.

62. Deo RP, Wang J, Block I, Mulchandani A, Joshi KA, Trojanowicz M, et al. Determination of organophosphate pesticides at a carbon nanotube/organophosphorus hydrolase electrochemical biosensor. *Anal Chim Acta* [Internet]. 2005;530(2):185–9. Available from: <http://linkinghub.elsevier.com/retrieve/pii/S0003267004012875>
63. Lu D, Shao G, Du D, Wang J, Wang L, Wang W, et al. Enzyme entrapped nanoporous scaffolds formed through flow-induced gelation in a microfluidic filter device for sensitive biosensing of organophosphorus compounds. *Lab Chip* [Internet]. 2011;11(3):381–4. Available from: <http://www.ncbi.nlm.nih.gov/pubmed/21152493>
64. Nistor C, Rose A, Farré M, Stoica L, Wollenberger U, Ruzgas T, et al. In-field monitoring of cleaning efficiency in waste water treatment plants using two phenol-sensitive biosensors. *Anal Chim Acta* [Internet]. 2002;456(1):3–17. Available from: <http://linkinghub.elsevier.com/retrieve/pii/S0003267001010157>
65. Lin Y, Timchalk CA, Matson DW, Wu H, Thrall KD. Integrated microfluidics/electrochemical sensor system for monitoring of environmental exposures to lead and chlorophenols. *Biomed Microdevices*. 2001;3(4):331–8.
66. Reshetilov AN, Semenchuk IN, Iliasov P V., Taranova LA. The amperometric biosensor for detection of sodium dodecyl sulfate. *Anal Chim Acta* [Internet]. 1997;347(1–2):19–26. Available from: <http://www.sciencedirect.com/science/article/pii/S0003267097000718>
67. Taranova L, Semenchuk I, Manolov T, Iliasov P, Reshetilov A. Bacteria-degraders as the base of an amperometric biosensor for detection of anionic surfactants. *Biosens Bioelectron* [Internet]. 2002;17(8):635–40. Available from: http://ac.els-cdn.com/S0956566301003074/1-s2.0-S0956566301003074-main.pdf?_tid=4384c9d8-c159-11e2-8edb-00000aacb35e&acdnat=1369060170_83aa6e3128ebd22962e5d6360e82d7ca
68. Masadome T, Kugoh S, Ishikawa M, Kawano E, Wakida S. Polymer chip incorporated with anionic surfactant-ISFET for microflow analysis of anionic

- surfactants. *Sensors Actuators B Chem* [Internet]. 2005;108(1–2):888–92.
Available from: <http://linkinghub.elsevier.com/retrieve/pii/S0925400504008305>
69. Mitrovski SM, Nuzzo RG. An electrochemically driven poly(dimethylsiloxane) microfluidic actuator: oxygen sensing and programmable flows and pH gradients. *Lab Chip*. 2005;5(6):634–45.
 70. Nomura Y, Ikebukuro K, Yokoyama K, Takeuchi T, Arikawa Y, Ohno S, et al. Application of a linear alkylbenzene sulfonate biosensor to river water monitoring1. *Biosens Bioelectron* [Internet]. 1998;13(9):1047–53. Available from: <http://www.sciencedirect.com/science/article/pii/S0956566397000778>
 71. Svoboda M, Slouka Z, Schrott W, Šnita D. Cation exchange membrane integrated into a microfluidic device. *Microelectron Eng*. 2009;86(4–6):1371–4.
 72. Marrazza G, Chianella I, Mascini M. Disposable DNA electrochemical biosensors for environmental monitoring. *Anal Chim Acta*. 1999;387(3):297–307.
 73. Laschi S, Mascini M. Planar electrochemical sensors for biomedical applications. *Med Eng Phys*. 2006;28(10):934–43.
 74. Laschi S, Fránek M, Mascini M. Screen-printed electrochemical immunosensors for PCB detection. *Electroanalysis*. 2000;12(16):1293–8.
 75. Tossanaitada B, Masadome T, Imato T. Sequential injection analysis of thiocyanate ions using a microfluidic polymer chip with an embedded ion-selective electrode. *Anal Sci* [Internet]. 2014;30(4):507–11. Available from: <http://www.ncbi.nlm.nih.gov/pubmed/24717662>
 76. Ercole C, Del Gallo M, Pantalone M, Santucci S, Mosiello L, Laconi C, et al. A biosensor for *Escherichia coli* based on a potentiometric alternating biosensing (PAB) transducer. *Sensors Actuators, B Chem*. 2002;83:48–52.
 77. Gabig-Ciminska M, Holmgren A, Andresen H, Bundvig Barken K, Wümpelmann M, Albers J, et al. Electric chips for rapid detection and quantification of nucleic acids. *Biosens Bioelectron*. 2004;19(6):537–46.

78. Tsai H, Doong R. Simultaneous determination of pH, urea, acetylcholine and heavy metals using array-based enzymatic optical biosensor. *Biosens Bioelectron* [Internet]. 2005;20(9):1796–804. Available from: <http://linkinghub.elsevier.com/retrieve/pii/S0956566304003197>
79. Law K a., Higson SPJ. Sonochemically fabricated acetylcholinesterase micro-electrode arrays within a flow injection analyser for the determination of organophosphate pesticides. *Biosens Bioelectron*. 2005;20(10 SPEC. ISS.):1914–24.
80. Puckett LG, Dikici E, Lai S, Madou M, Bachas LG, Daunert S. Investigation into the applicability of the centrifugal microfluidics platform for the development of protein-ligand binding assays incorporating enhanced green fluorescent protein as a fluorescent reporter. *Anal Chem*. 2004;76(24):7263–8.
81. Burger R, Reith P, Kijanka G, Akujobi V, Abgrall P, Ducreé J. Array-based capture, distribution, counting and multiplexed assaying of beads on a centrifugal microfluidic platform. *Lab Chip*. 2012;12(7):1289.
82. Steigert J, Grumann M, Brenner T, Mittenbühler K, Nann T, Rühle J, et al. Integrated sample preparation, reaction, and detection on a high-frequency centrifugal microfluidic platform. *JALA - J Assoc Lab Autom*. 2005;10(5):331–41.
83. Wozel E, Hermanowicz SW, Holman HYN. Developing a biosensor for estrogens in water samples: Study of the real-time response of live cells of the estrogen-sensitive yeast strain RMY/ER-ERE using fluorescence microscopy. *Biosens Bioelectron*. 2006;21(8):1654–8.
84. García-Alonso J, Greenway GM, Hardege JD, Haswell SJ. A prototype microfluidic chip using fluorescent yeast for detection of toxic compounds. *Biosens Bioelectron* [Internet]. 2009 Jan 1 [cited 2016 Feb 17];24(5):1508–11. Available from: <http://www.sciencedirect.com/science/article/pii/S0956566308004260>
85. Védrine C, Leclerc JC, Durrieu C, Tran-Minh C. Optical whole-cell biosensor using *Chlorella vulgaris* designed for monitoring herbicides. *Biosens Bioelectron*. 2003;18(4):457–63.

86. Endo T, Okuyama A, Matsubara Y, Nishi K, Kobayashi M, Yamamura S, et al. Fluorescence-based assay with enzyme amplification on a micro-flow immunosensor chip for monitoring coplanar polychlorinated biphenyls. *Anal Chim Acta*. 2005;531(1):7–13.
87. Aota A, Date Y, Terakado S, Sugiyama H, Ohmura N. Analysis of Polychlorinated Biphenyls in Transformer Oil by Using Liquid–Liquid Partitioning in a Microfluidic Device. *Anal Chem* [Internet]. 2011 Oct 15;83(20):7834–40. Available from: <http://dx.doi.org/10.1021/ac2015867>
88. Kubo I, Kanamatsu T, Furutani S. Microfluidic Device for Enzyme-Linked Immunosorbent Assay (ELISA) and Its Application to Bisphenol A Sensing. *Sensors Mater*. 2014;26(8):615–21.
89. Doong R, Shih H, Lee S. Sol–gel-derived array DNA biosensor for the detection of polycyclic aromatic hydrocarbons in water and biological samples. *Sensors Actuators B Chem* [Internet]. 2005;111–112:323–30. Available from: <http://linkinghub.elsevier.com/retrieve/pii/S0925400505005988>
90. Taylor CJ, Bain L a., Richardson DJ, Spiro S, Russell DA. Construction of a whole-cell gene reporter for the fluorescent bioassay of nitrate. *Anal Biochem*. 2004;328:60–6.
91. Xi Y, Templeton EJ, Salin ED. Rapid simultaneous determination of nitrate and nitrite on a centrifugal microfluidic device. *Talanta* [Internet]. 2010;82(4):1612–5. Available from: <http://dx.doi.org/10.1016/j.talanta.2010.07.038>
92. Tschmelak J, Proll G, Gauglitz G. Optical biosensor for pharmaceuticals, antibiotics, hormones, endocrine disrupting chemicals and pesticides in water: Assay optimization process for estrone as example. *Talanta* [Internet]. 2005;65(2):313–23. Available from: <http://www.sciencedirect.com/science/article/pii/S0039914004003832>
93. Tschmelak J, Proll G, Gauglitz G. Ultra-sensitive fully automated immunoassay for detection of propanil in aqueous samples: steps of progress toward sub-

- nanogram per liter detection. *Anal Bioanal Chem* [Internet]. 2004;379(7–8):1004–12. Available from: <http://www.ncbi.nlm.nih.gov/pubmed/15241578>
94. Mallat E, Barzen C, Abuknesha R, Gauglitz G, Barceló D. Fast determination of paraquat residues in water by an optical immunosensor and validation using capillary electrophoresis-ultraviolet detection. *Anal Chim Acta*. 2001;427(2):165–71.
95. Mallat E, Barzen C, Abuknesha R, Gauglitz G, Barceló D. Part per trillion level determination of isoproturon in certified and estuarine water samples with a direct optical immunosensor. *Anal Chim Acta*. 2001;426:209–16.
96. Rodriguez-Mozaz S, Reder S, Lopez De Alda M, Gauglitz G, Barceló D. Simultaneous multi-analyte determination of estrone, isoproturon and atrazine in natural waters by the River ANALyser (RIANA), an optical immunosensor. *Biosens Bioelectron*. 2004;19:633–40.
97. Duford† DA, Xi†† Y, Salin*† ED, Duford DA, Xi Y, Salin ED. Enzyme Inhibition-Based Determination of Pesticide Residues in Vegetable and Soil in Centrifugal Microfluidic Devices. *Anal Chem* [Internet]. 2013 Aug 20;85(16):7834–41. Available from: <http://dx.doi.org/10.1021/ac401416w>
98. Tschmelak J, Proll G, Gauglitz G. Sub-nanogram per litre detection of the emerging contaminant progesterone with a fully automated immunosensor based on evanescent field techniques. *Anal Chim Acta* [Internet]. 2004;519(2):143–6. Available from: <http://linkinghub.elsevier.com/retrieve/pii/S000326700400772X>
99. Hua P, Hole J, Wilkinson J, Proll G, Tschmelak J, Gauglitz G, et al. Integrated optical fluorescence multisensor for water pollution. *Opt Express* [Internet]. 2005;13(4):1124–30. Available from: <http://www.ncbi.nlm.nih.gov/pubmed/19494980>
100. Tschmelak J, Kumpf M, Käppel N, Proll G, Gauglitz G. Total internal reflectance fluorescence (TIRF) biosensor for environmental monitoring of testosterone with commercially available immunochemistry: antibody characterization, assay

development and real sample measurements. *Talanta* [Internet].

2006;69(2):343–50. Available from:

<http://www.ncbi.nlm.nih.gov/pubmed/18970572>

101. van Oordt T, Stevens GB, Vashist SK, Zengerle R, von Stetten F. Rapid and highly sensitive luciferase reporter assay for the automated detection of botulinum toxin in the centrifugal microfluidic LabDisk platform. *RSC Adv* [Internet]. 2013;3(44):22046. Available from: <http://xlink.rsc.org/?DOI=c3ra44482a>
102. Date A, Pasini P, Daunert S. Integration of spore-based genetically engineered whole-cell sensing systems into portable centrifugal microfluidic platforms. *Anal Bioanal Chem*. 2010;398(1):349–56.
103. Kasai A, Hiramatsu N, Meng Y, Yao J, Maeda S, Kitamura M. Fast-track DRESSA: a bioassay for fast, sensitive, and selective detection of halogenated and polycyclic aromatic hydrocarbons. *Anal Biochem* [Internet]. 2005;337(1):84–8. Available from: <http://www.ncbi.nlm.nih.gov/pubmed/15649379>
104. Berno E, Pereira Marcondes DF, Ricci Gamalero S, Eandi M. Recombinant *Escherichia coli* for the biomonitoring of benzene and its derivatives in the air. *Ecotoxicol Environ Saf* [Internet]. 2004;57(2):118–22. Available from: <http://www.sciencedirect.com/science/article/B6WDM-4B4YWX8-4/2/ae8ff5a254d279de82a586899bdded91>
105. Kostrzynska M, Leung KT, Lee H, Trevors JT. Green fluorescent protein-based biosensor for detecting SOS-inducing activity of genotoxic compounds. *J Microbiol Methods*. 2002;48:43–51.
106. Maehana K, Tani H, Kamidate T. On-chip genotoxic bioassay based on bioluminescence reporter system using three-dimensional microfluidic network. *Anal Chim Acta* [Internet]. 2006 Feb [cited 2016 Feb 17];560(1–2):24–9. Available from: <http://www.sciencedirect.com/science/article/pii/S0003267005020957>
107. Jin HL, Mitchell RJ, Byoung CK, Cullen DC, Man BG. A cell array biosensor for environmental toxicity analysis. *Biosens Bioelectron*. 2005;21:500–7.

108. Zhao X, Dong T. A microfluidic device for continuous sensing of systemic acute toxicants in drinking water. *Int J Environ Res Public Health*. 2013;10(12):6748–63.
109. Petänen T, Romantschuk M. Use of bioluminescent bacterial sensors as an alternative method for measuring heavy metals in soil extracts. *Anal Chim Acta*. 2002;456(1):55–61.
110. Liao VH-C, Chien M-T, Tseng Y-Y, Ou K-L. Assessment of heavy metal bioavailability in contaminated sediments and soils using green fluorescent protein-based bacterial biosensors. *Environ Pollut*. 2006;142(1):17–23.
111. Enzymatique LDG, Cnrs U, Marquette CA, Degiuli A, Blum LJ. Fiberoptic biosensors based on chemiluminescent reactions. *Appl Biochem Biotechnol* [Internet]. 2000;89(2):107–15. Available from: <http://dx.doi.org/10.1385/ABAB:89:2-3:107>
112. Choi S. A portable toxicity biosensor using freeze-dried recombinant bioluminescent bacteria. *Biosens Bioelectron* [Internet]. 2002;17(5):433–40. Available from: <http://www.sciencedirect.com/science/article/pii/S0956566301003037>
113. Johnson RD, Badr IHA, Barrett G, Lu Y, Madou MJ, Bachas LG, et al. Development of a Fully Integrated Analysis System for Ions Based on Ion-Selective Optodes and Centrifugal Microfluidics Development of a Fully Integrated Analysis System for Ions Based on Ion-Selective Optodes and Centrifugal Microfluidics. *Anal Chem*. 2001;(February 2016).
114. Chee GJ, Nomura Y, Ikebukuro K, Karube I. Optical fiber biosensor for the determination of low biochemical oxygen demand. *Biosens Bioelectron* [Internet]. 2000;15(7–8):371–6. Available from: <http://www.ncbi.nlm.nih.gov/pubmed/11219750>
115. Hemmi A, Usui T, Moto A, Tobita T, Soh N, Nakano K, et al. A surface plasmon resonance sensor on a compact disk-type microfluidic device. *J Sep Sci*. 2011;34(20):2913–9.

116. Seifert M, Haindl S, Hock B. Development of an Enzyme Linked Receptor Assay (Elra) for Estrogens and Xenoestrogens. *Anal Chim Acta*. 1999;386(3):191–9.
117. Koubová V, Brynda E, Karasová L, Škvor J, Homola J, Dostálek J, et al. Detection of foodborne pathogens using surface plasmon resonance biosensors. *Sensors Actuators B Chem* [Internet]. 2001;74(1–3):100–5. Available from: <http://www.sciencedirect.com/science/article/pii/S0925400500007176>
<http://linkinghub.elsevier.com/retrieve/pii/S0925400500007176>
118. Mauriz E, Calle a, Abad a, Montoya a, Hildebrandt a, Barceló D, et al. Determination of carbaryl in natural water samples by a surface plasmon resonance flow-through immunosensor. *Biosens Bioelectron* [Internet]. 2006;21(11):2129–36. Available from: <http://www.ncbi.nlm.nih.gov/pubmed/16309901>
119. Marchesini GR, Meulenber E, Haasnoot W, Irth H. Biosensor immunoassays for the detection of bisphenol A. *Anal Chim Acta* [Internet]. 2005;528(1):37–45. Available from: <http://www.sciencedirect.com/science/article/pii/S0003267004008177>
120. Bard AJ, Faulkner LR. *Fundamentals and applications. Electrochem Methods*. 2001;2.
121. Costard J, Ender M, Weiss M, Ivers-Tiffée E. Three-Electrode Setups for Lithium-Ion Batteries II. Experimental Study of Different Reference Electrode Designs and Their Implications for Half-Cell Impedance Spectra. *J Electrochem Soc*. 2017;164(2):A80–7.
122. Wilson GS, Gifford R. Biosensors for real-time in vivo measurements. *Biosens Bioelectron*. 2005;20(12):2388–403.
123. Sakaguchi T, Morioka Y, Yamasaki M, Iwanaga J, Beppu K, Maeda H, et al. Rapid and onsite BOD sensing system using luminous bacterial cells-immobilized chip. *Biosens Bioelectron*. 2007;22(7):1345–50.

124. Chen S-M, Chzo W-Y. Simultaneous voltammetric detection of dopamine and ascorbic acid using didodecyldimethylammonium bromide (DDAB) film-modified electrodes. *J Electroanal Chem.* 2006;587(2):226–34.
125. Sanger K, Zór K, Bille Jendresen C, Heiskanen A, Amato L, Toftgaard Nielsen A, et al. Lab-on-a-disc platform for screening of genetically modified *E. coli* cells via cell-free electrochemical detection of p-Coumaric acid. *Sensors Actuators B Chem* [Internet]. 2017;253:999–1005. Available from: <http://www.sciencedirect.com/science/article/pii/S0925400517312030>
126. Liao JC, Mastali M, Gau V, Suchard MA, Møller AK, Bruckner DA, et al. Use of electrochemical DNA biosensors for rapid molecular identification of uropathogens in clinical urine specimens. *J Clin Microbiol.* 2006;44(2):561–70.
127. Liu H, Xiang Y, Lu Y, Crooks RM. Aptamer-based origami paper analytical device for electrochemical detection of adenosine. *Angew Chemie.* 2012;124(28):7031–4.
128. Vasantha VS, Chen S-M. Electrocatalysis and simultaneous detection of dopamine and ascorbic acid using poly (3, 4-ethylenedioxy) thiophene film modified electrodes. *J Electroanal Chem.* 2006;592(1):77–87.
129. Simoyi MF, Falkenstein E, Van Dyke K, Blemings KP, Klandorf H. Allantoin, the oxidation product of uric acid is present in chicken and turkey plasma. *Comp Biochem Physiol Part B Biochem Mol Biol.* 2003;135(2):325–35.
130. Wang J, Chatrathi MP, Tian B. Capillary electrophoresis microchips with thick-film amperometric detectors: separation and detection of phenolic compounds. *Anal Chim Acta* [Internet]. 2000;416(1):9–14. Available from: <http://www.sciencedirect.com/science/article/pii/S0003267000008679>
131. Nie Z, Deiss F, Liu X, Akbulut O, Whitesides GM. Integration of paper-based microfluidic devices with commercial electrochemical readers. *Lab Chip.* 2010;10(22):3163–9.
132. Balasubramanian K, Burghard M. Biosensors based on carbon nanotubes. *Anal Bioanal Chem.* 2006;385(3):452–68.

133. Zhang S, Wang N, Niu Y, Sun C. Immobilization of glucose oxidase on gold nanoparticles modified Au electrode for the construction of biosensor. *Sensors Actuators B Chem.* 2005;109(2):367–74.
134. Wang J, Musameh M, Lin Y. Solubilization of carbon nanotubes by Nafion toward the preparation of amperometric biosensors. *J Am Chem Soc.* 2003;125(9):2408–9.
135. Shi M, Xu J, Zhang S, Liu B, Kong J. A mediator-free screen-printed amperometric biosensor for screening of organophosphorus pesticides with flow-injection analysis (FIA) system. *Talanta [Internet].* 2006;68(4):1089–95. Available from: <http://www.sciencedirect.com/science/article/pii/S0039914005004248>
136. Grundl T. A review of the current understanding of redox capacity in natural, disequilibrium systems. *Chemosphere [Internet].* 1994;28(3):613–26. Available from: <http://www.sciencedirect.com/science/article/pii/0045653594903034>
137. Noyhouzer T, Valdinger I, Mandler D. Enhanced Potentiometry by Metallic Nanoparticles. *Anal Chem [Internet].* 2013 Sep 3;85(17):8347–53. Available from: <http://dx.doi.org/10.1021/ac401744w>
138. Weber HF. Untersuchungen über das Elementargesetz der Hydrodiffusion. *Ann Phys.* 1879;243(7):469–87.
139. King D, O’Sullivan M, Ducreé J. Optical detection strategies for centrifugal microfluidic platforms. *J Mod Opt [Internet].* 2014;61(2):85–101. Available from: <http://www.tandfonline.com/doi/abs/10.1080/09500340.2013.873496>
140. Clesceri LS, Greenberg AE, Eaton AD. Standard methods for the examination of water and wastewater (20th ed.). Washington, DC, Am Public Heal Assoc [variously paged]. 1998;
141. Kaufman EN, Jain RK. Effect of bivalent interaction upon apparent antibody affinity: experimental confirmation of theory using fluorescence photobleaching and implications for antibody binding assays. *Cancer Res.* 1992;52(15):4157–67.

142. Murphy C, Stack E, Krivelo S, McPartlin D a., Byrne B, Greef C, et al. Detection of the cyanobacterial toxin, microcystin-LR, using a novel recombinant antibody-based optical-planar waveguide platform. *Biosens Bioelectron* [Internet]. 2015;67:708–14. Available from: <http://linkinghub.elsevier.com/retrieve/pii/S0956566314008380>
143. Vira S, Mekhedov E, Humphrey G, Blank PS. Fluorescent-labeled antibodies: Balancing functionality and degree of labeling. *Anal Biochem*. 2010;402(2):146–50.
144. Lakowicz JR, Gratton E, Cherek H, Maliwal BP, Laczko G. Determination of time-resolved fluorescence emission spectra and anisotropies of a fluorophore-protein complex using frequency-domain phase-modulation fluorometry. *J Biol Chem*. 1984;259(17):10967–72.
145. Lata S, Gavutis M, Tampé R, Piehler J. Specific and stable fluorescence labeling of histidine-tagged proteins for dissecting multi-protein complex formation. *J Am Chem Soc*. 2006;128(7):2365–72.
146. Ward LD. [22] Measurement of ligand binding to proteins by fluorescence spectroscopy. *Methods Enzymol*. 1985;117:400–14.
147. Van de Weert M, Stella L. Fluorescence quenching and ligand binding: a critical discussion of a popular methodology. *J Mol Struct*. 2011;998(1):144–50.
148. Aragay G, Pons J, Merkoçi A. Recent trends in macro-, micro-, and nanomaterial-based tools and strategies for heavy-metal detection. *Chem Rev*. 2011;111(5):3433–58.
149. Blake DA, Jones RM, Blake RC, Pavlov AR, Darwish IA, Yu H. Antibody-based sensors for heavy metal ions. *Biosens Bioelectron*. 2001;16(9):799–809.
150. Friend RH, Gymer RW, Holmes AB, Burroughes JH, Marks RN, Taliani C, et al. Electroluminescence in conjugated polymers. *Nature*. 1999;397(6715):121–8.

151. Wang S, Chen Q, Wei X, Wu J, Wang C, Liu J. A competitive luminol chemiluminescence immunosensor based on a microfluidic chip for the determination of ractopamine. 2017;
152. Blackburn GF, Shah HP, Kenten JH, Leland J, Kamin RA, Link J, et al. Electrochemiluminescence detection for development of immunoassays and DNA probe assays for clinical diagnostics. *Clin Chem*. 1991;37(9):1534–9.
153. Eltoukhy H, Salama K, Gamal A El. A 0.18- μm CMOS bioluminescence detection lab-on-chip. *IEEE J Solid-State Circuits*. 2006;41(3):651–62.
154. Yamane T, Davidson N. On the Complexing of Desoxyribonucleic Acid (DNA) by Mercuric Ion¹. *J Am Chem Soc* [Internet]. 1961 Jun 1;83(12):2599–607. Available from: c:%5CBack_up%5CReferences%5CYamane_jacs_1961.pdf
155. Yu Q, Chen S, Taylor AD, Homola J, Hock B, Jiang S. Detection of low-molecular-weight domoic acid using surface plasmon resonance sensor. *Sensors Actuators B Chem*. 2005;107(1):193–201.
156. Nwankire CE, Venkatanarayanan A, Glennon T, Keyes TE, Forster RJ, Ducreé J. Label-free impedance detection of cancer cells from whole blood on an integrated centrifugal microfluidic platform. *Biosens Bioelectron* [Internet]. 2015;68:382–9. Available from: <http://dx.doi.org/10.1016/j.bios.2014.12.049>
157. Höfflin J, Torres Delgado SM, Suárez Sandoval F, Korvink JG, Mager D. Electrifying the disk: a modular rotating platform for wireless power and data transmission for Lab on a disk application. *Lab Chip* [Internet]. 2015;15(12):2584–7. Available from: <http://pubs.rsc.org/en/content/articlehtml/2015/lc/c5lc00138b>

Chapter 3: A novel microfluidic analytical sensing platform for the simultaneous detection of three algal toxins in water

Chapter Foreword

As discussed in the Chapter 2, there is a need for the development of environmental sensing platforms. Therefore, the purpose of this chapter is address some of these needs through the investigation and development of a hand-held algal toxin detection system which uses centrifugal microfluidics. Firstly, the reader will be presented with the background information of three high interest algal toxins (microcystin, saxitoxin and domoic acid), followed by the current methods of detection. Finally, a novel algal toxin centrifugal microfluidic platform, with a complementary detection system, will be presented. This generic algal-toxin detection platform uses an inverse-based fluorescence assay detection of these three-separate high interest algal toxins with a response time after 20 min (Figure 3.1).

The limit of detection (LOD) of the device was determined to be 7.2 ng/mL, 20 ng/mL and 50 ng/mL for microcystin-LR, domoic acid and saxitoxin respectively. The disparity between the LODs for each analyte was primarily due to significant more optimisation of the microcystin-LR assay and these parameters were then used to detect the other analytes without further optimisation. It is believed that further optimisation would have improved the detectability of the other analytes. The lower limit of quantification was approximated as 2.5 times the limit of detection, with a sigmodal trend, detected after 10000 ng/mL, used as the higher limit of quantification.

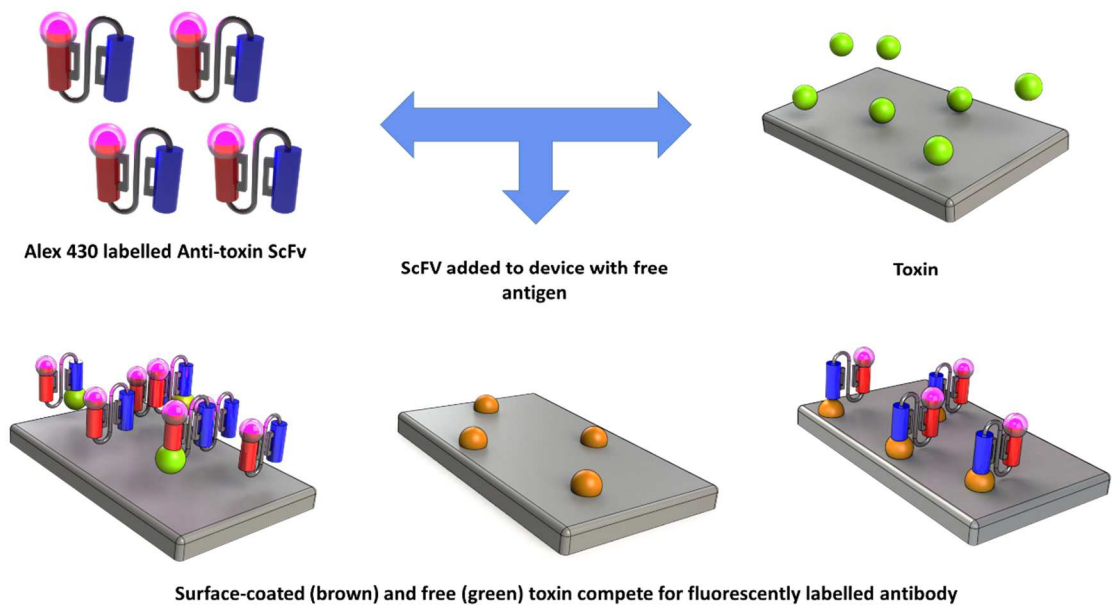


Figure 3.1: The inverse assay toxin detection strategy used in the algal-toxin detection platform.

Therefore, the dynamic range was identified to be $\sim 18 - 10000$ ng/mL. Three notable interferences clearly impeded measurements; Optical alignment, electronic configuration of the detection system and difficulties in toxin adhesion to the biosensor surface. The optical alignment of the disc with the detector proved troublesome initially, and required a revamping of the alignment pins used in the disc. This significantly increased the repeatability measurements of the disc. The electronic configuration of the disc underwent many different orientations and redesigns. Initially a bottom-up detector was employed, but due to difficulties with inconsistent transparency after toxin adhesion to the biosensor surfaces, the recorded signal became unreliable. Therefore, a top-down optical orientation was used which proved more successful. Finally, due to the prototyping nature of the electronics controller board incorporated within the system, electronic signal saturation occurred. This was rectified by incorporating several capacitors within the system to remove external electrical noise.

Summary of the nature and extent of candidate's work present in this chapter:

Joint first author (50% contribution), initiation, key ideas, design and engineering of platform, integration of components and modification of initial electronic prototype (*collaboration with Dr. Brendan Heery*), disc fabrication, biosensor integration (*collaboration with Dr. Jenny Fitzgerald*), data collection and analysis (*collaboration with Dr. Jenny Fitzgerald*), manuscript development and writing up (*collaboration with Dr. Jenny Fitzgerald*).

Summary of the nature and extent of work not performed by candidate present in this chapter:

Antibody Characteristics (including performance, selection and labelling of the antibodies) was performed by Dr. Jenny Fitzgerald (50% contribution), while design and initial prototype building of electronics for the detection system was performed by Dr. Brendan Heery.

A novel microfluidic analytical sensing platform for the simultaneous detection of three algal toxins in water

Ivan Maguire[†], Jenny Fitzgerald[†], Brendan Heery, Charles Nwankire, Richard O’Kennedy, Jens Ducreé and Fiona Regan

[†] These authors contributed equally

The article was received on 8 Feb 2018, accepted on 25 May 2018.

ACS Omega (DOI: 10.1021/acsomega.8b00240)

3.1 Abstract

Globally, the need for ‘on-site’ algal-toxin monitoring has become increasingly urgent due to the amplified demand for fresh-water and for safe, ‘toxin-free’ shellfish and fish stocks. Herein, we describe the first reported, Lab-On-A-Disc (LOAD) based-platform developed to detect microcystin levels *in-situ*, with initial detectability of saxitoxin and domoic acid also reported. Using recombinant antibody technology, the LOAD platform combines immunofluorescence with centrifugally driven microfluidic liquid handling to achieve a next-generation disposable device capable of multi-analyte sampling. A low-complexity ‘LED-Photodiode’ based optical sensing system was tailor-made for the platform, which allows the fluorescence signal of the toxin-specific reaction to be quantified. This system can rapidly and accurately detect the presence of microcystin-LR, domoic acid and saxitoxin in 30 mins, with a minimum of less than 5 mins end-user interaction for maximum reproducibility. This method provides a robust ‘point of need’ diagnostic alternative to the current laborious and costly methods used for qualitative toxin monitoring.

3.2 Introduction

With the rapid incline of population growth, the global demand and pressure for clean water supplies has never been more apparent. The resultant anthropogenic environmental impacts are predicted to increase freshwater harmful cyanobacterial and algal bloom prevalence and duration(1,2). These impacts include both global warming and water quality degradation, particularly due to eutrophication. Human, ecological and economic health can all be negatively impacted by harmful cyanobacterial and algae blooms formed due to eutrophication(3,4).

Microcystis aeruginosa is one of the most recurrent toxin-producing species of freshwater cyanobacteria, and commonly prevails in fresh and brackish water. One of the most dangerous toxins produced from harmful algal blooms (HABs) is microcystin-LR (MC-LR), produced directly by *Microcystis aeruginosa*, and is shown in Figure 3.2.**Left**. MC-LR can cause significant health issues for both humans and animals(5), particularly by inflicting hepatotoxicity and carcinogenesis through ingestion(6). In the EU, regulatory levels for MC-LR in water is 1 ng/mL for drinking water and bathing sites, with a >20 ng/mL concentration eliciting further action(3). One of the most extreme cases of human exposure transpired in Caruaru, Brazil in 1996 in a haemodialysis clinic(7). It was reported that 86% of the 116 patients undergoing dialysis in this clinic experienced severe MC-LR related symptoms including liver failure, resulting in the death of 52 patients.

A second documented marine toxin is domoic acid (DA), also demonstrated in **Figure 3.2.Centre**, which is a highly potent neurotoxin. Naturally manufactured by variant species of diatom, originating from the *genus Pseudonitzschia*, it can be responsible for eliciting the amnesic shellfish poisoning (ASP) illness(8). Following human exposure, some responses to ASP can include gastrointestinal distress, confusion, disorientation, seizures, permanent short-term memory loss, and in the most severe cases death(8,9). The earliest documented case of ASP contamination was in 1987 on the eastern coast of Prince Edward Island, Canada, where harvested mussels, contaminated with DA, were consumed(8–11). This case reported the death of 4 people, with a total of 143 people presenting similar ASP illness. Following the Canadian ASP event of 1987, and to protect seafood consumers, authorities established an action limit for DA of 20 µg DA/g shellfish

tissue(8). As there is no well-defined action limit for free DA in drinking water, a method of extraction of DA from shellfish for detection using antibody technology(12), which involved a 250-fold dilution step, was used to translate the action limit for free DA to approximately 80 ng/mL in water.

A third highly prevalent marine toxin is saxitoxin (STX), also illustrated in **Figure 3.2.Right**, which is another potent neurotoxin. It is most notably responsible for paralytic shellfish poisoning (PSP) and is produced by the genus *Alexandrium spp.* Some of the human responses following exposure to PSP can include gastrointestinal symptoms, numbness/tingling in mouth, dizziness, headache, fever, ataxia, respiratory distress, and death(13). Although there is currently no statutory guideline for STX contamination of drinking water, a suggested 3 ng/mL informal guideline concentration of for STX is currently used(14).

These relatively low guideline levels illustrate the importance of continuous environmental monitoring, and in particular, on-site algae-toxin monitoring.

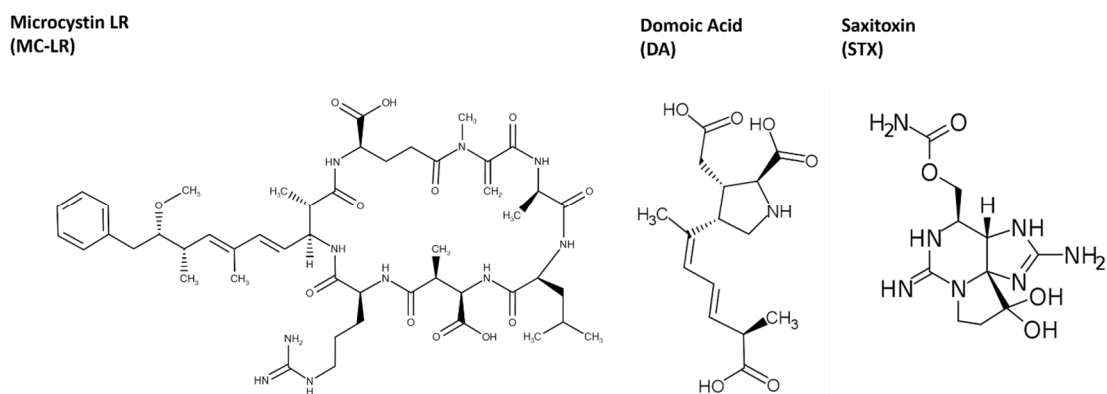


Figure 3.2: The chemical structures of microcystin-LR (MC-LR), domoic Acid (DA) and saxitoxin (STX) in their predominant congener form.

Currently, there are several *in-situ* based systems with the potential to monitor toxin presence, and in particular MC-LR, where one such case was developed by Mackenzie *et al.* in 2004(15). This approach uses a technique, referred to as solid phase adsorption toxin tracking (SPATT), which has since been adapted to allow the detection and monitoring of toxic algal blooms and shellfish contamination events(16). This technique, while beneficial, does require lab-based liquid chromatography-mass spectrometry (LC-

MS) analysis on the previously deployed and recovered materials. This limits the potential of the analysis system, preventing continuous autonomous analysis. Another disadvantage of this method is the low throughput capabilities, as well as the inability of real-time data capture, due to a weekly-based deployment and recovery sampling regime. These limitations also illustrate the requirement for highly trained technicians who are capable of handling and characterising weekly samples, consequently increasing the associated costs significantly. These increased costs would also negatively impact the ability of this approach to perform multiplexed, high density sampling in sites of interest. Other alternative biosensor-based methods, which have been used in the detection of MC-LR, have also been limited by this requirement of laboratory-based analysis. *Chianella et al.*(17) detailed a novel molecularly imprinted polymer (MIP)-based piezoelectric sensor for MC-LR with a low detection limit for 0.35 nM (0.35 ng/mL) using in-laboratory analysis. Similarly, electrochemical biosensors with reported sensitivities of 0.1 µg/L (0.1 ng/mL) for MC-LR (18) and 9.0×10^{-11} M (~ 0.09 ng/mL) for a MC-LR specific gene sequence(19), which again requires the use laboratory-based instrumentation. A highly sensitive immunosensor for MC-LR has also been demonstrated(20), whereby a graphene–gold nanocomposite/functional conducting polymer/gold nanoparticle/ionic liquid composite film with electrodeposition achieved MC-LR detection limits of as low as 3.7×10^{-17} M ($\sim 4 \times 10^{-5}$ ng/mL). Another immunosensor based-method by presented by Queirós *et al.*(21), demonstrates the use of a Fabry–Pérot interferometer combined with an optical fibre, coated with a sol–gel imprinted sensing membrane, attained a MC-LR detection sensitivity of 12.4 ± 0.7 nm.L/µg (~ 0.08 nm⁻¹.(ng/mL)). Finally, a cantilever-based immunosensor was also developed, which could assess MC-LR concentrations as low as 1pg/mL (0.001 ng/mL) in varying water sources(22). While these methods achieve highly desirable detection sensitivities, they all suffer from the common requirement of expensive laboratory equipment, with specially trained personnel, in order to perform the analysis. However, an *in-situ* based method has been previously reported by Long and colleagues(23), whereby a commercially available portable trace organic pollutant analyser (TOPA) was used to detect MC-LR, however the limit of detection of the assay was significantly higher than any of the lab-based methods at 0.03 µg.mL⁻¹ (30 ng/mL), which is above the 1 ng/mL,

and 20 ng/mL, action limits for MC-LR in drinking water, and bathing sites, respectively(3).

In order to facilitate toxin monitoring at the 'site of interest', *in-situ* toxin detection can be alternatively achieved using Lab-On-A-Chip (LOC) technologies. This can be achieved through precisely controlling and manipulating of small quantities of liquids contained within a LOC platform, in order to process and analyse a sample as if in lab environments, even when *in-situ*. These relatively new technologies are highly customisable and commercially-viable alternatives to the current detection methods which have been previously employed for environmental monitoring. LOC-based platforms have been used to specifically target *in-situ* environmental monitoring, including the detection of phosphate(24–27) and *Escherichia coli* (*E. coli*)(28,29), with the potential to also detect polycyclic aromatic hydrocarbons (PAHs), endocrine disruptors (EDCs), inorganic ions and heavy metals, by utilising already developed microfluidic techniques(30). Whilst LOC platforms are highly convenient, cost-effective and highly adaptive, the pumping technologies often required to drive sample progression through a LOC cartridge can be expensive. This is primarily due to the high costs associated with precise pumping mechanisms. A derivative of the LOC platform, circumventing these externally required expenditures is the Lab-On-A-Disc platform (LOAD)(31,32).

The LOAD centrifugal microfluidic platform replaces these previously required pumping mechanisms with a centrifugal driving force, utilising a more cost-effective motor system. To date, on-chip water quality assessment systems have been primarily developed using LOC systems, with only a few examples reported on centrifugal disc (CD) platforms(33,34). There are multiple advantages associated with LOAD platforms including; automation of system through precisely-timed sample actuation using centrifugal forces, precise liquid handling, control of samples using valves, ability to multiplex assays using identical test conditions and a myriad of detection techniques compatible on disc, making it an ideal technique for *in-situ* environmental monitoring.

In this paper, the first reported multi-analyte LOAD algal toxin sensor is described. The purpose of this sensor is to advance the first generation LOAD platform(35), whereby multi-toxin detection of a single, pre-lysed sample was confirmed using a fluorescent microscope. The novelty of this system includes the use of highly-specific recombinant

antibody technology, coupled with highly sensitive immunoaffinity purified antibodies from chicken, which have far greater sensitivity than their commercial counterparts. The production of specific DA and STX antibodies in chickens allowed for large quantities of highly sensitive Immunoglobulin Y (IgY) to be purified with relative ease and minimum cost. The LOAD platform combines immunofluorescence with centrifugally driven microfluidic liquid handling to achieve a next-generation disposable device for *in-situ* high-throughput sampling. Recombinant antibodies (rAb) were selected over alternative antibody technologies. rAb ensure consistent bio-sensing detection, with high purity yielded from production and minimal batch-to-batch manufacturing variation. A low-cost, 'LED-photodiode' based optical sensing system was tailor-made for the platform. This optical sensing system allows the fluorescence signal of the toxin-specific reaction to be quantified. This system can rapidly and accurately detect the presence of the targeted toxins in approximately 30 mins, with a maximum of 5 mins of user-interaction and high reproducibility. Due to the imminent requirement for a rapid and reliable qualitative assessment of waterbodies at the point of need, this sensor has the potential to provide an *in-situ* alternative to the current laborious and laboratory-based methods used for multiple toxin detection.

3.3 Results and discussion

The system design was largely inspired by the limitations of current *in-situ* environmental monitoring techniques. The system itself was specifically designed to prioritise some of these limiting factors, such as portability, reliability and ease-of-use, where it is envisaged that future assembly line manufacturing will offer further reproducibility and cost-effectiveness improvements. This compact, rapid system was achieved through small hardware size, simultaneous multi-sample detection in separate assay form, and reduced assay runtime through minimal user interaction and incubation periods.

3.3.1 Microfluidic disc characterisation

Reliable fluid manipulation is vital in order to conduct accurate assay protocols. For this reason, the on-disc fluidic dynamics were assessed, with the results demonstrated in

Figure 3.3 and Supplementary Video¹. The manual valve approach demonstrated excellent control of liquid, with minimal premature sample leakage between reservoir transitions. As this technique indirectly controls sample progression, via direct pneumatic air actuation, therefore there was no additional cross-reactivity between sample and microvalve material. This phenomenon occurs as the sample, while progressing within a microchannel with a $\sim 7.5 \times 10^{-8} \text{ m}^2$ cross-sectional area, experiences an increased surface tension force. This increased surface tension then prevents air-sample pass-through, resulting in an air compression proportional to the centrifugal force acting on the sample. Therefore, with the liquid acting as a cap for the succeeding reservoir, a pressure release through a valve is required to further sample progression. This pneumatic valving strategy can also be future automated, as described by *Kim et al.*(36) It is expected that with the integration of a motor(26,37), sampler(38), and multi-disc changer(39–41), long-term autonomous sensor deployment could be achievable.

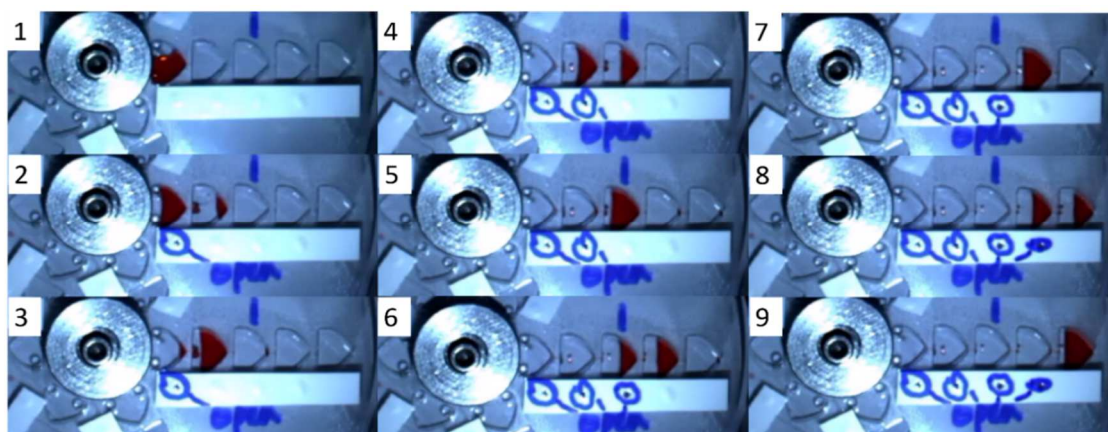


Figure 3.3: Fluid dynamic characterisation of microfluidic disc using a coloured-aqueous solution.

Sample was initially loaded into the 'load' reservoir (1). Once the first valve was manually opened while the disc was stationary, spinning of the disc allows sample progression only to the succeeding 'incubation' reservoir (2), with minimal premature leakage into the test reservoir (3). The second valve was opened then for the sample to pass to the test reservoir (4) and halted (5), with the process repeated until the sample has passed into the control reservoir (6) and halted for the allocated time (7), where it was then moved (8) and stored (9) in the waste chamber.

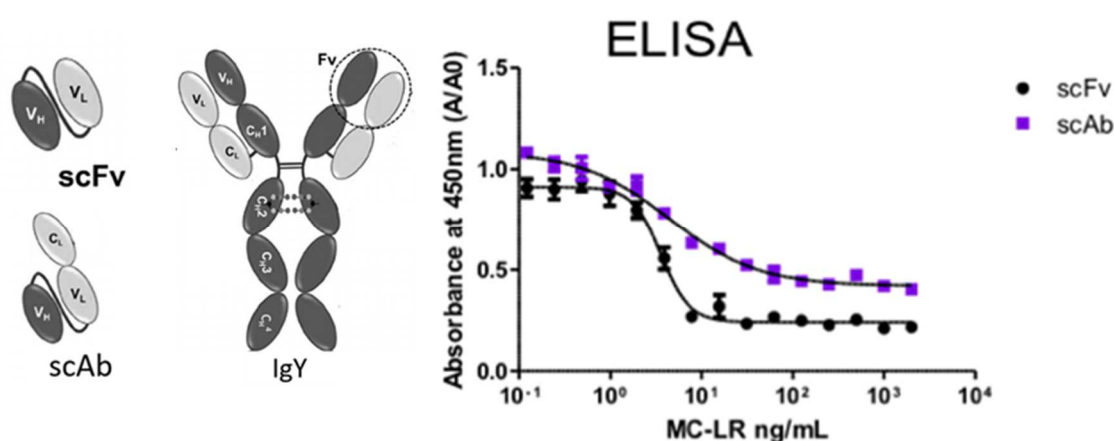
¹ Supplementary video included in publication available at:
<https://drive.google.com/open?id=16BV2FcXIBdJiAKtJnNN8UWaMn6SjPLS1>

3.3.2 Biosensor characterisation

Due to the potential human health hazard posed by MC-LR, DA and STX (which shall be generically referred to as 'toxin'), and the repercussions associated with a false qualitative screening of waterbodies, including human health, fishery, recreational and economic impacts, a screening method needs to be capable of detecting toxins with a significant degree of confidence. An assessment of the screening data variability or coefficients of variation is critical in determining the reproducibility of the assay format. Initial experimental design approaches were investigated to evaluate and determine the optimal assay parameters for use with the system.

3.3.2.1 Biosensor selection

In order to attain the low levels of relevant detection (ng/ml), highly sensitive biosensors were an essential component in achieving this detectability. All Abs (recombinant for MC-LR, and polyclonal for STX and DA) were produced in-house with MC-LR antibody fragments assessed (Figure 3.4). In the case of domoic acid, it was also reported that the in-house produced scFv performed better than the commercial counterparts (sourced by Abcam Ltd.) (Figure 3.5).



Antibody variant	ELISA IC ₉₀ -IC ₁₀
scFv	1.6-7.9 ng/mL
scAb	0.4-52.8 ng/mL

Figure 3.4: The comparison of the performance of the microcystin scFv vs scAb antibody form.

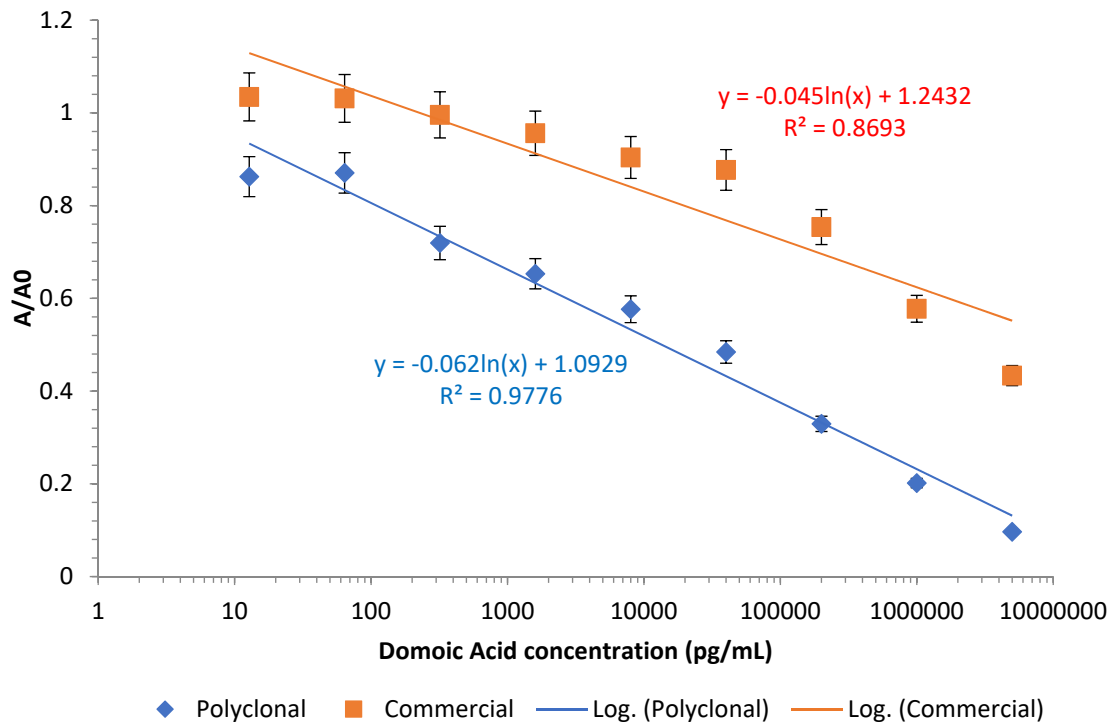


Figure 3.5: In-house highly specific recombinant antibody technology vs. commercial counterparts (supplied by Abcam Ltd.)

3.3.2.2 Assay optimisation studies

As the detection system was limited to an 11-bit ADC reference readout (in the form of '0-2047' fluorescence response units' for the end-user), it was important to identify the system's maximum fluorescent readability threshold. Therefore, the amount of fluorescent antibody required for this assay format was investigated by analysing varying concentrations of primary antibody to ascertain the dynamic range of the system. There are several parameters that primarily influence direct planar assay performance; these include antibody/antigen concentration, contact time and flowrate. These parameters were evaluated for this assay, with a rotational frequency of 35 Hz constant spin rate was used for the final assay procedure. Figure 3.6 illustrates the averaged results ($n = 3$) of a direct binding assay performed on the disc to assess optimal antibody concentration and determined by the system *via* fluorescence at 430 nm.

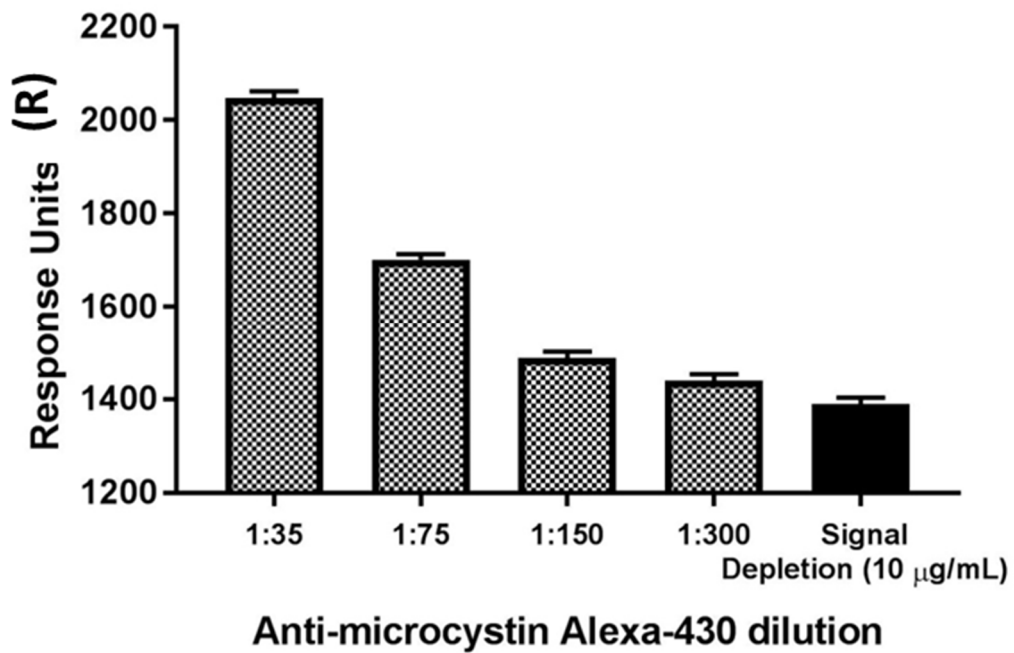


Figure 3.6: Direct binding assay measured by the system.

A set concentration of MC-LR-BSA coated on the test wells of a disc was probed with varying concentrations of the Alexa-430-labelled anti-MC-LR scFv. The scFv were excited fluorescently at 430 nm with the emission signal recorded. The system readout was limited to '0-2047' response units (R), therefore any dilution factor below 1:75 produced a signal outside of the detectable range.

It was observed that the optimum concentration of anti-MC-LR-Alexa-430 labelled-scFv to be used in the assay for MC-LR detection was approximately 40 µg/mL (1/75 dilution), as observed in Figure 3.6. This was subsequently calculated to be approx. 12 µg/mL and 20 µg/mL for anti-DA-Alexa-430 labelled-scFv and STX-Alexa-430 labelled-scFv, respectively. These antibodies will be generically referred to as 'anti-toxin'-Alexa-430 labelled-scFv to avoid repetition. Once the assay conditions were established, and direct binding of the antibody to the surface of the disc was successfully quantified, inter/intra assay studies were performed to develop a calibration curve. Method precision and accuracy for the assay was evaluated using validation standards in the same complex matrix as the study samples; i.e. lake water samples.

3.3.2.3 Performance studies

In order to assess the performance of the system with each of the toxins, a number of studies were conducted to identify the variation between assays readings on the same disc (intra-day) and between separate disc readings on different days (inter-day). Six microfluidic discs, with six assay tests per disc, were manufactured for each toxin. Each of the six assays were set to be injected with varying toxin concentrate (0, 1, 10, 100, 1000, and 10000 ng/mL), resulting in triplicate results (over two separate days) for each concentration. The PMMA discs were treated and functionalised at the test zone with 'toxin'-conjugate, and the control zone with anti-chicken antibody. The incubation zone was coated *via* passive adsorption with 'anti-toxin-Alexa-430 labelled-antibodies. A silanization approach was also deemed the most effective in coating the disc surfaces with the detection molecule of interest, namely, a toxin-BSA conjugate. Issues arose with the level of background noise observed from the un-coated discs. The background noise was circumvented by coating the perimeter of each well with black acrylic paint to negate any inherent optical interference generated from the PMMA discs.

To determine the inter-day variation of results, calibration curves were generated for each toxin in the range 0 – 10000 ng/mL. The co-efficients of variation (CV) values between the inter-day batches were then calculated via calibration curve analysis. For the intra-day studies; lake water aliquots (1 mL) were spiked with toxin at concentrations of 0, 1, 10, 100, 1000, and 10000 ng/mL. Sample progression, through each assay step (see Figure 3.9), was achieved using the spin cycle approach discussed in microfluidic disc characterisation. The sample progression included pass-through of the incubation chamber, where the anti-toxin-Alexa-430 labelled-scFv was coated. This was resuspended by incubation for 5 min with the toxin sample prior to passage over the test chamber, whereby toxin in the sample and immobilized toxin on the disc compete for binding to the anti-toxin scFv. Following resuspension of the antibodies at the incubation-zone (see Figure 3.9), the sample was centrifuged to propel the sample through the test, control and waste chambers respectively.

Binding was fluorescently observed in both the test and control chamber separately. Bound scFv was quantified *via* fluorescence measurement with a 430 nm excitation LED, with the pre-filtered optical range above 475 nm collected, including the emission peak

at 545 nm. Fluorescence measurement occurred after assay completion, with each single fluorescence value programmed to consist of an averaged ($n = 640$, with n sampled every $8 \mu\text{s}$) reading generated every $\sim 0.5 \text{ s}$, with a further averaging of data captured over a 30 s run. The signal generated from the bound scFv was found to be inversely proportional to the amount of toxin present in the test sample. The sample was then passed from the test chamber to the control chamber where scFv was picked up by the control anti-chicken antibody. Once signal could be observed in this control chamber, it was used as a qualitative measure to ensure that the sample had successfully passed through all zones of the disc, thus signifying cessation of the assay. The readings generated from assessment of these lake-water spiked standards formed the calibration curves for each toxin whereby the system's performance could be determined.

To determine the detection capabilities of the system, equal volume lakewater samples were spiked with varying concentrations of 'Toxin' (0, 1, 10, 100, 1000, and 10000 ng/mL). The spiked lakewater samples were individually applied and run through the pre-functionalised PMMA disc. The fluorescent response units (R) of the system were then normalised by dividing the max achievable fluorescence of the blank (0 ng/mL) response (R_0). The intra-assay analysis of each of the toxins, shown in Figure 3.7, was performed in triplicate within the same assay. The observed co-efficients of variation for this assay was $< 0.05\%$, proving considerable quantitative agreement between the intra-assay standards. A best-fit calibration curve was applied to the mean data, with assay accuracy determined by comparing the error of predicted concentrations against known standards. These results are shown in Table 3.

The precision analysis shown in Table 3 demonstrates excellent correlation $< 20\%$ for high concentrations of MC-LR when estimated from the calibration curve. This is evident by the estimated concentration error recorded, from use of the calibration curve for validation standards, down to as low as 100 ng/mL of MC-LR. However, it was noted that assessment of lower levels of MC-LR not as accurate, determined by the larger relative standard deviation. This may be due to steric hindrance effects during the binding event, when low or non-competing levels of MC-LR are present, and full capacity binding of the antibodies at the test zone is attempted(42). Ng *et al.* (43) discuss the use of long flexible linkers such as polyethyleneimine (PEI) and dextran (DEX) being more

favourable for covalent attachment than shorter linkers such as 3-aminopropyltriethoxysilane (APTES), as the long flexible linkers circumvent problems associated with antibody accessibility and steric limitations, which could be a contributing factor to the low sensitivity observed within the assay. Taking these hindrance effects into consideration, and the lower optimum concentration of anti-toxin-Alexa-430 labelled-Ab used for the DA and STX assays, an increased averaged error correlation (Table 3) of < 26% and < 32% respectively, was not unsurprising.

Quantitative immunoassays rely on calibration correlations to determine the analyte concentration in samples from the strength of the signal produced. Figure 3.8 illustrates how the log of analyte concentration is plotted against the percentage antibody bound. The latter is the signal level expressed as a normalised function of the total signal response units per response in the presence of no competitive agent (R/R0)). The bottom graph shown in Figure 3.8 illustrates the assessment of MC-LR down to 1 ng/mL in spiked lake water samples. Intra-day co-efficients of variation (CV) (n= 3) were calculated as < 0.1% for replicates within the same assay (Figure 3.7), and the inter-assay (Figure 3.8) CV (n=2) were calculated as < 0.27% for the average calibration curve of MC-LR. These CV values confirm the reproducibility of the assay. The detection capacity of this assay as observed from the validated standards is approximately 7.2 ng/mL.

Table 3: Precision determination of 'back-calculated' concentration percentage error extrapolated from the calibration curve by estimation of the actual concentrations of free 'toxin' (ng/mL).

Actual toxin concentration	Microcystin recovery variance (expected value ± reported value difference)	Domoic acid recovery variance (expected value ± reported value difference)	Saxitoxin recovery variance (expected value ± reported value difference)
(ng/mL)	(ng/mL) (n=3)	(ng/mL) (n=3)	(ng/mL) (n=3)
10,000	10,000 ± 1,560	10,000 ± 181	10,000 ± 3,640
1,000	1,000 ± 192	1,000 ± 221	1,000 ± 350
100	100 ± 15.5	100 ± 43.6	100 ± 17.6
10	10 ± 3.28	10 ± 4.69	10 ± 4.2
1	1 ± 0.368	1 ± 0.131	n/a

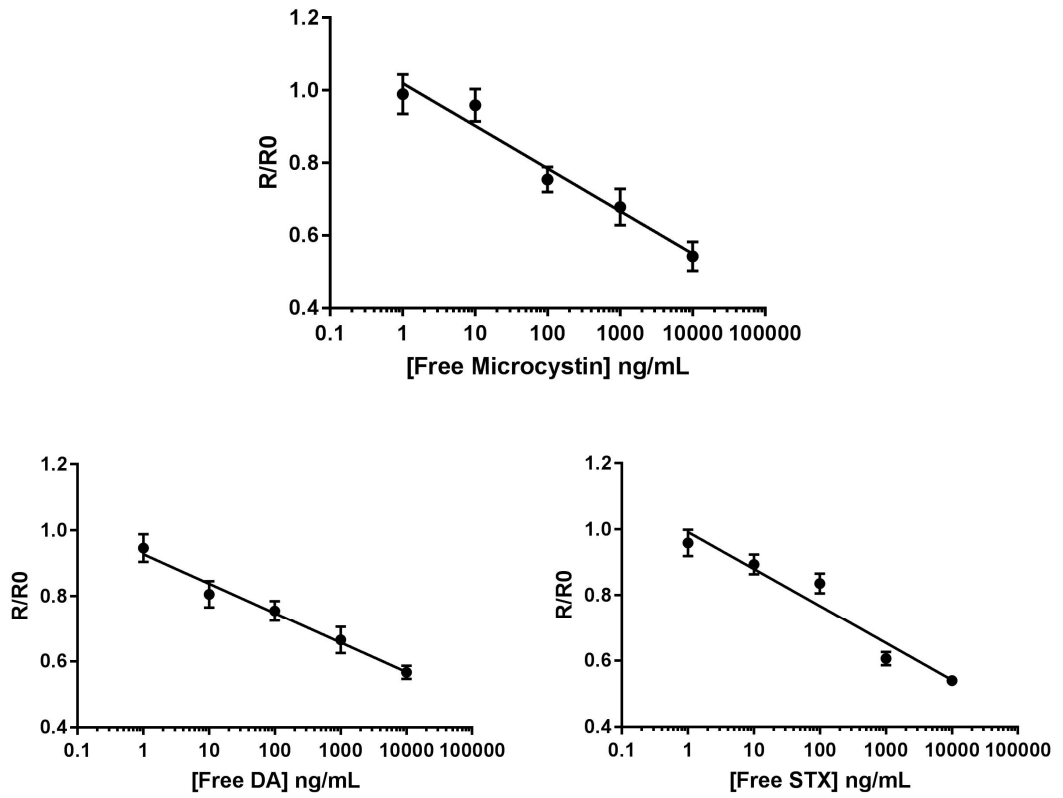


Figure 3.7: Intra-assay analysis (n=3) for microcystin (MC-LR), domoic acid (DA) and saxitoxin (STX) measured on the microfluidic sensor.

Spiked concentrations of 'Toxin' were incubated with anti-toxin-Alexa-430 labelled-scFv. The sample was passed to the test zone to interact with coated toxin conjugate. Signal was observed by fluorescent measurement at the test zone at 430nm.

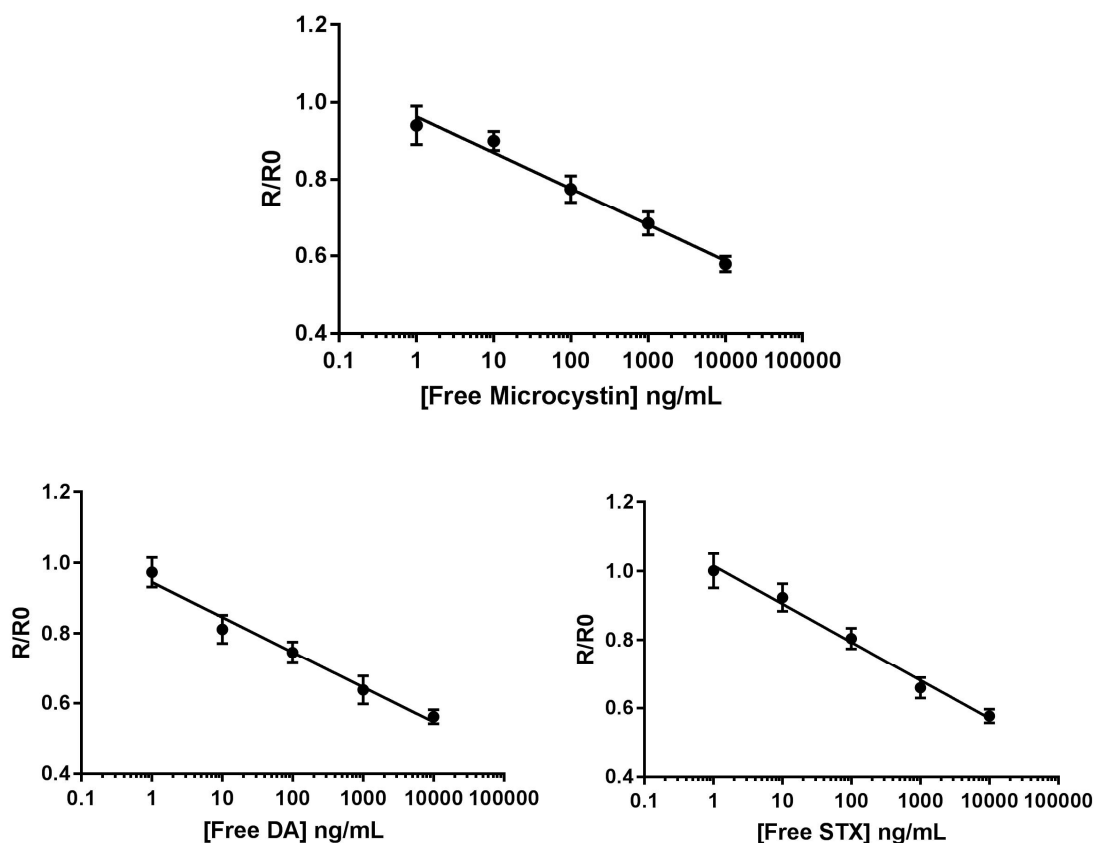


Figure 3.8: Inter-assay analysis for microcystin (MC-LR), domoic Acid (DA) and saxitoxin (STX) measured on the microfluidic sensor.

Lakewater samples spiked with concentrations of DA and STX were incubated with anti-toxin-Alexa-430 labelled antibody. The sample was passed to the test zone to interact with coated Toxin conjugate. Signal was observed by fluorescent measurement at the test zone at 430nm

The limit of detection (LOD) for the system was observed by using **Equation 1**. The LOD was calculated to be 7.2 ng/mL for MC-LR for this assay. This LOD meets the need for an early warning system capable of providing an early warning assessment of bathing water bodies when MC-LR is present, while it is short of the 1 ng/ml detection limit for drinking water currently. The detection limit observed from the inter-day analysis of DA and STX using the detection system was found to be approximately 20 ng/mL and 50 ng/mL respectively. It was also expected that individual optimisations of the antibody/antigen concentration, contact time and flowrate for each of the DA and STX would have further reduced the LOD. The co-efficients of variation of the DA and STX assay from the intra-assay studies (Figure 3.7) were both determined to be less than 0.05 %, with the

precision of the assay determined from the inter-assay studies (Figure 3.8) found to be within 95% and 90% agreement with actual spiked concentrations respectively.

Equation 1: Limit of detection of instrument (LOD)

$$LOD = I_{blank} + 3\sigma_{blank}$$

Where, LOD the concentration of toxin corresponding to the signal intensity, I_{blank} is the mean signal intensity of blank toxin and σ_{blank} is the standard deviation of the blank

Recent detection methods described for the detection of MC-LR include biosensor-based methods (44–47) or ELISA-based methods (48) or even MALDI-TOF (49) analysis. These methods suffer from extensive automation requirements or laborious testing via specially trained personnel, the methods are also not applicable for testing *in-situ* at the ‘point of need’. The qualitative method described herein, illustrates a method for routine use as a future-autonomous rapid warning system for water quality, with results in 30 mins with minimal end-user interaction. This assay represents several notable advantages; firstly, the system is made of inexpensive materials suitable for mass replication, and secondly, the simple design offers the potential to become a rapid and easy-to-use instrument for direct use in the field at the point of need. It has a high within-assay response-reproducibility and a negligible assay turnaround time. The limitations of the proposed assay relate to potential deviations induced to individual discs due to each of the discs currently being manufactured and assembled by hand, which it is hoped in the future can be produced using industry standard assembly lines(50). Also, while the biosensor application within the disc is initially complex, it is hoped that through mass production breakthroughs such as automated assembly line production, that this platform could become significant faster and more cost-effective to produce. This proof of concept system shows detection of low levels of toxins, which makes it highly applicable for use as a warning system for the qualitative assessment of recreational or fishing waters. Due to the system being designed for detection of ‘free toxin’, the addition of a lysing step for extracting toxin from the species for improving the sensitivity of the system requires would be beneficial, and has been previously demonstrated either on disc(32) or through a pre-loading mechanism(51). The system will be coupled with a wireless communications platform, motor and automatic sampler

for use as an automated rapid warning, integrated system. This would include monitoring, analysing, interpreting, and distribution monitoring data, in which continuous real-time detection can be performed for offering generic warning or trigger an alarm as required, similar to the deployable MARIABOX system(38).

3.4 Conclusion

Intoxication events due consumption of contaminated seafood and water supplies due to prevailing marine toxins is becoming a global problem. Ideally, the monitoring of harmful toxins like microcystin (MC-LR), domoic acid (DA) and saxitoxin (STX) should be performed on a device *in-situ*, which is sensitive enough to perform accurate detection toxin outbreaks in a complex aquatic matrix. Currently, there is a high priority for the development of an easy-to-use, rapid, robust and non-expensive devices for monitoring of the required low action level concentrations of toxins. Herein, a rapid system capable of providing an early warning system for the presence of toxic residues in water samples *in-situ* is described. This system is capable of detecting algal toxin residues in lakewater matrices using recombinant antibody technology and immuno-affinity purified antibodies with fluorescent-labelling. The advantages of the system are the incorporation of these elements into a rapid assay for the concurrent detection of three algal toxins at the point of need. The antibodies are produced under minimum cost conditions and made in very large quantities. The instrument provided reproducible dynamic linear ranges and rapid assay times. The rapid fabrication techniques used in disc generation offered a platform, whereby tailoring of the prototype's size, shape, reservoir volume and surface structure for rapid assay integration became feasible. This allowed facilitation of a fully enclosed platform, specifically optimised for minimal end-user interaction. In addition, the disposable discs can be mass produced, allowing convenient and safe 'on site' toxin handling, with future possibilities aimed at fully autonomous system deployment. While these toxin analytes were used as a 'proof of concept' to determine functionality of the system, the system is designed generically to allow for future multiplexing and with testing of numerous toxin variants. This method could alleviate the costly laboratory procedures associated with frequent toxin monitoring.

3.5 Materials and methods

3.5.1 Chemical and biological reagents used

Bis[3-(trimethoxysilyl)propyl]amine (cat no. 413356), Micro90 (cat no. Z281565), ethanol, isopropanol and phosphate buffered saline (PBS) were all obtained from Sigma Aldrich, Ireland Limited, Arklow, County Wicklow, Ireland. 1-Ethyl-3-(3-dimethylaminopropyl)carbodiimide bovine serum albumin (Imject EDC BSA) and 1-Ethyl-3-(3-dimethylaminopropyl)carbodiimide keyhole limpet hemocyanin (Imject EDC KLH) spin conjugation kits were obtained from Fisher Scientific (UK). Alexa Fluor 430 (Alexa-430) fluorescent kit (cat no. A10171) was obtained from Bio-Sciences Ltd., Charlemont Terrace, Crofton Rd, Dún Laoghaire, Dublin, Ireland. MC-LR (cat no. ALX-350-012-M001) was obtained from Enzo life sciences (UK) Ltd. Domoic acid polyclonal antibody was obtained from Abcam Ltd. Cambridge, United Kingdom. Donkey anti-chicken IgY Fab was obtained from Gallus Immunotech (Antibodies-online GMBH). Lake water samples were obtained from Leixlip reservoir in Dublin, Ireland and stored in RNase and DNase free tubes (Fisher Scientific, UK) at 4 degrees. Black acrylic paint (obtained from Tiger Direct™) was also used for biosensor signal enhancement.

3.5.2 Preparation of conjugates and fluorescent antibodies

MC-LR-BSA conjugates and the recombinant anti-MC-LR-Alexa-430 were prepared, as per the method by Murphy *et al.* (52). All animal models used were approved by the Department of Health and Children, Ireland licensing authority under the Cruelty to Animals Act 1876 as amended, for Dublin City University under license ref no. B100/2705. Domoic-Acid and STX conjugates were prepared using an Imject EDC KLH spin conjugation kit (Fisher), as per the manufacturer's instructions. A Leghorn chicken was initially immunised sub-cutaneously with of equal parts solution of DA-KLH/STX KLH conjugate and Freund's complete adjuvant. The final concentration of the initial immunisation was 200 µg/mL. The first boost (day 14) was then administered using 100 µg/mL of each conjugate in PBS, mixed in a 1:1 ratio with Freund's incomplete adjuvant, in a final volume of 1 mL. The final 4 boosts that followed (days 36, 52 and 66) all contained 100 µg/mL of each conjugate and were administered in the same manner as the first boost using incomplete adjuvant. Serum antibodies were isolated from the chicken and subsequently labelled with Alexa-430.

3.5.3 Microfluidic disc manufacturing

The microfluidic disc was designed and developed as a single-assay version of the previously reported multi-toxin detection disc (35). The previously reported multi-toxin detection disc was fluidically optimised for sample metering between three separate assays via pneumatic-based valving with detection performed using a fluorescent-based microscope, whereas this single assay format, shown in Figure 3.9, was fabricated primarily to fully characterise a toxin detection performance on a microfluidic disc platform using an in-house built fluorescence-based complementary system. The microfluidic disc platform was manufactured from poly(methyl methacrylate) (PMMA) sheets and “pressure sensitive adhesive” (PSA) sheets (ARseal™90880), obtained from Radionics™ and Adhesives Research™ respectively. The discs were manufactured through assembling consecutive layers of PMMA and PSA(53–55). The roof was additionally covered using PSA to act as a manual active microfluidic valve layer. The reservoir floor of the biosensor was laser etched to improve binding process (70% power, 60% using Epilog Zing 16, Epilog Laser USA) with the surrounding reservoir walls painted black, using acrylic paint, before full disc assembly.

3.5.4 Preparation of reservoir surface for bio-activation

The PMMA layers of the disc were thoroughly surface cleaned in a class-1000 clean room with the assistance of ultrasonication; A 2% (v/v) solution, consisting of Micro-90™ in deionised water was prepared to remove any present oil, grease, resin and any biological material on PMMA layers prior to assembly. This solution was placed in a heat-sealed bag with the all of the PMMA layers and ultrasonicated at 50°C for 30 min. Subsequently, the PMMA layers were each rinsed three times, with deionised (DI) water, followed by isopropanol. Finally, the PMMA layers were then rinsed a final time with DI water and dried using nitrogen. Following this, the PMMA and PSA disc layers were assembled as two halves (the lower half (LH) and upper half (UH)), with a centre point at the floor of the reservoirs, leaving the reservoir floors exposed on the LH for antibody immobilisation treatment. After cleaning and assembly, the two halves of the discs were then placed in heat-sealed bags for storage, while the biosensor components were being integrated to the LH of the disc. Following this integration, the two halves were then combined to form a single disc.

3.5.5 Amine surface functionalisation of biosensor reservoir floor by liquid phase

Following the cleaning process, the LH of several discs were then exposed to a microwave-induced O₂ plasma, allowing multiple reservoir floor surfaces to be treated simultaneously, using the plasma cleaner (Harrick plasma, USA). The O₂ gas stream was regulated by the integrated mass flow controller until the required operating pressure within the chamber adjusted to approximately 1000 mT. The exposure duration of the LH of the discs were exposed to the O₂ plasma for 10 min on the 'high setting'. A 3% APTES solution was prepared in 98% ethanol to functionalise the PMMA disc reservoirs. This solution was then immediately applied to the detection reservoirs (reservoir 3 "Test" and reservoir 4 "Control") of the surface-activated discs to provide a binding bridge between the surface oxidation of the reservoir floor, and hydroxylation (-OH groups) of the toxin conjugates and toxin-specific antibodies. The discs were then incubated at room temperature for 1 h in a fumehood in a 15 cm diameter petri dish with cover. Following functionalisation, the discs were then cleaned twice, using a solution of 98% ethanol under ultrasonication for 15 min. The discs were baked at 60°C for 2 h in an oven, where significant cracking of the PMMA discs was noted at high temperatures. The discs were then allowed to cool to room temperature, at which point the toxin conjugate/antibodies were added to reservoir floor.

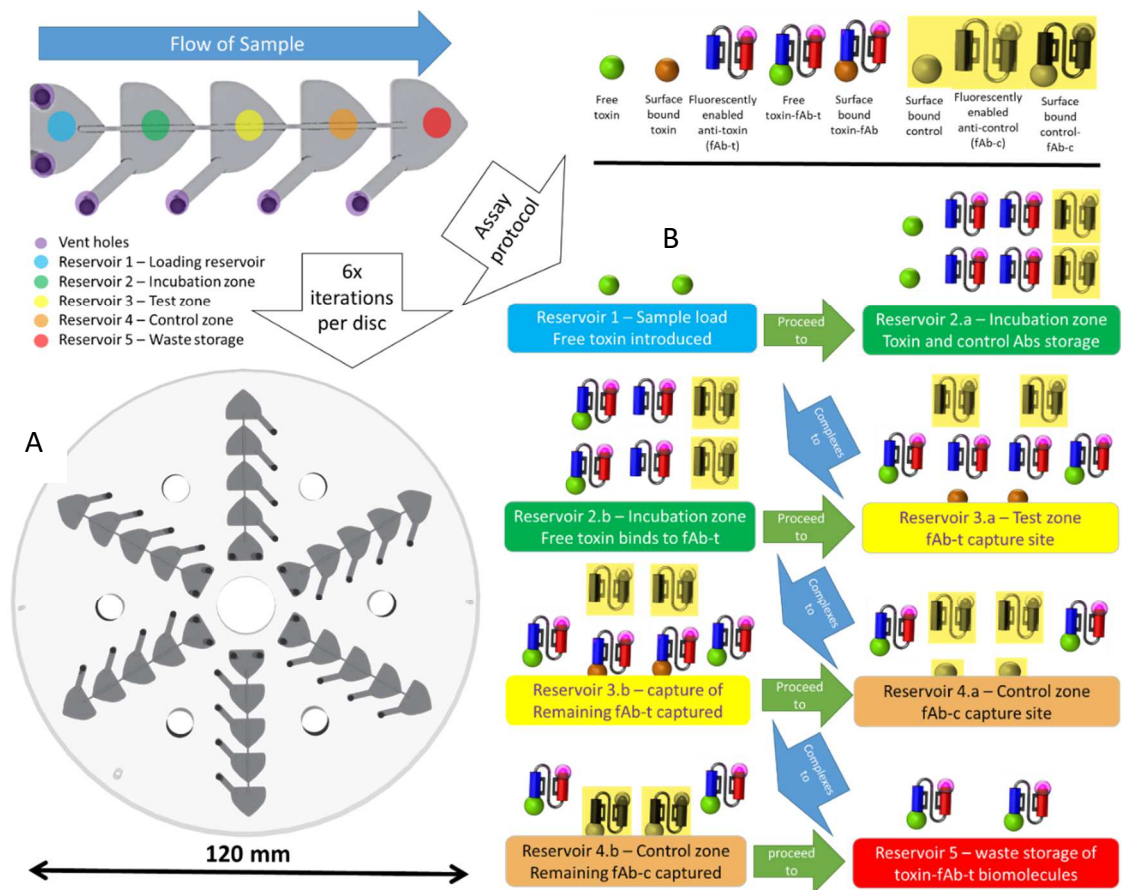


Figure 3.9: The competitive toxin detection assay protocol represented by functional microfluidic reservoirs.

A) The microfluidic assay structure consists of five reservoirs (loading, incubation, test, control and waste) in radial alignment connected by microchannels, each with separate ventilation systems, and 6 replicates per disc respectively. Each reservoir is a single step in the competitive assay protocol (B). This inverse assay demonstrates how a loaded sample, containing pre-lysed microcystis, interacts with the reservoir of fluorescent (Alexa 430)-anti-MC-LR antibodies (Abs), with the control Abs available for quantification through a separate capture site to act as a positive control.

3.5.6 Microfluidic disc characterisation

The fluidic motion on the microfluidic discs was assessed using a customised, in-house developed “spin stand”(56) (shown in Figure 3.10), as previously demonstrated by Kirby *et al.*(57). Briefly, the centrifugation of the discs was regulated using a computer operated spindle motor (Faulhaber Minimotor SA, Switzerland). A highly sensitive, short-exposure camera (Pixelfly, PCO, Germany) was combined with a stroboscopic-programmed light source (Drelloscop 3244, Drello, Germany), which was synchronised

with the spindle motor using in-house built electronics, for visualising on-disc fluidic performance under centrifugation. Furthermore, as the roof was covered using PSA to act as a manual active microfluidic valve layer, actuation of the microvalves was attained by pin puncture, allowing pneumatic pressure release which had prevented sample progression to occur. In summary, the discs were spun at 35 Hz for 30 s to transport sample to the subsequent reservoir, followed by halting of the disc for the required incubation period per reservoir. After this wait period, the sequential manual microvalve was opened. This cycle repeated until the sample had successfully completed the full assay protocol.

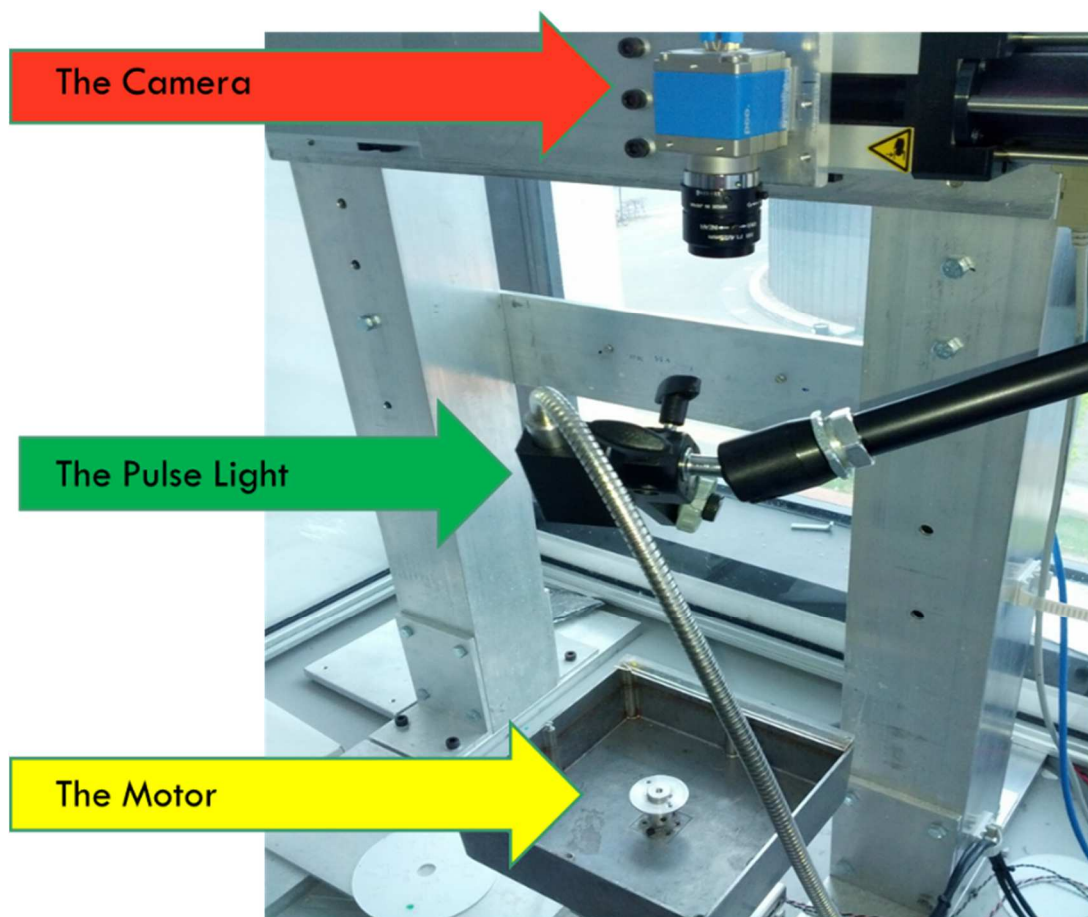


Figure 3.10: The 'Spin stand' used for microfluidic characterisation.

This observation setup had a triggering mechanism for actuation of camera and pulse light every $2\pi n$ rotations (whereby n is a natural number and dependant on rotational speed). This give the viewer the perspective of a stationary disc with fluidic motion, giving precise liquid characterisation whilst simultaneously running assay to be tested in the detection system.

3.5.7 Optimisation of antibody concentration

Preliminary studies were performed to determine the optimal labelled-antibody concentration for use in the final assay. An optimal antibody concentration will provide sufficient signal observation when interacted with the immobilised toxin conjugate on the surface, and subsequently measured fluorescently at 430 nm on the system. Varying dilutions of each antibody from 1/35, 1/75, 1/150, 1/300 were assessed fluorescently, by applying 100 μ L of each to the inlet channel on a functionalised disc and spinning the disc on a spin stand at 35 Hz for 1 min. A depletion sample which included 10 μ g/mL of free toxin with 1/75 dilution of antibody at equal volumes was assessed also. The amount of bound antibody was determined via fluorescent measurement at 430 nm.

3.5.8 Toxin Conjugate and control antibody binding to biosensor surfaces

The Alexa-430 labelled specific Ab's were coated on the 2nd radially-aligned 'incubation zone' reservoir (see Figure 3.9) where 100 μ L of optimally determined antibody concentration was added (40 μ g/mL). As this reservoir was not functionalised prior to coating, the antibody was passively adsorbed onto the reservoir floor of the incubation zone. The sequential release of the sample was then required for antibody resuspension within the incubation zone. MC-LR, conjugated to BSA (1 μ g/mL) was prepared in a PBS solution, where 100 μ L was then added to each of the 3rd radially-aligned 'test' reservoir (see Figure 3.9). 100 μ L of a commercially available anti-chicken IgY (H+L), at approximately 10 μ g/mL (Gallus Immunotech Inc., Canada), was added to each of the 4th radially-aligned 'control' reservoir (see Figure 3.9). The coated discs were stored at 4°C covered for 12 h. To avoid any non-specific binding from occurring on the biosensor reservoir floor, the remaining activated amine sites were then subsequently blocked with 200 μ L of 3% BSA (in PBS solution) added to each reservoir. The blocking agent was left to incubate at 37°C for 1 h, after which it was aspirated. Finally, the disc assembly was completed and the prepared disc was ready for toxin determination.

The exact same procedure to determine the calibration curve for DA was followed as was outlined previously for the MC-LR calibration curve. The variables used for DA include approximately 12 μ g/mL of antibody as assessed via ELISA. The conjugate coated on the test well was 1 μ g/mL of DA-BSA conjugate prepared in-house in DCU. The control

antibody used in the control well was the anti-chicken IgY (H+L) 100 µL, a commercial antibody from Gallus Immunotech Inc., Canada.

Similarly, the exact same procedure to determine the calibration curve for STX was followed as was outlined in section for the MC-LR calibration curve. The variables used for STX include approximately 20 µg/mL of antibody as assessed via ELISA. The conjugate coated on the test well was 1 µg/mL of STX-BSA conjugate prepared in-house in DCU. The control antibody used in the control well was the anti-chicken IgY (H+L) 100 µL, a commercial antibody from Gallus Immunotech Inc., Canada.

3.5.9 Manufacture of the detection platform

The detection system shown in Figure 3.11, was 3D-printed from acrylonitrile butadiene styrene (ABS), to hold the disc, with an incorporated fluorescent detection apparatus to separately capture fluorescence values at both reservoirs three and four on the disc (see Figure 3.9). The detection system utilised a top-down detection configuration with a 405 nm excitation LED (cat no. 713-4898, Radionics Ltd Ireland), a 475 nm long pass filter (cat no. 64-617, Edmund Optics Ltd) and a photo-LED emission detector sensitive from 420–675 nm (cat no. 708-2813, Radionics Ltd Ireland). This in-house developed system was controlled by a Pololu Wixel microcontroller (cat no. 785, Cool Components Ltd), which transmits communications to a user interface via USB and/or wirelessly (using a second Pololu Wixel microcontroller). While this model does not contain a motor, as microfluidic characterisation was done using the previously described 'spin stand', motor incorporation will be done in future models similarly to those described by *Duffy et al.*(26,27,37)

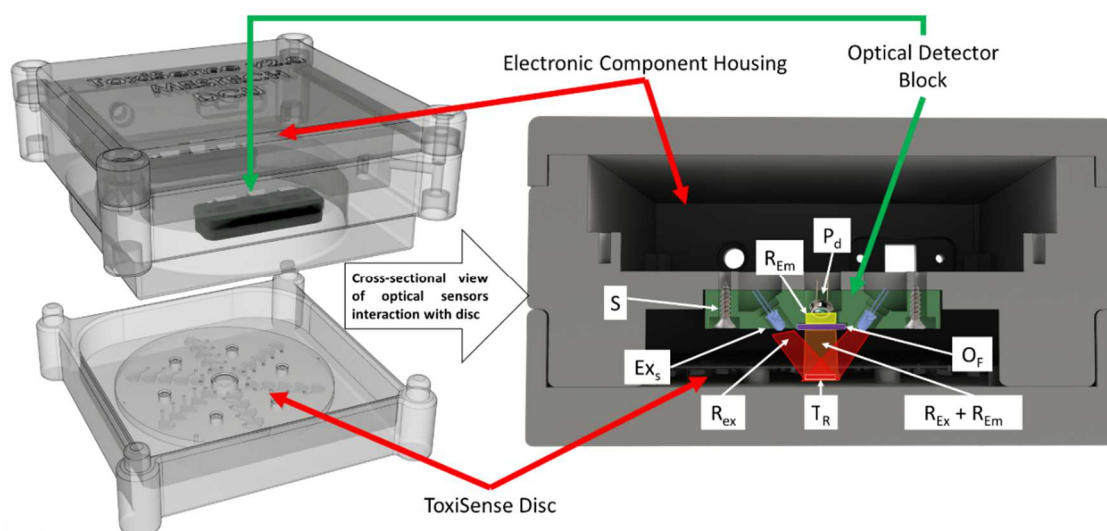


Figure 3.11: The Detection system.

This 3-D printed system was designed to allow in-situ detection of MC-LR applied to the Lab-On-A-Disc (LOAD) platform. It is configured for a top-down detection method of the test reservoir (T_R) (see reservoir three in see Figure 3.9) with a 405 nm (R_{ex}) excitation source (EX_s), a 475 nm long pass filter (O_F) and a photo-LED emission detector (P_d) for collecting the emission radiation (RE_M). The optical components all stored in a swappable 'Optical Detection Block' and is adhered to the bottom of the 'Electronic Component Housing' by screw (S). This in-house developed system is controlled by a Pololu Wixel Microcontroller, stored in the 'Electronic Component Housing', which can transmit communications to user via USB and/or wirelessly (using a second Pololu Wixel).

3.5.10 Measurement of toxin binding

The preliminary assay was performed at room temperature in the lab using the developed system box connected to a portable laptop facilitating analysis via the Pololu Wixel software. The analysis was performed by adding 100 μ L of the lake water sample via pipette to the sample load zone on the disc. When spun at 35 Hz the water sample travels from the sample loading zone into the incubation zone. The water sample is allowed to interact with the now reconstituted antibody in the incubation zone for ten minutes and the disc is spun again at 35 Hz. The water sample with potential toxin and resuspended anti-toxin antibody then advanced to the test zone, whereby toxin in the water sample and toxin coated on the wells of the test zone compete for binding to the fluorophore conjugated antibody. Bound antibody on the wells of the test zone is inversely proportional to the amount of toxin present in the water sample. The water sample continues through to the control zone, whereby anti-chicken antibodies capture

the fluorophore labelled anti-chicken antibodies, this signifies successful transition of the water sample from the loading zone through the incubation and test zones and to the control zone. The water sample then flows from the control zone to the waste zone, and the fluorescent readings are measured. Readings from the system are taken every 0.5 seconds, these values are exported into excel and an average of 10 measurements is taken for each fluorescent analysis.

3.6 Acknowledgment

This work was supported by the FP7 EU-funded MARIABOX project. The MARIABOX project receives funding from the European Union Seventh Framework Programme - Grant Agreement No: 614088.

3.7 Author Information

Ivan Maguire; ivan.maguire2@dcu.ie, Jenny Fitzgerald; jenny.fitzgerald@dcu.ie,
Brendan Heery; brendanheery@gmail.com, Charles Nwankire;
Charles.nwankire@gmail.com, Richard O' Kennedy; richardokennedy@gmail.com,
Jens Ducreé, jens.ducree@dcu.ie, Fiona Regan; Fiona.regan@dcu.ie.

3.8 Supplementary Information

- Additionally, a **Supplementary Video**² is included to demonstrate visualisation of fluidic motion on disc platform using the “spin stand’ method

² Supplementary video included in publication available at:
<https://drive.google.com/open?id=16BV2FcXIBdJiAKtJnNN8UWaMn6SjPLS1>

3.9 References

1. Hudnell HK, Dortch Q, Zenick H. An overview of the interagency, International Symposium on Cyanobacterial Harmful Algal Blooms (ISOC-HAB): advancing the scientific understanding of freshwater harmful algal blooms. In: Cyanobacterial Harmful Algal Blooms: State of the Science and Research Needs. Springer; 2008. p. 1–16.
2. Paerl HW, Huisman J. Blooms like it hot. *Science*. 2008;320(5872):57.
3. World Health Organization, Chorus I, Bartram J. Toxic Cyanobacteria in Water: A guide to their public health consequences, monitoring and management. Retrieved March. E & FN Spon; 1999. 400 p.
4. Carmichael W. A world overview—One-hundred-twenty-seven years of research on toxic cyanobacteria—Where do we go from here? In: Cyanobacterial harmful algal blooms: State of the science and research needs. Springer; 2008. p. 105–25.
5. Mackintosh C, Beattie K a., Klumpp S, Cohen P, Codd G a. Cyanobacterial microcystin-LR is a potent and specific inhibitor of protein phosphatases 1 and 2A from both mammals and higher plants. *FEBS Lett*. 1990;264(2):187–92.
6. Rinta-Kanto JM, Konopko E a., DeBruyn JM, Bourbonniere R a., Boyer GL, Wilhelm SW. Lake Erie Microcystis: Relationship between microcystin production, dynamics of genotypes and environmental parameters in a large lake. *Harmful Algae*. 2009;8(5):665–73.
7. Azevedo SMF. FO, Carmichael WW, Jochimsen EM, Rinehart KL, Lau S, Shaw GR, et al. rober. *Toxicology*. 2002;181(December):441–6.
8. Lefebvre KA, Robertson A. Domoic acid and human exposure risks: a review. *Toxicon*. 2010;56(2):218–30.
9. Perl TM, Bédard L, Kosatsky T, Hockin JC, Todd ECD, Remis RS. An outbreak of toxic encephalopathy caused by eating mussels contaminated with domoic acid. *N Engl J Med*. 1990;322(25):1775–80.

10. Bates SS. Domoic acid producing diatoms: another genus added. *J Phycol.* 2000;36(6):978–83.
11. Wright JLC, Boyd RK, Freitas ASW de, Falk M, Foxall RA, Jamieson WD, et al. Identification of domoic acid, a neuroexcitatory amino acid, in toxic mussels from eastern Prince Edward Island. *Can J Chem.* 1989;67(3):481–90.
12. Garthwaite I, Ross KM, Miles CO, Hansen RP, Foster D, Wilkins AL, et al. Polyclonal antibodies to domoic acid, and their use in immunoassays for domoic acid in sea water and shellfish. *Nat Toxins* [Internet]. 1999 May 26;6(3-4):93–104. Available from: [https://doi.org/10.1002/\(SICI\)1522-7189\(199805/08\)6:3/4%3C93::AID-NT15%3E3.0.CO](https://doi.org/10.1002/(SICI)1522-7189(199805/08)6:3/4%3C93::AID-NT15%3E3.0.CO)
13. Stommel EW, Watters MR. Marine neurotoxins: Ingestible toxins. *Curr Treat Options Neurol.* 2004;6(2):105–14.
14. Fitzgerald JD, Cunliffe DA, Burch MD. Development of health alerts for cyanobacteria and related toxins in drinking water in South Australia. *Environ Toxicol* [Internet]. 1999 Jan 14;14(1):203–9. Available from: [https://doi.org/10.1002/\(SICI\)1522-7278\(199902\)14:1%3C203::AID-TOX26%3E3.0.CO](https://doi.org/10.1002/(SICI)1522-7278(199902)14:1%3C203::AID-TOX26%3E3.0.CO)
15. MacKenzie L, Beuzenberg V, Holland P, McNabb P, Selwood A. Solid phase adsorption toxin tracking (SPATT): a new monitoring tool that simulates the biotoxin contamination of filter feeding bivalves. *Toxicon.* 2004;44(8):901–18.
16. MacKenzie LA. In situ passive solid-phase adsorption of micro-algal biotoxins as a monitoring tool. *Curr Opin Biotechnol.* 2010;21(3):326–31.
17. Chianella I, Piletsky SA, Tothill IE, Chen B, Turner APF. MIP-based solid phase extraction cartridges combined with MIP-based sensors for the detection of microcystin-LR. *Biosens Bioelectron.* 2003;18(2):119–27.
18. Chen K, Liu M, Zhao G, Shi H, Fan L, Zhao S. Fabrication of a novel and simple microcystin-LR photoelectrochemical sensor with high sensitivity and selectivity. *Environ Sci Technol.* 2012;46(21):11955–61.

19. Yan F, Erdem A, Meric B, Kerman K, Ozsoz M, Sadik OA. Electrochemical DNA biosensor for the detection of specific gene related to *Microcystis* species. *Electrochem commun* [Internet]. 2001 May [cited 2017 Mar 11];3(5):224–8. Available from: <http://linkinghub.elsevier.com/retrieve/pii/S1388248101001497>
20. Ruiyi L, Qianfang X, Zaijun L, Xiulan S, Junkang L. Electrochemical immunosensor for ultrasensitive detection of microcystin-LR based on graphene–gold nanocomposite/functional conducting polymer/gold nanoparticle/ionic liquid composite film with electrodeposition. *Biosens Bioelectron*. 2013;44:235–40.
21. Queirós RB, Silva SO, Noronha JP, Frazão O, Jorge P, Aguilar G, et al. Microcystin-LR detection in water by the Fabry–Pérot interferometer using an optical fibre coated with a sol–gel imprinted sensing membrane. *Biosens Bioelectron*. 2011;26(9):3932–7.
22. Ding Y, Mutharasan R. Highly sensitive and rapid detection of microcystin-LR in source and finished water samples using cantilever sensors. *Environ Sci Technol*. 2010;45(4):1490–6.
23. Long F, He M, Zhu AN, Shi HC. Portable optical immunosensor for highly sensitive detection of microcystin-LR in water samples. *Biosens Bioelectron*. 2009;24(8):2346–51.
24. Cleary J, Slater C, McGraw C, Diamond D. An autonomous microfluidic sensor for phosphate: On-site analysis of treated wastewater. *IEEE Sens J*. 2008;8(5):508–15.
25. Cleary J, Maher D, Diamond D. Development and Deployment of a Microfluidic Platform for Water Quality Monitoring. In: Mukhopadhyay SC, Mason A, editors. *Smart Sensors for Real-Time Water Quality Monitoring SE - 6* [Internet]. Springer Berlin Heidelberg; 2013. p. 125–48. (Smart Sensors, Measurement and Instrumentation; vol. 4). Available from: http://dx.doi.org/10.1007/978-3-642-37006-9_6
26. Duffy G, Maguire I, Heery B, Nwankire C, Ducrée J, Regan F. PhosphaSense: A fully integrated, portable lab-on-a-disc device for phosphate determination in water. *Sensors Actuators B Chem*. 2017;246:1085–91.

27. Duffy G. Development and optimisation of colourimetric microfluidic sensors for water quality monitoring, Phd Thesis [Internet]. Dublin City University; 2017. Available from: <http://doras.dcu.ie/22045/>
28. Beyor N, Seo TS, Liu P, Mathies RA. Immunomagnetic bead-based cell concentration microdevice for dilute pathogen detection. *Biomed Microdevices*. 2008;10(6):909–17.
29. Dharmasiri U, Witek MA, Adams AAA, Osiri JJK, Hupert MML, Bianchi TTS, et al. Enrichment and detection of *Escherichia coli* O157: H7 from water samples using an antibody modified microfluidic chip. *Anal Chem*. 2010;82(7):2844–9.
30. Nandagopal MSG, Antony R, Rangabhashiyam S, Selvaraju N. Advance approach on environmental assessment and monitoring. *Res J Chem Environ*. 2014;18(7):7.
31. Ducreé J, Haeberle S, Lutz S, Pausch S, Zengerle R, Stetten F Von, et al. The centrifugal microfluidic Bio-Disk platform. *J Micromechanics Microengineering* [Internet]. 2007 Jul 1 [cited 2013 Nov 7];17(7):S103–15. Available from: <http://dx.doi.org/10.1088/0960-1317/17/7/s07>
32. Burger R, Ducreé J. Handling and analysis of cells and bioparticles on centrifugal microfluidic platforms. *Expert Rev Mol Diagn* [Internet]. 2012 May;12(4):407–21. Available from: <http://www.ncbi.nlm.nih.gov/pubmed/22616705>
33. Czugala M, Gorkin III R, Phelan T, Gaughran J, Curto VF, Ducreé J, et al. Optical sensing system based on wireless paired emitter detector diode device and ionogels for lab-on-a-disc water quality analysis. *Lab Chip*. 2012;12(23):5069–78.
34. Hwang H, Kim Y, Cho J, Lee JY, Choi M-SS, Cho Y-KK. Lab-on-a-disc for simultaneous determination of nutrients in water. *Anal Chem*. 2013;85(5):2954–60.
35. Maguire I, Fitzgerald J, McPartlin D, Heery B, Murphy C, Nwankire C, et al. A centrifugal microfluidic-based approach for multi-toxin detection for real-time marine water-quality monitoring. In: *OCEANS 2017 - Aberdeen*. 2017. p. 1–8.
36. Kim T-H, Abi-Samra K, Sunkara V, Park D-K, Amasia M, Kim N, et al. Flow-enhanced electrochemical immunosensors on centrifugal microfluidic platforms. *Lab Chip*

- [Internet]. 2013;13(18):3747–54. Available from: <http://pubs.rsc.org/en/Content/ArticleHTML/2013/LC/C3LC50374G%5Cnhttp://dx.doi.org/10.1039/C3LC50374G%5Cnhttp://www.ncbi.nlm.nih.gov/pubmed/23900555>
37. Duffy G, Maguire I, Heery B, Gers P, Ducreé J, Regan F. ChromiSense: A colourimetric lab-on-a-disc sensor for chromium speciation in water. *Talanta* [Internet]. 2018 Sep [cited 2017 Sep 26];178(Supplement C):392–9. Available from: <http://www.sciencedirect.com/science/article/pii/S0039914017310081>
 38. Bonasso M, Barattini P, Isticato R, Donadio G, Giusti A, Philimis P, et al. MariaBox: First prototype of a novel instrument to observe natural and chemical pollutants in seawater. In: *OCEANS 2017 - Aberdeen*. 2017. p. 1–5.
 39. Nakayama M. Disc changer and disc holder and box for use with such a changer. Google Patents; 1985.
 40. Kadrmas KA. Automatic disc changer apparatus [Internet]. Google Patents; CA2024839A1, 1991. Available from: <https://patents.google.com/patent/CA2024839A1>
 41. Yankowski CJ. Compact disc changer utilizing disc database [Internet]. Google Patents; CA2227519A1, 1998. Available from: <https://patents.google.com/patent/CA2227519A1/en>
 42. Helmerhorst E, Chandler DJ, Nussio M, Mamotte CD. Real-time and label-free bio-sensing of molecular interactions by surface plasmon resonance: a laboratory medicine perspective. *Clin Biochem Rev*. 2012;33(4):161.
 43. Ng AHC, Uddayasankar U, Wheeler AR. Immunoassays in microfluidic systems. *Anal Bioanal Chem*. 2010;397(3):991–1007.
 44. Zhang J, Sun Y, Dong H, Zhang X, Wang W, Chen Z. An electrochemical non-enzymatic immunosensor for ultrasensitive detection of microcystin-LR using carbon nanofibers as the matrix. *Sensors Actuators B Chem*. 2016;233:624–32.

45. Tan F, Saucedo NM, Ramnani P, Mulchandani A. Label-free electrical immunosensor for highly sensitive and specific detection of microcystin-Lr in water samples. *Environ Sci Technol*. 2015;49(15):9256–63.
46. Catanante G, Espin L, Marty J-L. Sensitive biosensor based on recombinant PP1 α for microcystin detection. *Biosens Bioelectron*. 2015;67:700–7.
47. Devlin S, Meneely JP, Greer B, Campbell K, Vasconcelos V, Elliott CT. Production of a broad specificity antibody for the development and validation of an optical SPR screening method for free and intracellular microcystins and nodularin in cyanobacteria cultures. *Talanta*. 2014;122:8–15.
48. Liu L, Xing C, Yan H, Kuang H, Xu C. Development of an ELISA and immunochromatographic strip for highly sensitive detection of microcystin-LR. *Sensors*. 2014;14(8):14672–85.
49. Kadlec KM, Turczyn A, Grant J. Comparative Analysis of ELISA and MALDI-TOF Mass Spectrometry Methods for Microcystins in Freshwater Samples. *FASEB J*. 2016;30(1 Supplement):1121–2.
50. Chin CD, Linder V, Sia SK. Commercialization of microfluidic point-of-care diagnostic devices. *Lab Chip*. 2012;12(12):2118–34.
51. Regan F, Fitzgerald J, Murphy C, Maguire I, O’Kennedy R. Convenient ‘one-step’ extraction method for autonomous sensing of marine algal toxins. In: *OCEANS 2017-Aberdeen*. IEEE; 2017. p. 1–5.
52. Murphy C, Stack E, Krivelo S, McPartlin D a., Byrne B, Greef C, et al. Detection of the cyanobacterial toxin, microcystin-LR, using a novel recombinant antibody-based optical-planar waveguide platform. *Biosens Bioelectron* [Internet]. 2015;67:708–14. Available from: <http://linkinghub.elsevier.com/retrieve/pii/S0956566314008380>
53. Becker H, Locascio LE. Polymer microfluidic devices. *Talanta*. 2002;56(2):267–87.

54. Bartholomeusz DA, Boutté RW, Andrade JD. Xurography: rapid prototyping of microstructures using a cutting plotter. *J Microelectromechanical Syst.* 2005;14(6):1364–74.
55. Nayak NC, Lam YC, Yue CY, Sinha AT. CO₂-laser micromachining of PMMA: the effect of polymer molecular weight. *J Micromechanics Microengineering.* 2008;18(9):95020.
56. Grumann M, Brenner T, Beer C, Zengerle R, Ducrée J. Visualization of flow patterning in high-speed centrifugal microfluidics. *Rev Sci Instrum.* 2005;76(2):25101.
57. Kirby D, Siegrist J, Kijanka G, Zavattoni L, Sheils O, O’Leary J, et al. Centrifugomagnetophoretic particle separation. *Microfluid Nanofluidics.* 2012;13(6):899–908.

Chapter 4: Enabling fluidic predictability using a pneumatic valve enhancement strategy for highly integrated Lab-on-a-disc platforms

Chapter Foreword:

In order to further build on the toxin detection strategy and make it compatible for incorporation within the *Marine environmental in-situ assessment and monitoring toolBox 'MARIABOX' in-situ*, there is a need for development of an automation mechanism for the centrifugal microfluidic platform. Inclusion of this mechanism would additionally benefit non-specialist users for potential on site sampling. Therefore, the purpose of this chapter is tackle some of these needs through the investigation of a highly reliable, yet low-complexity, autonomous microfluidic valve mechanism. Firstly, the reader will be presented with the background information of current microfluidic valving mechanisms. This will be followed by an introduction to a novel pneumatic microvalve mechanism, and the extensive characterisation process used to develop a corresponding rotational valve actuation program. The combination of both these elements results in a powerful, easy-to-use microvalve mechanism for automation of centrifugal microfluidic platforms. Also, with the requirement of the MARIABOX platform for storage and use of manually, mass produced centrifugal microfluidic prototypes, this study also investigated the recalibrations required of the disk rotational program in order to maximise complete assays due to potential misalignments and unintentional variations in pneumatic chamber size.

It was found that using a standard modelling strategy for liquid state actuation was predicted to be unsuccessful for as high as ~48% of the microvalves used. This model

was then modified by shifting the model trend based on both the highest averaged and raw actuation values observed. This resulted in an improvement of 72% of predictability of valves in the case of the averaged data set, with up to 100% improvement using the raw data.

Summary of the nature and extent of candidate's work present in this chapter:

First author, initiation, key ideas, disc fabrication (*collaboration with Kevin Alazet and Niamh Aine Kilcawley*), data collection, data analysis (*collaboration with Prof. Turlough Downes*), manuscript development and writing up.

Enabling fluidic predictability using a pneumatic valve enhancement strategy for highly integrated Lab-on-a-disc platforms

Ivan Maguire, Kevin Alazet, Niamh Aine Kilcawley, Turlough Downes, Jens
Ducrée, Fiona Regan

The article was received on 5 June 2018. (subject to change based on journal recommendations)

Sensors and Actuators B: Chemical

4.1 Abstract

Fluid flow control is key for defining the sequence and timing of liquid handling protocols at the backbone of automating bioanalytical protocols for sample preparation and detection on Lab-on-a-disc (LOAD) platforms. The requirements on the reliability of the valving techniques significantly increases with the degree of functional integration and parallelisation of liquid handling steps. During the prototyping stage, simplification of microfluidic systems can initially benefit the assay optimisation, but to further improve the cost-effectiveness of the system, multi-iteration integration of the desired assay protocols is desirable. It would also be advantageous for synchronised multi-assay execution to occur in the device as it would reduce the overall runtime duration of microsystem protocol. Therefore, achieving a successful highly-integrated microsystem with synchronised multi-assay execution, reliable and predictable microfluidic valves are essential. We present here a characterisation of the operational inconsistencies of microfluidic features, with particular emphasis on a microfluidic pneumatic valve strategy, due to rapid-prototyping manufacturing process. In this paper, as part of the liquid behavioural model, characterisation of set microfluidic features was conducted on a centrifugal platform at varying drive forces and radii from the centre of rotation. These were aimed at enhancing current dissolvable film-based microvalve strategies. The study involved three liquid phase changes of interest; from 'loaded liquid' to

'normalisation' against a centrifugal force, from 'normalisation' of liquid to liquid 'passthrough' in microchannels, and from liquid 'passthrough' to a 'compression' of a pneumatic chamber, where a dissolvable microvalve would be suitably positioned. These models were then calibrated to be used as a rotational frequency protocol for autonomous use, with demonstration of the MariaBox Platform used as an example. The paper shows that the predictability of these liquid phase changes, through a 4.5-7 Hz increase in rotational frequency of the liquid phase change base models, can experience up to ≈ 72 -100% improvement, respectively. This improvement in reliability will significantly enhance the ability of LOAD platform for performing assay protocols in autonomous, *in-situ* environments. This work aims to promote more efficient and effective use of LOAD-based platforms as autonomous, reliable and robust detection strategies.

4.2 Introduction

There is significant interest in the development of micron-scale integrated chemical/biological analytical devices, also referred to as Lab-on-a-Chip systems(1–3). The development history of microfluidic-enabled solutions involves a number of fields such as molecular biology and analysis, and microelectronics(4). Microfluidic systems, which can perform bio-analytical assays, are generally reported as three primary types of platforms; Lab-On-A-Chip (LOC)(5–7), Lab-On-A-Disc (LOAD)(1,2,8,9) (Figure 4.1), and paper-fluidic platforms(10–13). The specific role of these devices is to perform a desired biological/chemical required to conduct specific assay protocol which would normally be conducted within a laboratory environment. This requires the devices to be capable of performing experimental functions such as sample transportation(5,8), separation(14–16), reagent mixing(17) and storage(18,19), heating(20) and detection(9,21). To conduct these experimental functions for the required assay duration, integration of protocol-required time delays is essential for the assay success. This can be achieved through the addition of reliable pumping and/or valving mechanisms. In bio and chemical assays, these pumping systems can be very complex and therefore, extensive efforts have been made to develop simple and reliable micro pumping/valving schemes(22) that can be employed in microfluidic systems. There are

a number of approaches which can be taken in order to integrate valving onto a microfluidic platform, but they can usually be split into two primary categories(22,23), active microvalves and passive microvalves.

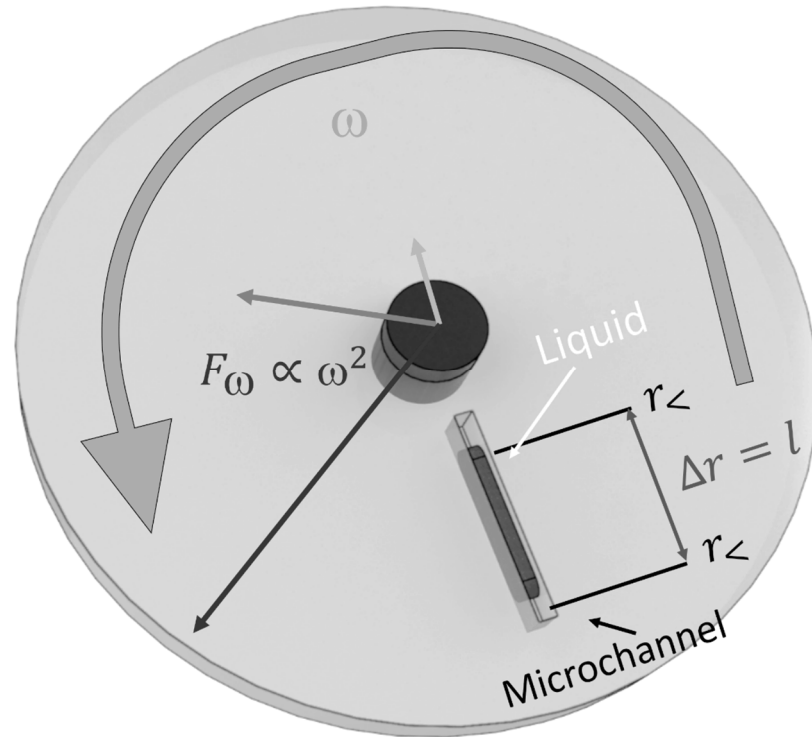


Figure 4.1: The Lab-On-A-Disc (LOAD) platform concept.

This illustration demonstrates how the centrifugal force (F_{ω}) increases radially on a disc during centrifugation, with constant rotational frequency ω . Microfeatures, such as microchannels and valves which are radially positioned on disc, will have a constant activation force based on their physical parameters. Therefore, a constant F_{ω} should be acting on the sample during microfeature interaction to maintain reliability, which can be tuned by decreasing ω as radius r increases. (Authors own image)

Active microvalves are microfluidic valves which require a physical parameter change by external or separate interaction for actuation to occur. The actuation method can be mechanical (magnetic(24), electrical(25), piezoelectric(26), thermal(27), bistable(28)), non-mechanical (electrochemical(29), phase change(30,31), rheological(32)) and external (modular(33), pneumatic(34)). In the case presented by *Gorkin et al.*¹⁶, similar to Figure 4.2.a, an active, non-mechanical and air-tight microvalve, polyvinyl-alcohol-based water-soluble dissolvable film (DF), undergoes phase change upon liquid contact

by where it dissolves. This is a very useful set-up, as liquid-DF contact will not occur until the pneumatic chamber storing the DF valve reaches sufficient compression, which can be achieved through a generated centrifugal force, although sample loss is illustrated per iteration use of the valve which could prove problematic for largely integrated devices. While KC-35 film (made from SOLUBLON® and sourced from *Harke Packpro, Germany*) was the only used DF material during this report, with a dissolution time of approximately 30 s, there are a also number of different materials currently available, with a study carried out to determine the dissolution time of each.(35) Another example of an active valve was demonstrated by *Lee et al.*(36) and *Park et al.*(37), illustrated by Figure 4.2.b, whereby microchannels can be closed using a ferrowax microvalve, which can be melted using a laser source, allowing further sample progression.

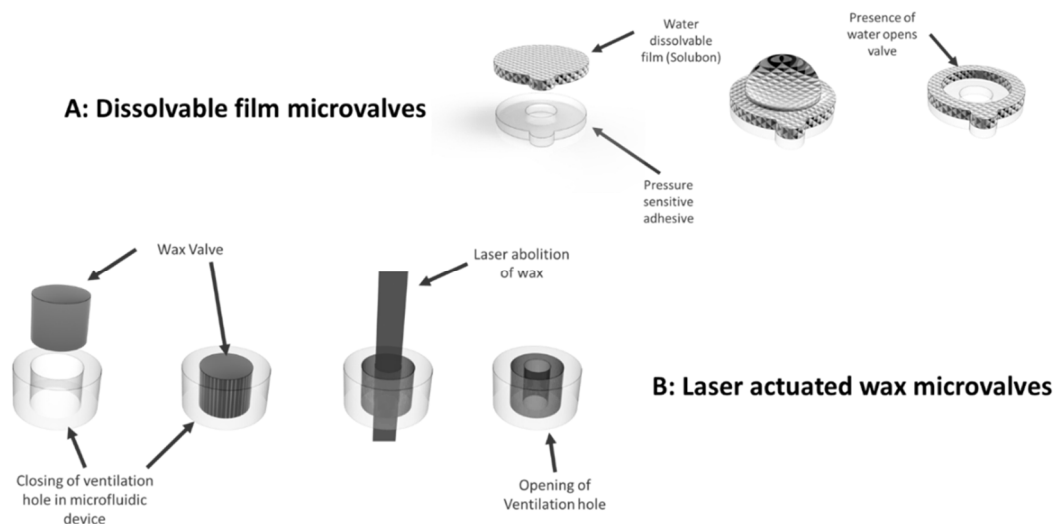


Figure 4.2: Active valving systems integrated into microfluidic platforms.

A) illustrates the structural design and scale of a dissolvable film (DF) valve. In this case, the valve halts sample temporarily often by pneumatic compression, until the liquid solution reaches the DF and dissolves the material, thereby releasing any generated air pressure. B) demonstrates how ferro-wax microvalves can be also used to prevent pneumatic release, thus halting sample progress, until laser abolition of valve creates a vent to release compressed air. (Authors own image)

Passive microvalves refer to valves which don't require external interaction for actuation due to the valve's natural physical parameters, which can be overcome through sample interaction; mechanical (check valve(38)), non-mechanical (capillary(39)). In comparison to a standard microchannel (A), three examples of passive microvalves are illustrated in

Figure 4.3; capillary valve (B), hydrophobic valve (C) and siphon valve (D). In each case, the microvalve can be overcome, without modifying the physical parameters of the valve, by increasing the centrifugal force beyond the activation threshold of a particular valve. While passive valves are generally easier to integrate into microfluidic systems than active microvalves, a usual trade-off is microvalve reliability due to not being externally actuated.(22)

Generally, once a microfluidic platform has been fully characterised to show successful assay integration and performance, the subsequent step would be the integration of further 'assays-of-interest' and/or replication of desired assays for increased sampling capabilities per single microfluidic platform. An example of this can be demonstrated with the MariaBox microfluidic platform(40), whereby the system was targeting the long-term monitoring (up to 6 months), *in-situ* monitoring of eight separate marine analytes. Due to the limited storage specifications on the buoy-based detection system, inclusion on the microfluidic platform of multiple multi-assay detection iterations was required. The microfluidic system was developed gradually, as described in Figure 4.4, whereby initially the development of a single-assay microfluidic platform which incorporated an inverse-assay based protocol with manual microvalve actuation, was used to fully characterise successful assay integration. Due to the ease of development of this platform, large-scale production using current prototyping techniques was possible, and thus allowed considerable assay optimisation studies to be rapidly conducted.

However, due to the storage constraints associated within the MariaBox platform, the number of assays was required to be increased from 6 (single assay x 6) to 24 (octuple-assay x 3). Initially, the expansion of the 'single-analyte disc' to the 'triple-analyte disc' was conducted to increase the number of sampling assays to 9, which also utilised a single sample loading reservoir which metered the sample between individual assays, as well as an enhanced pneumatic microvalve strategy. As each assay experienced the same wait periods between each assay step, considerable effort was focused into developing this highly reliable valve strategy which could consistently open all of valves at the same radial position, allowing synchronised assay execution.

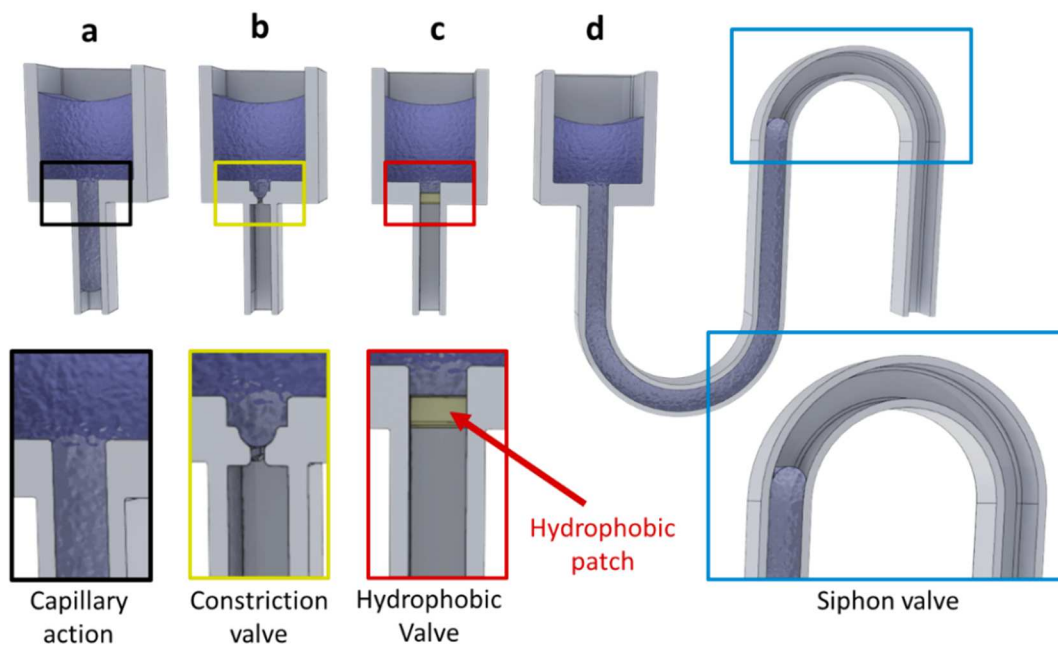


Figure 4.3: Passive valving solutions for microfluidic platforms.

Presented here are three microfluidic valve concepts, with respect to a standard capillary action microchannel (a), which require a separate specific force for liquid to overcome either constriction (b), hydrophobic (c) or siphon (d) obstacles. (Authors own image)

This format was then further upscaled to the ‘octuple-analyte’ disc, which had four assays per loaded sample, as in this specific case(40), there was four biological and four chemical analytes of interest with differing preloading treatments required. This platform was also made ~20% thicker to allow the same volume of sample (50 μ L) per assay as previously used with a reduced x-y spatial footprint for increased reservoir quantity.

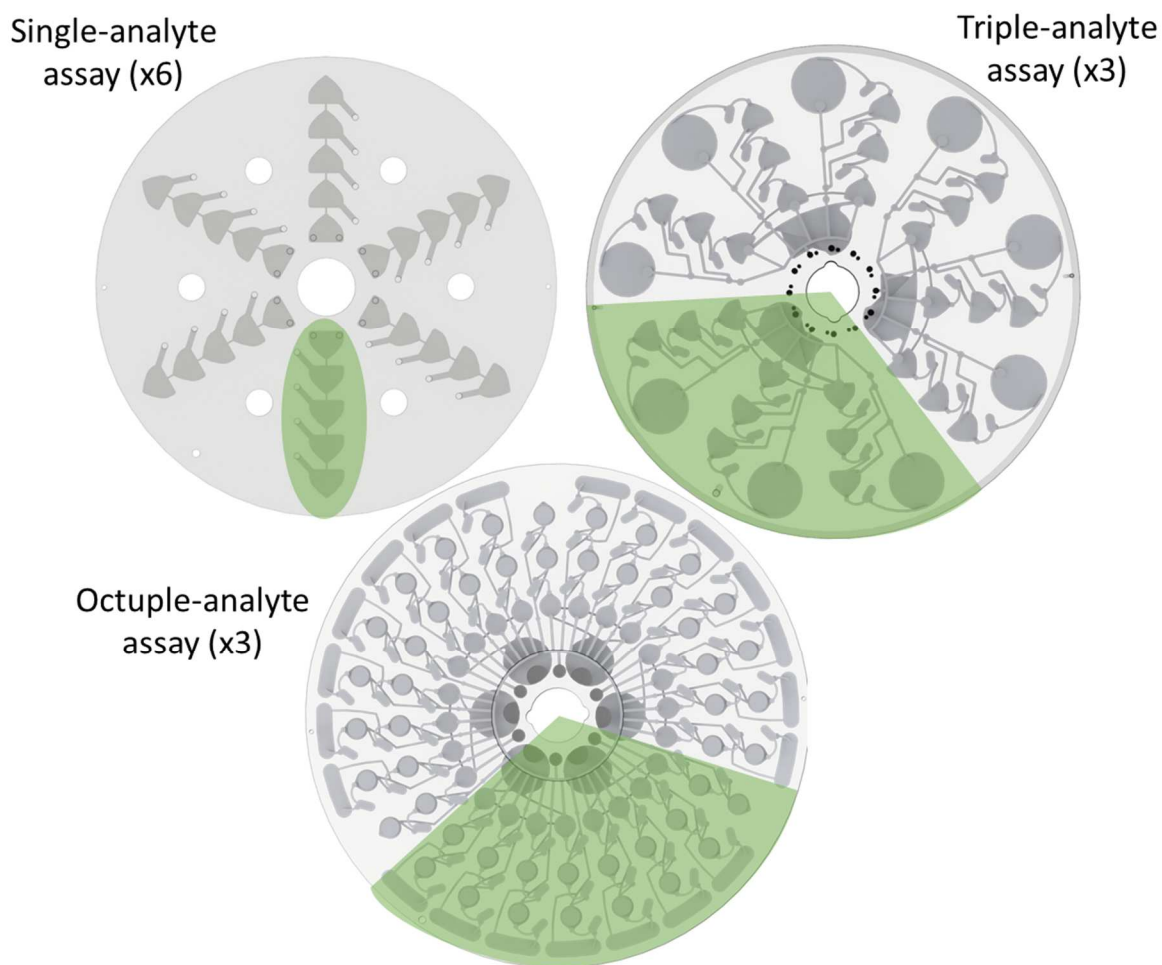


Figure 4.4: The development stages of a highly integrated LOAD microfluidic platform summarised as three microfluidic platforms.

Top-left) A microfluidic platform which targets 'single-analyte assay' performance characterisation in the microfluidic platform with minimal microfluidic features. The simplicity of this platform offered ease-of-manufacturing, thus allowing mass production of disc for significant assay characterisation studies to be conducted both cost- and time-effectively. Top-Right) Expansion of the previous test disc to include triple-analyte detection with an enhanced pneumatic microvalve incorporated for synchronised assay execution. Bottom) Augmentation of the previous test disc, the final MariaBox microfluidic platform⁽⁴⁰⁾ incorporated the same microvalve strategy for the synchronous detection of eight separate analytes from two loaded sample. This platform was also made ~ 2.5 mm thicker to maintain consistent $50 \mu\text{l}$ sample-per-assay, as per previous test discs.

In this work, a characterisation of the operational inconsistencies of microfluidic features due to the rapid-prototyping development process, and with particular emphasis on an enhanced microfluidic pneumatic valve strategy, is presented. This

includes the design and characterisation of a pneumatic-based microfluidic feature for enhancing the previously reported DF microvalve strategy developed by *Gorkin et al.*¹⁶. As part of this strategy, intentional rotation of microfeatures, with respect to the radial axis, was done to replicate possible misalignments may occur during the manufacturing and assembly stages of rapid-prototyping, which can significantly affect the predictability of sample-microfeature interactions. Also, as this microfluidic strategy was targeting synchronised assay execution with minimal sample loss per microfeature iteration, a full characterisation of sample-microfeature interactions at varying radii and rotational frequencies was conducted to generate a complementary liquid performance model. Therefore, we present here, a non-simulation-based approach for assessing and modelling microfeature performance to develop a complementary ‘spin program’ for high reliability liquid actuation. It is hoped that this strategy of modelling microfeature operational conditions in a non-simulation-based approach will assist in the development of more reliable, autonomously-predictable LOAD platforms.

4.3 Results and discussion

Initially, a reservoir-reservoir-pneumatic-chamber (RRPC) feature (shown in Figure 4.5) was specifically used to simultaneously assess the rotational frequencies of the non-pneumatic ‘passthrough’ of liquid between reservoirs, where low rotational frequencies were sufficient, and the compressibility of pneumatic chambers, where high rotational frequencies were required. This was then used in determining the required low and high disc rotational frequency regimes, with respect to the radial placements of both microchannel, for sample progression, and microvalve, for halting sample progression temporarily. In effort to increase the error due to rapid-prototype manufacturing as well as reduce the effect of liquid driving due centrifugal magnitude growth, a spiral pattern was also utilised, whereby the RRCP features became further rotated, with respect to the radial axis, as the radius increased (Figure 4.5). It was expected that the operational range of required rotational frequencies would resultantly be reduced on the premise that the features intentionally became misaligned with the vector of centrifugal force with respect to radius, thus reducing the effect of liquid driving by centrifugation, as well as replicate the effects due to poor manufacturing and assembly during the rapid

prototyping process. It was also predicted that due to the manufacturing techniques used, being xurography and laser cutting which work of the premise of an x-y coordinate-based system, that the resolution of the microfluidic features would be diminished upon rotation. This reduction in resolution was predicted to be in proportion to the squared root of the combined squared resolutions in the x and y axis, whereby if the resolutions of each axis was identical, then the error would be increased by a factor of $\sqrt{2}$.

4.3.1 Disc characterisation

Once the microfluidic discs were manufactured and assembled, they were continuously spun from 2-50 Hz with a liquid settlement period of 10 secs before image capture at each incremental increase of 1 Hz. This was to ensure that liquid movement did not change between each increment. The RRCP pattern was used to assess three liquid phase changes of interest; from 'loaded liquid' to 'normalisation' against a centrifugal force, from 'normalisation' of liquid to liquid 'passthrough' in microchannels, and from liquid 'passthrough' to a 'compression' of a pneumatic chamber (as demonstrated by Figure 4.5). The images for each rotational frequency per disc were then collected and analysed to determine the correct rotational frequency required to initiate a liquid phase change (as per Figure 4.5). The averaged ($n=3$) rotational frequency (ω) where liquid phase change occurred at radial position (r) from axis of rotation, is shown in Figure 4.6.

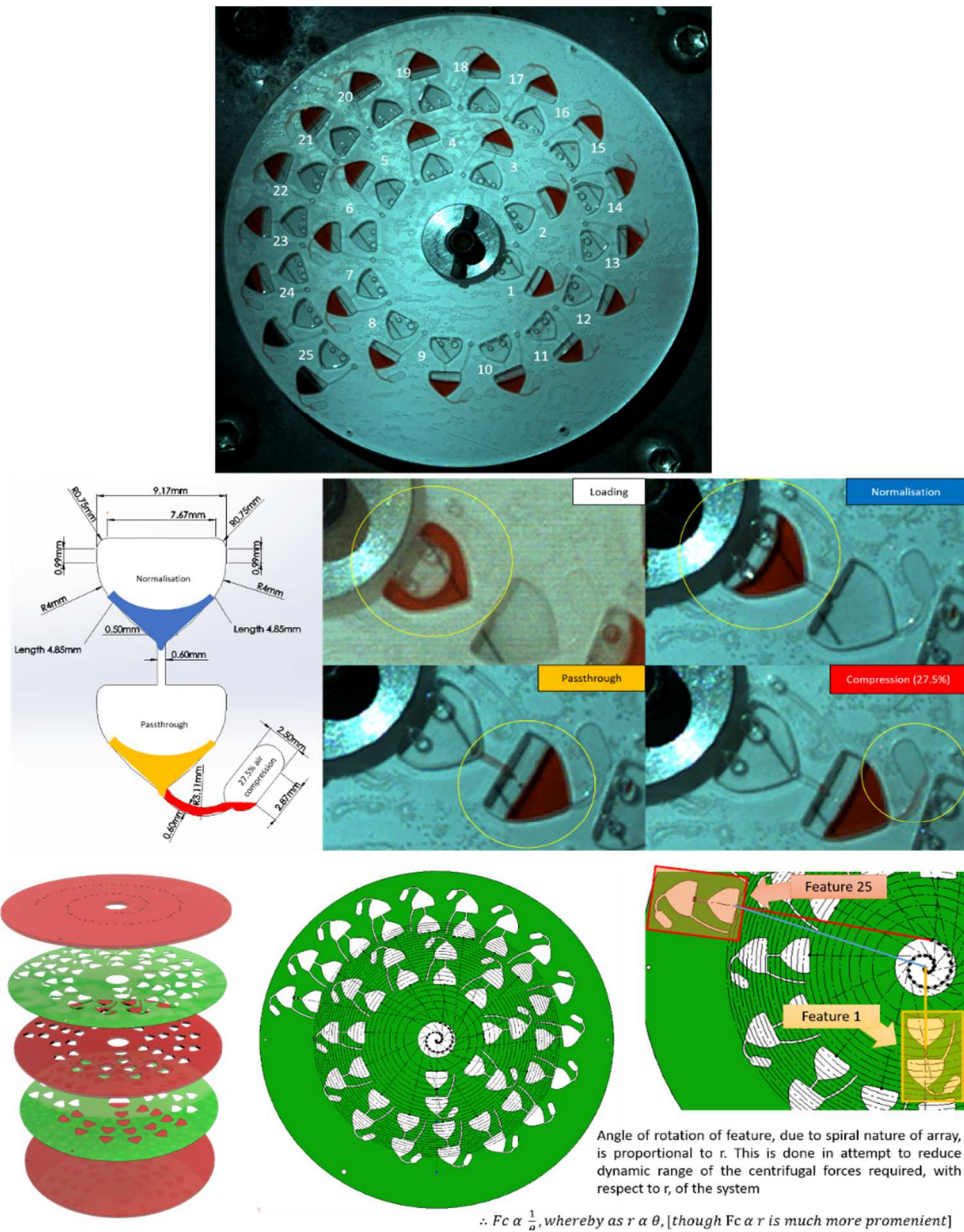


Figure 4.5: The Microfluidic disc with spiral arraying of reservoir-reservoir-Pneumatic-chamber (RRPC) microfluidic features.

Top) The assembled microfluidic disc, at rotational frequency of 50hz. Middle) The RRPC pattern dimensions and associated liquid phases during centrifugation; 'Loading', 'Normalisation', 'Passthrough' and 'Compression' of pneumatic valve at 27.5%. Bottom-left) The centrifugal microfluidic platform layers, including 2mm thick PMMA (Red) and 150 μ m thick pressure sensitive adhesive (Green) sheets. Bottom-middle) The innermost reservoir-reservoir-Pneumatic-chamber (RRPC) pattern initially aligns directly with the radial centrifugal force which is arrayed in a spiral pattern. Bottom-right) This results in an intentional unalignment of the pattern of the centrifugal force to reduce the effective magnitude of the centrifugal force driving the liquid as the placement radius increases, therefore reducing the dynamic range of required rotational frequencies for the study, as well as replicate the effects of poor manufacturing and assembly during the rapid prototyping process.

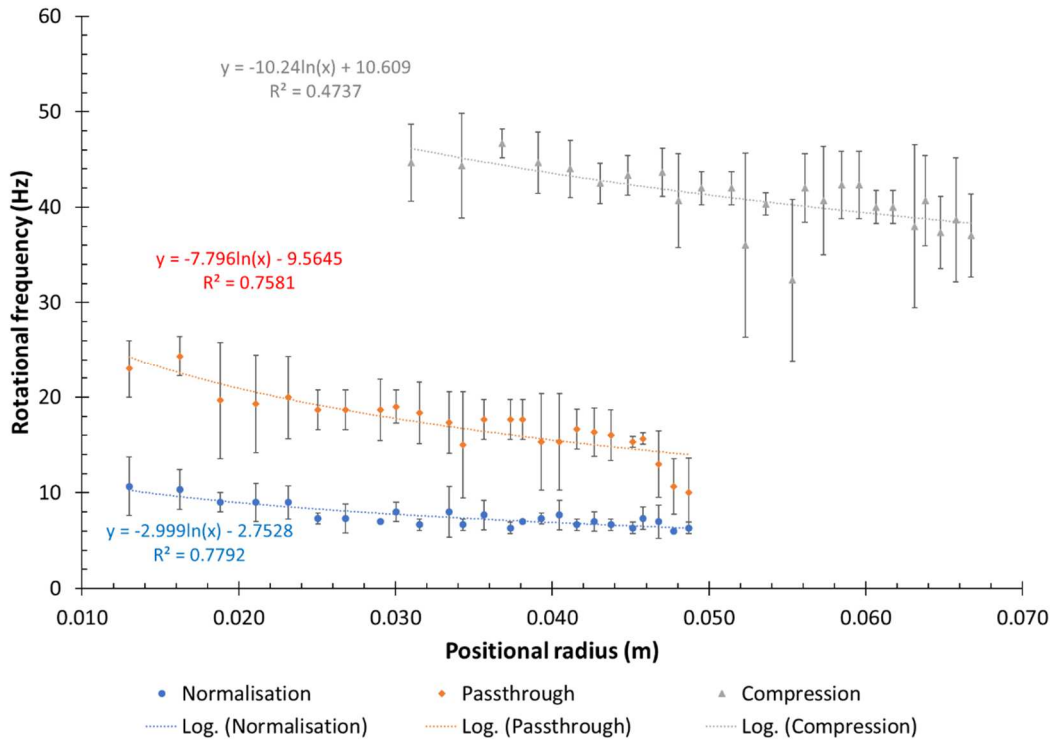


Figure 4.6: The averaged ($n=3$) rotational frequency vs positional radius from centre of rotation, whereby liquid phase change occurred.

This graph indicates the occurrence of three distinct liquid phase change models; liquid shape conforms to the centrifugal force in the load reservoir (Normalisation), normalised liquid passthrough a microchannel with compression (Passthrough) and liquid passes through a microchannel whilst simultaneously compresses air by 27.5% (Compression). Also evident is the large error most likely prominent due to the manufacturing and manual-assembly process of the discs.

This data reflects the significant unpredictability of liquid phase change due to the necessary manual-manufacturing of individual layers, most likely occurring during due to assembly misalignments and/or manufacturing inaccuracies. This also emphasises the difficulty in transitioning from a prototype device to a fully developed platform, for which an automatic fluidic actuation protocol can be easily predicted throughout sample progression within a centrifugal microfluidic platform. It is clear from Equation 20, that there is be a logarithmic-based proportionality between ω and r , which was used as a base model for assessing the unpredictability, corresponding to the coefficient of determination (RSD).

Equation 20: Derivation of centrifugal force (F_c), in the form of rotational frequency (ω)

$$F_c = m \cdot \omega^2 \cdot r = \text{const.}$$

$$\rightarrow \frac{F_c}{m} = \omega^2 \cdot r$$

$$\rightarrow \omega^2 \propto \frac{1}{r}$$

$$\rightarrow \omega \propto \sqrt{\frac{1}{r}}$$

Where F_c is the required centrifugal force induced, m is the mass of the liquid, ω is the rotational frequency of the disc and r is the radial distance from the centre of rotation. Therefore, there is an inverse logarithmic relationship between ω and r , as depicted by the data in Figure 4.6.

4.3.2 Outlier removal

Due to the poor RSD values indicated (< 0.8), an initial step of outlier removal was required in this case to further improve model accuracy. This was achieved by setting a maximum standard deviation (STD) error as the threshold for outlier removal. This was done using Excel™ solver, where the optimisation of RSD was maximised by changing the STD error tolerance threshold, with the requirement of a minimal averaged ($n=3$) sample count of five. The output of these settings is given by Table 4, and illustrated in Figure 4.7.

Table 4: Outlier removal settings using logarithmic regression analysis.

Liquid Phase change	% STD Error tolerance	Sample count after outlier removal	RSD
Normalisation	29	24	0.787
Passthrough	13	10	0.911
Compression	7	10	0.878

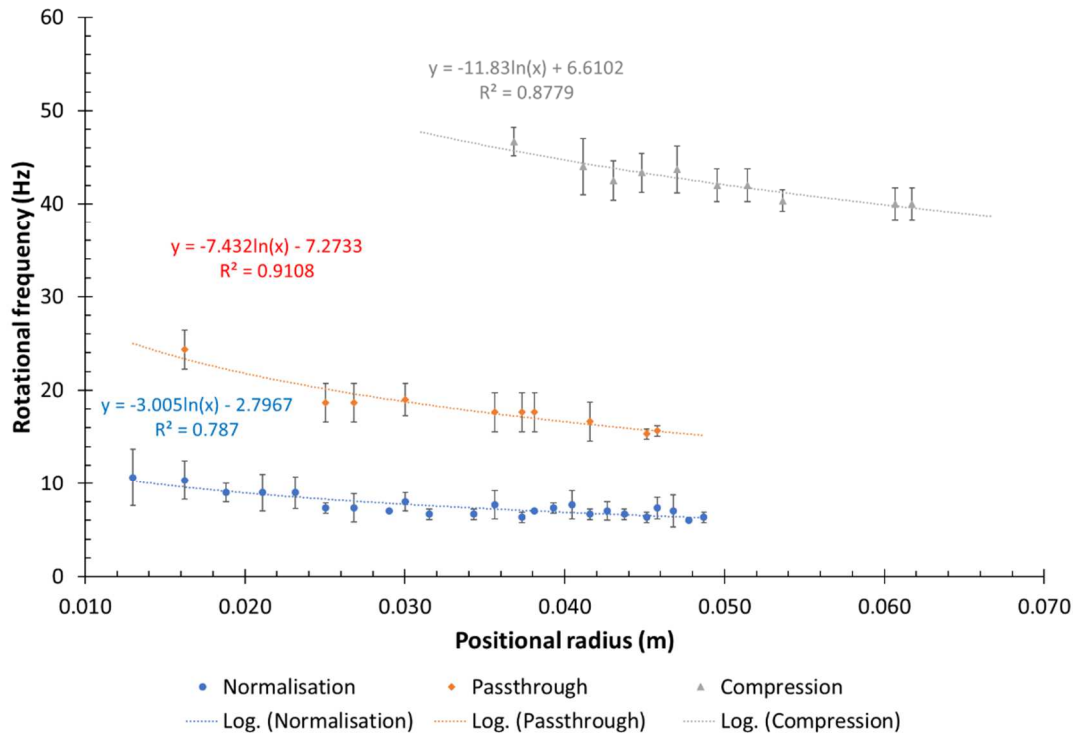


Figure 4.7: Averaged rotational frequency vs positional radius of feature from centre of rotation, whereby liquid phase change occurred, with outliers excluded as per settings described in Table 4.

4.3.3 Initial Model generation

These data points were then used to assess the specific force required to enact liquid phase change. As Equation 20 indicates, a directly proportional relationship between ω and r^{-2} should occur. However, as the reservoir, microchannel and compression valve shape are constant at varying radii throughout the disc, the 'specific force required to induce liquid phase change' (P) should also be constant. As this model is only based on the rotational frequency and radial position parameters, liquid phase change should occur as the centrifugal force (F_c) becomes equal to the force required to initiate liquid phase change (F_p). Therefore, as Equation 21 demonstrates, P is constant for enacting a particular liquid phase change, and is represented by the squared slope of this relationship. This data is illustrated in Figure 4.8 and summarised in Table 5.

Equation 21: Derivation of theoretical rotational frequency ($\omega_{\text{theoretical}}$) required to generate the force of liquid phase change (F_p).

$$F_p = F_c = m.(\omega^2).r = \text{const.}$$

$$\Rightarrow P = \frac{F_c}{m} = (\omega^2).r$$

$$\Rightarrow \omega = \sqrt{\frac{F_p}{m} \cdot \frac{1}{r}} = \sqrt{\frac{P}{r}}$$

$$\Rightarrow \frac{\partial y}{\partial x} = \frac{\partial(\omega)}{\partial\left(\sqrt{\frac{1}{r}}\right)} = \sqrt{\frac{F_p}{m}} = P^{0.5}$$

$$\therefore P = \left(\frac{\partial y}{\partial x}\right)^2$$

Where F_p is the force required to initiate liquid phase change, F_c is the required centrifugal force induced, m is the mass of the liquid, r is the radial distance from the centre of rotation, P is the specific force required to initiate liquid phase change of mass m , which can be determined through linear regression analysis between ω and the square-rooted inverse of r (as illustrated in Figure 4.8).

Table 5: Specific force of liquid phase change model data using linear regression analysis.

Liquid Phase change	STD Error % tolerance	Sample count after outlier removal	RSD	Slope $\text{m}^{1/2}.\text{s}^{-1}$	Squared slope $\text{m}^1.\text{s}^{-2}$ or N/Kg	Y-intercept
Normalisation	29	24	0.816	0.995	0.989	1.890
Passthrough	13	10	0.928	2.484	6.170	4.241
Compression	7	10	0.888	5.223	27.284	18.630

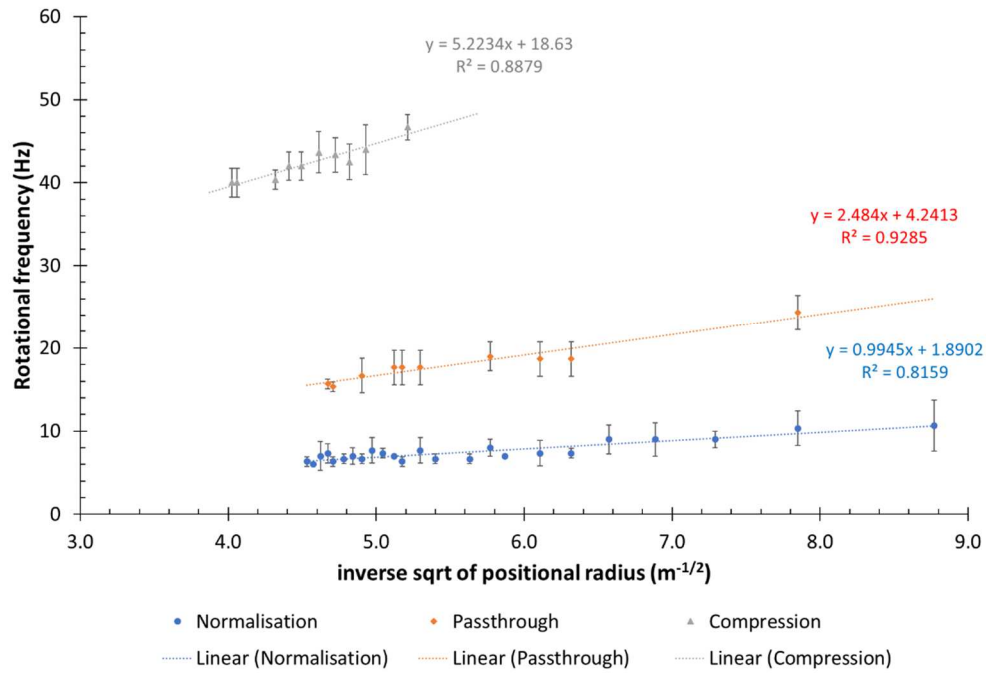


Figure 4.8: The averaged rotational frequency (with outliers excluded) at the inverse square root positional radius of feature from centre of rotation, whereby liquid phase change occurred.

This graph was used to extrapolate the specific force determined by linear regression (as per Equation 21) and used to generate a model representation (as per Equation 22).

It is also important to note that Figure 4.8 does not demonstrate a directly proportional relationship between ω and r as theoretically postulated, and the addition of the y-intercept value (ω_{const}) can be attributed to the misalignment of the features with respect to the radial centrifugal force, disc layer assembly and manufacturing issues and unaccounted-for liquid-surface and liquid-air interactions, which should otherwise be constant with respect to r and ω . Therefore, the initial characterisation model (ω_{Model}) was generated as to include both a $\omega(r)$ and ω_{const} element, as demonstrated in Equation 22.

Equation 22: Characterisation of experimental rotational frequency required for liquid phase change (ω_{model})

$$\omega_{experimental} = \left(\sqrt{\frac{F_c}{m} \cdot \frac{1}{r}} \right) + const. = \left(\sqrt{\frac{P}{r}} \right) + (\omega_{const})$$

$$\left[\omega_{\left(\frac{1}{r} \rightarrow 0\right)} = \lim_{r \rightarrow \infty} (\omega_{experimental}) = \lim_{r \rightarrow \infty} \left(\sqrt{\frac{F_c}{m} \cdot \frac{1}{r}} + \omega_{const} \right) = \omega_{const} \right]$$

$$\therefore \omega_{Model} = \left(\sqrt{\frac{F_c}{m} \cdot \frac{1}{r}} \right) + const. = \omega(r) + \omega_{const}$$

Where $\omega_{experimental}$ is the true experimental rotational frequency at which liquid phase change occurred, F_c is the required centrifugal force induced, m is the mass of the liquid, r is the radial distance from the centre of rotation, ω_{const} represents the y-intercept value as ($r \rightarrow \infty$), $\omega(r)$ corresponds to the rotational frequency of the disc at r .

4.3.4 Spin protocol generation

As the models determined from Table 5 offer a valid model of liquid phase change, they are not yet suitable for use as a guaranteed liquid phase change threshold, as is visible in Figure 4.9. Therefore, a shift in the y-intercept was initially conducted using Equation 23, which is based on using the largest positive y-residual value determined initially from the averaged data set, in order to set to maximise liquid phase change successful transitions. However, as shown in Figure 4.10, it is again evident that the y-intercept shift based on the averaged data (solid) is insufficient, with a significant number of failed liquid phase changes likely. Therefore, the y-intercept shift was again repeated to using the max raw residual value (dotted).

Equation 23: Modification of model to include positive outliers

$$\omega_{Model} = \left(\sqrt{\frac{P}{r}} \right) + \omega_{const}$$

$$\omega_{res,x}(r) = \text{Max} \left[(\omega_x - \omega_{Model})|_r = (\omega_x)|_r - \left(\sqrt{\frac{P}{r}} + \omega_{const} \right) \right]$$

Where $\omega_{res,x}$ is the maximum positive residual difference of the rotational frequency at r radial position between the x dataset [averaged, raw], and the model. $\omega_{res,x}$ was then used to recalibrate ω_{const} in the base model to $\omega_{(const_recalibrated,x)}$ by,

$$\omega_{(const_recalibrated,x)} = \sqrt{\frac{P}{r}} \cdot \ln(r_x(\omega_{res,x})) - \omega_{res,x}$$

With the recalibrations using averaged and raw datasets demonstrated in Figure 4.9 and Figure 4.10, respectively.

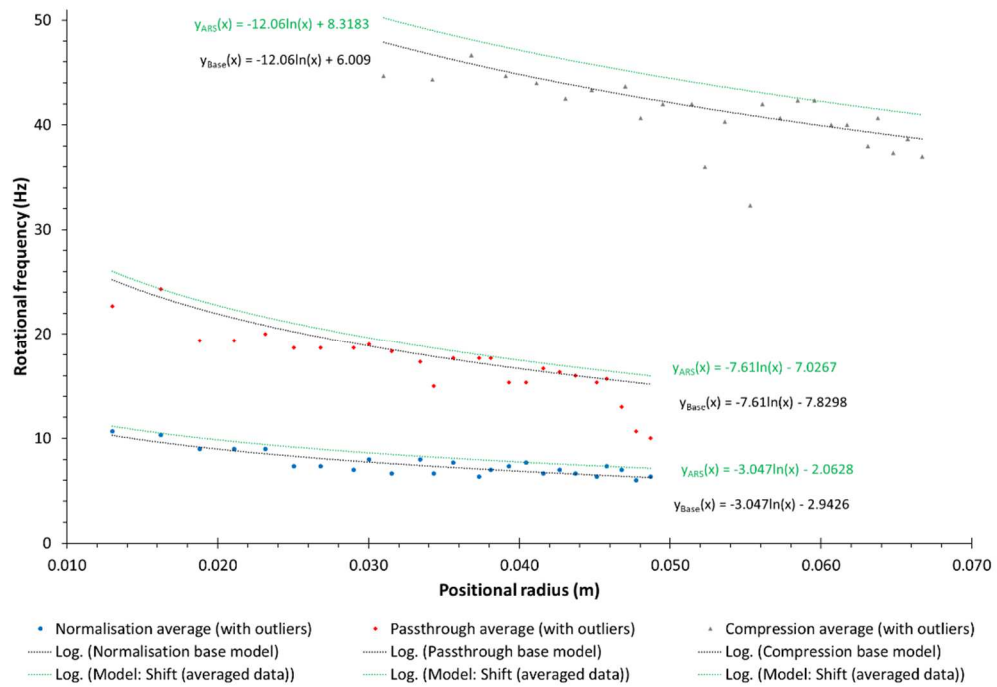


Figure 4.9: Averaged ($n=3$) rotational frequency vs positional radius from centre of rotation whereby liquid phase change occurred (including outliers) compared to model.

Two trends are included in this graph for comparison; the initial liquid phase characterisation model (Y_{Base}), as per Equation 22, and the recalibrated model using the averaged dataset (Y_{ARS}), as per Equation 23. This recalibrated model demonstrates a up to 35% improvement in predictability, corresponding to a maximum rotational increase of ~ 4.5 Hz.

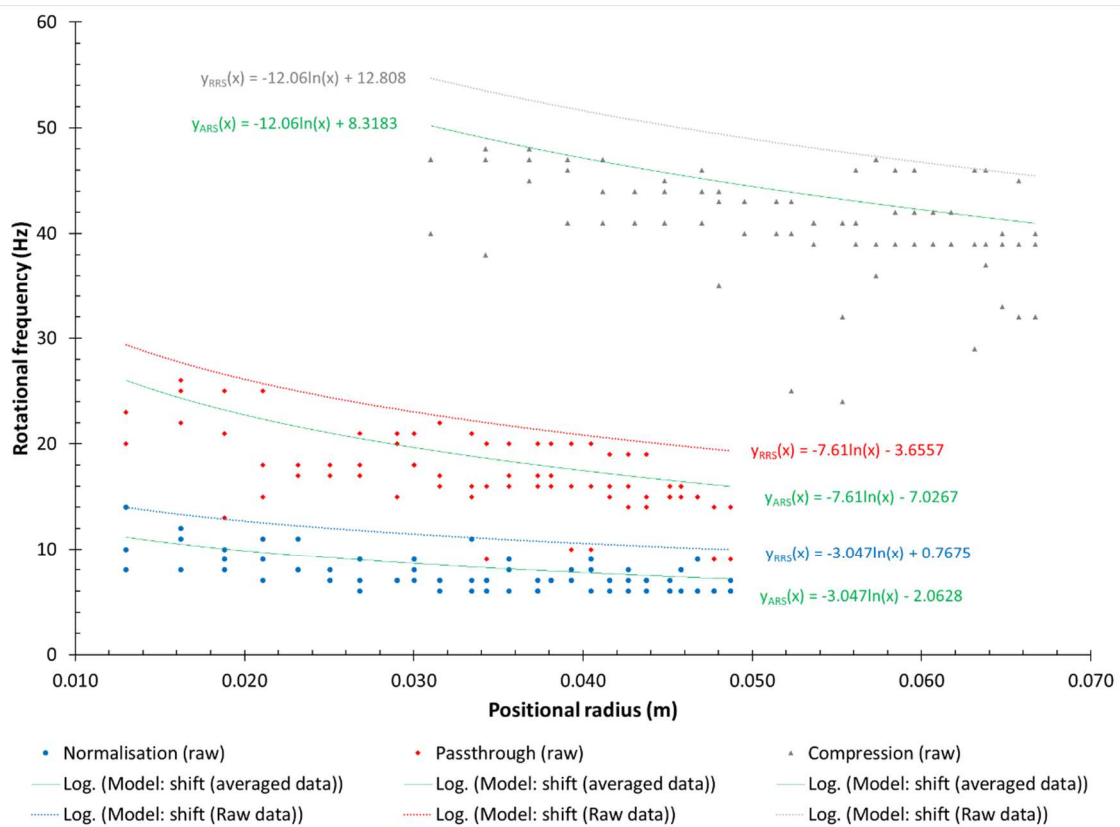


Figure 4.10: Raw rotational frequencies of the three discs vs positional radius from centre of rotation whereby liquid phase change occurred (including outliers) compared to model.

Two trends are included in this graph for comparison; and the recalibrated model using the averaged dataset (Y_{ARS}) and recalibrated model using the raw dataset (Y_{RRS}), as per Equation 23. This graph demonstrates up to 26% failure of liquid phase change with recalibration using the averaged dataset vs the raw dataset, corresponding to a maximum rotational increase of ~ 7 Hz.

4.3.5 Summary

Table 6 summarises the expectant success of each model variation per liquid phase change, based on the original raw data, if used as a ‘spin speed’ protocol. In this table, it is evident that a recalibration of the model significantly reduced the failure rate of all of the liquid phase change predictions, with a considerable reduction in missed points particularly evident with the compression liquid phase change. The recalibration of the base model corresponded to ~ 4.5 Hz and ~ 7 Hz increase, based on the averaged and raw residuals, respectively. While these recalibrations would lead to a higher compression percentile in the case of the compression liquid phase change, risking premature dissolvable microvalve rupture, a stronger or thicker DF could be incorporated to

counteract the excess pressure generated whilst maintaining the lower failure rate. Alternatively, as per the setup demonstrated in the MariaBox platform(40,41), an additional DF valve can be included to assist in liquid deceleration before compression (Figure 4.11). In this case, DF microvalve one was used to prevent premature air compression in the pneumatic chamber, while DF microvalve two acted to prevent air release until sufficient pneumatic compression is achieved.

Table 6: Model comparison of the initial model, the modified model based on averaged residual shift and the modified model based on the raw residual shift.

y-intercept adjustments	Liquid phase change	y-intercept based on initial model (Hz)	Raw points missed (x/75)	% of raw points missed
Initial model	Liquid normalisation in start reservoir	-2.943	29	38.67
	Liquid microchannel passthrough	-7.830	25	33.33
	Air compression by 27.5%	6.009	36	48.65
		y-intercept based on averaged data max residual (Hz)		
Averaged data	Liquid normalisation in start reservoir	-2.063	16	21.33
	Liquid microchannel passthrough	-7.027	20	26.67
	Air compression by 27.5%	8.318	10	13.51
		y-intercept based on raw data max residual (Hz)		
Raw data	Liquid normalisation in start reservoir	0.767	0	0
	Liquid microchannel passthrough	-3.656	0	0
	Air compression by 27.5%	12.808	0	0

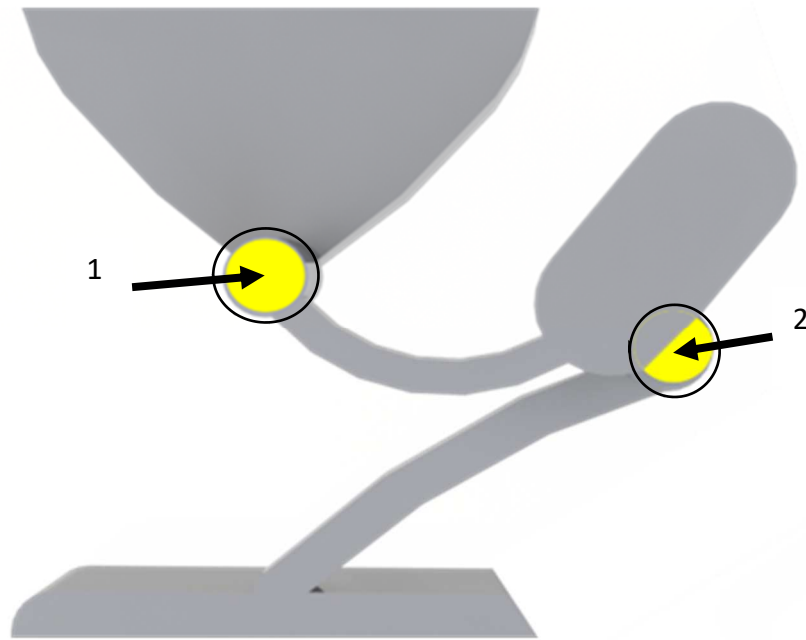


Figure 4.11: Ideal dissolvable valve locations.

1) prevents premature air compression during deceleration of rotational frequency from high frequency ('Compression') to low frequency ('Passthrough'). 2) prevents air release, which halts sample progression, until sufficient air compression within the pneumatic chamber is achieved, allowing the sample to contact and dissolve the microvalve.

Liquid phase changes are essential components in developing a microfluidic platform. Understanding and predicting how liquids normalise, travel through microchannels and interact with microvalves is key in the success of a microfluidic device. To develop a highly reliable autonomous rotational frequency program to run a LOAD assay protocol, a characterisation of the specific force required to initiate a liquid phase change should be performed and related the liquid driving force, or in the case of the LOAD platform, the centrifugal force. There should also be a clear distinction between the specific force required to drive a liquid through a microchannel and interact with a microvalve if high reliability is to be achieved. In the case of a pneumatic chamber for DF-based microvalves, how they are integrated with other microfeatures can largely affect actuation performance and efficiency. Larger pneumatic chambers can increase reduce the required activation force, making differentiation between microchannel passthrough more difficult, while smaller pneumatic chambers would result in larger

required actuation forces, therefore tuning of the pneumatic chamber should be considered carefully. As is demonstrated in the MariaBox platform(40) (Figure 4.12), the combination of the liquid phase change models can then be mapped to the respective microfluidic feature, whereby the change between liquid phase changes is determined by the individual assays step durations. This program can then be used to autonomous LOAD management *in-situ*.

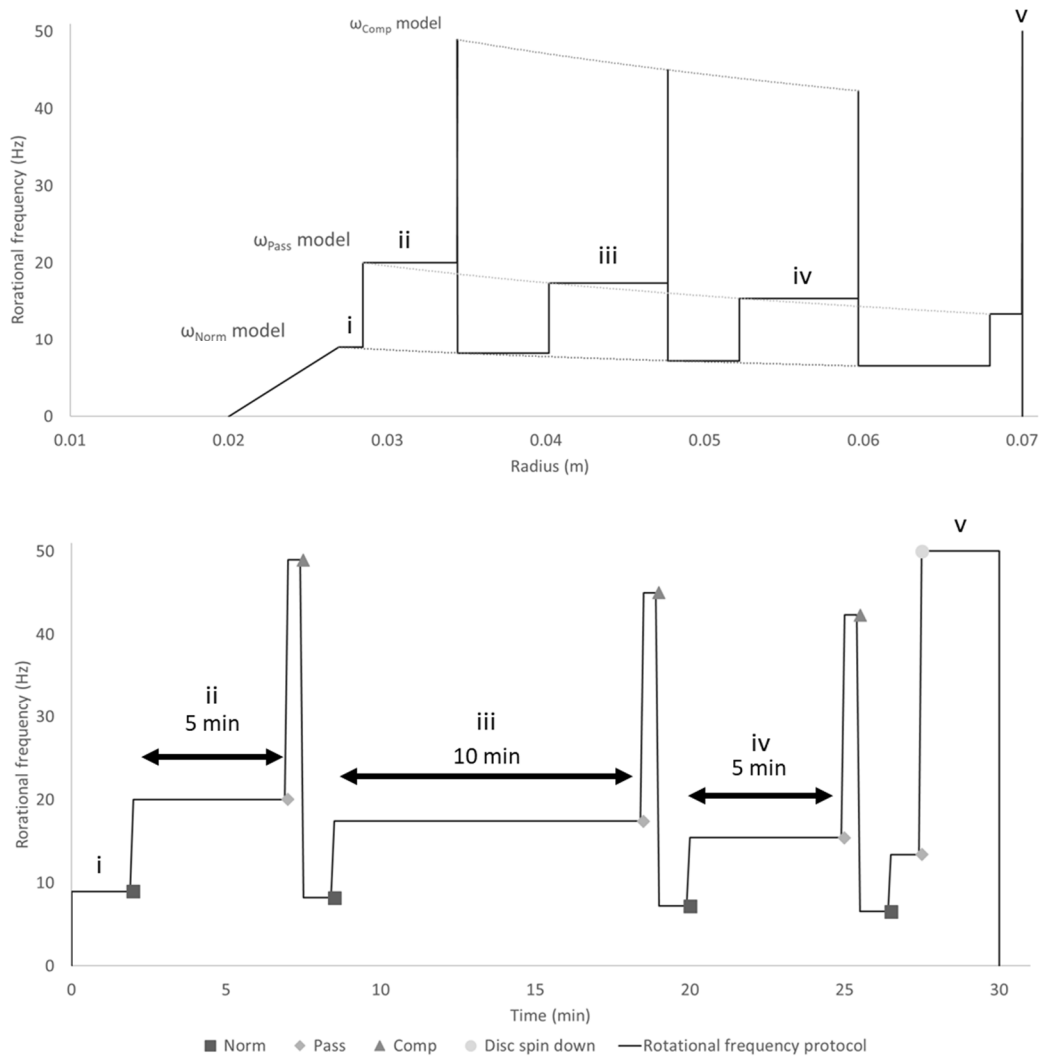


Figure 4.12: The rotational frequency protocol used for the MariaBox microfluidic platform(40), either by varying radius (top) or time (below), based on the normalisation, passthrough and compression models. The assay steps in this example are loading and normalisation(i), metering and incubation (ii), test (iii), control (iv), and complete disc spin-down (v).

With the increased abilities of highly complex microfluidic devices, achieved through an increasing the quantity of microfeatures present, there is also a corresponding reduction in success rate of the system proportional to the reliability and predictability of the utilised, particularly in an autonomous setting. Therefore, it is essential to maximise the corresponding actuation model in order to achieve a successful, highly integrated microfluidic platform.

4.4 Conclusion

A characterisation of possible manufacturing errors associated with the rapid-prototyping of microfluidic platforms and their effects on liquid manipulation has been performed. This was achieved through the use of a novel designed 25-iteration reservoir-reservoir-pneumatic chamber (RRPC) feature set, joined by microchannels, and aligned in a spiral patterning at varying radii. The purpose of this was to identify and fully characterise three liquid phase transitions which occur during assay execution; from loaded liquid to normalisation against a centrifugal force (Normalisation), from normalisation of liquid to liquid passthrough in microchannels (Passthrough), and from liquid passthrough to a compression of a pneumatic chamber where a microvalve would normally be installed (Compression). These models were used to develop a corresponding 'spin speed' protocol for increased valve reliability for autonomous use, whereby a 4.5-7 Hz increase on microvalve model corresponded to a \approx 72-100% improvement in successful compression reliability respectively. Within this protocol development, a comparative study was conducted between the use of either the averaged and raw activation spin speeds to develop spin speed protocols with high predictability. These protocols were based on a logarithmic regression model which an intercept shift based the maximum residual difference between either the averaged or raw data sets. After characterisation, these valves were successfully integrated into both the 'triple-assay' and fully integrated 'octuple-assay' MariaBox microfluidic discs for autonomous, *in-situ* deployment.

4.5 Acknowledgment

This work was supported by the FP7 EU-funded MARIABOX project. The MARIABOX project receives funding from the European Union Seventh Framework Programme - Grant Agreement No: 614088.

4.6 Materials and Methods

4.6.1 Microfluidic disc manufacturing

The Microfluidic disc, shown in Figure 4.5, was manufactured from poly(methyl methacrylate) (PMMA) sheets (2 mm for top and bottom, 0.5 mm for pneumatic chamber) and “pressure sensitive adhesive” (PSA) sheets (ARseal™90880), sourced from Radionics™ and Adhesives Research™ respectively. The discs were manufactured through assembling consecutive layers of PMMA and PSA using xurographic and laser-based rapid prototyping strategies(42–44).

4.6.2 Microfluidic disc characterisation

A “spin stand”(45), as described by Kirby *et al* (15) was used to characterise liquid motion on the microfluidic platform. In short, centrifugation of the discs was controlled via computer operated spindle motor (Faulhaber Minimotor SA, Switzerland). A high sensitivity, short-exposure time camera (Pixelfly, PCO, Germany) and a stroboscopic light source (Drelloscop 3244, Drello, Germany) were combined and synchronized with the spindle motor using custom electronics to allow visualisation of hydrodynamic performance of the discs during centrifugation. 50 µL of de-ionised water with red food colouring added to each load reservoir, images were captured of the liquid phases in each of the 25 RRPC patterns (2-50 Hz rotational frequencies, with a 10 S wait period before each 1 Hz increment) for 3 separate test discs, as shown in Figure 4.5. The liquid phases were then compared to the preset profiles (shown in Figure 4.5.Bottom), whereby ‘Loading’ represents liquid shape before spinning, ‘Normalisation’ represents the liquid conformity, normal to a centrifugal force, and before progression from reservoir to microchannel, ‘Passthrough’ represents a reservoir-to-reservoir liquid transfer via microchannels unimpeded by air pneumatics, and ‘Compression’ represents the point at which the liquid has entered the larger slot-shaped pneumatic valve causing liquid trapping above the microvalve location (Figure 4.5).

4.7 Reference

1. Haeberle S, Zengerle R, Mark D, Von Stetten F, Zengerle R. Microfluidic platforms for lab-on-a-chip applications. *Lab Chip* [Internet]. 2007 Sep;7(9):1094. Available from: <http://xlink.rsc.org/?DOI=b706364b>
2. Kong LX, Perebikovskiy A, Moebius J, Kulinsky L, Madou M. Lab-on-a-CD: A Fully Integrated Molecular Diagnostic System. *J Lab Autom* [Internet]. 2015;2211068215588456-. Available from: <http://jla.sagepub.com/content/early/2015/06/16/2211068215588456.abstract>
3. Ducrée J, Zengerle R, Newman J. *FlowMap: microfluidics roadmap for the life sciences*. Books on Demand; 2004.
4. Whitesides GM. The origins and the future of microfluidics. *Nature* [Internet]. 2006;442(7101):368–73. Available from: <http://www.scopus.com/inward/record.url?eid=2-s2.0-33747117373&partnerID=40&md5=0074130e4ce504444efcdd2a9e1f92d4>
5. Mark D, Haeberle S, Roth G, von Stetten F, Zengerle R. Microfluidic lab-on-a-chip platforms: requirements, characteristics and applications. *Chem Soc Rev* [Internet]. 2010;39(3):1153–82. Available from: <http://pubs.rsc.org/en/content/articlehtml/2010/cs/b820557b>
6. Gardeniers JGE, Van Den Berg A. Lab-on-a-chip systems for biomedical and environmental monitoring. *Anal Bioanal Chem*. 2004;378(7):1700–3.
7. Stone HA, Stroock AD, Ajdari A. ENGINEERING FLOWS IN SMALL DEVICES Microfluidics Toward a Lab-on-a-Chip. *Annu Rev Fluid Mech* [Internet]. 2004;36(1):381–411. Available from: <http://arjournals.annualreviews.org/doi/abs/10.1146/annurev.fluid.36.050802.122124>
8. Ducrée J, Haeberle S, Lutz S, Pausch S, Zengerle R, Stetten F Von, et al. The centrifugal microfluidic Bio-Disk platform. *J Micromechanics Microengineering* [Internet]. 2007 Jul 1 [cited 2013 Nov 7];17(7):S103–15. Available from: <http://dx.doi.org/10.1088/0960-1317/17/7/s07>

9. Burger R, Amato L, Boisen A. Detection Methods for Centrifugal Microfluidic Platforms. *Biosens Bioelectron* [Internet]. 2015;(January 2016):1–14. Available from: <http://linkinghub.elsevier.com/retrieve/pii/S0956566315302463>
10. Imdieke J, Fu E. Porous stamp-based reagent patterning for lateral flow immunoassays. *Anal Methods*. 2017;9(18):2751–6.
11. Dong M, Wu J, Ma Z, Peretz-Soroka H, Zhang M. Rapid and Low-Cost CRP Measurement by Integrating a Paper-Based Microfluidic Immunoassay with Smartphone (CRP-Chip). *Sensors*. 2017;
12. Zou L, Tian Y, Zhang X, Fang J, Hu N. A competitive love wave immunosensor for detection of okadaic acid based on immunogold staining method. *Sensors Actuators B*. 2017;
13. Babrak L, Lin A, Stanker L, McGarvey J, Hnasko R. Rapid microfluidic assay for the detection of botulinum neurotoxin in animal sera. *Toxins (Basel)*. 2016;
14. Nwankire CE, Maguire I, Kernan D, Glynn M, Kirby D, Ducree J. SIZE- and deformability-based particle sorting by strategic design of obstacle arrays in continuous centrifugal sedimentation mode. In: 2015 Transducers - 2015 18th International Conference on Solid-State Sensors, Actuators and Microsystems, TRANSDUCERS 2015. 2015. p. 1854–6.
15. Kirby D, Siegrist J, Kijanka G, Zavattoni L, Sheils O, O’Leary J, et al. Centrifugo-magnetophoretic particle separation. *Microfluid Nanofluidics*. 2012;13(6):899–908.
16. Boettcher M, Jaeger MS, Riegger L, Ducreé J, Zengerle R, Duschl C. Lab-on-chip-based cell separation by combining dielectrophoresis and centrifugation. *Biophys Rev Lett*. 2006;1(04):443–51.
17. Clime L, Brassard D, Geissler M, Veres T. Active pneumatic control of centrifugal microfluidic flows for lab-on-a-chip applications. *Lab Chip* [Internet]. 2015;15(11):2400–11. Available from: <http://dx.doi.org/10.1039/C4LC01490A>

18. Abi-Samra K, Hanson R, Madou M, Gorkin R a. Infrared controlled waxes for liquid handling and storage on a CD-microfluidic platform. *Lab Chip*. 2011;11(4):723–6.
19. Garcia-Cordero JL, Benito-Lopez F, Diamond D, Ducree J, Ricco AJ, Ducreé J. Low-Cost Microfluidic Single-Use Valves and On-Board Reagent Storage using Laser-Printer Technology. *Ieee Int Conf Micro Electro Mech Syst Proc* [Internet]. 2009 Jan 25;439–42. Available from: http://pubget.com/paper/pgtmp_9612e20a010d754c6a68393dc8fe6b92/low-cost-microfluidic-single-use-valves-and-on-board-reagent-storage-using-laser-printer-technology
20. Duffy G, Maguire I, Heery B, Gers P, Ducreé J, Regan F. ChromiSense: A colourimetric lab-on-a-disc sensor for chromium speciation in water. *Talanta* [Internet]. 2018 Sep [cited 2017 Sep 26];178(Supplement C):392–9. Available from: <http://www.sciencedirect.com/science/article/pii/S0039914017310081>
21. King D, O’Sullivan M, Ducreé J. Optical detection strategies for centrifugal microfluidic platforms. *J Mod Opt* [Internet]. 2014;61(2):85–101. Available from: <http://www.tandfonline.com/doi/abs/10.1080/09500340.2013.873496>
22. Ahn KWO and CH, Oh KW, Ahn CH. A review of microvalves. *J Micromechanics Microengineering* [Internet]. 2006;16(5):R13. Available from: <http://stacks.iop.org/0960-1317/16/i=5/a=R01>
23. Kim J, Kido H, Rangel RH, Madou MJ. Passive flow switching valves on a centrifugal microfluidic platform. *Sensors Actuators B Chem* [Internet]. 2008;128(2):613–21. Available from: <http://www.sciencedirect.com/science/article/pii/S0925400507005217>
24. Terry SC, Jerman JH, Angell JB. A gas chromatographic air analyzer fabricated on a silicon wafer. *IEEE Trans Electron Devices*. 1979;26(12):1880–6.
25. Goll C, Bacher W, Büstgens B, Maas D, Ruprecht R, Schomburg WK. An electrostatically actuated polymer microvalve equipped with a movable membrane electrode. *J Micromechanics Microengineering*. 1997;7(3):224.

26. Shao P, Rummeler Z, Schomburg WK. Polymer micro piezo valve with a small dead volume. *J micromechanics microengineering*. 2003;14(2):305.
27. Rich CA, Wise KD. A high-flow thermopneumatic microvalve with improved efficiency and integrated state sensing. *J microelectromechanical Syst*. 2003;12(2):201–8.
28. Ren H, Gerhard E. Design and fabrication of a current-pulse-excited bistable magnetic microactuator. *Sensors Actuators A Phys*. 1997;58(3):259–64.
29. Neagu CR, Gardeniers JGE, Elwenspoek M, Kelly JJ. An electrochemical microactuator: principle and first results. *J Microelectromechanical Syst*. 1996;5(1):2–9.
30. Benito-Lopez F, Byrne R, Răduță AM, Vrana NE, McGuinness G, Diamond D, et al. Ionogel-based light-actuated valves for controlling liquid flow in micro-fluidic manifolds. *Lab Chip*. 2010;10(2):195–201.
31. R. G, C.E. N, J. G, X. Z, G.G. D, M. R, et al. Centrifugo-pneumatic valving utilizing dissolvable films. *Lab a Chip - Miniaturisation Chem Biol* [Internet]. 2012;12(16):2894–902. Available from: <http://ovidsp.ovid.com/ovidweb.cgi?T=JS&PAGE=reference&D=emed10&NEWS=N&AN=2012436014>
32. Hartshorne H, Backhouse CJ, Lee WE. Ferrofluid-based microchip pump and valve. *Sensors Actuators B Chem*. 2004;99(2):592–600.
33. Oh KW, Park C, Namkoong K, Kim J, Ock K-S, Kim S, et al. World-to-chip microfluidic interface with built-in valves for multichamber chip-based PCR assays. *Lab Chip*. 2005;5(8):845–50.
34. Go JS, Shoji S. A disposable, dead volume-free and leak-free in-plane PDMS microvalve. *Sensors Actuators A Phys*. 2004;114(2):438–44.
35. Kinahan DJ, Kearney SM, Dimov N, Glynn MT, Ducrée J. Event-triggered logical flow control for comprehensive process integration of multi-step assays on centrifugal microfluidic platforms. *Lab Chip*. 2014 Jul;14(13):2249–58.

36. Lee W, Jung J, Hahn YK, Kim SK, Lee Y, Lee J, et al. A centrifugally actuated point-of-care testing system for the surface acoustic wave immunosensing of cardiac troponin I. *Analyst* [Internet]. 2013;138(9):2558–66. Available from: <http://www.ncbi.nlm.nih.gov/pubmed/23478433>
37. Park J-M, Cho Y-K, Lee B-S, Lee J-G, Ko C. Multifunctional microvalves control by optical illumination on nanoheaters and its application in centrifugal microfluidic devices. *Lab Chip*. 2007;7(5):557–64.
38. Yang EH, Han SW, Yang SS. Fabrication and testing of a pair of passive bivalvular microvalves composed of p+ silicon diaphragms. *Sensors Actuators A Phys*. 1996;57(1):75–8.
39. Andersson H, van der Wijngaart W, Griss P, Niklaus F, Stemme G. Hydrophobic valves of plasma deposited octafluorocyclobutane in DRIE channels. *Sensors Actuators B Chem*. 2001;75(1):136–41.
40. Bonasso M, Barattini P, Isticato R, Donadio G, Giusti A, Philimis P, et al. MariaBox: First prototype of a novel instrument to observe natural and chemical pollutants in seawater. In: *OCEANS 2017 - Aberdeen*. 2017. p. 1–5.
41. Maguire I, Fitzgerald J, McPartlin D, Heery B, Murphy C, Nwankire C, et al. A centrifugal microfluidic-based approach for multi-toxin detection for real-time marine water-quality monitoring. In: *OCEANS 2017 - Aberdeen*. 2017. p. 1–8.
42. Becker H, Locascio LE. Polymer microfluidic devices. *Talanta*. 2002;56(2):267–87.
43. Bartholomeusz DA, Boutté RW, Andrade JD. Xurography: rapid prototyping of microstructures using a cutting plotter. *J Microelectromechanical Syst*. 2005;14(6):1364–74.
44. Nayak NC, Lam YC, Yue CY, Sinha AT. CO₂-laser micromachining of PMMA: the effect of polymer molecular weight. *J Micromechanics Microengineering*. 2008;18(9):95020.

45. Grumann M, Brenner T, Beer C, Zengerle R, Duccrée J. Visualization of flow patterning in high-speed centrifugal microfluidics. *Rev Sci Instrum.* 2005;76(2):25101.

Chapter 5: A Centrifugal Microfluidic-Based Approach for Multi-Toxin Detection for Real-Time Marine Water-Quality Monitoring

Chapter Foreword:

Building on the previously presented algal toxin detection system (Chapter 3) and the autonomous microvalve mechanism (Chapter 4), the summation of both platforms will be presented in this chapter. This will specifically include the furtherment of the single-toxin detection platform presented in Chapter 3 into a simultaneous multi-toxin monitoring platform, achieved through the integration of the autonomous microvalve mechanism demonstrated in Chapter 4. This platform was used as stepping-stone to the final eight-analyte centrifugal microfluidic platform designed for MariaBox project, discussed further in Chapter 6.

The limit of detection (LOD) of the platform could not be determined due to the larger size of the disc being incompatible with the detection system presented in Chapter 3. This platform was specifically tailor-made for compatibility with the MARIABOX device, and it was hoped that optical detection could have been comprehensively performed using this system. Unfortunately, MARIABOX detection platform was not ready in time for this study. Therefore, fluorescence microscopy was used to confirm successful assay execution after integration of the autonomous microvalve mechanism.

Summary of the nature and extent of candidate's work present in this chapter:

First author, initiation, key ideas, design and engineering of platform, disc fabrication, biosensor integration (*collaboration with Dr. Jenny Fitzgerald*), data collection and analysis (*collaboration with Dr. Jenny Fitzgerald*), manuscript development and writing up.

Summary of the nature and extent of work not performed by candidate present in this chapter:

Antibody Characteristics (including performance, selection and labelling of the antibodies) was performed by Dr. Jenny Fitzgerald.

A Centrifugal Microfluidic-Based Approach for Multi-Toxin Detection for Real-Time Marine Water-Quality Monitoring

Ivan Maguire, Jenny Fitzgerald, Daniel McPartlin, Brendan Heery, Caroline Murphy, Charles Nwankire, Richard O'Kennedy, Jens Ducreé, Fiona Regan

The article was published on 26 October 2017.
IEEE - OCEANS 2017 - Aberdeen (10.1109/OCEANSE.2017.8084975)

5.1 Abstract

Globally, fresh and brackish water sources are constantly under threat of exposure to toxins. Two of the most prevalent toxins from fresh and brackish water blooms are the cyclic peptide toxins of the microcystin family, formed from cyanobacterial, and the kainic acid analog neurotoxin known as domoic acid. There is therefore a significant need for constant and cost-effective 'on-site' algal-toxin monitoring to respond to constantly increasing demand for safe and 'toxin-free' fresh-water, shellfish and fish stocks. Herein, we describe a Lab-On-A-Disc (LOAD) platform which was developed to assess microcystin and domoic acid concentration levels *in-situ*. Using recombinant antibody technology, the LOAD platform combines immunofluorescence with centrifugally driven microfluidic liquid handling to achieve a next-generation disposable device for high throughput sampling.

5.2 Introduction

5.2.1 Overview of the problem

To sustain a rapidly increasing of population growth, the global demand for clean, safe water supplies has never been more apparent. It has been previously reported, and predicted, that anthropogenic environmental impacts will continue to increase the prevalence and duration of harmful freshwater cyanobacterial and algae blooms.(1,2) Other influences also reported are global warming and water quality degradation,

particularly due to eutrophication. Human, ecological and economic health can all be negatively impacted by harmful cyanobacterial blooms formed due to eutrophication. (3,4)

One of the most dangerous toxins documented is the cyclic peptide cyanobacterial toxin microcystin-LR (MC-LR), shown in Figure 5.1-**Left**. MC-LR is the predominant congener of the microcystin family which derived from the cyanobacteria *microcystis aeruginosa*, and commonly recorded in fresh and brackish water. Significant health issues can arise through ingestion of MC-LR for humans and animals alike (5), with patients often presenting with hepatotoxicity and carcinogenesis (6). In the EU, concentration limits for microcystin which elicit action are regulatory levels for is 1 ng/mL for drinking water and 20 ng/mL for bathing sites. (4) One of the most noted cases of human exposure occurred in a haemodialysis clinic in Caruaru, Brazil in 1996 (7,8). In this case, it was reported that of the 116 patients undergoing dialysis, 89% experienced severe symptoms, and 100 of these patients developed liver failure resulting in the death of 52 patients.

Another well documented marine toxin is Domoic acid (DA), shown in Figure 5.1-**Right**, which is a highly potent neurotoxin. It is naturally produced by several diatom species of the *genus Pseudonitzschia*, and is responsible for the amnesic shellfish poisoning (ASP) illness.(9) Some of the human responses following exposure to ASP include gastrointestinal distress, confusion, disorientation, seizures, permanent short-term memory loss, and in the most severe cases death.(9,10) The first documented case of ASP poisoning was noted in 1987 on the eastern coast of Prince Edward Island, Canada, where harvested mussels, contaminated with DA, were consumed.(9–12) This case resulted in the death of 4 people of some total 143 reporting similar DA associated symptoms. Following the Canadian ASP event of 1987 and to protect seafood consumers, authorities established an action limit for DA of 20 mg DA/g shellfish tissue.(9)

These case studies demonstrate not only the importance of continuous environmental monitoring, with special regard to on-site algae-toxin monitoring, but also the need for a multi-toxin detection platform. Therefore, preceding this will be several both lab- and in-situ- based toxin monitoring solutions.

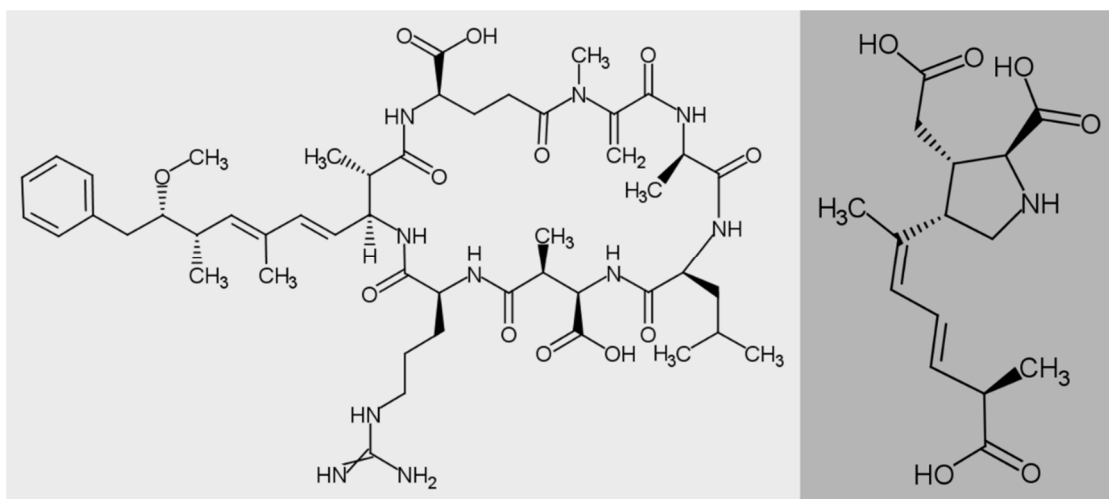


Figure 5.1: The chemical structures of microcystin-LR (left) and domoic acid (right) in their predominant congener forms

5.2.2 Current approaches for toxin analysis

5.2.2.1 MC-LR detection solutions

There is currently multiple in-field based platforms capable of monitoring MC-LR, with solution suggested by MacKenzie and colleagues in 2004.(13) This solution is referred to as solid phase adsorption toxin tracking (SPATT), and has since been further adapted to detect and monitor toxic algal blooms as well as shellfish contamination events (14). While this technique is useful, it requires a deployment and recovery process for lab-based liquid chromatography-mass spectrometry (LC-MS) analysis. This limits it as a semi-*in-situ* analysis system and prevents autonomous continuous monitoring. Another limitation of this approach is the relatively low sample rate due to the weekly deployment and recovery process, thus impeding the throughput capabilities and potential of real-time data capture. These limitations also indicate a requirement for trained experts for handling and characterisation of weekly samples, therefore increasing associated costs significantly and reducing the ability of rapid, high density sampling of sites.

Other previously reported biosensor-based methods for microcystin detection have been limited by the requirement for laboratory-based analysis. Chianella and colleagues reported a novel molecularly imprinted polymer (MIP)-based-piezoelectric sensor for Microcystin-LR with a low detection limit for 0.35nM for in-laboratory analysis (15).

Similarly, electrochemical biosensors with demonstrated sensitivities of $0.1 \mu\text{g}/\text{L}^{-1}$ for microcystin-LR (16) and $9.0 \times 10^{-11} \text{ M}$ for a microcystin specific gene sequence (17) were reported, however both of these methods are primarily laboratory-based. A highly sensitive immunosensor for microcystin has previously been reported (18), based on graphene–gold nanocomposite/functional conducting polymer/gold nanoparticle/ionic liquid composite film with electrodeposition with detection limits as low as $3.7 \times 10^{-17} \text{ M}$. Another immunosensor based-method by Queirós et al., reported the use of a Fabry–Pérot interferometer using an optical fibre coated with a sol–gel imprinted sensing membrane with a sensitivity of $12.4 \pm 0.7 \text{ nm}/\text{L}/\mu\text{g}^{-1}$ (19). A cantilever immunosensor was reported which tested microcystin concentrations as low as $1 \text{ pg}/\text{mL}^{-1}$ in varying water sources (20). These methods, however sensitive, all suffer from the requirement of expensive laboratory equipment and specially trained personnel to perform the analysis. An in-situ based method was previously reported by Long and colleagues, who used a commercially available portable trace organic pollutant analyser (TOPA) for the detection of microcystin, however the limit of detection of the assay was significantly higher than any of the lab-based methods at $0.03 \mu\text{g}/\text{mL}^{-1}$ (21).

5.2.2.2 DA detection solutions

It has been previously reported that surface plasmon resonance (SPR) (22,23), antibody technology (24,25) and optical MIP-based molecular recognition sensors (26) can be used in detecting DA. Lotierzo *et al* and Stevens *et al*. reported a detection limit of $5 \mu\text{g}.\text{l}^{-1}$ and $3 \mu\text{g}.\text{l}^{-1}$, respectively. (22,23) The antibody-based approaches taken by Zhou *et al*. and Micheli *et al*. observed a $100 \mu\text{g}.\text{l}^{-1}$ and $5 \mu\text{g}.\text{l}^{-1}$ detection limit respectively. (24,25). The MIP-based approach, taken by Henry *et al*. reported a detection limit of $5 \mu\text{g}.\text{l}^{-1}$ also. (26)

5.2.3 A Lab-On-A-Chip (LOAC) solution to toxin monitoring

In order to facilitate detection of microcystin at the ‘point of need’ On-site algal toxin monitoring can alternatively be achieved using Lab-On-A-Chip (LOAC) technologies. This is possible as small volumes of liquids can be precisely controlled and manipulated to undergo assessment as if in lab environments, even when in-situ. These relatively new technologies are highly customisable and commercially-viable alternatives to the

current detection methods employed for environmental monitoring. LOAC-based platforms, previously designed for environmental monitoring, are currently capable of detecting phosphate(27–29) and E. Coli (30,31), whilst also offering the capabilities of detecting polycyclic aromatic hydrocarbons (PAHs), endocrine disruptors (EDCs), inorganic ions and heavy metals, by utilising already developed microfluidic techniques (32). Whilst LOAC platforms are highly convenient, cost-effective and highly adaptive, the pumps often required to drive sample progression through a LOAC cartridge can be expensive. This is primarily due to the high costs associated with precise pumping mechanisms. A derivative of the LOAC platform, circumventing these externally required expenditures is the Lab-On-A-Disc platform (LOAD)(33,34).

5.2.4 Proposed Lab-On-A-Disc (LOAD) alternative solution

The LOAD centrifugal microfluidic platform replaces the previously required pumping mechanisms with a centrifugal driving force, utilising a more cost-effective motor system. To date, on-chip water quality assessment systems have been primarily developed using LOAC systems, with only a few examples reported on centrifugal disc (CD) platforms (Czugala et al., 2012; Hwang et al., 2013). There are multiple advantages associated with LOAD platforms including; autonomous pumping using centrifugal forces, precise liquid handling, control of samples using valves, ability to multiplex assays using identical test conditions and a myriad of detection techniques compatible on disc, making it an ideal technique for in-situ environmental monitoring.

In this paper, a novel LOAD-based platform, which has been developed to assess both M-LR and DA toxin levels *in-situ*, with the additional capabilities for deployment as a long-term, real-time microcystin monitor will be presented (Figure 5.2-Left). Using highly-specific recombinant antibody technology, the LOAD platform combines immunofluorescence with centrifugally driven microfluidic liquid handling to achieve a next-generation disposable device for high throughput sampling. Recombinant antibodies (RAs) were selected over alternative antibody technologies. This was because RAs would ensure a consistent bio-sensing detection as the RAs would remain homogeneous indefinitely.

A stockpile of these LOAD platforms will then be incorporated into the MARIABOX deployable system for a targeted deployment of 6 months. This deployable system will

incorporate a high sensitivity ‘LED-Photodiode’ based fluorescent detection system which was tailor-made for the LOAD platform (Figure 5.2-Right). The optical sensing system utilises the fluorescence signal of the toxin-specific reaction to be quantified, thus allowing rapid and accurate detection of the presence of M-LR and DA toxins simultaneously in less than 15 min with minimum user interaction and maximum reproducibility. The LOAD platform was first assessed using a simplified single assay detection system a replica electronics configuration stored in handheld 3-D printed casing. This method provides a low-cost diagnostic-alternative to the current laborious and costly methods used for toxin detection, and can be easily adapted for further alternative toxin monitoring.

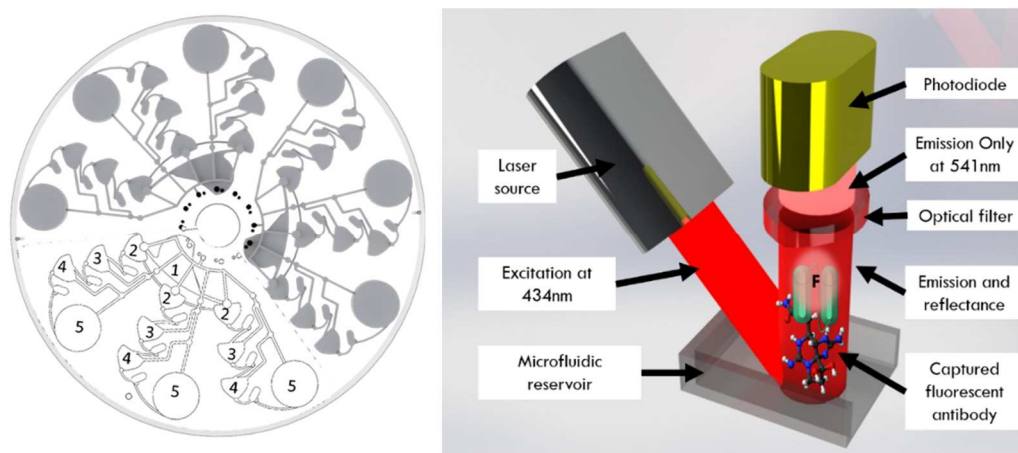


Figure 5.2: The MARIABOX platform and detection.

Left) The centrifugal Microfluidic platform with for triplicate triple-toxin detection. Each triplicate has a separate load zone, marked as ‘1’, which separates and mixes with the relevant detection antibodies located in zone ‘2’. Zones ‘3’, ‘4’ and ‘5’ represent the test detection zone, control detection zone and waste collection zone respectively. Right) The fluorescent detection setup which will be incorporated within the MARIABOX platform for determining the remainder of fluorescently-enabled anti-body presence after toxin conjugate pass-through has occurred. This is will be performed at zones ‘3’ and ‘4’, where toxin concentration can be inversely determined based on the recorded fluorescent intensity.

5.3 Results and discussion

The LOAD design was largely inspired by the limitations of current environmental monitoring techniques. The system itself was therefore designed to overcome some of these limiting factors; portability, cost-effectiveness, multiplexed sampling and ease-of-

use. This was achieved through small system size, low cost per assay with higher sample throughput, simultaneous multi-analyte detection in single assay form and reduced assay runtime through minimal user interaction and incubation periods. Due to the potential human health hazard posed by MC-LR and DA, and the repercussions associated with a false qualitative screening of waterbodies, including human health, fishery, recreational and economic impacts, a screening method needs to be capable of toxin detection with a significant degree of confidence. Therefore, both reliability of sampling handling and confirmation of fluorescent presence was required before a full calibration of the MARIABOX platform.

5.3.1 Characterisation of sample handling

The microfluidic platform was assessed whilst under centrifugation to confirm reliable and consistent sample handling. Figure 5.3 illustrates how close each assay pathway is with regards to progression with near synchronise movement occurring. While some microvalves did rupture before others, which falls within the expected rupture deviation of the Solublon™ material, this was also to be expected due to the manual manufacturing process of both the microvalves and LOAD platform which lead to some inconsistencies.

5.3.2 Fluorescent assessment of microfluidic

It was important to assess that binding was present before calibration of the MARIABOX platform. This was done through fluorescent microscopy. Figure 5.4 demonstrates the competitive inverse assay used on the LOAD platform, whereby the larger the toxin concentration within the loaded sample, the lower the fluorescent signal detected. This was initially compared to the expected thresholds of a reservoir containing the same population of fluorescent antibodies which would be used within the assay to determine a control high and low. From this, a comparison between a high toxin concentration of MC-LR and DA could then be done.

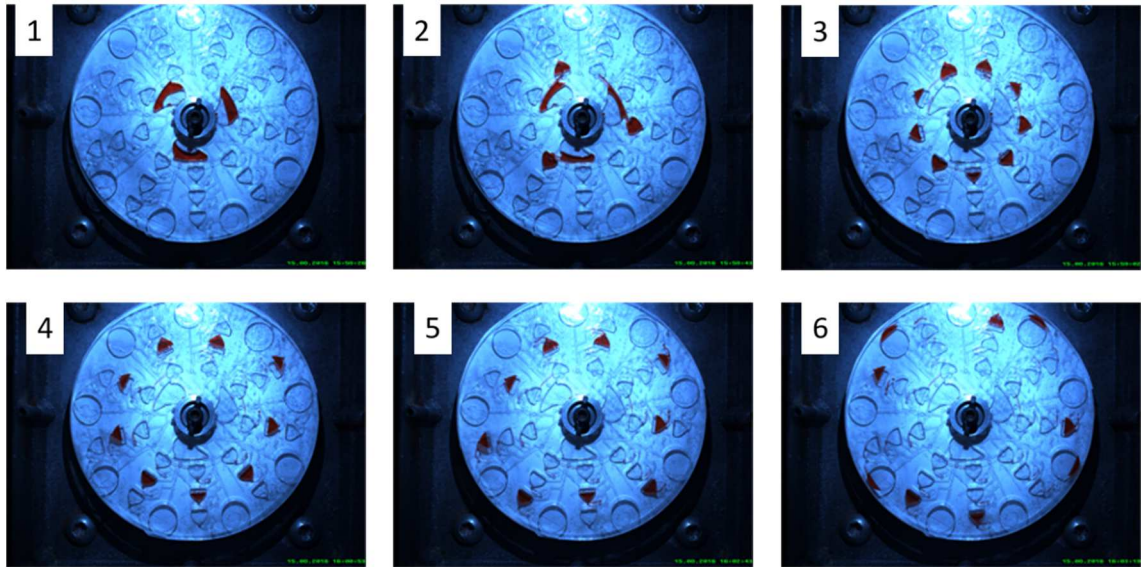


Figure 5.3: – Microfluidic disc characterisation.

1-6) illustrate the sample flow through each of the assay steps, represented by the reservoirs. Each valve is opened by pulsing the speed from low to high. This reduces the possibility of premature valve rupturing to maintain a consistent time delay in each reservoir.

5.3.3 Next steps to be taken

With confirmation of the LOADs reliability and the detectability of the fluorescence at varying concentrations of DA and MC-LR, integration and calibration of MARIABOX prototype will take place. This will include deployment in Oslo, Norway on the *MS Color Fantasy* in collaboration with NIVA, Oslo.

5.4 Conclusion

It has been observed that both microcystin and domoic acid can be simultaneously detected on a LOAD platform. While this has only been assessed using a fluorescent microscope, future work will include a full calibration assessment on the MARIABOX platform. Once this complete calibration has been achieved, it is aimed that the MARIABOX platform will be deployed for up to six months of autonomous use.

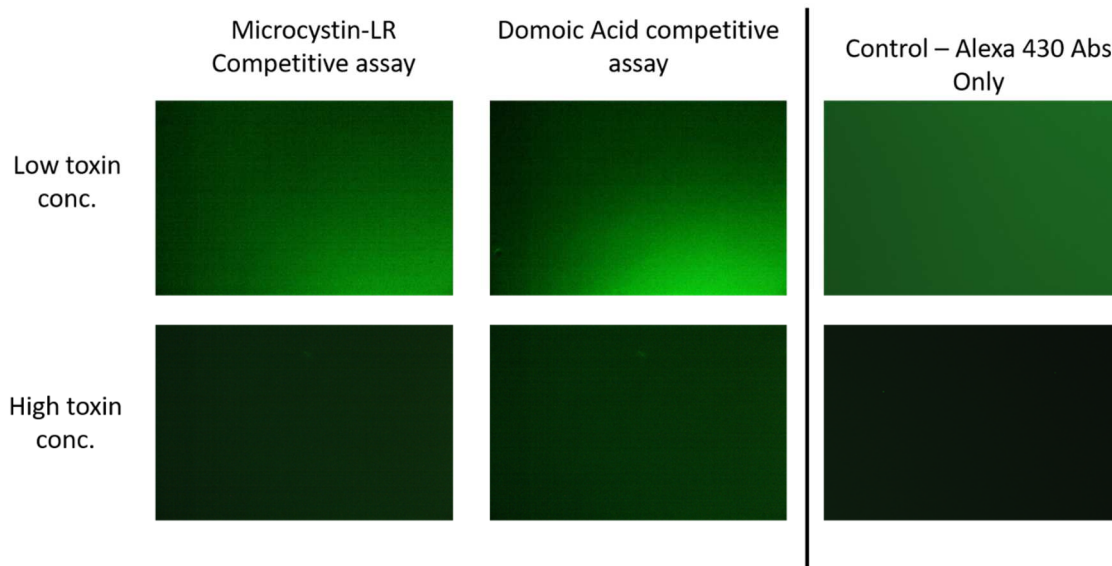


Figure 5.4: – Fluorescent microscopy images taken from the test reservoir floors.

Left) illustrates the fluorescence captured using a fluorescent microscope to assess the competitive assays of both microcystin-LR and domoic acid. Right) demonstrates the expected fluorescence levels with a high concentration of fluorescently enabled antibodies vs no antibody presence.

5.5 Methods and Materials

5.5.1 Chemical and biological reagents used:

MC-LR was sourced from Enzo life sciences (UK) Ltd. (cat no. ALX-350-012-M001). Alexa Fluor 430 (Alexa-430) fluorescent kit was sourced from Bio-Sciences Ltd., Charlemont Terrace, Crofton Rd, Dún Laoghaire, Dublin, Ireland. (cat no. A10171). Bis[3-(trimethoxysilyl)propyl]amine (cat no. 413356), Micro90 (cat no. Z281565), Ethanol, isopropanol and PBS were all sourced from Sigma Aldrich, Ireland Limited, Arklow, County Wicklow, Ireland. Donkey anti-Chicken IgY Fab was sourced from Gallus Immunotech (Antibodies-online GMBH). Black acrylic paint (sourced from Tiger Direct™) was also used for biosensor signal enhancement. Lake water samples were sourced from Leixlip reservoir in Dublin, Ireland.

5.5.2 Preparation of MC-LR and DA conjugates and fluorescent antibodies:

MC-LR and DA conjugates and the recombinant anti-Microcystin-LR-Alexa-430 and anti-Domoic-Acid-Alexa-430 were prepared, as described by Murphy et al. (35)

5.5.3 Microfluidic disc manufacturing:

The LOAD disc, shown in Figure 5.2-**Left**, was manufactured from PMMA sheets and PSA (ARseal™90880), sourced from Radionics™ and Adhesives Research™ respectively. The discs were manufactured through assembling consecutive layers of poly(methyl methacrylate) (PMMA) and pressure sensitive adhesive (PSA). (36–38)

5.5.4 Dissolvable film valves:

Dissolvable film (DF) valves were manufactured as reported by Gorkin *et al.* (39) Briefly, the DF was arranged on the disc to act as pneumatic valves which would become activated upon contact with sample, as shown in Figure 5.5 and Figure 5.6. The DF used, referred to as KC-35 film, was supplied by Harke Packpro, Germany. While its composition is proprietary, the KC-35 film is formed from SOLUBLON®, a water-soluble film based on the synthesis of polyvinyl alcohol (PVA). As the film is non-adhesive, it was adhered to PSA to create sticky tabs. One-tab geometry was used for all valves and were placed after each reservoir section. A two-valve arrangement both before and in the pneumatic valve was utilised to keep all liquids in separate sections of the disc from moving in sync with each other through the assay protocol.

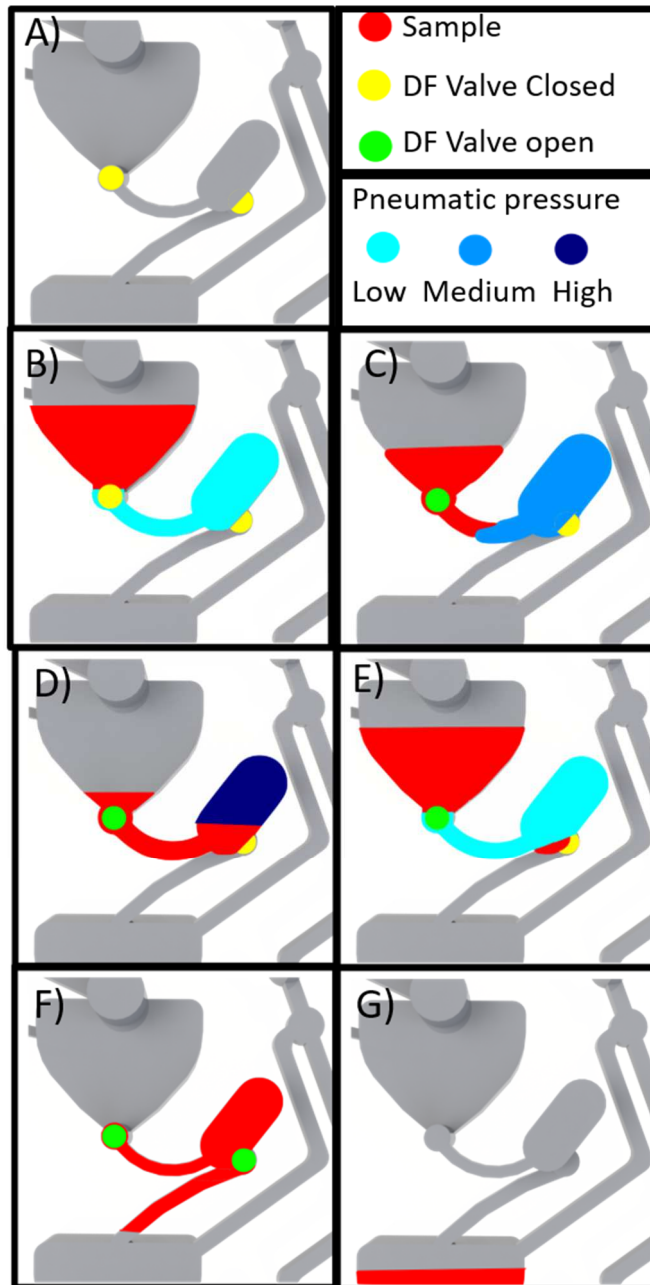


Figure 5.5: – An illustration to demonstrate how sample progression can be halted for a set period of time using a pneumatic stop approach, which was determined by a specific disc spin cycle.

A) The pneumatic stop (PS) consists of a narrow-to-wide microchannel with a DF valve (with a 30 secs time to dissolved upon contact with sample) located both at the start and midpoint of the PS. The purpose of these valves is to have a set volume of trapped air in each case, hence improving reliability of each valve. B-C) Once the first DF valve has dissolved, the sample will require an increase of disc spin speed in order to compress the trapped air by approximately 40%. D-E) Once this is achieved, the spin speed is dropped back to a lower value, with a small portion of the sample remaining trapped with the PS, where the second DF valve is located. F-G) Once this DF valve is dissolved, the trapped air within the pneumatic stopped is released and sample will progress to the next reservoir.

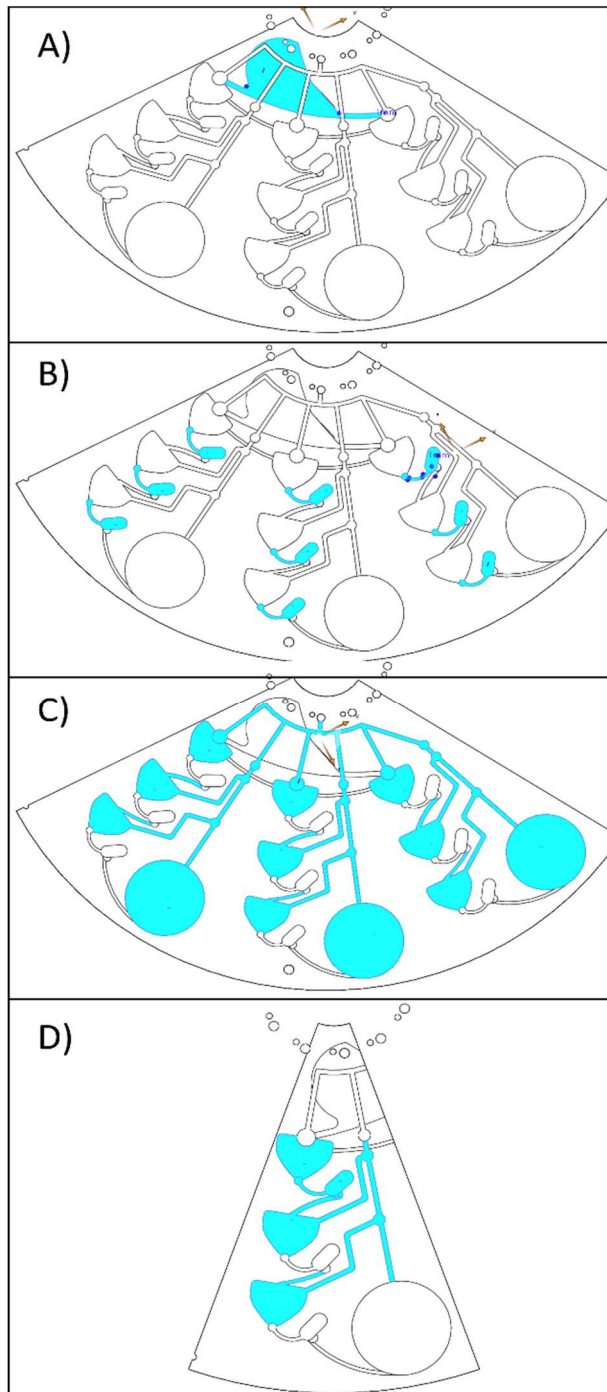


Figure 5.6: – An illustration of a triple-test assay on the disc, with the 5-step assay protocol in triplicate; Load reservoir (1), mixing reservoir (2), analyte detection zone (3), Control analyte detection zone (4) and waste storage (5) (see Figure 5.2-Left). One third of a disc will be used per run with up to three separate analyte detections occurring on a loaded sample. A) Shows the portion of the disc used per run, with the loading reservoir. This reservoir delivers the sample to the outer microchannels, followed by metering into the central reservoir. B) The locations of the pneumatic stops, with DF valves both before and after (see Figure 5.5.C) the collective microfluidic channels (sample transportation and ventilation) throughout the disc highlighted. D) illustrates a single assay with the features described in A-C.

5.5.5 Preparation of reservoir surface for bio-activation:

Before complete assembly of discs, the lower half (LH) of the discs, where antibody immobilisation was due to occur, were cleaned using a thorough surface cleaning process, which was then followed by O₂ plasma treatment. All the PMMA layers of the discs were initially cleaned in a class 1000 clean room using ultrasonication; A 2% (v/v) solution of Micro-90™ was used to remove oil, grease, resin and any biological material by ultrasonication at 50°C for 30 min. Subsequently, the PMMA layers discs were rinsed three times with deionised (DI) water and a 100% (v/v) solution of isopropanol. The PMMA discs were then rinsed a final time with DI water and dried using nitrogen. After cleaning, the LH of the discs were then assembled and placed in plastic bags for transportation to the O₂ plasma cleaner.

5.5.6 Amine surface functionalisation of biosensor reservoir floor by liquid phase:

The LH of the discs were placed in the plasma cleaner (Harrick plasma, USA) to expose the PMMA surfaces to a microwave-induced O₂ plasma. The operating pressure of the chamber was set using a scroll pump and a mass flow controller. The O₂ was applied as a gas stream, regulated by the integrated mass flow controller and adjusted to approximately 1000 mT. The PMMA discs were exposed to the O₂ plasma for 10 min. The detection reservoirs of the surface-activated discs were immediately coated in a solution of APTES to provide a binding bridge between the surface oxidation and hydroxylation (-OH groups) of the PMMA surface and the toxin conjugates of MC-LR/DA/Anti-chicken (Control) antibodies; A 3% APTES solution was prepared in 98% ethanol to functionalise the PMMA disc reservoirs. The discs were then placed in a 15 cm diameter petri dish with cover and incubated at room temperature for 1 h in a fumehood. After functionalisation, the discs were ultrasonically cleaned for 15 min (2x) using a solution of 98% ethanol. The discs were baked in an oven at 60°C for 2 h. If the temperature of the oven was set higher, significant cracking of the PMMA discs was noted. The discs were then cooled to room temperature before adding of the toxin conjugate/antibodies to surface.

5.5.7 Toxin conjugate binding/Control antibody binding to biosensor surface:

The Alexa-430 labelled specific scFv were coated on the 2nd radially-aligned reservoirs, also referred to as the 'incubation' zone (see Figure 5.2). The sequential release of the liquid following incubation is required to resuspend antibody coated on the surface of the immobilisation zone, as this area is not functionalised prior to coating, the antibody is passively adsorbed onto the surface and resuspended following incubation with the solution. Toxin, representing both MC-LR and DA, conjugated to BSA (1 µg/mL), was prepared in PBS solution, where 100 µL was then added to each of the 3rd (radially) reservoirs, also referred to as the 'test' reservoir. Anti-chicken IgY (H+L) 100 µL, a commercial antibody from Gallus Immunotech Inc., Canada, was added to each of the 4th radially-aligned reservoirs, also referred to as the 'control' reservoir (see Figure 5.2). The coated discs were stored at 4°C covered for 12 h. To prevent any non-specific binding occurring on the biosensor reservoir surface, the remaining activated amine sites were blocked by the addition of 200 µL of 3% BSA to each reservoir. This was left to block at 37°C for 1 hour. The blocking agent was aspirated and the prepared disc was ready for toxin determination.

5.5.8 Microfluidic disc characterisation:

The microfluidic discs were characterized on an in-house developed "spin stand" (40) as described by Kirby *et al.* (41) In short, centrifugation of the discs was controlled via computer operated spindle motor (Faulhaber Minimotor SA, Switzerland). A high sensitivity, short-exposure time camera (Pixelfly, PCO, Germany) and a stroboscopic light source (Drelloscop 3244, Drello, Germany) were combined and synchronized with the spindle motor using custom electronics to allow visualisation of hydrodynamic performance of the discs during centrifugation. Additionally, with the discs using manually activated microvalves, opening of the microvalves was achieved by pin puncture, allowing sample progression to occur. In summary, the disc was spun at 35 Hz, followed stopping the disc and opening the sequential microvalve, with this cycle repeated until the liquid had successfully passed through each reservoir.

5.5.9 Fluorescent microscope analysis:

Fluorescent microscope images were captured using the Optika fluorescent Microscope (XDS-3 FL4 Inverted trinocular EPI fluorescence microscope HBO illumination system) combined with the Alexa-430-Fluor Filter (EOPT-39008), all supplied by Lennox Ireland.

5.6 Acknowledgment

This work was supported by the FP7 EU-funded MARIABOX project. The MARIABOX project receives funding from the European Union Seventh Framework Programme - Grant Agreement No: 614088.

5.7 References

1. Hudnell HK, Dortch Q, Zenick H. An overview of the interagency, International Symposium on Cyanobacterial Harmful Algal Blooms (ISOC-HAB): advancing the scientific understanding of freshwater harmful algal blooms. In: Cyanobacterial Harmful Algal Blooms: State of the Science and Research Needs. Springer; 2008. p. 1–16.
2. Paerl HW, Huisman J. Blooms like it hot. *Science*. 2008;320(5872):57.
3. Carmichael W. A world overview—One-hundred-twenty-seven years of research on toxic cyanobacteria—Where do we go from here? In: Cyanobacterial harmful algal blooms: State of the science and research needs. Springer; 2008. p. 105–25.
4. World Health Organization, Chorus I, Bartram J. Toxic Cyanobacteria in Water: A guide to their public health consequences, monitoring and management. Retrieved March. E & FN Spon; 1999. 400 p.
5. Mackintosh C, Beattie K a., Klumpp S, Cohen P, Codd G a. Cyanobacterial microcystin-LR is a potent and specific inhibitor of protein phosphatases 1 and 2A from both mammals and higher plants. *FEBS Lett*. 1990;264(2):187–92.
6. Rinta-Kanto JM, Konopko E a., DeBruyn JM, Bourbonniere R a., Boyer GL, Wilhelm SW. Lake Erie Microcystis: Relationship between microcystin production, dynamics of genotypes and environmental parameters in a large lake. *Harmful Algae*. 2009;8(5):665–73.
7. Azevedo SMF, FO, Carmichael WW, Jochimsen EM, Rinehart KL, Lau S, Shaw GR, et al. rober. *Toxicology*. 2002;181(December):441–6.
8. Yuan M, Carmichael WW, Hilborn ED. Microcystin analysis in human sera and liver from human fatalities in Caruaru, Brazil 1996. *Toxicon*. 2006;48(6):627–40.
9. Lefebvre KA, Robertson A. Domoic acid and human exposure risks: a review. *Toxicon*. 2010;56(2):218–30.

10. Perl TM, Bédard L, Kosatsky T, Hockin JC, Todd ECD, Remis RS. An outbreak of toxic encephalopathy caused by eating mussels contaminated with domoic acid. *N Engl J Med*. 1990;322(25):1775–80.
11. Bates SS. Domoic acid producing diatoms: another genus added. *J Phycol*. 2000;36(6):978–83.
12. Wright JLC, Boyd RK, Freitas ASW de, Falk M, Foxall RA, Jamieson WD, et al. Identification of domoic acid, a neuroexcitatory amino acid, in toxic mussels from eastern Prince Edward Island. *Can J Chem*. 1989;67(3):481–90.
13. MacKenzie L, Beuzenberg V, Holland P, McNabb P, Selwood A. Solid phase adsorption toxin tracking (SPATT): a new monitoring tool that simulates the biotoxin contamination of filter feeding bivalves. *Toxicon*. 2004;44(8):901–18.
14. MacKenzie LA. In situ passive solid-phase adsorption of micro-algal biotoxins as a monitoring tool. *Curr Opin Biotechnol*. 2010;21(3):326–31.
15. Chianella I, Piletsky SA, Tothill IE, Chen B, Turner APF. MIP-based solid phase extraction cartridges combined with MIP-based sensors for the detection of microcystin-LR. *Biosens Bioelectron*. 2003;18(2):119–27.
16. Chen K, Liu M, Zhao G, Shi H, Fan L, Zhao S. Fabrication of a novel and simple microcystin-LR photoelectrochemical sensor with high sensitivity and selectivity. *Environ Sci Technol*. 2012;46(21):11955–61.
17. Yan F, Erdem A, Meric B, Kerman K, Ozsoz M, Sadik OA. Electrochemical DNA biosensor for the detection of specific gene related to *Microcystis* species. *Electrochem Commun [Internet]*. 2001 May [cited 2017 Mar 11];3(5):224–8. Available from: <http://linkinghub.elsevier.com/retrieve/pii/S1388248101001497>
18. Ruiyi L, Qianfang X, Zaijun L, Xiulan S, Junkang L. Electrochemical immunosensor for ultrasensitive detection of microcystin-LR based on graphene–gold nanocomposite/functional conducting polymer/gold nanoparticle/ionic liquid composite film with electrodeposition. *Biosens Bioelectron*. 2013;44:235–40.

19. Queirós RB, Silva SO, Noronha JP, Frazão O, Jorge P, Aguilar G, et al. Microcystin-LR detection in water by the Fabry–Pérot interferometer using an optical fibre coated with a sol–gel imprinted sensing membrane. *Biosens Bioelectron.* 2011;26(9):3932–7.
20. Ding Y, Mutharasan R. Highly sensitive and rapid detection of microcystin-LR in source and finished water samples using cantilever sensors. *Environ Sci Technol.* 2010;45(4):1490–6.
21. Long F, He M, Zhu AN, Shi HC. Portable optical immunosensor for highly sensitive detection of microcystin-LR in water samples. *Biosens Bioelectron.* 2009;24(8):2346–51.
22. Lotierzo M, Henry OYF, Piletsky S, Tothill I, Cullen D, Kania M, et al. Surface plasmon resonance sensor for domoic acid based on grafted imprinted polymer. *Biosens Bioelectron.* 2004;20(2):145–52.
23. Stevens RC, Soelberg SD, Eberhart B-TL, Spencer S, Wekell JC, Chinowsky TM, et al. Detection of the toxin domoic acid from clam extracts using a portable surface plasmon resonance biosensor. *Harmful Algae.* 2007;6(2):166–74.
24. Zhou Y, Zhang Y-Y, Shen Q-F, Lu S-Y, Ren H-L, Li Y-S, et al. Development of a novel antibody probe useful for domoic acid detection. *Biosens Bioelectron.* 2009;24(10):3159–63.
25. Micheli L, Radoi A, Guarrina R, Massaud R, Bala C, Moscone D, et al. Disposable immunosensor for the determination of domoic acid in shellfish. *Biosens Bioelectron.* 2004;20(2):190–6.
26. Henry OYF, Cullen DC, Piletsky SA. Optical interrogation of molecularly imprinted polymers and development of MIP sensors: a review. *Anal Bioanal Chem.* 2005;382(4):947–56.
27. Cleary J, Slater C, McGraw C, Diamond D. An autonomous microfluidic sensor for phosphate: On-site analysis of treated wastewater. *IEEE Sens J.* 2008;8(5):508–15.

28. Cleary J, Maher D, Diamond D. Development and Deployment of a Microfluidic Platform for Water Quality Monitoring. In: Mukhopadhyay SC, Mason A, editors. *Smart Sensors for Real-Time Water Quality Monitoring SE - 6* [Internet]. Springer Berlin Heidelberg; 2013. p. 125–48. (Smart Sensors, Measurement and Instrumentation; vol. 4). Available from: http://dx.doi.org/10.1007/978-3-642-37006-9_6
29. Duffy G, Maguire I, Heery B, Nwankire C, Ducreé J, Regan F. PhosphaSense: A fully integrated, portable lab-on-a-disc device for phosphate determination in water. *Sensors Actuators B Chem.* 2017;246:1085–91.
30. Beyor N, Seo TS, Liu P, Mathies RA. Immunomagnetic bead-based cell concentration microdevice for dilute pathogen detection. *Biomed Microdevices.* 2008;10(6):909–17.
31. Dharmasiri U, Witek MA, Adams AAA, Osiri JJK, Hupert MML, Bianchi TTS, et al. Enrichment and detection of *Escherichia coli* O157: H7 from water samples using an antibody modified microfluidic chip. *Anal Chem.* 2010;82(7):2844–9.
32. Nandagopal MSG, Antony R, Rangabhashiyam S, Selvaraju N. Advance approach on environmental assessment and monitoring. *Res J Chem Environ.* 2014;18(7):7.
33. Burger R, Ducreé J. Handling and analysis of cells and bioparticles on centrifugal microfluidic platforms. *Expert Rev Mol Diagn* [Internet]. 2012 May;12(4):407–21. Available from: <http://www.ncbi.nlm.nih.gov/pubmed/22616705>
34. Ducreé J, Haeberle S, Lutz S, Pausch S, Zengerle R, Stetten F Von, et al. The centrifugal microfluidic Bio-Disk platform. *J Micromechanics Microengineering* [Internet]. 2007 Jul 1 [cited 2013 Nov 7];17(7):S103–15. Available from: <http://dx.doi.org/10.1088/0960-1317/17/7/s07>
35. Murphy C, Stack E, Krivelo S, McPartlin D a., Byrne B, Greef C, et al. Detection of the cyanobacterial toxin, microcystin-LR, using a novel recombinant antibody-based optical-planar waveguide platform. *Biosens Bioelectron* [Internet]. 2015;67:708–14. Available from: <http://linkinghub.elsevier.com/retrieve/pii/S0956566314008380>

36. Bartholomeusz DA, Boutté RW, Andrade JD. Xurography: rapid prototyping of microstructures using a cutting plotter. *J Microelectromechanical Syst.* 2005;14(6):1364–74.
37. Becker H, Locascio LE. Polymer microfluidic devices. *Talanta.* 2002;56(2):267–87.
38. Nayak NC, Lam YC, Yue CY, Sinha AT. CO₂-laser micromachining of PMMA: the effect of polymer molecular weight. *J Micromechanics Microengineering.* 2008;18(9):95020.
39. R. G, C.E. N, J. G, X. Z, G.G. D, M. R, et al. Centrifugo-pneumatic valving utilizing dissolvable films. *Lab a Chip - Miniaturisation Chem Biol* [Internet]. 2012;12(16):2894–902. Available from: <http://ovidsp.ovid.com/ovidweb.cgi?T=JS&PAGE=reference&D=emed10&NEWS=N&AN=2012436014>
40. Grumann M, Brenner T, Beer C, Zengerle R, Ducrée J. Visualization of flow patterning in high-speed centrifugal microfluidics. *Rev Sci Instrum.* 2005;76(2):25101.
41. Kirby D, Siegrist J, Kijanka G, Zavattoni L, Sheils O, O’Leary J, et al. Centrifugo-magnetophoretic particle separation. *Microfluid Nanofluidics.* 2012;13(6):899–908.

Chapter 6: Development of a novel multi-analyte marine bio-sensor lab-on-a-disc platform: A design pipeline from concept to actuality

Chapter Foreword:

This Chapter will act as an executive summary of the design strategies pertaining to the development of a multi-analyte centrifugal microfluidic platform for the MariaBox project. Presented to the author is the fragmented design strategy used in developing this platform, whereby an efficient and cost-effective testing of each stepwise is made possible through the development of low-complexity replica discs eventually being integrated together, once optimised. This strategy will cover a number of stages; conceptualisation, assay integration, microvalve development, integration with the MariaBox Platform and the final deployable outputs.

Summary of the nature and extent of candidate's work present in this chapter:

First author, initiation, key ideas, input and management of biosensor development (collaboration with Dr. Jenny Fitzgerald, Dr. Caroline Murphy and Prof. Richard O'Kennedy), microvalves development (in collaboration with Prof. Jens Ducreé) and total system integration design strategies (in collaboration with Dr. Alessandro Giusti, Dr. Panayiotis Philimis, Dr. Rachele Isticato, Dr. Giuliana Donadio, Prof. Sabato D'Auria, Dr. Antonio Varriale, Dr. Maria Staiano, Dr. Anna Pennacchio, Prof. Kevin Thomas, Dr. Stephen J. Sayfritz), large scale fabrication, assisted in integration troubleshooting,

collection of all relevant 'MARIABOX' project information and analysis from partners, manuscript development and writing up.

Summary of the nature and extent of work not performed by candidate present in this chapter:

Methodology development for biosensor integration conducted primarily by Dr. Jenny Fitzgearld and Dr. Antonio Varriale. Heavy metal methodology developed by Dr. Giuliana Donadio.

Development of a novel multi-analyte marine biosensor lab-on-a-disc platform: A design pipeline from concept to actuality

I. Maguire, J. Fitzgerald, C. Murphy, R. O'Kennedy, J. Ducreé, F. Regan, A. Giusti, P. Philimis, R. Isticato, G. Donadio, S. D'Auria, A. Varriale, M. Staiano, A. Pennacchio, K. Thomas, S. J. Sayfritz

The article was received on 9 July 2018. (subject to change based on journal recommendations)

Emerald Sensors Review

6.1 Abstract

The development of microfluidic sensors as cost-effective strategies for environmental monitoring has been a primary goal for the platform since the 1980s. It has played a pivotal role in the downsizing of sample ranges and complex assay protocols used in analyte detection. This article aims to demonstrate the technical steps involved the designing, integrating and testing of biochemical assays on a centrifugal microfluidic platform for environmental applications, using MariaBox project as case in point. A gradual up-scaling design approach was used to allow development of the individual steps of the analytical assays on-chip, accommodating incremental testing. The concept to enable analysis of eight analytes on-chip simultaneously, with each requiring different assay methods, was the driver for the study. The final 8-analyte disc evolved through the testing process and emerged as a different, but effective design. The findings of the paper illustrate the complexities in developing a multi-analyte centrifugal microfluidic platform, and the incremental optimisation practices that should be employed. This will cover an initial conceptualisation, biosensor assay integration methods with surface modifications parameters used, microvalve development for synchronised assay execution, workarounds for integrations within the MariaBox system, and the final deployable outputs.

6.2 Introduction

The ideal criteria for environmental monitoring tools include; autonomous deployment, robust, quantitative and qualitative output, and cost-effectiveness. It is important to have a highly flexible monitoring platform which can process a large variety of analytes under different conditions. One such platform capable of this flexibility is the lab-on-a-disc centrifugal platform (LOD) (1,2), a derivative of the lab-on-a-chip (LOC) (3–6) microfluidic platform.

The flexibility of microfluidic platforms is primarily due to the significant advancement and more readily available micro-scale manufacturing technologies.(7) This has led to an exponential surge in many varying and novel applications to target the miniaturisation of laboratory-based techniques for conducting highly specific bio-chemical assay.(8) This is achieved through the combination of microfluidic features which can manipulate fluids, and their contents, with high precision; reservoirs for liquid storage, microchannels for liquid transport, microvalves for assay pause sequences, and transducing elements for detection. Advancement of each of these components is essential for platform success.(1,7,9) Common fluidic inputs can range from micro-litres (10^{-6}) to atto-litres (10^{-18}), depending on assay requirements. These low sample sizes correspond to a reduction in consumption of samples, reagents, materials, and detection times, whilst offering enhanced systematic detection resolution and sensitivity. Therefore, the overall associated development carbon footprint and cost of microfluidics, due to these advantages, is decreased.(10)

In order to develop a centrifugal microfluidic platform for environmental monitoring, a number of factors must be considered; sample/reagent type/size, analyte characteristics, sample matrix, assay protocols, transduction method, targeted style of use (autonomous, handheld), usage (single, multiuse). With regards to detection strategy on centrifugal microfluidics, there are currently a myriad of transducing solutions currently employed in microfluidic platforms for biosensing (2) and electrochemical sensing (11). The key to developing a successful, multi-analyte environmental processing unit lies within the integration and adaptation of new and current microfluidic features and transducing elements in microfluidic platforms.(12)

The “**Marine environmental *in-situ* Assessment and monitoring tool **Box****” (MariaBox) is a FP7 project (13), funded by the European Commission under the Horizon 2020 framework, which was developed in response to a number of European directives outlining the priority of marine environmental protection;

- “Strategies against pollution of water” - Article 16 of the Water Framework Directive (2000/60/EC)
- “Establishing the list of priority substances in the field of water policy and amending Directive 2000/60/EC” – Commission Decision (2455/2001/EC)
- “Laying down, pursuant to Directive (2000/60/EC) of the European Parliament and of the Council, technical specifications for chemical analysis and monitoring of water status.” - Commission directive (2009/90/EC)

As such, the MariaBox autonomous sensing platform was designed to be used as a tool which could assist in the decision-making process behind the development of European strategy for the marine protection and exploitation. Incorporated within the MariaBox platform is an autonomous, wireless analytical device, capable of long-term, real-time *in-situ* water monitoring when integrated onto a buoy, a free-floating device or a ship. The device utilises a multi-analyte centrifugal microfluidic processing unit (mCPU), incorporating novel biosensors, as a detection strategy. The purpose of this paper is to outline the design strategy undertaken during the development of the microfluidic bio-sensor disc from concept to delivery of the final 8-analyte disc.

6.3 Methodology

6.3.1 Chemical and biological reagents used

(3-Aminopropyl)triethoxysilane (APTES) (cat no. 440140), nickel powder (cat no. 266981), ethanol, isopropanol and phosphate buffered saline (PBS) were all obtained from Sigma Aldrich, Ireland Limited, Arklow, County Wicklow, Ireland. 1-Ethyl-3-(3-dimethylaminopropyl)carbodiimide bovine serum albumin (Imject EDC BSA) and 1-Ethyl-3-(3-dimethylaminopropyl)carbodiimide keyhole limpet hemocyanin (Imject EDC KLH) spin conjugation kits were obtained from Fisher Scientific (UK). Alexa Fluor 430 (Alexa-430) fluorescent kit (cat no. A10171) was obtained from Bio-Sciences Ltd.,

Charlemont Terrace, Crofton Rd, Dún Laoghaire, Dublin, Ireland. MC-LR (cat no. ALX-350-012-M001) was obtained from Enzo life sciences (UK) Ltd. Domoic acid polyclonal antibody was obtained from Abcam Ltd. Cambridge, United Kingdom. Donkey anti-chicken IgY Fab was obtained from Gallus Immunotech (Antibodies-online GMBH). Chelex® 100 Resin (cat no. 1422822) was acquired from Bio-Rad Laboratories.

6.3.2 Microfluidic disc manufacturing

The mCPUs were manufactured from poly(methyl methacrylate) (PMMA) sheets (ranging from ~0.5 - 2 mm in thickness) and “pressure sensitive adhesive” (PSA) sheets (ARseal™90880) (ranging from ~80 - 160 µm in thickness), sourced from Radionics™ and Adhesives Research™ respectively. The discs. Briefly, the PMMA and PSA sheets were laser- and knife-cut, respectively, where the layers were then intermittently stacked and pressure rolled. (14–16)

6.3.3 Microfluidic disc fluidic characterisation

Fluidic actuation studies were performed on an in-house developed “spin stand” (17), as described by (18). Briefly, disc centrifugation was achieved using a computer operated spindle motor (Faulhaber Minimotor SA, Switzerland), synchronized, using custom electronics, with a high sensitivity, short-exposure time camera (Pixelfly, PCO, Germany) and a stroboscopic light source (Drelloscop 3244, Drello, Germany) pairing.

6.3.4 Pre-storage of analyte conjugate and control on disc

The Alexa-430 labelled analyte specific antibodies (anti-analyte) and chicken IgY antibodies were coated on the 2nd radially-aligned ‘incubation zone’ reservoir where 100 µL of each antibody concentration was added (40 µg/mL). As this reservoir was not functionalised prior to coating, the anti-analyte was passively adsorbed onto the reservoir floor of the incubation zone. The sequential release of the analyte-containing sample was then required for antibody resuspension within this zone. Anti-analyte, conjugated to BSA (1 µg/mL) was prepared in a PBS solution, where 100 µL was then added to each of the 3rd radially-aligned ‘test’ reservoir (see Figure 6.1.a). 100 µL of a commercially available anti-chicken IgY (H+L), at approximately 10 µg/mL (Gallus Immunotech Inc., Canada), was added to each of the 4th radially-aligned ‘control’ reservoir (see Figure 6.1.a). The coated discs were stored at 4°C covered for 12 h. To avoid any non-specific binding from occurring on the biosensor reservoir floor, the

remaining activated amine sites were then subsequently blocked with 200 μL of 3% BSA (in PBS solution) added to each reservoir. The blocking agent was left to incubate at 37°C for 1 h, after which it was aspirated. Finally, the disc assembly was completed and the prepared disc was ready for toxin determination.

6.3.5 Biosensor integration

6.3.5.1 *Surface modification*

This method allows activating the top of the surface with chemical groups able to react towards the COOH and/or NH₂ residues present in the biomolecules. The surface derivatization was made through the incubation of 50 μL of 3% APTES in 98% Ethanol for 1 hour. The discs were placed in 15 cm diameter petri dishes to prevent the 3% APTES in EtOH from evaporating. The disc was then rinsed twice with 98% ethanol, baked at 85°C oven for 2 hours and then allowed to cool before adding the analytes-conjugate.

6.3.5.2 *Functionalization of the surface with analytes-conjugate.*

After the derivatization step, the surface is functionalized through two main steps. First, the analytes-conjugate (5 $\mu\text{g}/\text{mL}$) was pre-incubated for 20 minutes in a solution of 5 mM 1-ethyl-3-[3-dimethylaminopropyl] carbodiimide hydrochloride (EDC) and 5 mM N-hydroxysuccinimide (NHS) in HEPES 20 mM pH 6.0 and after added (100 μL) to each well and the disks are left coating at 4°C covered overnight. Then, the surface was washed three times with PBS buffer. The selected surface was derivatized first with the amino reactive group and then functionalized with specific analytes-conjugate, such as the pre-developed glutamine-perfluorooctanoic acid (GlnBP-PFOA), glutamine-naphthalene (GlnBP-NAFTHA) and casein-camphechlor (Casein-CHOR). to prevent any non-specific binding occurring on the biosensor reservoir surface, the remaining activated amine sites were blocked by the addition of 200 μL of 3% of protein (BSA and/or OVA) to each reservoir. This was left to block at 37°C for 1 hour. The blocking agent was aspirated and the prepared disc is ready for analytes determination. The bio-functionalized surfaces were then characterized for their ability to selectively bind to the biological targets.

6.3.6 Heavy metals assay integration

To conduct the total heavy metal assay, nickel-saturated Chelex 100 resin was added into the 3rd radially positioned reservoir until completely filled. The resin was prepared by re-suspending 50mg of resin in 500 Mm Nickel solution, followed by stirring for 20

min. This was followed by several washes in de-ionised water to remove any excess metal.

6.3.7 Manufacturing of a detection platform

The assay detectability was conducted using a 3d printed fluorescence detector, as described by (19), as a proof of concept for the MariaBox fluorescence detection system. In summary, the final fluorescence detection reader was 3D-printed from acrylonitrile butadiene styrene (ABS) and incorporated a top-down detection configuration, inclusive of a 405 nm excitation LED (cat no. 713-4898, Radionics Ltd Ireland), a 475 nm long pass filter (cat no. 64-617, Edmund Optics Ltd) and a 420–675 nm photo-LED emission detector (cat no. 708-2813, Radionics Ltd Ireland). This was controlled using a programmable IC (Pololu Wixel, cat no. 785, Cool Components Ltd).

6.4 Discussion

6.4.1 Analytes

Eight different analytes (summarised in Table 7), four algal toxins and four priority pollutant analytes, were targeted. In the case of the algal toxins, pre-lysed samples of azaspiracid, domoic acid, microcystin (and structurally related variants), and saxitoxin (and derivatives) were required to be quantitatively detected. While this was initially done manually before loading onto the disc, lysing on disc has been previously reported (20)(21) but was too complicated to achieve in the MariaBox mCPU also. Therefore the MariaBox platform incorporated a custom lysing instrument for sample handling prior to sample loading onto disc platform.(22) Targeted priority pollutant chemicals included camphechlor, naphthalene, perfluorooctanoic acid, and total heavy metals. A generic competitive inverse assay protocol, as described in Figure 6.1.a, was implemented for the fluorescence detection of all of the analytes, except for the total heavy metals which had minor deviations (Figure 6.1.b).

Table 7: List of chemical pollutants and algal toxins initially targeted by the MariaBox centrifugal processing unit.

	Category	Analyte	Partner	Ref.
Chemical pollutants	PAHs	Naphthalene	CNR - Consiglio Nazionale delle Ricerche	-
	Pesticides	Camphechlor	CNR - Consiglio Nazionale delle Ricerche	-
	PFCAs	Perfluorooctanoic acid	CNR - Consiglio Nazionale delle Ricerche	(23)
	Total Heavy Metals	Cu ²⁺ , Zn ²⁺	University of Naples Federico II	(24)
Algal toxins	Dinoflagellate, Alexandrium	Saxitoxin and derivatives	Dublin City University	(19,22,25)
	Cyanobacteria	Microcystin and structurally related variants.	Dublin City University	(19,22,25)
	Oscillatoria, Nostoc.	Azaspiracid	Dublin City University	-
	Pseudo nitzschia sp.	Domoic acid	Dublin City University	(19,22,25)

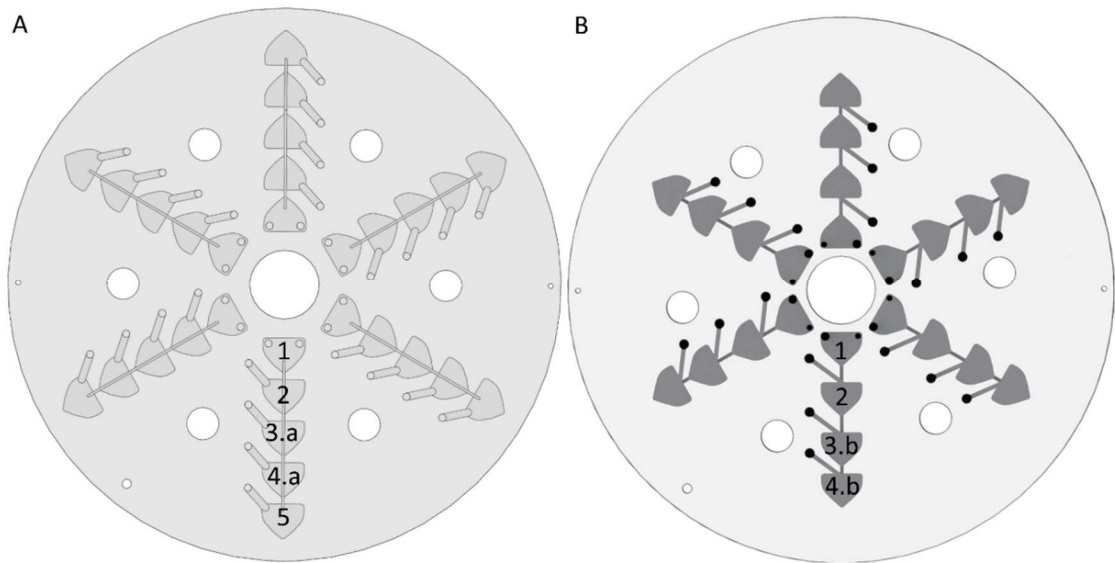


Figure 6.1: The inverse assay protocols used for fluorescence detection of both non-heavy metal analytes (A) and heavy metals (B), illustrated as a centrifugal microfluidic processing unit.

1) A sample containing the analyte of interest is loaded. 2) The analyte-containing sample is incubated with a fluorescently-enabled 'anti-analyte' to form a complex. Also present in this reservoir is fluorescently-enabled chicken antibodies to act as a control. 3.a) Any excess anti-analyte is then collected through interaction with the test biosensor for inverse quantification of analyte concentration. 3.b) The metal-containing complex is captured on the Chelex resin upon flow-through. Fluorescent measurement of this reservoir was used as a control mechanism for this assay. 4.a) The fluorescently-enabled chicken antibodies (control) interacts with the surface bound anti-chicken control antibody, confirming successful sample passthrough of test zone. 4.b) Any excess fluorescently-enabled anti-analyte is collected for inverse quantification of analyte concentration. 5) The sample holding the complex is then stored within the waste reservoir for dry measurement of the test and control reservoirs.

The inverse assay protocol can be represented by a microfluidic structure consists of different reservoirs, with each reservoir acting as a functional assay step (Figure 6.1). On-disc, these reservoirs are in radial alignment and connected by microchannels, with connected to a separate ventilation system. Depending of microfluidic structure complexity, multiple replicas are also possible on each disc. Below we summarise the operational steps that compose the final assay configuration, with the operational steps are similar in all versions of the discs used throughout the MariaBox final validations and demos.

1. The water sample is loaded into the first inner most reservoir.
2. The water sample is then transported and incubated with Alexa-430 labelled specific antibody (anti-analyte), coated on the 2nd radially-aligned reservoirs, also referred to as the 'incubation zone'. The liquid, following a 5-min incubation, resuspends the antibody coated on the surface.
3. The liquid complex is then transported and incubated with the assay biosensor zone, also referred to as the 'test zone', for 10 min. For the chemical assays, in the test reservoirs, the analytes are conjugated to the carrier protein (50 µg/mL), prepared in PBS solution at pH 7.4. For the biological assays, the PBS is not required.
4. Commercially available anti-chicken antibodies, which was previously bound to the control surface, interact with the fluorescently-enabled free chicken antibodies where a positive signal indicates correct sample-biosensor pass-over.
5. The sample is then transported to a waste reservoir to allow dry reading of biosensor and control zones.

This inverse assay demonstrates how a loaded sample interacts with anti-analytes, labelled with Alexa Fluor 430, and how excess of anti-analytes available are used for inverse quantification of analyte concentration.

In the case of the detection of total heavy metals, the detection assay deviated slightly. Firstly, a nickel-saturated Chelex resin was added within the disc for heavy metals only. This particular assay also had a reduction in steps from five to four, as no waste reservoir was required (see Figure 6.1.b). The order of assay steps also differed slightly from the main five step assay, with the first steps of sample loading and peptide mixing remaining the same, but the 3rd step involved Chelex resin flow-through with test detection as step 4. The fluorescent measurement of both the resin and the test zone was then used to approximate the fluorescent intensity ratio; i.e. the initial premix fluorescence of the protein should be the same intensity as the combined population of both the Chelex-bound fluorescent protein and fluorescent protein remaining in the collected sample after pass-through. The control mechanism used is a summation of fluorescence intensity values from both the test and Chelex resin reservoirs, where a set threshold should be reached to confirm a valid test.

6.4.2 Disc development process

6.4.2.1 *Design and Manufacturing*

The discs were designed using CAD software, where a layer-by-layer, hand-assembled manufacturing approach was employed (Figure 6.2). This was determined to be the easiest method for rapid modifications; such as inclusion of additional layers, change of material, and compatibility with both laser and knife cutter instruments. Generally, the microfluidic discs were engineered from sheets of poly(methyl methacrylate) (PMMA) ranging from 2 mm to 0.5 mm in thickness, with interlocking layers of modified “pressure sensitive adhesive” (PSA) sheets (ARseal™90880), sourced from Radionics™ and Adhesives Research™ respectively.(14–16) The design and development strategy used encompassed five stages (Figure 6.3);

- Conceptualisation – The conceptualisation stage was used to set a target of expected platform outcome. It is a particularly important stage for ensuring efficient collaborations, particularly emphasising realistic objectives, whilst also focusing the initial platform configuration.
- Assay integration – The assay integration stage is inclusive of designing, and optimising, of the fluidic actuation on-disc, modification and functionalisation of microfluidic features for conducting assay protocols, and the detectability of the assay results after completion.
- Microvalve integration – The microfluidic valve stage substitutes manually actuated elements within the disc for autonomous strategies. This reduces the user interaction, as well as minimising the expertise level, required to use the platform.
- System integration – The system integration stage offers potential collaborators to offer input into the design and development strategy for compatibility with their project elements. This could include minor modifications to the platform which could enhance the integration compatibility with the overall system, such as additional slots for autonomous manipulation, low complexity calibration replicas for rapid testing, and issue reporting.
- Deployable outputs – The deployable output stage includes the testing and the optimisations of the final platforms, operating with all the integrated partner elements, within the targeted environment.

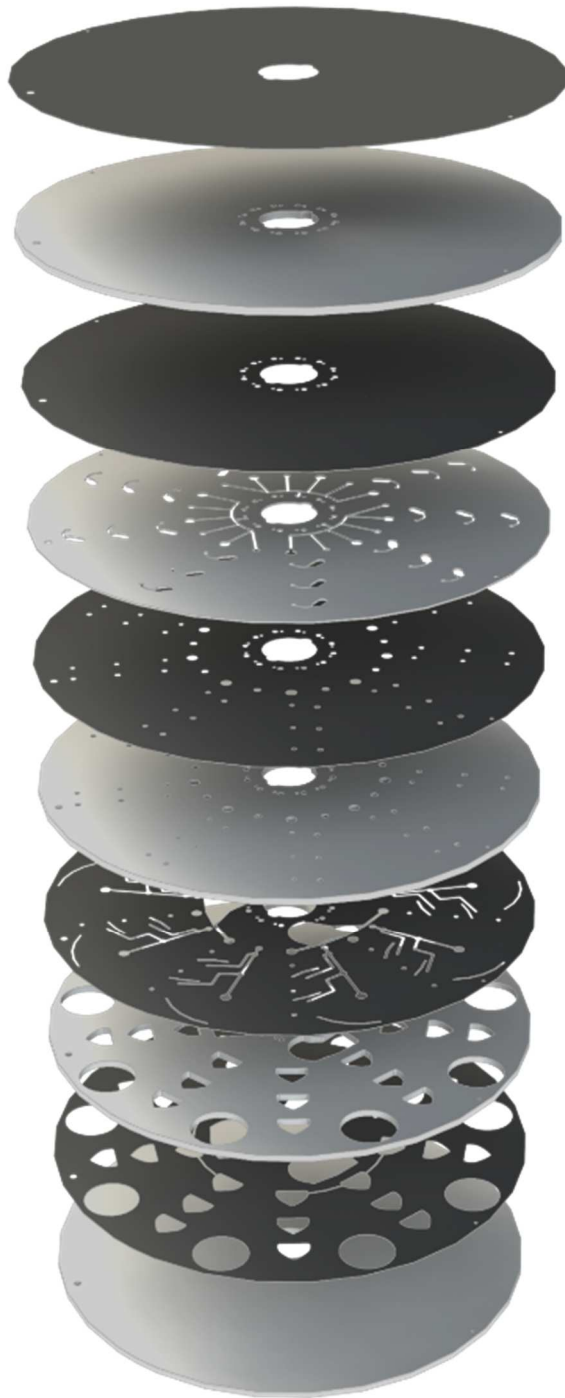


Figure 6.2: Layer-by-layer disc design approach using CAD software for ease of compatibility and rapid modification.

Poly(methyl methacrylate) (PMMA) Layers (white), ranging from 0.5 - 2 mm in thickness, are interlocked with pressure sensitive adhesive (PSA) layers (black), ranging from 80 – 150 μm in thickness. The thickness dimensions of both the PMMA and PSA make them ideal for μl liquid storage, and capillary action transportation, respectively.

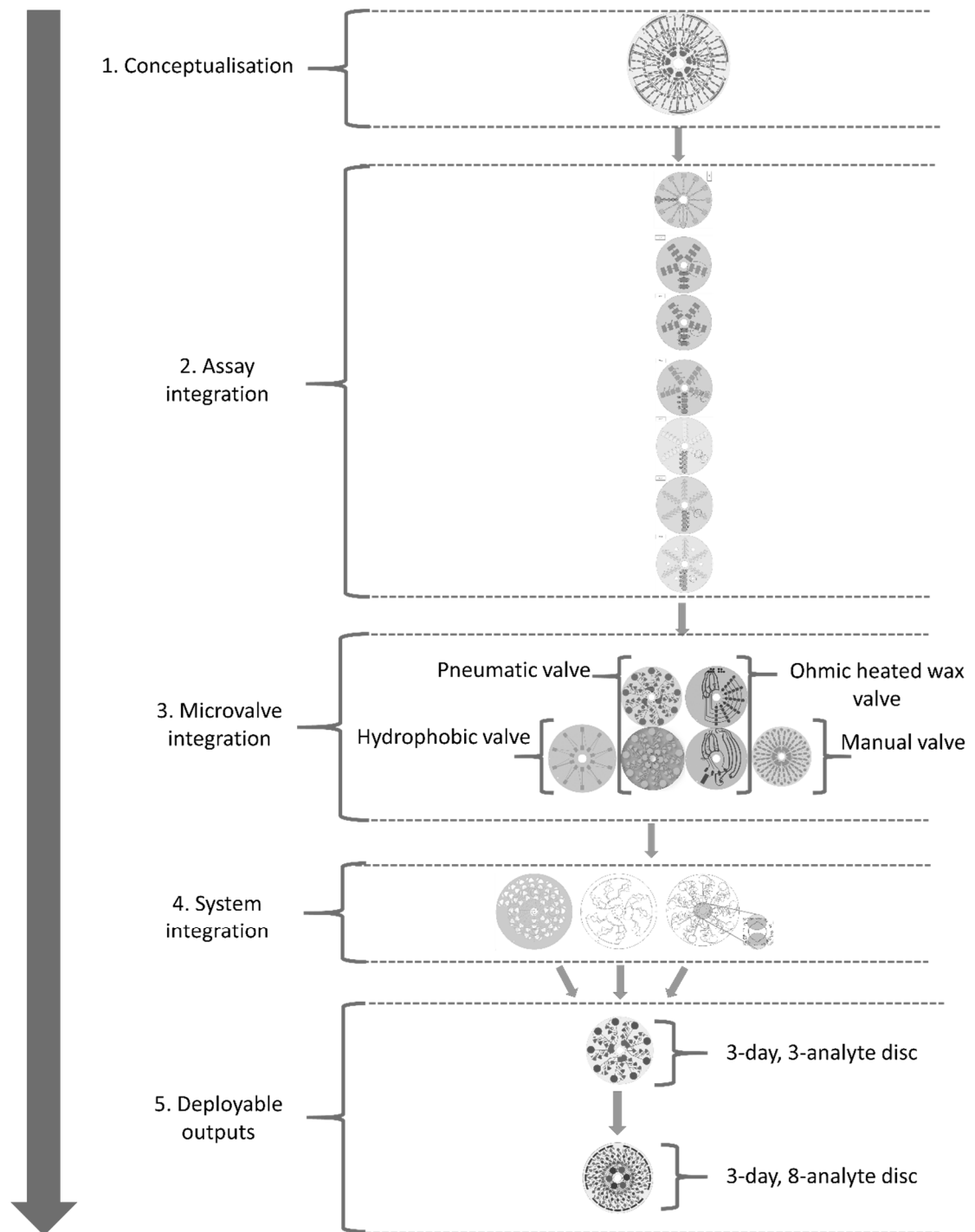


Figure 6.3: The design tree for the MariaBox centrifugal processing unit (mCPU).

Illustrated here, are the design fragmentations based on the initial conceptualisation design. In order of development, assay integration was prioritised to give the partners a proof of concept for testing assay integration. Next, microvalve integration strategies were investigated to automate assay protocol. This was then followed by development and distribution of calibration and test discs to partners for compatibility troubleshooting with the MariaBox platform. Finally, any compatibility issues were rectified, with two final deployable mCPU variants for the MariaBox platform produced; 3-day, 3-analyte disc (Biological analytes only) and 3-day, 8-analyte disc (all analytes).

6.4.2.2 Conceptualisation

As there were a number of individual and international partners involved in the development MariaBox analyte detection strategy, identification and agreement of the minimum requirements for conducting each partner's designated analyte detection protocols was conducted. This included specifically inputted liquid sample sizes required to conduct each assay (50 μL), the maximum number of assay steps (five) and the detection strategy (fluorescence spectroscopy). Based on these parameters, and in combination with the solutions presented by *Lai et al.*(26) and *Lee et. al.*(27), an initial conceptualisation of the MariaBox centrifugal processing unit (mCPU), encompassing the targeted analytes (shown in Table 7) detection assays was designed (Figure 6.4). A platform design tree (Figure 6.3) was designed, based on this mCPU concept, which was filled during the course of the study.

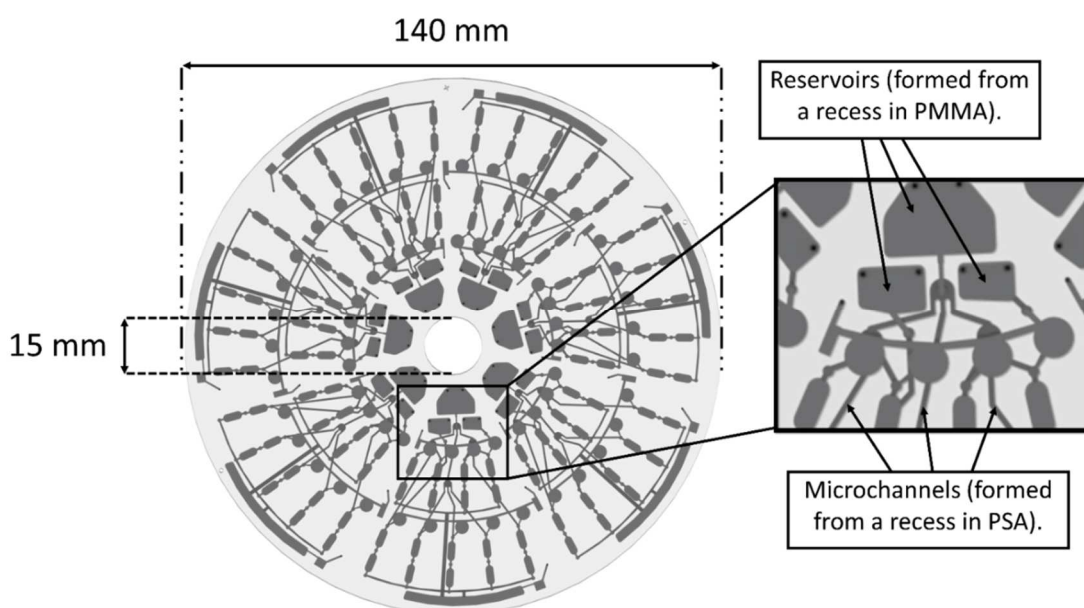


Figure 6.4: Initial conceptualisation of the MariaBox centrifugal processing unit (mCPU).

In this initial concept, integration of the minimum requirements required to perform the detection assay protocols were prioritized over fluidic actuation and device cost-effectiveness. This design was not manufactured, but rather used as an end target goal, with the design fragmented into simpler microfluidic features for ease of manufacturing, reproducibility and cost-effectiveness.

6.4.2.3 Assay integration

Initial efforts were focused on simplification of the mCPU concept to a single assay form. V1.0, illustrated in Figure 6.5. This disc had the same manufacturing issues associated with the concept disc, such as thickness, expensive and no autonomous valving mechanism for assay automation. Therefore, by reducing the number of performable assays, the required thickness could be reduced with an expansion of reservoir in the x-y plane.

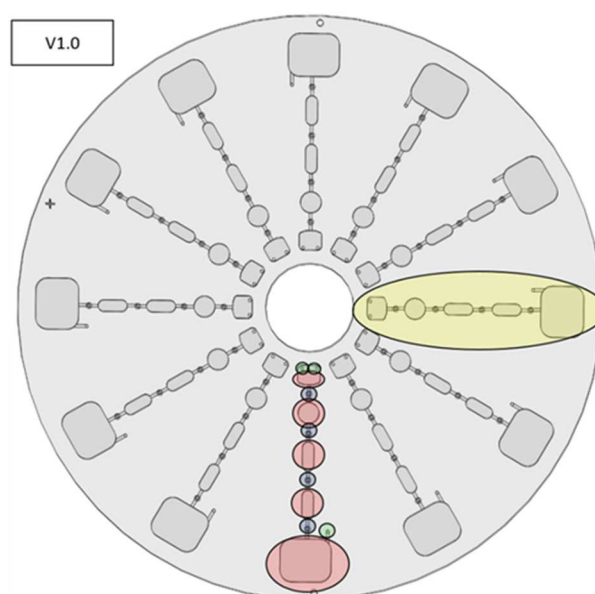


Figure 6.5: The single assay concept (v1.0).

The microfeatures contained within the disc consists of vents (green), reservoirs (red), microvalves (blue), manual vent caps (green with dark green dot). Modifications from the previous version is illustrated by yellow.

6.4.2.3 (a) Assay integration – fluidic actuation

A low complexity, 3-to-5 step assay protocol for assessing liquid transfer between reservoirs on the disc was developed (Figure 6.6). In the first iteration (V1.1), liquid transportation between the 3 reservoirs unintentionally halted when rotational frequency was constant due to the pneumatic trapping of air halting sample progression. Therefore, the subsequent version (V1.2) was a modified in such that each reservoir had a separate ventilation mechanism, which was capped. Transfer between desired reservoirs was only achieved by rupturing the adjacent ventilation cap of the

desired reservoir manually. With the successful liquid actuation of this version, this was then further expanded from a 3-step assay protocol proof of concept to a 4- and 5-step assay protocol, in V1.3 and V1.4 respectively. However, due to the non-rounded reservoir shape, sample loss occurred in these versions also. Therefore, in V1.5, a rounded reservoir modification was implemented prevent sample loss during assay execution.

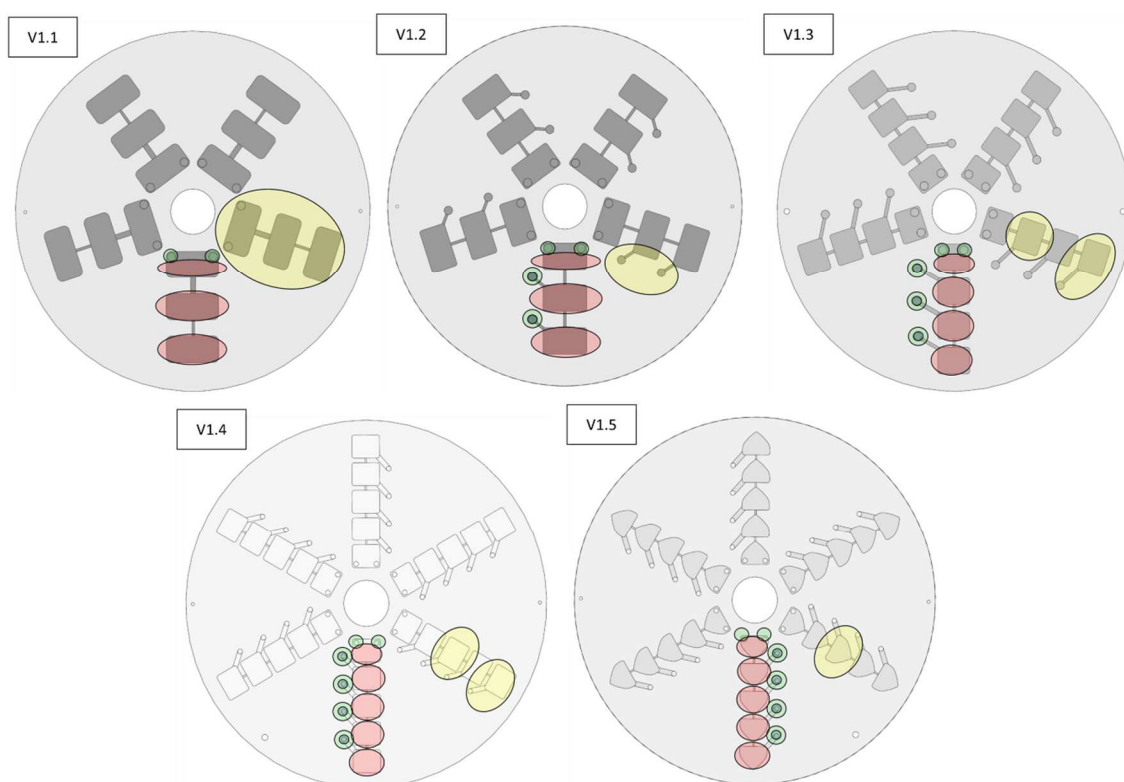


Figure 6.6: The design refinement process of the initial assay development with manual microvalve mechanism (V1.1-1.5).

The microfeatures contained within the disc consists of vents (green), reservoirs (red), microvalves (blue), manual vent caps (green with dark green dot). Modifications from the previous version is illustrated by yellow.

6.4.2.3 (b) Assay integration – biosensor integration

Modification of the PMMA surface was required in order to adhere a functionalisation complex for assay detection. The chemical based approach with EDC/NHS protocol (28), often used in SPR sensors, was modified in order to obtain active groups on the PMMA surface. These active groups are chemical molecules that react with the COOH and/or

NH₂ residues present in the biomolecules. Then, the reactive group present on the surface, reacts with the biomolecules through a chemical EDC/NHS reaction. In particular, after the activation of the surface with the APTES, the conjugates were attached. In Figure 6.7, the flowchart of the reaction using the APTES-EDC/NHS protocol is shown. Initially, the PMMA surface is O₂ plasma treated (Harrick plasma-USA, 1000 mT for 10 mins on high settings) and reacted with APTES to produce a silanization of the surface. After the silanization procedure, an amino reactive group was available on the surface for reaction. Then, the analyte conjugate was pre-incubated, with a solution of EDC/NHS, and added to the disc surface. This allowed the obtaining of a stable and permanent binding of the conjugate to the surface. This process was not required for the heavy metals assay, as this step was replaced by the use of Chelex resin.

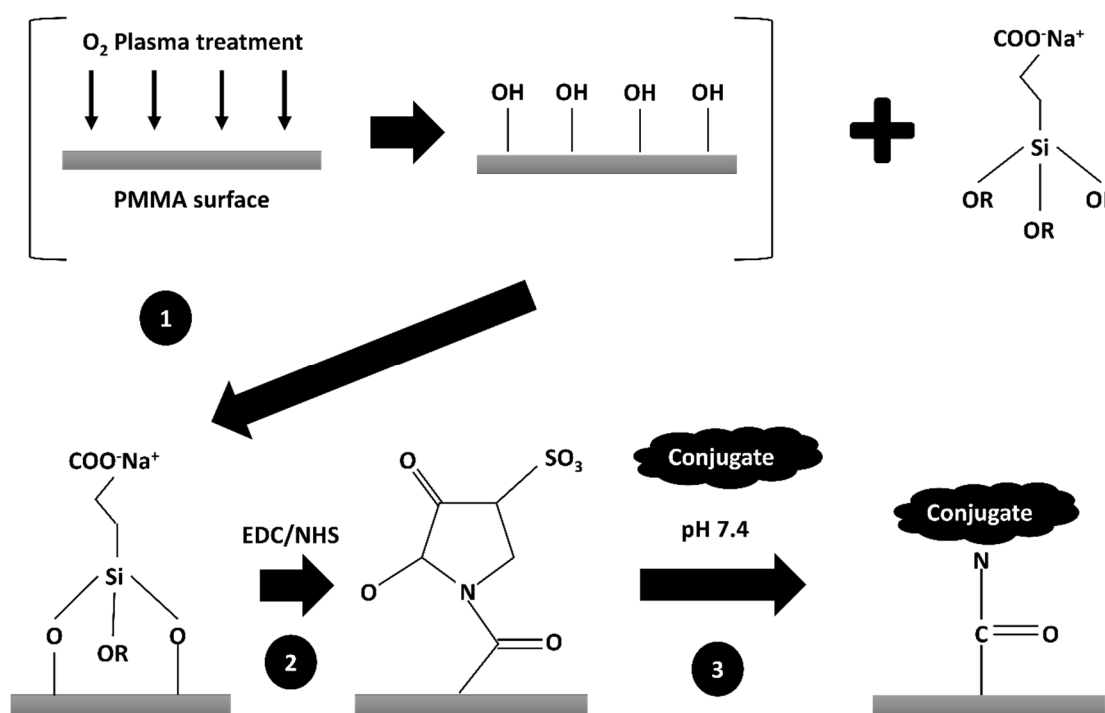


Figure 6.7: Flowchart of the APTES-EDC/NHS surface functionalisation chemical method.

6.4.2.3 (c) Assay integration – detectability

Finally, this mCPU V1.5 was tested using the first detection platform (Figure 7-left), which presented misalignment issues with the detection platform. This was rectified through the addition of alignment holes and pillars, which were integrated in V1.6, and

the succeeding detection platform (Figure 7-right), respectively. The performance of the liquid actuation using a cap vent valving mechanism for the mCPU V1.6 was also previously demonstrated (19). For convenience and rapid assay optimisation studies, a chip and holder mechanism (Figure 6.8), replicating the 3rd and 4th reservoir (test and control assay zones) in the mCPU, was also produced. This chip platform offered ease of assay optimisation by being compatible for use with both the detection platform (Figure 7-right) and a fluorescence microscope. This facilitated the optimisation and testing of the reservoir surface modification, whereby successfulness of an immobilised capture target could be determined.

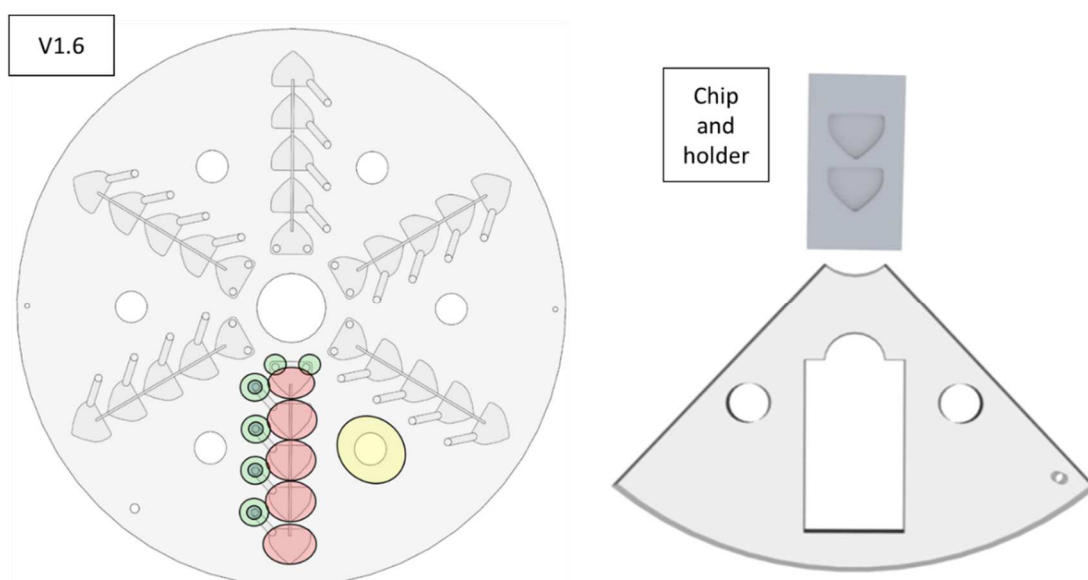


Figure 6.8: The detection optimised mCPU with manual microvalve mechanism (V1.6), and reservoir replica chip and holder for rapid biosensor integration.

The microfeatures contained within the disc consists of vents (green), reservoirs (red), microvalves (blue), manual vent caps (green with dark green dot). Modifications from the previous version is illustrated by yellow.

6.4.2.4 Disc Testing

Before a centrifugal microfluidic platform can be used *in-situ*, the platform must be rigorously tested and optimised to ensure correct assay execution. This assessment should include both a characterisation of the liquid actuation on disc and the assay detectability. The microfluidic platform fluidic performance was generally characterised

using a custom built “spin-stand” mechanism (17), as described by (18). In short, a high sensitivity, short-exposure time camera (Pixelfly, PCO, Germany) was paired with a stroboscopic light source (Drelloscop 3244, Drello, Germany), and synchronised with a spindle motor, was used in recording still images of the microfluidic platform whilst under centrifugation.

The assay detectability was conducted using a custom-made, 3d-printed fluorescence detector system, as described by (19), as a proof of concept for the MariaBox fluorescence detection system. The first detection platform iteration (Figure 6.9-left) was manufactured to complement the mCPU V1.5. This in-house built fluorescence detection system, however, was flawed. Firstly, this detection strategy was designed similar to a compact disc reader, in that it operated a bottom-up detection method (Figure 7-left). It was found that the surface modification of the reservoir floor during the capture target immobilisation resulted in a major degradation of the optical transparency of the surface. Secondly, alignment with the detection elements proved very difficult, with a temporary ‘2-pin’ mechanism used to lock the disc in place. This set-up was insufficiently rigid, whereby minor movement resulted in major fluctuations in the recorded optical signal. The final iteration (Figure 6.9-right) amended these issues. Firstly, the optical detection configuration was rotated to a top-down detection method, illustrated in (Figure 6.9-right), which vastly improved the maximum optical signal readout that was previously lost due to poor transmission through the bottom of the disc. Secondly, the alignment mechanism was upgraded from a ‘2-pin’ approach to a ‘6-pillar’ strategy, whereby the disc holder had 6 extruded pillars which aligned with the array of circular holes present in the mCPU V1.6. The degree of freedom of this approach was minute, particularly in comparison to the ‘2-pin’ strategy.

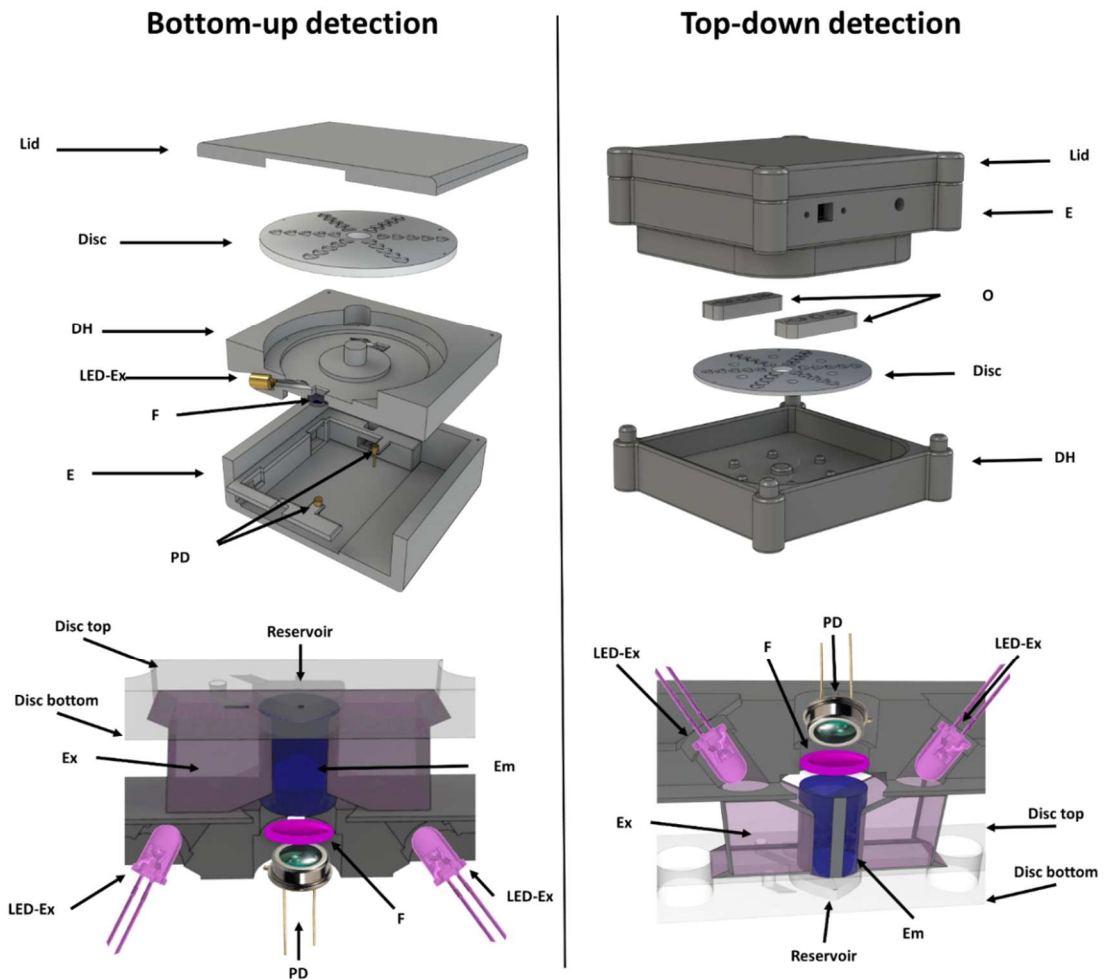


Figure 6.9: The Evolution of the detection platform for the MariaBox centrifugal processing unit.

The tested fluorescence detection strategies used on the MariaBox centrifugal processing unit (mCPU). A) The bottom-up approach used on the detection platform V1.0-2.0. This method proved inaccurate due to the loss in optical transparency due to surface modification of the reservoir floor during functionalisation. B) The top-down approach used in the detection platform V3.0. This configuration seemed unaffected by the functionalisation of the reservoir.

The ability of this system (mCPU V1.6 and final detection platform) was previously characterised, with a 7.2 ng/mL limit of detection microcystin-LR (19). While the system was also optimised for MC-LR detection as a proof of concept, a limit of detection of both domoic acid and saxitoxin was also reported to be approximately 20 ng/mL and 50 ng/mL, respectively, where it was predicted that further optimisations of the domoic acid and saxitoxin assays could have further reduced these limits of detections.

6.4.2.5 Microvalve development

With the assay integration on a proof of concept successful, development of appropriate microfluidic valving mechanisms was required to conduct autonomous assay execution. A number of microvalve strategies (Figure 6.10) were considered and tested to determining difficulty in application, reliability and ease of autonomous actuation *in-situ*;

- a) The cap valve (19) – With the success of the mCPU V1.6, the cap valve was designed to allow for the expansion of the number of test assays per disc with minimal additional microfeatures. However, as this approach was easy to apply and highly reliable, it was deemed that autonomous actuation *in-situ* would be too difficult. This was due to difficulties in integrating and operating a reliable puncturing mechanism in a turbulent marine environment, therefore this valve was not investigated beyond conceptualisation.

- b) Wax valve (29) – Through the use of a paraffin-graphite (1 g : 1.17 g) wax valve, in combination with a silver screen printed layer, an alternative to the cap valve (a) was developed, whereby the semi-conductive material would melt due to the ohmic heating effect. While this valve was successful, it was problematic to consistently integrate within the disc, guaranteeing contact between the screen-printed layer and the valve, as well as ensuring the vent was completely closed, was difficult. This was amplified by the quantity of microvalve to be integrated per disc, whereby one was required for every reservoir.

- c) The wax valve multiplex – Due to the difficulties in integrating the wax valve within the disc, the wax valve multiplex solution was developed in an attempt to reduce the number of valves per disc, with a single valve actuating multiple reservoirs with the same radial positioning. This approach again was difficult to implement as the communal ventilation system also a sharing of initial sample loading inlets preventing pneumatic compression and sample progression halting. This was somewhat rectified by a resealing of the loading inlets, however as this would be difficult to achieve autonomously in-field, this approach was not further investigated.

- d) The hydrophobic valve – The use of a hydrophobic valve for halting liquid progression has been previously reported.(30,31) A hydrophobic valve strategy

was integrated by spray-coating the microfluidic channels using a sol-gel composite, similar to (32), whereby the in-house designed sol-gel recipe was paired with methylated fumed silica to achieve a hydrophobic coating (surface contact angle $<130^\circ$). However, in this case, the hydrophobicity proved to promote liquid transportation over liquid halting. It was stipulated that this was caused by a non-uniform spreading of the coating of the reservoir due to the spray-coating procedure.

- e) The pneumatic valve for air actuation – A pneumatic compression valve was investigated whereby an air-tight, but water dissolvable, material (Solublon™) as an alternative to the cap valve (a), based on the event-trigger valving mechanism (33). In this method, a threshold centrifugal force is required for liquid progression to reach and compress a pneumatic chamber containing a dissolvable valve, whereby the opening this valve would uncap the ventilation for the subsequent reservoir and release pneumatic compression. This valve proved difficult to implement, as the centrifugal forces required to actuate the microvalve were too similar to the forces required for liquid transportation between reservoirs, making the valves highly unreliable in this configuration in high uncertainty of success.

- f) The pneumatic valve for liquid actuation (25) – The pneumatic valve for liquid actuation was a variant, and less complex configuration to the pneumatic valve for air actuation (e). In this case, a standalone pneumatic chamber prevented liquid progression unless relatively high centrifugal forces were generated, with the need for capping of the ventilation system. This case proved very successful and was used as the main valve for the deployable mCPU outputs.

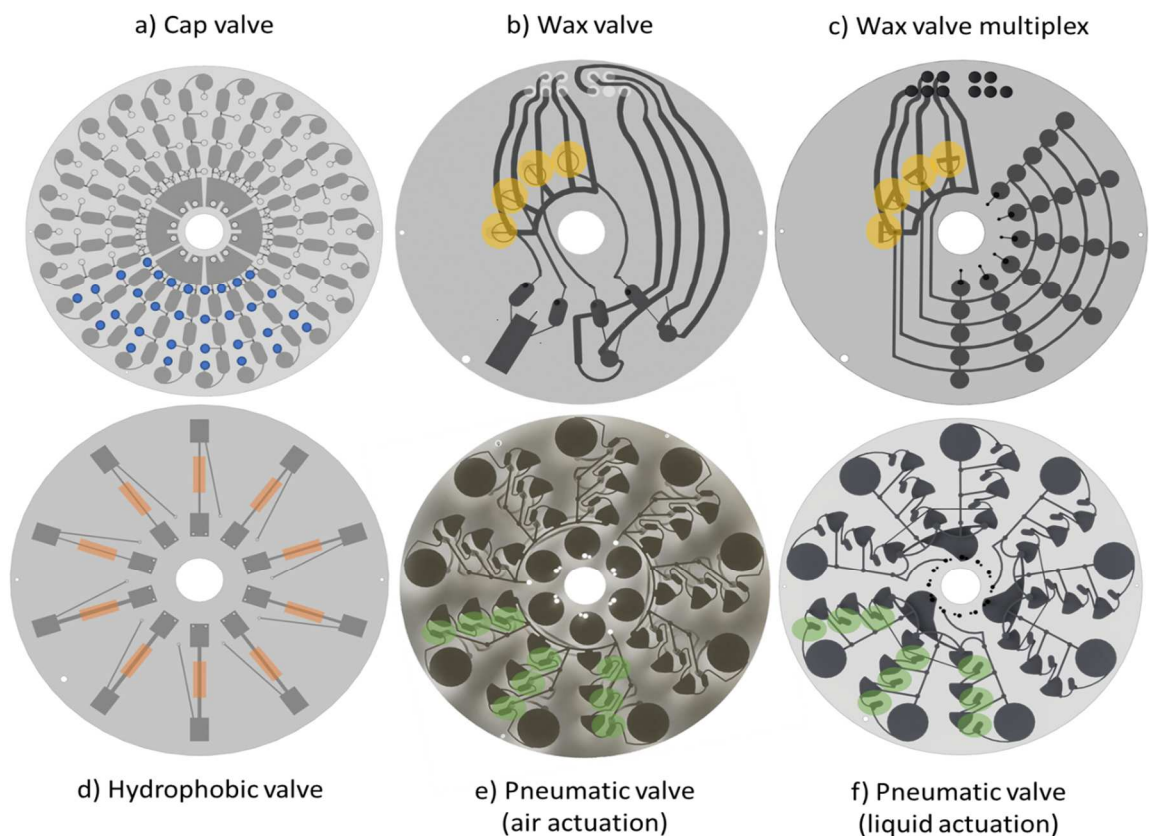


Figure 6.10: The microvalve mechanisms investigated for autonomous assay execution.

a) The cap valve (blue) was designed as an upscaled version of the mCPU V1.6 which also required external puncturing of the roof membrane. B) A paraffin-graphite wax valve (yellow), combined with a silver screen printed layer, was used as an alternative to the cap valve (a), whereby the semi-conductive material would melt due to the ohmic heating effect. C) The paraffin-graphite wax valve multiplex (yellow) was developed to amend the difficulties associated with (b), by attempting to use a single valve per multiple reservoirs at the same radial distance. d) A hydrophobic valve (orange) used to halt liquid progression. This valve was integrated by spray-coating the microfluidic channels using a sol-gel composite, similar to (32), whereby the in-house designed sol-gel recipe was paired with methylated fumed silica to achieve a hydrophobic coating. E) The pneumatic valve (green) for air actuation utilised an air-tight, but water dissolvable, material as an alternative to the cap valve (a), whereby liquid progression would be halted until it reached the dissolvable valve, thus opening the valve. f) The pneumatic valve (green) for liquid actuation was an alternative and less complex configuration to the pneumatic valve for air actuation (e), whereby the ventilation system remained uncapped but an isolated pneumatic chamber prevented liquid progression unless relatively high centrifugal forces were generated.

6.4.2.6 *Integration of microfluidic platform with autonomous MariaBox platform*

With assay integration and a reliable microfluidic valving mechanism implemented, the MariaBox platform required calibration in order to correctly use the mCPU. As autonomous assay execution was handled on the mCPU, the MariaBox platform was only required to transport the disc to different zones within the system, rotate the disc using a specific test protocol, and fluorescently read the test and control reservoirs of the disc. Firstly, the central hole mCPU was slightly modified to allow interaction via a magnetic ball lifting mechanism as requested by the engineering partners (Figure 6.11.a). This was to allow ease of transport and manipulation of the mCPU from a cold storage zone to the motor and fluorescence detection zone. Secondly, a full characterisation of the pneumatic valve for liquid actuation, at varying rotation frequencies and radial positions, was conducted (Figure 6.11.B). This was used in developing an accurate spin speed protocol to complement the autonomous assay execution cycle on the mCPU. Thirdly, a simple microfluidic platform was produced which could be completely loaded with a fluorophore-enriched liquid (Figure 6.11.C). This was used as a method for initial calibration the detection elements with the MariaBox platform without wasting the deployable mCPUs.

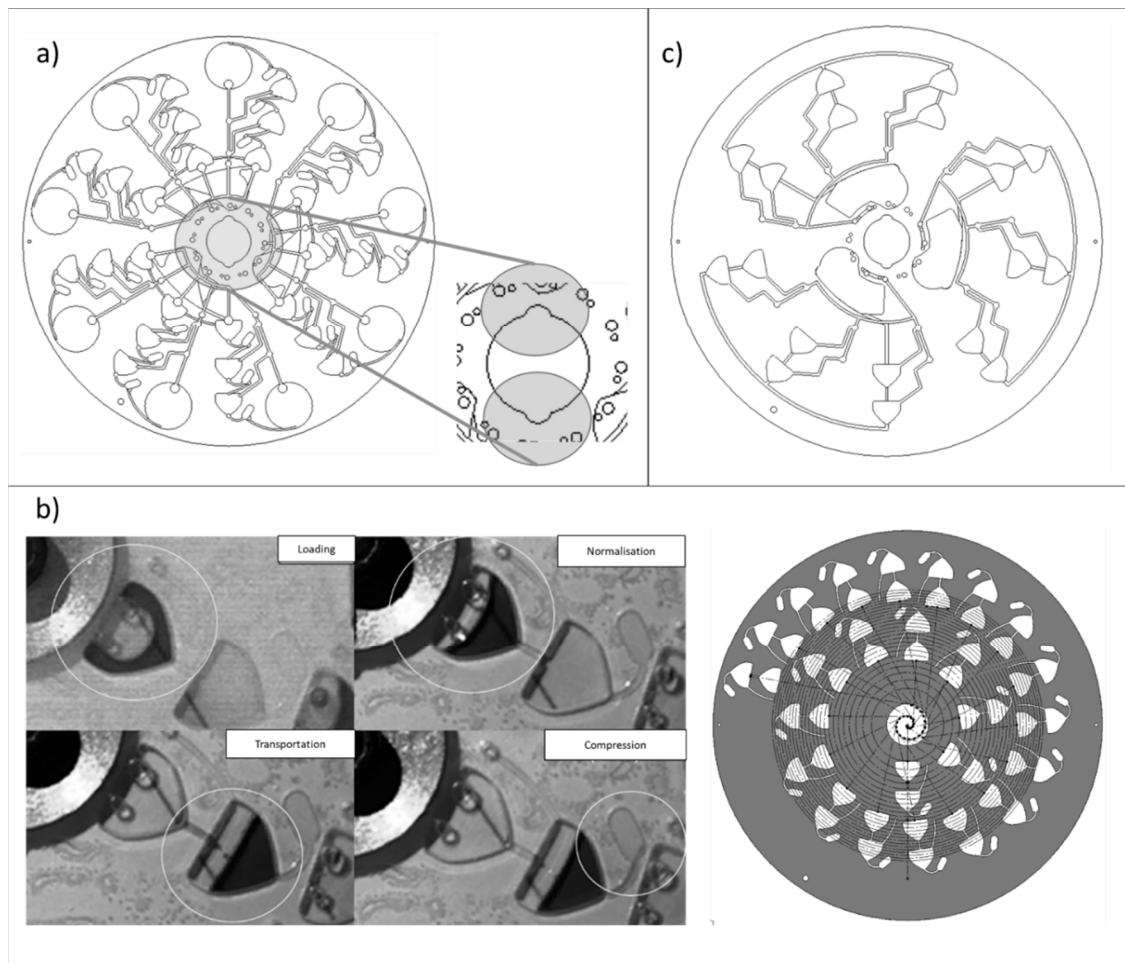


Figure 6.11: Modifications and calibration discs required for integration of microfluidic platform with autonomous MariaBox platform.

A) Integration of an alignment slot in the mCPU for instalment of a magnetic ball lifting mechanism, as requested by the engineering partners. This was for easier manipulation and transportation of the mCPU inside of the MariaBox system. B) The microvalve characterisation disc. Using this disc, liquid actuation, at varying rotation frequencies and radial positions, was validated. This validation was then directly used in the generation of a specific spin speed protocol to complement the autonomous assay execution cycle on the mCPU. C) The fluorescence detection calibration disc. This disc was relatively simple microfluidic platform whereby the disc could be completely loaded with a fluorophore-enriched sample, for use as a sample for initial calibration the detection elements within the MariaBox platform, without the wastage of complex, deployable mCPUs.

6.4.2.7 Deployable outputs

As disc storage was limited to approximately 26 concept mCPU discs, with a thickness of 20mm each, seven replications of the multi-analyte detection strategy were initially included in the design to target the six-months (182 days) deployment duration required

of the MariaBox platform. It was found later however, that optimisation of the design towards a 3-day disc, as opposed to the conceptualised 7-day disc, reduced the disc thickness by ~65%, allowing for the storage of 69 discs within the same space, corresponding to an increase in potential test days to 207. Following this optimisation, the first deployable mCPU was produced the 3-day, triple-assay disc (3D3A) disc (Figure 6.12), encompassing all of the successful discs from each of the stages prior. The 3A3D disc was used as an initial stage to bridge the gap between a single assay disc (mCPU v1.9) and the octuple-assay disc. This disc allowed the multiplex processing of a single sample for the conduction of three separate biological samples only, and is further described by (25).

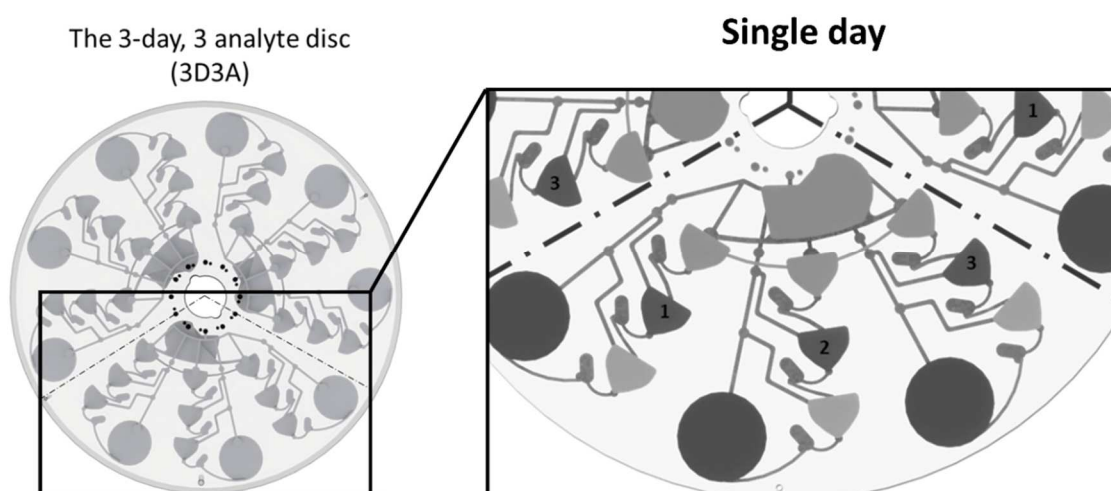


Figure 6.12: The deployable 3-day, 3 analyte (3D3A) MariaBox centrifugal processing unit.

This was used as a bridging disc between the single assay disc mCPU 1.6 and the final octuple-assay disc (Figure 6.14). 1-3) The detection assays for Saxitoxin, microcystin, and domoic acid respectively.

In summary, the sample is loaded, and metered between the second reservoir of the three separate assays. Using the pneumatic valve for liquid actuation, the sample conducted the remaining steps of the assay for the required duration. This mCPU verified fluorescence signal change proportional to the concentration of analytes present, however, as this disc had a 10 mm larger radius, it was not compatible for quantitative analysis using the detection platform (Figure 7-right) which could only be carried out using the MariaBox system. Unfortunately, the first tests were inconclusive due to partner distribution issues, whereby a whitening of the adhesive layers significantly degraded the optical clarity of the discs, resultantly saturating the optical

data results (Figure 6.13.left). This was rectified in the second generation of 3D3A discs, where whitening was reduced by removal of excess adhesive above and below reservoir zones, as well as increased rolling pressure in activating adhesive (Figure 6.13.right).



Figure 6.13: Issues associated with the optical transparency of the discs during transportation.

Right) significant whitening of the disc completely degraded the quality of the optical data, resulting in inconclusive results. Left) The rectified 3D3A disc, whereby whitening was reduced by removal of excess adhesive above and below reservoir zones, as well as increased rolling pressure in activating adhesive.

During the testing of the 3D3A discs, and in order to meet the project end-date, the 3-day, the octuple-assay (3D8A) disc (Figure 6.14) was simultaneously produced. This was an upscaled version of the 3D3A disc, where the reservoir size was maintained through upscaling, with a spatial reduction in the x-y plane accounted for by a 2 mm increase in disc thickness. This allowed the testable assay quantity to be increased from 9 to 24, with sufficient room for the pneumatic valve mechanism. However, the significant complexity associated with disc impeded the manufacturing time due to the manually achieved rapid prototyping approach used. The target goals of the project required distribution of these final 3D8A discs to be used in 3 separate MariaBox platforms, therefore only 6 discs, containing 3 iterations each, was available for each test site. As these systems also had not had the opportunity to be fully calibrated in the handling of these discs, but rather the lower complexity discs, an initial recalibration of the system prior to deployment was required. This further reduced the yield of data collected to 12

measurements per site, per day, whilst in autonomous deployment. This made it extremely difficult to assess which components (disc, optical system, mechanical system, electrical systems, computational system, etc...), if any, may have acted incorrectly whilst in the marine environment. This lack of component surveillance, combined with the low levels of analytes expected during the time of deployment (winter), particularly with regards to minimal toxin presence, further emphasised the additional validation required by the system. However, it is worth noting that significant steps have been made in development of a fully autonomous, *in-situ* deployable marine monitoring system, from conceptualisation to realisation, and had more time been available to conduct this additional validation, as well as the production of extra 3D8A mCPUs, it is believed that the end-target could have been achieved.

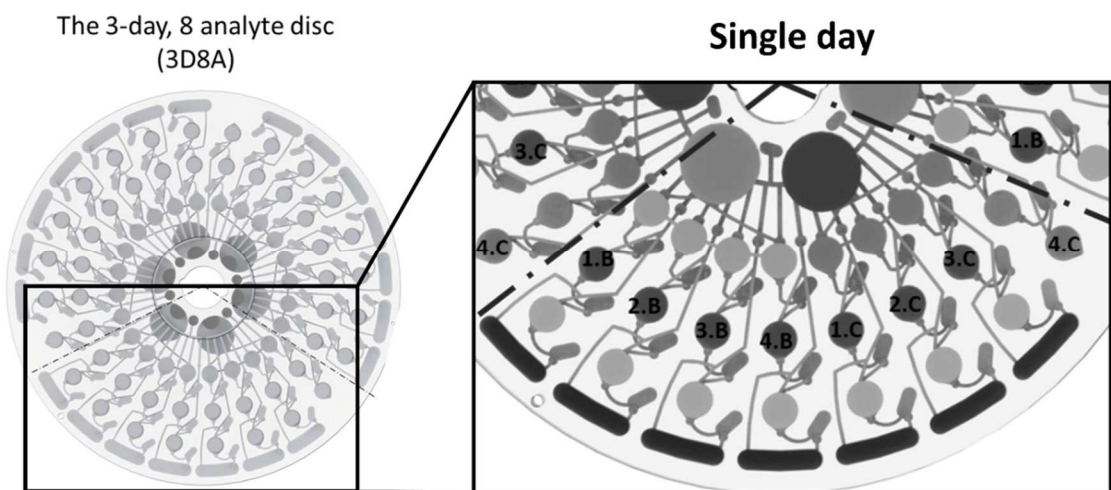


Figure 6.14: The deployable 3-day, 8 analyte (3D8A) MariaBox centrifugal processing unit.

This was the final realisation of the original concept, for the detection of all of the target analytes. 1-4.B) The detection assays for Saxitoxin, microcystin, azaspiracid, and domoic acid respectively. 1-4.C) The detection assays for naphthalene PFOS, Camphechlor, and total heavy metals respectively.

6.4.3 Summary and lessons learned

There has had a number of successful outcomes and lessons learned from working on the highly complex and integrated MariaBox project. Whilst this report primarily discusses the design developments associated with the MariaBox mCPU, notable work which falls outside the scope of this report includes;

- The development of novel assay strategies for the detection of analytes which have not been detectable *in-situ* prior to this project.
- The development of a highly integrated and deployable marine-monitoring system, inclusive of attachable peripheral sensors, with cloud-based networking for instantaneous data capture and processing.
- The investigation into the requirement for deployable systems in marine-based environments, and the associated governmental legislation required for the correct installation and implementation of monitoring systems.
- The accumulation of an interdisciplinary expertise networking consortium, inclusive of both academic, institutional and industrial, with future exploration of collaboration opportunities.

With regards to microfluidic disc development for a highly challenging, long term deployment, a strategy from conceptual ion to realisation was developed. This was achieved through the development of a conceptual design, encompassing all of the required end target goals, which was then fragmented into simpler microfluidic discs for ease of manufacturing, reproducibility, simultaneous testing and optimisation of individual functional microfeatures, and cost-effectiveness. These simpler microfluidic discs, once optimised, could then be integrated together to gradually approach the requirements of the conceptual design. These fragment integration stages included; conceptualisation, assay integration, microvalve integration, partner compatibility and deployable outputs. A summary of the design changes for the mCPU during assay integration is summarised in Table 8. This table illustrates the lessons learned during each mCPU design iteration, with the optimal manually-actuated mCPU V1.6 could be used as a simple generic approach for alternative 5-step assay protocols, or further modified for the inclusion of more, or less, assay steps as required. Reservoir replica chips were also recommended for the rapid, cost-effective optimisation of the multi-parameter surface functionalisation process.

Table 8: MariaBox centrifugal processing unit design log summary.

Version	Issue	Design modifications
V1.0	Disc too thick for initial testing, no valving solution for automation	Reduction in number of performable assays, wider reservoirs, thinner disc, automatic valving solution investigated
V1.1	Sample not progressing through reservoirs	ventilation added to each reservoir
V1.2	Requires a control reservoir to be integrated, sample not stopping in reservoirs	Control reservoir added, PSA used to cover each reservoir ventilation hole where popping allows progression: Manual valve (Vent)
V1.3	Anti-body mixing section required for powdered antibody storage	Anti-body mixing reservoir added
V1.4	Sample loss more obvious with addition reservoirs	Reservoirs rounded to reduce sample lose
V1.5	Alignment with detection difficult, bottom-up detection failing due to white PPT forming after surface modification	Alignment holes added to disc, detection system converted to a top-down detection.
V1.6	Manufacturing time to slow at high cost for surface modification optimisation (~ 5 discs per week = 30 tests per week at material wastage)	Chip based replicas of test and control reservoirs created (~ 15 chips per day = 75 tests per week at low material wastage)
Chip	Chip no longer compatible with ToxiSense detection system for comparison with fluorescent microscope	Chip holder accessory with alignment holes manufactured
Chip Holder	none	none.

A simple assay detection system, which would be representative of the final optical detection setup used in the MariaBox system, was developed to complement both the optimal mCPU and replica chip. A summary of the design changes for the detection platform during assay integration is summarised in Table 9. While the end-target was a fully autonomous detection system, value was identified in the production of a portable, low-cost detection system. Therefore, a custom designed and 3d-printed detection platform was manufactured. During assay integration, however, it was notated that

optical transparency issues due to surface functionalisation impelled the orientation of the optical detection, with the ‘Top-down’ approach selected as the optimum detection configuration.

Table 9: Detection platform design log summary.

Version	Issue	Design modifications
Bottom-up	Alignment of disc difficult and causing varying detection results, Surface modification of disc creating white PPT which detection optics must travel	Alignment extrudes added, systems converted to a top-down detection system
Top-down	None	None

Finally, a summary of the disc production for the entire MariaBox project, which only included on-disc assay integration, is presented in Table 10. Clearly evident in Table 10, is the correlation between disc complexity, given by number of individual ‘layers with disc’, and the quantity of discs produced. Due to the manual manufacturing of the mCPUs, this trend became unavoidable. If this process was automated, significant improvement in the yield of produced discs is expected, but until such a procedure is implemented, it is recommended that this fragmented development strategy is implemented to minimise disc complexity and maximise testable disc yield.

Table 10: Microfluidic disc production summary during duration of MariaBox project.

Disc model	Layers within disc	Dates	Quantity	Partner distribution	Feedback from partners following usage of discs	Modifications arising from feedback from tests done on discs by partners
ToxiSense test design	5	2014-2016	50	N/A - DCU solo testing	Assay performance and quantification successful on the ToxiSense platform	N/A
3-Day discs (with toxin coated within the discs)	10	Jan-17	3	CYRIC	None	N/A
Lucifer yellow discs – developed by DCU to test the detection system in Cyprus	10	Jan-17	2	CYRIC	Brief summary of final results, request of alignment slot on disc	Due to lack of results, analysis of results could not be carried out to decide further modifications, alignment slot incorporated
3-Day discs (without toxin coated with the discs)	10	Mar-17	5	NIVA	YES: Detection wells became whitened due oxidation of glue over detection wells during transportation	Further optical enhancement of detection zones
3-Day discs (without toxin coated with the discs)(Optically enhanced)	10	Oct-17	10	NIVA	YES: Detection wells remained transparent for testing. Liquid traveling beyond detection zones before detection occurs.	Clarification to partners that this was always the case and detection is supposed to occur after liquid has travelled to waste zone, therefore discs functioning correctly
8-day discs (Full) calibration	12	Nov-17	3x2 (6)	Galway, Barcelona, CYRIC	Discs are leaking, sample not progressing correctly, Detection not functioning correctly	Request of returned disc to assess why liquid is no longer correctly flowing, Detection zone verified by DCU. Detection issue with MariaBox. Suggested simplification of discs for characterising MariaBox performance with reading detection zone only.
8-day discs (Full) Test pilot	12	Dec-17	3x4 (12)	Galway, Barcelona, CYRIC	N/A-System pilots not complete	N/A

6.5 Conclusion

The development of microfluidic bio-sensors as cost-effective strategies for environmental monitoring has been a primary goal for the platform since the 1980s. It has played a pivotal role in the downsizing of sample ranges and complex assay protocols used in analyte detection. In order to develop a successful, highly integrated centrifugal microfluidic platform, from initial concept to final employed disc, for a large scale, interdisciplinary project, a number of design stages must be undertaken and optimised. Depending on the complexity of the project, autonomous multi-assay integration and execution studies may be required, with microvalve technology which allows minimal external interaction for maximum automation. In achieving this, compromises and assistance must be provided to project partners, such as modifications and/or calibration devices, in order to attain the proposed project target. Throughout this paper, the design and development strategy implemented in the MariaBox centrifugal processing unit was used as an example of how to develop a highly-integrated, microfluidic centrifugal processing unit, from conceptualisation to realisation. As part of this, a concept-fragmentation strategy is demonstrated for the development and optimisation of single microfeature elements prior to amalgamation into a complete and fully integrated platform. The benefits of this approach allow the complete characterisation and optimisation of each microfeature required separately in a low-complexity, high production yield device. This approach also allows for maximised research output opportunities during the development process, whilst offering insight into the 'most feasible' selection practice for large-scale integration compatibility and success.

6.6 Acknowledgment

This work was supported by the FP7 EU-funded MARIABOX project. The MARIABOX project receives funding from the European Union Seventh Framework Programme - Grant Agreement No: 614088.

6.7 Supplementary Information

- Additionally, the design portfolio of the microfluidic discs and detection systems for assay integration has been included.

6.8 References

1. Kong LX, Perebikovskiy A, Moebius J, Kulinsky L, Madou M. Lab-on-a-CD: A Fully Integrated Molecular Diagnostic System. *J Lab Autom* [Internet]. 2015;2211068215588456-. Available from: <http://jla.sagepub.com/content/early/2015/06/16/2211068215588456.abstract>
2. Ducr e J, Haeberle S, Lutz S, Pausch S, Zengerle R, Stetten F Von, et al. The centrifugal microfluidic Bio-Disk platform. *J Micromechanics Microengineering* [Internet]. 2007 Jul 1 [cited 2013 Nov 7];17(7):S103–15. Available from: <http://dx.doi.org/10.1088/0960-1317/17/7/s07>
3. Haeberle S, Zengerle R, Mark D, Von Stetten F, Zengerle R. Microfluidic platforms for lab-on-a-chip applications. *Lab Chip* [Internet]. 2007 Sep;7(9):1094. Available from: <http://xlink.rsc.org/?DOI=b706364b>
4. Stone HA, Stroock AD, Ajdari A. ENGINEERING FLOWS IN SMALL DEVICESMicrofluidics Toward a Lab-on-a-Chip. *Annu Rev Fluid Mech* [Internet]. 2004;36(1):381–411. Available from: <http://arjournals.annualreviews.org/doi/abs/10.1146/annurev.fluid.36.050802.122124>
5. Mark D, Haeberle S, Roth G, von Stetten F, Zengerle R. Microfluidic lab-on-a-chip platforms: requirements, characteristics and applications. *Chem Soc Rev* [Internet]. 2010;39(3):1153–82. Available from: <http://pubs.rsc.org/en/content/articlehtml/2010/cs/b820557b>
6. Liu Y, Sun Y, Sun K, Song L, Jiang X. Recent developments employing new materials for readout in lab-on-a-chip. *J Mater Chem* [Internet]. 2010;20(35):7305–11. Available from: <http://dx.doi.org/10.1039/C0JM00576B>
7. Whitesides GM. The origins and the future of microfluidics. *Nature* [Internet]. 2006;442(7101):368–73. Available from: <http://www.scopus.com/inward/record.url?eid=2-s2.0-33747117373&partnerID=40&md5=0074130e4ce504444efcdd2a9e1f92d4>

8. Figeys D, Pinto D. Lab-on-a-chip: a revolution in biological and medical sciences. *Anal Chem.* 2000;72(9):330–A.
9. Sharma S, Zapatero-Rodríguez J, Estrela P. Point-of-care diagnostics in low resource settings: present status and future role of microfluidics. *Biosensors.* 2015;
10. Manz A, Harrison DJ, Verpoorte EMJ, Fettinger JC, Paulus A, Lüdi H, et al. Planar chips technology for miniaturization and integration of separation techniques into monitoring systems: Capillary electrophoresis on a chip. *J Chromatogr A* [Internet]. 1992;593(1–2):253–8. Available from: <http://www.sciencedirect.com/science/article/pii/0021967392802934>
11. Wang J. Electrochemical detection for microscale analytical systems: a review. *Talanta.* 2002;56(2):223–31.
12. Maguire I, O’Kennedy R, Ducreé J, Regan F. A review of centrifugal microfluidics in environmental monitoring. *Anal Methods.* 2018;10(13):1497–515.
13. Bonasso M, Barattini P, Isticato R, Donadio G, Giusti A, Philimis P, et al. MariaBox: First prototype of a novel instrument to observe natural and chemical pollutants in seawater. In: *OCEANS 2017 - Aberdeen.* 2017. p. 1–5.
14. Becker H, Locascio LE. Polymer microfluidic devices. *Talanta.* 2002;56(2):267–87.
15. Bartholomeusz DA, Boutté RW, Andrade JD. Xurography: rapid prototyping of microstructures using a cutting plotter. *J Microelectromechanical Syst.* 2005;14(6):1364–74.
16. Nayak NC, Lam YC, Yue CY, Sinha AT. CO₂-laser micromachining of PMMA: the effect of polymer molecular weight. *J Micromechanics Microengineering.* 2008;18(9):95020.
17. Grumann M, Brenner T, Beer C, Zengerle R, Ducreé J. Visualization of flow patterning in high-speed centrifugal microfluidics. *Rev Sci Instrum.* 2005;76(2):25101.

18. Kirby D, Siegrist J, Kijanka G, Zavattoni L, Sheils O, O’Leary J, et al. Centrifugo-magnetophoretic particle separation. *Microfluid Nanofluidics*. 2012;13(6):899–908.
19. Maguire I, Fitzgerald J, Heery B, Nwankire C, O’Kennedy R, Ducreé J, et al. A novel microfluidic analytical sensing platform for the simultaneous detection of three algal toxins in water. *ACS Omega* [Internet]. 2018;3(6):6624–6634. Available from: <https://pubs.acs.org/doi/pdf/10.1021/acsomega.8b00240>
20. Burger R, Ducreé J. Handling and analysis of cells and bioparticles on centrifugal microfluidic platforms. *Expert Rev Mol Diagn* [Internet]. 2012 May;12(4):407–21. Available from: <http://www.ncbi.nlm.nih.gov/pubmed/22616705>
21. Lee C-Y, Lee G-B, Lin J-L, Huang F-C, Liao C-S. Integrated microfluidic systems for cell lysis, mixing/pumping and DNA amplification. *J Micromechanics Microengineering*. 2005;15(6):1215.
22. Regan F, Fitzgerald J, Murphy C, Maguire I, O’Kennedy R. Convenient “one-step” extraction method for autonomous sensing of marine algal toxins. In: *OCEANS 2017 - Aberdeen*. 2017.
23. Cennamo N, Zeni L, Tortora P, Regonesi ME, Giusti A, Staiano M, et al. A High Sensitivity Biosensor to detect the presence of perfluorinated compounds in environment. *Talanta*. 2018;178:955–61.
24. Donadio G, Di Martino R, Oliva R, Petraccone L, Del Vecchio P, Di Luccia B, et al. A new peptide-based fluorescent probe selective for zinc (II) and copper (II). *J Mater Chem B*. 2016;4(43):6979–88.
25. Maguire I, Fitzgerald J, McPartlin D, Heery B, Murphy C, Nwankire C, et al. A centrifugal microfluidic-based approach for multi-toxin detection for real-time marine water-quality monitoring. In: *OCEANS 2017 - Aberdeen*. 2017. p. 1–8.
26. Lai S, Wang S, Luo J, Lee LJ, Yang S-T, Madou MJ. Design of a Compact Disk-like Microfluidic Platform for Enzyme-Linked Immunosorbent Assay. *Anal Chem* [Internet]. 2004 Apr 1;76(7):1832–7. Available from: <https://doi.org/10.1021/ac0348322>

27. Lee BS, Lee J-N, Park J-M, Lee J-G, Kim S, Cho Y-K, et al. A fully automated immunoassay from whole blood on a disc. *Lab Chip* [Internet]. 2009;9(11):1548–55. Available from: <http://dx.doi.org/10.1039/B820321K>
28. Fischer MJE. Amine Coupling Through EDC/NHS: A Practical Approach. In: Mol NJ, Fischer MJE, editors. *Surface plasmon resonance* [Internet]. Totowa, NJ: Humana Press; 2010. p. 55–73. Available from: http://link.springer.com/10.1007/978-1-60761-670-2_3
29. Maguire I, Heery B, Andlauer B, Gribbin S, Nwankire C, Ducreé J, et al. Battery-powered microcontroller with wireless communication for random, Ohmic actuation of novel wax valves on a Lab-on-a-Disc platform. In: *20th International Conference on Miniaturized Systems for Chemistry and Life Sciences, MicroTAS 2016*. 2016.
30. Feng Y, Zhou Z, Ye X, Xiong J. Passive valves based on hydrophobic microfluidics. *Sensors Actuators, A Phys*. 2003;108(1–3):138–43.
31. Ahn KWO and CH, Oh KW, Ahn CH. A review of microvalves. *J Micromechanics Microengineering* [Internet]. 2006;16(5):R13. Available from: <http://stacks.iop.org/0960-1317/16/i=5/a=R01>
32. Power AC, Barrett A, Abubakar J, Suarez L., Ryan L, Wencel D, et al. Versatile Self-Cleaning Coating Production Through Sol–Gel Chemistry. *Adv Eng Mater* [Internet]. 2015 Jul 1;18(1):76–82. Available from: <https://doi.org/10.1002/adem.201500112>
33. Kinahan DJ, Kearney SM, Dimov N, Glynn MT, Ducreé J. Event-triggered logical flow control for comprehensive process integration of multi-step assays on centrifugal microfluidic platforms. *Lab Chip*. 2014 Jul;14(13):2249–58.

Chapter 7: Final Conclusion

The development of low-cost sensors for the monitoring of the precious resource that is water is of critical importance worldwide. As these sensors reduce in cost, complexity and size, their ability to be implemented in large scale autonomous and/or hand-held networks allows for more frequent and extensive monitoring of environments. As outlined at the start of this thesis, the primary technical challenge of this thesis was the development of low-cost, microfluidic platforms for environmental water quality monitoring. The project was sponsored by the FP7 EU-Funded 'MARIABOX project', as part of the European Union Seventh Framework Program (grant agreement No: 614088). Presented within this thesis, was the staged development process for achieving an autonomous, multi-assay detection strategy for environmental monitoring, through the use of centrifugal microfluidic platforms. Included within this development strategy are both the individual and integration advancements towards a successful, autonomous environmental sensor which has the potential to be used *in-situ*.

As the MARIABOX project deliverables included the requirement to develop a microfluidic platform with eight separate on-board biosensors (four biological, four chemical). This platform was also required to be compatible with a deployable analytical system developed by external partners, in which contained modules of sample preparation and delivery, disc and reagent storage, detection capabilities, as well as network communications. To achieve this target, a conceptual fragmentation strategy was utilised, whereby an initial high-cost centrifugal platform was developed and simplified for the individual optimisation of microfluidic components. Therefore, as part of this project, a proof-of-concept toxin detection system was developed and tested. This generically designed platform demonstrated capability for detecting 3 of the 4 separate toxins required by the MariaBox system. This platform was then further enhanced to include a simple, yet robust microvalve mechanism, allowing for simultaneous assay execution. This was then followed by further expansion of the platform for the inclusion of 8 separate analytes.

Centrifugal microfluidic technology was selected as the ideal sensor platform for hand-held systems due to the current gap in research, adaptability of the platform and low cost of implementation and actuation. Requiring only a motor to propel a sample within a centrifugal microfluidic platform, complex assay protocols can be integrated within the platform through coupling with biosensing technology (1–3). This platform therefore offers huge potential in the enhancement of current environmental monitoring strategy limitations; portability and in-situ capability, cost-effectiveness, generical design for multi-analyte detectability, and the minimal required end-user interaction. As part of this thesis, the basic principles observed in microfluidic systems were investigated, as well as the current detection methodologies for marine based environments was conducted, which was then used in the translation of popular Lab-on-a-Chip technologies into centrifugal platforms.

Initially, high priority marine toxins were selected as the analytes of interest, including microcystin-LR, domoic acid, saxitoxin and azaspiracid (4,5). While antibody generation and ‘off-chip’ assay performance studies were separately performed by Dr. Jenny Fitzgerald, the design and optimisation of the ‘on-chip’ fluidic handling was conducted by the author. As is evident in chapter six, the design stage received several optimisation iterations, which varied based on the fluidic, assay and detection performances, before the final toxin detection platform was realised and presented in chapter 3. In chapter 3, it was demonstrated that a limit of detection of 7.2 ng/mL, 20 ng/mL and 50 ng/mL for microcystin-LR, domoic acid and saxitoxin respectively could be achieved when the ‘on-chip’ platform was integrated with the detection assays and paired with a low-cost fluorescence detection system. Considering the case of the microcystin detection assay, which received further optimisation, a detection limit of 7.2 ng/mL would be useful for monitoring bathing site, where a detectability of 20 ng/mL is required, but unfortunately it is well short of the required 1 ng/mL detection for drinking water. This shortage was determined to be due to the low-cost fluorescence detection system used, as it has been recently reported that alternative detection systems using similar assay protocols could

achieve < 1 ng/mL limits of detection for microcystin (6,7). However, in comparison with these systems, a reasonably similar detection response for microcystin-spiked water samples was noted.

Following the assay integration on a low-cost centrifugal microfluidic platform, precedence switched to the lowering the minimum required user interaction through the inclusion of microvalves within the system. The importance of these microvalves lies with their ability to allow each assay step to occur both in the correct order and for their set allotted time. Four separate microvalve strategies were investigated for their performance and ease-of integration with the MARIABOX platform as demonstrated in chapter 6; Manually-actuated valves, Ohmic-heated wax valves, pneumatic dissolvable valves, and hydrophobic valves. Of these valves, hydrophobic valves proved the least predictable, which was expected to be primarily due to the rapid spray-coat application technique used, and in some cases, it assisted in the promotion liquid flow. The ohmic heated valves were also found to be quite promising, however integration of the valve within the centrifugal platform proved quite difficult and often resulted a degrading of the optical transparency of the platform resulting in diminished detectability. This valve also required an additional electronic plug-and-play device to heat the wax valves. This device would have also needed to be integrated within the final MARIABOX platform, which was deemed to be unattainable by the project consortium. The manually-actuated valves used the same mechanism of preventative ventilation demonstrated in chapter 3, whereby a physical puncturing of the centrifugal platform surface released compressed air which was otherwise preventing liquid flow. However again, while this disc was highly successful and ideal for multiple-assay integration, it required an external puncturing mechanism similar to the laser abolition method previously reported (8), which again was determined to be too difficult to integrate within the final MARIABOX platform. Finally, the pneumatic dissolvable valves presented in chapter 4, became the compromise between microvalve actuation and integrability with the MARIABOX platform. As part of chapter 4, a complete characterisation of the pneumatic valve actuation was studied, whereby specific centrifugal forces would cause resultant

pneumatic compression within the microvalve. This principle was used to actuate each subsequent valve by the operation of a complementary disc rotational speed program.

As was demonstrated in chapter 5, the toxin detection centrifugal microfluidic platform (chapter 3) and the pneumatic microvalve mechanism (chapter 4) were combined within a single microfluidic disc. Given that there is interest in the use of optical biosensors for simultaneous detection of multiple analytes (9), this platform was also scaled up further to allow for the detection of up to 3 separate toxins in triplicate, while in this case, only microcystin and domoic acid were assessed with a blank assay used as a negative test, with the positive control included within the assay itself. Due to the increase size of this platform, it could not be qualitatively assessed using the same the detection platform discussed in chapter 3 as it was too large, and the MARIABOX detection prototype for which it was designed was not functional at the time. Therefore, the disc was analysed using both a 'spin-stand' mechanism, for fluidic performance characterisation, and fluorescence microscopy, for assay performance characterisation.

While this platform was demonstrated to be successful, as is shown in chapter 5, the scalability of the microvalve mechanism was difficult to achieve when the platform was further expanded to include triplicate detection of the eight separate MARIABOX target analytes, as discussed in chapter 6. This was due to the lack of autonomous tools available to assist with microvalve integration within the disc, thus leading to a more manually assembled platform than desired. The manufacturability of the final MARIABOX centrifugal platform was also impacted during the integration of this microvalve within the platform by way of a more complex, and significantly larger centrifugal platform. As a result, errors due to misalignment during assembly were more prominent and large-scale production of the platform for deployment proved difficult. However, while difficulties are commonplace during prototype development, which can often take up to 10 years to convert a prototype to an end-user commercial device, within this project, a deployable asset, from conceptualisation to realisation, with great

potential in the field of environmental monitoring has been realised within a four-year period, thanks to the culmination of efforts of the MARIABOX partnership.

It is hoped that these investigations will assist in the decision-making process of future environmental monitoring platforms, offering insight into the development of deployable environmental sensors.

7.1 References

1. Maguire I, O’Kennedy R, Ducreé J, Regan F. A review of centrifugal microfluidics in environmental monitoring. *Anal Methods*. Royal Society of Chemistry; 2018;10(13):1497–515.
2. Burger R, Amato L, Boisen A. Detection Methods for Centrifugal Microfluidic Platforms. *Biosens Bioelectron* [Internet]. 2015;(January 2016):1–14. Available from: <http://linkinghub.elsevier.com/retrieve/pii/S0956566315302463>
3. O’Kennedy R, Fitzgerald J, Cassedy A, Crawley A, Zhang X, Carrera S. Applications of antibodies in microfluidics-based analytical systems: challenges and strategies for success. *J Micromechanics Microengineering*. IOP Publishing; 2018;28(6):63001.
4. World Health Organization, Chorus I, Bartram J. *Toxic Cyanobacteria in Water: A guide to their public health consequences, monitoring and management*. Retrieved March. E & FN Spon; 1999. 400 p.
5. Girault M, Beneyton T, del Amo Y, Baret JC. Microfluidic technology for plankton research. *Curr Opin Biotechnol* [Internet]. Elsevier Ltd; 2019;55:134–50. Available from: <https://doi.org/10.1016/j.copbio.2018.09.010>
6. Yang R, Song D, Fang S, Liu Y, Zhou X, Long F, et al. Development of novel portable and reusable fiber optical chemiluminescent biosensor and its application for sensitive detection of microcystin-LR. *Biosens Bioelectron* [Internet]. Elsevier B.V.; 2018;121(June):27–33. Available from: <https://doi.org/10.1016/j.bios.2018.08.062>
7. Taghdisi SM, Danesh NM, Ramezani M, Ghows N, Mousavi Shaegh SA, Abnous K. A novel fluorescent aptasensor for ultrasensitive detection of microcystin-LR based on single-walled carbon nanotubes and dapoxyl. *Talanta* [Internet]. Elsevier; 2017;166(January):187–92. Available from: <http://dx.doi.org/10.1016/j.talanta.2017.01.053>
8. Mishra R, Reilly G, Agnew M, Garvey A, Rogers C, Andrade E, et al. Laser-actuated

centrifugo-pneumatic flow control towards “sample-to-answer” integrated detection of multi-marker panels at the point-of-care. Proc IEEE Int Conf Micro Electro Mech Syst. 2018;2018–January:1185–8.

9. Liao Z, Zhang Y, Li Y, Miao Y, Gao S, Lin F, et al. Microfluidic chip coupled with optical biosensors for simultaneous detection of multiple analytes: A review. Biosens Bioelectron [Internet]. Elsevier B.V.; 2018;126(August 2018):697–706. Available from: <https://linkinghub.elsevier.com/retrieve/pii/S095656631830928X>